Increased Oil Recovery from Mature Oil Fields Using Gelled Polymer Treatments

Final Report

Reporting Period
June 16, 1999 - June 31, 2002

G.P. Willhite, D.W. Green and C.S. McCool

May 2003

DE-AC26-99BC15209

The University of Kansas Center for Research, Inc.
Tertiary Oil Recovery Project
1530 W. 15th St.
Lawrence, Kansas 66045-7609

Abstract

Gelled polymer treatments are applied to oil reservoirs to increase oil production and to reduce water production by altering the fluid movement within the reservoir. This report describes the results of a three-year research program aimed at reducing barriers to the widespread use of gelled polymer treatments by (1) developing methods to predict gel behavior during placement in matrix rock and fractures, (2) determining the persistence of permeability reduction after gel placement, and (3) developing methods to design production well treatments to control water production. The work focused on the gel system composed of polyacrylamide and chromium acetate. The molar mass of the polymer was about six million. Chromium(III) acetate reacted and formed crosslinks between polymer molecules. The crosslinked polymer molecules, or pre-gel aggregates, combine and grow to eventually form a 3-dimensional gel.

A fundamental study to characterize the formation and growth of pre-gel aggregates was conducted. Two methods, flow field-flow fractionation (FFFF) and multi-angle laser light scattering (MALLS) were used. Studies using FFFF were inconclusive. Data taken using MALLS showed that at the gel time the average molar mass of gel aggregates increased by a factor of about three while the average size increase was approximately 50%.

Increased acetate concentration in the gelant increases the gel time. The in situ performance of an added-acetate system was investigated to determine the applicability for in-depth treatments. Increased acetate concentrations delayed the development of increased flow resistance during gelant injection in short sandpacks. The development of increased flow resistance (in situ gelation) was extended from 2 to 34 days by increasing the acetate-to-chromium ratio from 38 to 153. In situ gelation occurred at a time that was approximately 22% of the bulk gelation time.

When carbonate rocks are treated with gel, chromium retention in the rock may limit in-depth treatment. Chromium retention due to precipitation was investigated by flowing chromium acetate solutions through carbonate rock. Chromium precipitated faster in the rocks than in beaker experiments at similar conditions. A mathematical model previously developed fit the precipitation data reasonably well.

The stability of gels when subjected to stress was investigated by experiments with gels placed in tubes and in laboratory-scale fractures. Rupture pressures for gels placed in small diameter tubes were correlated with the ratio of tube length to tube ID. In fractures, fluid leakoff from the fracture to adjacent matrix rock affected gel formation and gel stability in a positive way.

Disproportionate permeability reduction (DPR) was studied in unconsolidated sandpacks and in Berea sandstone cores. A conceptual model was developed to explain the presence of DPR. The effect of a pressure gradient, imposed by injection of oil or brine, on the permeability of gel-treated cores was investigated. DPR increased significantly as the pressure gradient was decreased. The magnitude of the pressure gradient had a much larger effect on water permeability than on oil permeability.

Table of Contents

List of Figures

List of Tables and Exhibit

Executive Summary

Gelled polymer treatments are applied to oil reservoirs to increase oil production and to reduce water production by altering the fluid movement within the reservoir. This report describes the results of a three-year research program aimed at reducing barriers to the widespread use of gelled polymer treatments by (1) developing methods to predict gel behavior during placement in matrix rock and fractures, (2) determining the persistence of permeability reduction after gel placement, and (3) developing methods to design production well treatments to control water production. The work focused on the gel system composed of polyacrylamide and chromium acetate. The molar mass of the polymer was about six million. Chromium(III) acetate reacted and formed crosslinks between polymer molecules. The crosslinked polymer molecules, or pre-gel aggregates, combine and grow to eventually form a 3-dimensional gel.

Aggregate size during gelation. A fundamental study to characterize the formation and growth of pre-gel aggregates was conducted. Two methods, FFFF and MALLS, were developed and used to measure the size of aggregates during the gelation process. Flow field-flow fractionation (FFFF) is a technique that separates particles/molecules by different diffusion rates and determines their size based on flow phenomena through a narrow slit. Multi-angle laser light scattering (MALLS) is a technique that determines the molar mass and size of polymers in solution by directing a laser beam through the solution and measuring the amount of scattered light at several angles. Size distributions of gel aggregates were also measured using a procedure based on equilibrium dialysis (EqD).

The flow field-flow fractionation (FFFF) technique was capable of determining size distributions for polyacrylamide polymers. FFFF results for size distributions of aggregates in gelants indicated that the size of aggregates decreased during the gelation reactions up to the gel time of the systems. The FFFF results for gelants were not in agreement with data from other techniques. Further work is required to evaluate the use of FFFF for the measurement of size distributions of pre-gel aggregates.

A standard procedure using light-scattering measurements was developed for the determination of the weight-average molar mass and the z-average rms radius of polyacrylamide samples that are used in oilfield operations. Light scattering measurements on a polyacrylamide-chromium acetate gelant showed moderate increases in the molar mass and rms radius up to the time when the viscosity of the gelant increases rapidly (gel time). At the gel time, the molar mass approximately tripled in value and the rms radius increased on the order of 50%.

Acetate addition to delay gelation. Increased acetate concentration in the gelant increases the gel time. The in situ performance of an added-acetate system was investigated to determine the applicability for in-depth treatments. Increased acetate concentrations delayed the development of increased flow resistance during gelant injection in short sandpacks. The development of increased flow resistance (in situ gelation) was extended from 2 to 34 days by increasing the acetate-to-chromium ratio from 38 to 153. In situ gelation occurred at a time that was approximately 22% of the bulk gelation time.

Propagation of chromium through carbonate rock. In-depth treatment of carbonate matrix rock using gel systems containing chromium(III) may be limited by the poor propagation of chromium. Two competitive reactions occur: (1) the reaction between chromium acetate and polymer to form a crosslink, (2) precipitation of chromium hydroxide complex due to the increased solution pH caused by the dissolution of the carbonate rock.

Chromium retention was determined when chromium acetate solutions were injected through dolomite cores in the absence of polymer. Significant retention of chromium occurred as a result of precipitation of chromium hydroxide. Retention increased with the residence time in the dolomite cores. A chromium concentration gradient was established along the direction of flow. Presence of potassium chloride moderately increased chromium retention. Chromium precipitated faster in cores than in beaker experiments conducted at similar pH values. An induction period observed in beaker experiments was not observed in the dolomite cores.

Flow of oil/water through gels confined in tubes. Gels, after placement, are subjected to pressure gradients in the reservoir. Pressure gradients imparted by water and/or oil flow eventually create flow paths through gel that is placed in fractures and/or matrix rock. The development of flow paths through gels affects the persistence of a gel treatment and provides conduits for oil production.

Experiments were conducted to reveal characteristics of how gels respond to pressure gradients. The physical structure of the gels fails when the pressure gradient exceeds a critical value, termed the rupture pressure. Two types of gel failure were observed, termed *center-rupture* and *wall-rupture*. Center-rupture occurred when the injection fluid created a path down the centerline of the gel. The gel-tube bond was intact and a sizeable portion of the gel remained in the tube with subsequent oil or brine flow. Wall-rupture occurred when the gel detached from the tube and a significant amount of the gel was displaced from the tube with continued injection. The tube material and condition affected the adhesion strength of the gel to the tube wall. Rupture pressures increased linearly with the ratio of the tube length to tube ID and moderately increased with the time period the gel was allowed to mature.

Response of the gel to an applied pressure gradient that is below a value where rupture occurs depended on time and how the gel was confined. Part of the pressure was transmitted down the length of the gel immediately followed by a smooth increase in pressure transmission when the outlet end of the tube was closed. The smooth increase in pressure transmission was relatively slow and the magnitude decreased with the ID of the tube.

Different behavior was observed when the tube outlet was open which allowed greater deformation of the gel under the applied pressure gradient. Both oil and brine developed channels and flowed through or past the gel. The movement of oil and brine through the gel occurred intermittently. Small pressure gradients were observed along the length of the gel where the brine or oil had penetrated. Most of the applied pressure gradient was across a short section of gel downstream of the position to which the oil or brine had advanced. The oil or brine eventually penetrated the entire length of the gel.

Channel development through gels has implications on the performance of gelled polymer treatments. In production wells, injected brine can develop channels through the placed gel, possibly reducing the effectiveness of the treatment. In production wells, the development of channels by oil and water could affect the treatment's ability to reduce water production while sustaining oil production.

Leakoff during placement in fractures. Gelant leaks off to the adjoining matrix during placement of gelant in a fracture. Experiments were conducted to determine the effect of leakoff on the formation and strength of a gel placed in a fracture. Gel did not form in the fracture when the gelant was placed without leakoff due to reduced chromium levels. Chromium diffused into the brine in the adjoining matrix before gelation could occur. Gel formed in the fracture when leakoff occurred during placement in a fracture. Chromium in the leakoff fluid retarded diffusion from the fracture sufficiently to allow for gelation. Injection of brine into a gel placed in a fracture (with leakoff) ruptured the gel at a threshold pressure. Continued flow of brine after rupture eroded the gel in the fracture wall and displaced gel fragments from the fracture. Substantial resistance to fluid flow remained after the gel was ruptured, but this resistance was eroded by continuous brine injection.

Disproportionate permeability reduction. Treatment of porous rocks with a gelled polymer system usually reduces the permeability of water at residual oil saturation to a much greater extent than the reduction of permeability of oil at the water saturation that is immobile after treatment. This phenomenon is termed disproportionate permeability reduction (DPR). A model for the mechanism of DPR was proposed based on the interpretation of experimental data of the flow of oil and brine in unconsolidated sandpacks and in Berea sandstone cores, with and without residual oil saturation, after gel treatments.

Interpretation of the flow experiments indicated that oil permeability develops as oil penetrates into the gel-filled pore space, dehydrating the gel by displacing brine from the gel structure and creating "new flow" channels within or around the gel. The "*new pore space*" is a fraction of the original pore space, and the permeability to oil is reduced substantially from its value before placement and in situ gelation of the gelant. Subsequent brine injection displaces oil from these flow channels but traps some of the oil in the "*new pore space*" as a residual saturation. The trapping of residual oil in the "*new pore space*" causes the disproportionate reduction in brine permeability because the brine flows primarily in the pore channels created by dehydration of the gel even though the gel has some brine permeability. When gelant is placed in matrix containing residual oil, dehydration of the gel reconnects some of the trapped oil and the oil permeability increases. Subsequent brine displacement experiments conducted at the same pressure drop showed that initial brine permeability was reduced by factors of 100-1000 more than the oil permeability, verifying the existence of disproportionate permeability reduction.

The effect of a pressure gradient, imposed by injecting oil and brine, on the permeability of gel-treated Berea cores was investigated. The volume of dehydration, i.e., the volume of the new pore space created, increased with the pressure gradient imposed during the dehydration process. At the lower range of pressure gradients used for dehydration, permeability to water in the gel treated rock was reduced to a much greater extent than permeability to oil, i.e. there was a significant disproportionate permeability reduction (DPR). Permeabilities to oil and water in the

new pore space were a function of imposed pressure gradient, increasing as pressure gradient increased. Pressure gradient had a much larger effect on water permeability than on oil permeability, thus the magnitude of the DPR decreased as pressure gradient was increased. The large DPR values observed at the lower range of pressure gradients were attributed to relatively large residual oil saturation in the new pore space and the extremely water-wet nature of the new pore space.

Technology transfer. Presentations and technical papers that presented results from this work and work conducted in a previous DOE contract were documented.

Chapter 1

Introduction

Gelled polymer systems are applied to injection wells in mature oil fields for the purpose of in situ permeability modification to improve volumetric sweep efficiency in displacement processes such as waterflooding. Gelled polymers are also used to treat production wells to reduce water production and operating costs, prolonging the economic life of the wells. While the technology has been applied successfully, there are barriers to widespread utilization. These barriers generally involve a need to develop gel systems that can be used for in-depth treatment of matrix rock and a need for improved understanding of performance in matrix rock and fractures. This research program seeks to diminish these barriers through fundamental studies to predict gel behavior and placement in matrix rock and fractures and to develop a new approach to the control of water production in production wells.

A focus of studies for in-depth treatment in injection wells is the role of pre-gel aggregates which form during the gelation process. Aggregates affect gel placement and performance and information about their formation and growth can aid in the design of treatments so that the treatments can be made more reliable. A second focus is on gel systems that have long gel times due to the addition of ligands that slow the overall reaction rate. The added ligand systems have the potential to be placed deep in reservoirs, but their performance under flow conditions in porous media needs to be investigated.

The approach to water control in production wells is based on two-phase flow characteristics of gelled polymer systems that are dehydrated in the reservoir rock after placement. Development of successful treatment strategies will provide the means for oil operators to reduce costs, since water production commonly represents a significant portion of oilfield operational expenses.

This report presents work that was accomplished during the three-year program. Graduate students and research associates performed the laboratory work. Contributors are acknowledged at the beginning of each chapter.

The work described in this report focused on the polyacrylamide-chromium acetate gel system. Chromium(III) forms a complex ion that reacts with carboxyl groups on the polyacrylamide molecule. A crosslink is formed when two polymer molecules join the complex ion. A gel is formed as a result of the crosslinking process.

A study to develop procedures and to measure the size of polyacrylamide molecules and gel aggregates that form during gelation is described in Chapter 2. Two methods, multi-angle light scattering (MALLS) and flow field-flow fractionation (FFFF), were tested. Measurements on a polyacrylamide-chromium acetate gelant using MALLS showed moderate increases in the molar mass and rms radius up to the time when the viscosity of the gelant increases rapidly, or the gel point. The molar mass approximately tripled in magnitude and the rms radius increased on the order of 50%. Sizes of polyacrylamide samples were measured using FFFF. However, size measurements of pre-gel aggregates using FFFF were inconsistent with measurements using other techniques.

The in situ performance of an added-acetate system to determine the applicability for in-depth treatments was tested and the results are described in Chapter 3. Increased acetate concentrations delayed the development of increased flow resistance during gelant injection in short sandpacks. The development of increased flow resistance (in situ gelation) was extended from 2 to 34 days by increasing the acetate-to-chromium ratio from 38 to 153. In situ gelation occurred at a time that was approximately 22% of the bulk gelation time.

Chapter 4 describes a study of the propagation of chromium acetate through dolomite cores in the absence of polymer. Significant retention of chromium occurred and increased with the residence time in the dolomite cores. A chromium concentration gradient was established along the direction of flow. Presence of potassium chloride moderately increased chromium retention. Chromium precipitated faster in cores than in beaker experiments conducted at similar pH values. An induction period observed in beaker experiments was not observed in the dolomite cores.

Gels, after placement, are subjected to pressure gradients in the reservoir. Pressure gradients imparted by water and/or oil flow eventually create flow paths through gel that is placed in fractures and/or matrix rock. The development of flow paths through gels affects the persistence of a gel treatment and provides conduits for oil production. A study that revealed characteristics of how gels respond to pressure gradients is given in Chapter 5.

Gelant leaks off to the adjoining matrix during placement of gelant in a fracture. A study, described in Chapter 6, was conducted to determine the effect of leakoff on the formation and strength of a gel placed in a fracture. Gel did not form in the fracture when the gelant was placed without leakoff. Gels did form in the fracture when leakoff occurred during placement.

Chapters 7 and 8 describe studies on a phenomenon termed disproportionate permeability reduction (DPR), a property of a gel treatment where the water permeability is reduced to a greater extent than the oil permeability. A conceptual model of DPR is described in Chapter 7 that is based on the interpretation of flow experiments. A central feature of this model is the creation of a new pore space that is a result of dehydration of the gel. A study of the effect of the pressure gradient during the injection of oil and water through gel-treated rocks is given in Chapter 8. DPR decreased as the pressure gradient during injection of oil and water was increased.

A listing of presentations and technical papers that present results from this work and work conducted in our previous DOE contract is given in Chapter 9.

Chapter 2

Determination of Molar Mass and Size of Aggregates during the Gelation of a Polyacrylamide-Chromium(III) Acetate Gel System

Graduate Research Assistants: Pau Ying Chong, Tong Wang and Chunyu Wang

Introduction

The polyacrylamide-chromium(III) acetate gel system is used for permeability modification treatments to control fluid movement in oil reservoirs by reducing the permeability of selected zones in the oil reservoirs. The aqueous system forms a gel through the crosslinking of polymer molecules by a complex chromium(III) ion. The crosslinked polymer molecules are referred to here as pre-gel aggregates. The aggregates combine and grow in size to eventually form a 3-dimensional gel. During flow through reservoir rocks, the aggregates filter from the solution. The retained aggregates eventually develop significant flow resistance, diverting gelant flow to zones that were previously less permeable and retarding the depth of placement.

This chapter describes a fundamental study to characterize the formation and growth of the pre-gel aggregates. Two methods, FFFF and MALLS, were tested to determine their capability to measure the size of aggregates during the gelation process. Flow field-flow fractionation (FFFF) is a technique that separates particles/molecules by different diffusion rates and determines their size based on flow phenomena through a narrow slit. Multi-angle laser light scattering (MALLS) is a technique that determines the molar mass and size of polymers in solution by directing a laser beam through the solution and measuring the amount of scattered light at several angles. In addition, aggregate size distributions were measured using a tedious procedure based on equilibrium dialysis (EqD).

The objective of this work was to develop methods based on FFFF and MALLS and then measure the size distributions of pre-gel aggregates as a function of reaction time. Experimental challenges and equipment failure resulted in only partial success in achieving the type and quantity of data that was originally proposed. Size distributions of polymer samples were measured but the results of the size distributions for pre-gel aggregates with FFFF were inconclusive. Average sizes and average molar masses of pre-gel aggregates were measured as a function of time using the MALLS technique.

This chapter reviews the work reported in the annual reports [Willhite et al., 2001, 2002] and presents the results achieved during the third year of the project. Development work for experimental procedures is described in the previous annual reports [Willhite et al., 2001, 2002].

Experimental Techniques and Materials

Flow Field-Flow Fractionation. Flow field-flow fractionation (FFFF) is a technique that separates particles/molecules based on different diffusivities of different size particles/molecules [Giddings et al., 1986; Meyers, 1997]. The separation process of FFFF is conducted in a thin ribbon-like channel that is open and contains no packing material. A schematic of FFFF channel is shown in Figure 2.1. The sample is introduced into the channel through an injector valve and is carried through the channel by the carrier solvent stream. The top and bottom of the channel

are fabricated from a porous ceramic frit, which allows a second solvent stream (crossflow) to flow across, perpendicular to the channel.

The crossflow stream is the driving force for sample retention. The crossflow stream forces the polymer molecules in the sample to move toward the bottom of the channel which is called the accumulation wall. A semi-permeable membrane placed on the accumulation wall allows for solvent passage but not passage of large molecules in the sample. The polymer molecules diffuse back toward the center of the channel. The diffusion rates are related to the molecular size. Smaller polymer molecules diffuse further from the wall. The polymer molecules form an exponential concentration distribution that has a maximum concentration at the accumulation wall and decreases towards the center of the channel at steady-state. The solvent flow stream through the channel is laminar and has a parabolic velocity profile where the flow velocity is zero at the wall and has a maximum value at the center of the channel. Differential elution of sample component occurs when the different axial flow velocities intercept the sample component with different concentration distributions. An inline UV detector attached to the channel outlet determines the mass of the polymer molecules as a function of elution time from the fractionator.

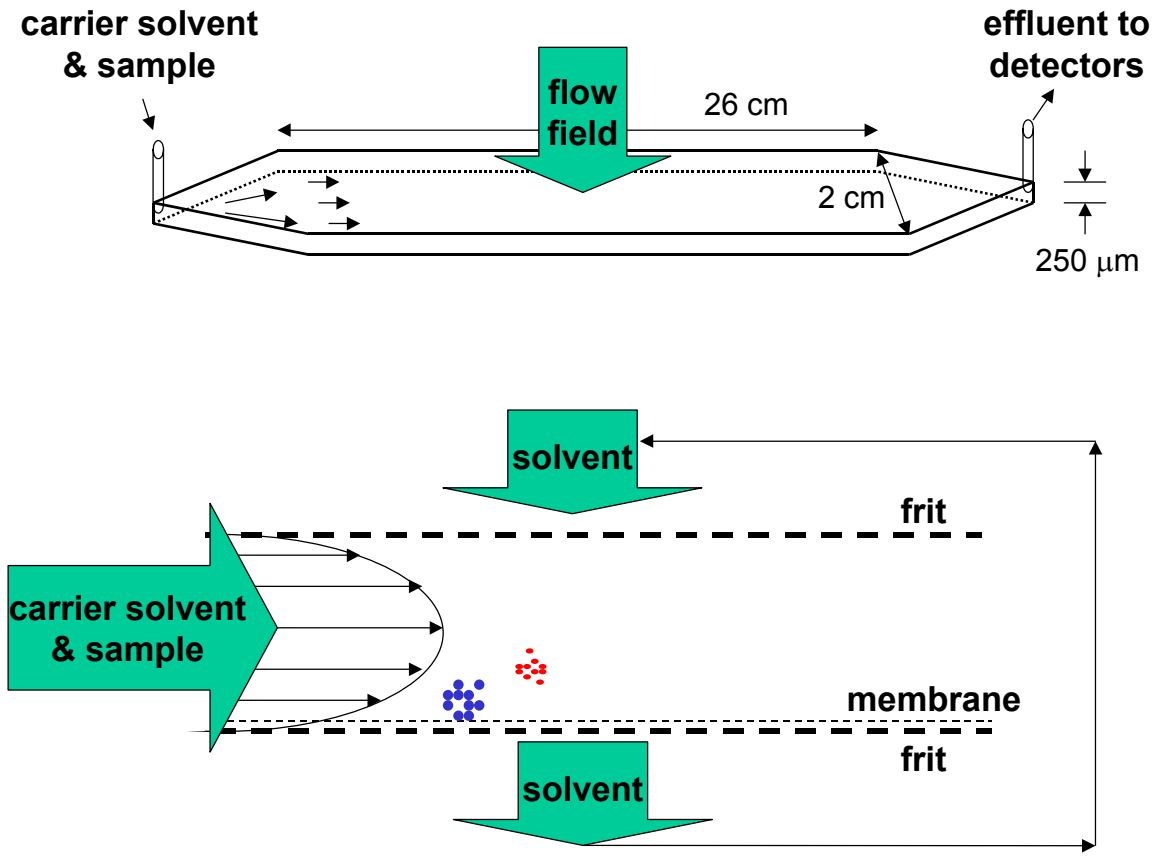

Figure 2.1 - Schematic of channel for the flow field-flow fractionator.

The relationship between elution time and particle size is derived from theoretical models of the transport processes (laminar flow along the channel length, viscous drag and diffusion in the direction of the crossflow) and the Stokes-Einstein equation that relates particle size to the diffusion coefficient [Giddings et al., 1976]. Equation 2.1 is the relationship between particle diameter, d, and elution time, t

$$t = \frac{t^o}{\frac{2kTV^o}{\pi\eta d w^2 V_c} - 12\left(\frac{kTV^o}{3\pi\eta d w^2 V_c}\right)^2} \qquad \text{Eq. 2.1}$$

where,

- d = diameter of particle
- k = Boltzmann's constant
- t = elution time
- t^o = time for non-retained particle to elute from channel (channel void volume/flow rate in channel)
- V^o = channel void volume
- V_c = volumetric rate of crossflow
- w = channel thickness
- T = temperature
- η = viscosity of carrier liquid

Eq. 2.1 is applicable for polymer molecules with diameters of approximately 1 μm or smaller. The cutoff size of 1 μm is dependent on the operating conditions. As the size of the polymer molecules become larger than the cutoff size, the separation mechanism in the channel undergoes a transition from normal FFFF to steric FFFF, where the size of the particle affects the concentration distribution from the accumulation wall. Large particles accumulate at the membrane and protrude into the stream where the flow is faster, eluting earlier than normal-flow theory predicts. Under this situation, calibration with standards of known size is necessary to relate sizes to elution times.

Modifications to the fractionator and operating procedures have improved the versatility and fractionating power of the method [Giddings, 1990]. A stop-flow procedure speeds the initial positioning the sample at the accumulation wall. The channel flow is stopped for a period of time after the sample has entered the channel allowing the crossflow to push the sample to the membrane. The frit outlet improves the detection capabilities by removing a significant portion of the effluent flow from the top of the channel. Only flow from the bottom of the channel next to the accumulation wall (which contains the sample) travels through the detector. The sample concentration is increased by this flow configuration.

Experiments were conducted with a Model F-1000 FIFO Universal Fractionator (FFFractionation, LLC; Salt Lake City, UT) equipped with a polycarbonate membrane (10 nm pore size diameter). The channel dimensions were 2.0 cm wide, 28 cm long and 0.0141 cm thick.

The channel was operated using the frit outlet. Three pumps were required for operation as shown in Figure 2.2. The channel flow pump provided flow through the sample injection valve, the channel and the detector. A second pump was configured to control flow out of the frit-outlet. The frit outlet and corresponding pump are used to draw a significant portion of the flow from the upper portion of the channel which does not contain the sample. A third pump was configured in a loop to control the inlet and outlet flow of the crossflow stream.

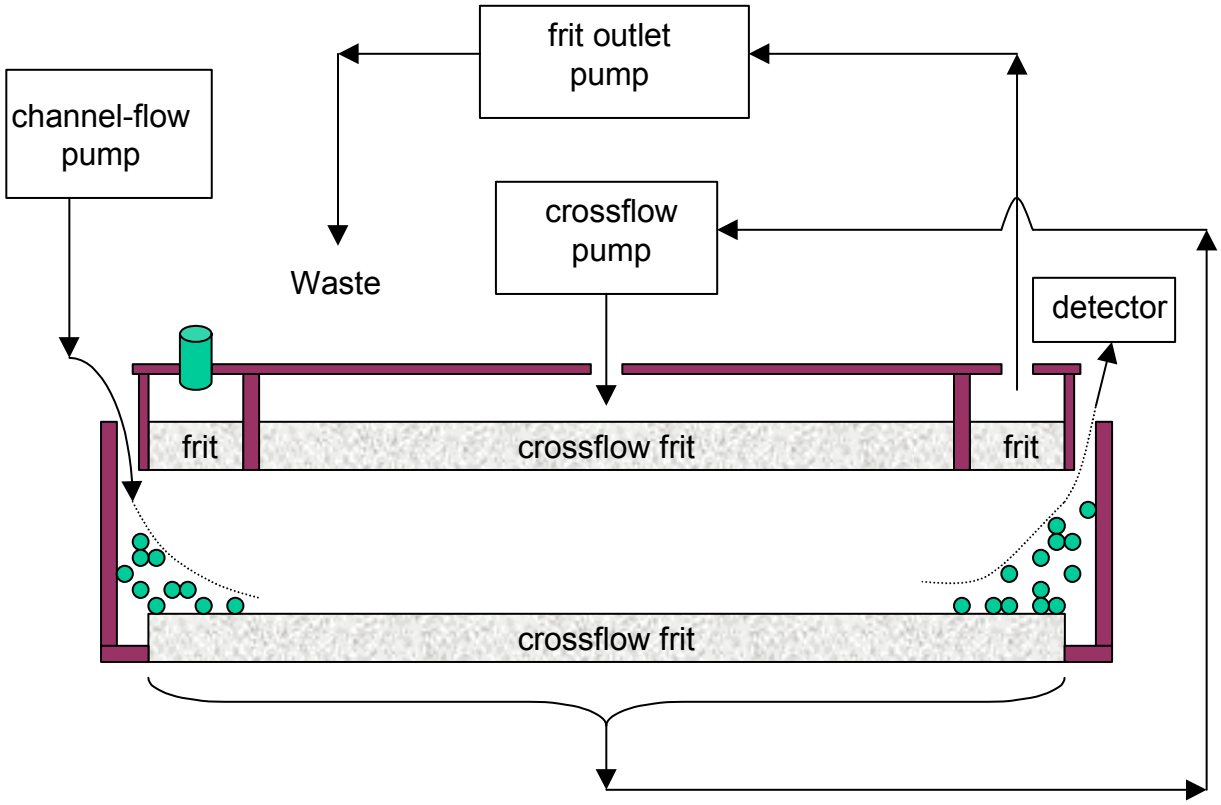

Figure 2.2 - Schematic of pumps and flow paths for FFFF channel.

Samples were introduced with an injection valve equipped with a 10 μL sample loop. The carrier solvent for all flow streams was a 1.0% potassium chloride brine which matched the solvent used for preparing polymer and gelant solutions. Material eluted from the channel was measured using a Waters 490 UV detector. Runs were controlled and data were collected by computer using the Flow-160 program (FFFractionation, LLC; Salt Lake City, UT). Operating conditions for a run are included on the figure that present the results. Data were analyzed on a computer using the FFF Analysis program (FFFractionation, LLC).

Multi-Angle Laser Light Scattering. Light is scattered by polymer molecules as it travels through a solution containing the polymer. The amount and direction that the light is scattered provides information on the molecular weight and size of the molecule. The principal equation relating the light scattering to physical characteristics of the polymer molecule is:

$$\frac{R(\theta)}{K^* c} = M_w P(\theta, r_g^2) - 2A_2 M_w^2 P^2(\theta, r_g^2) c \qquad \text{Eq. 2.2}$$

where,

- $R(\theta)$ = excess Rayleigh ratio; a measure of the fraction of light intensity that is scattered by the polymer molecule (a function of the scattering angle)
- K^* = light-scattering constant containing the wavelength of the incident light, the refractive index of the solvent, the refractive index increment (dn/dc) and other physical parameters and constants
- c = concentration of polymer
- M_w = weight-average molar mass
- $P(\theta,r_g^2)$ = scattering function (and is a function of the scattering angle and the mean square radius of the molecule)
- A_2 = second virial coefficient
- r_g^2 = mean square radius
- θ = scattering angle.

Wyatt [1993] and Huglin [1972] describe theory and measurement techniques of light scattering in detail. A light scattering experiment consists of measuring the amount of scattered light from a sample at various angles as shown in Figure 2.3. The polymer concentration must be known or measured by another detector in order to determine molar mass. Size can be measured without knowing the concentration. Other constants such as the refractive index of the solvent and the refractive index increment, dn/dc, must also be known or measured. The light scattering data along with the other known or measured parameters are used in Eq.2.2 along with specialized plotting techniques to determine the molar mass and the root-mean-square (RMS) radius of the polymer sample.

Two types of light scattering experiments are performed depending on whether the sample is fractionated or not fractionated. In batch mode when the sample is not fractionated, light scattering data are taken on samples that are prepared at a series of known concentrations. The data are displayed on a Zimm plot. Extrapolation of the data on the Zimm plot to a zero scattering angle and to zero concentration allows for the determination of the *weight-average* molar mass and the *z-average* root-mean-square (RMS) radius of the polymer. The batch mode of operation was used in this study.

The light scattering detector can also be used to take measurements on polymer samples that have been fractionated by size-exclusion chromatography or flow field-flow fractionation. This mode determines the distributions of molar mass and size. Coupling of MALLS and FFFF for distribution measurements was not accomplished during this study.

Light scattering measurements were conducted with a Dawn EOS Light Scattering Instrument (Wyatt Technology Corp., Santa Barbara, CA) that was configured in microbatch mode as shown in Figure 2.4. Solvent was continuously pumped through the instrument at a flow rate of 0.5 mL/min. Samples of polymer prepared at several known concentrations are inserted into the flow stream using an injection valve fitted with a 0.91-mL sample loop. The computer program ASTRA (Wyatt Tech. Corp.) was used to collect and process the light-scattering data.

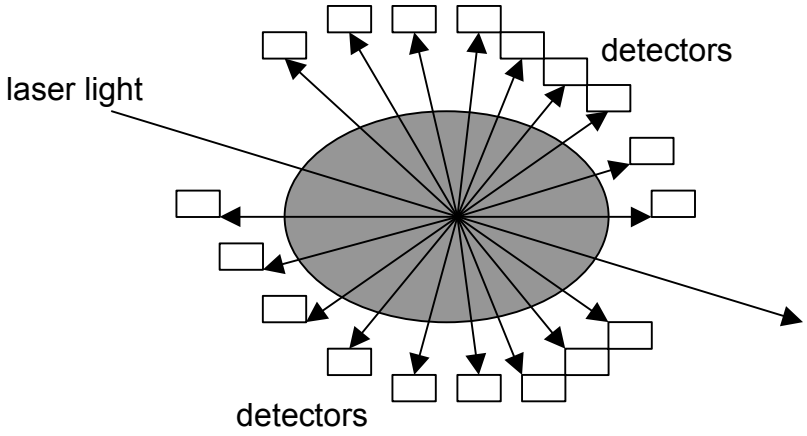

Figure 2.3 – Schematic of scattered light in cell of the multi-angel laser light scattering (MALLS) detector.

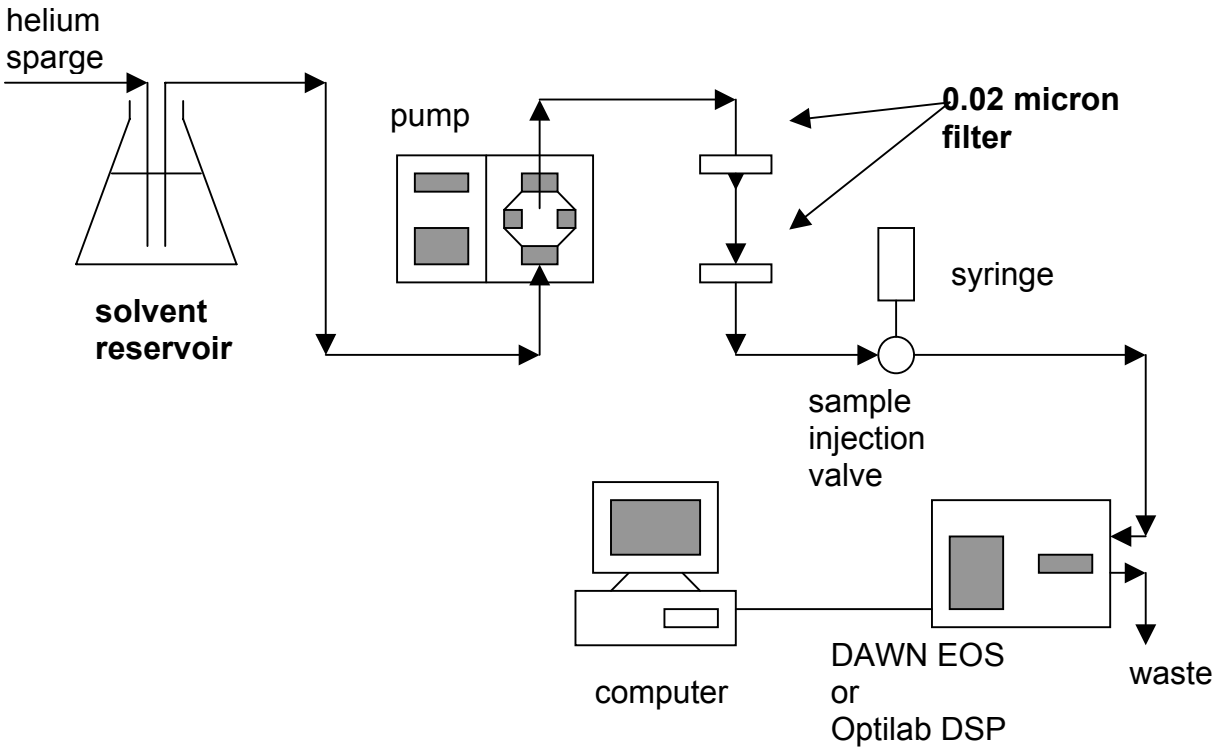

Figure 2.4 – Schematic of equipment used for light scattering measurements.

Runs were also conducted using the same flow system described in Figure 2.4 but using the Optilab DSP interferometric refractometer instrument and DNDC software (Wyatt Tech.Corp.). These measurements are used to determine the specific refractive index increment, dn/dc, which is the change of refractive index with the concentration of polymer. The average refractive index increment (dn/dc) FOR Alcoflood 935 was determined as 0.182 mL/g at 25°C in the 1% KCl aqueous solvent. Densities of the polymer solutions and the refractive index of the solvent were also measured. These measured values are required for the determination of molar mass and size parameters from the light scattering data. All of the instruments were calibrated according to manufacture's procedures.

A general procedure was developed to determine the weight-averaged molar mass and rms radius of polyacrylamide samples with molar masses on the order of 5 million Daltons. This procedure is outlined in Exhibit 2.1.

Determination of the active amount of polymer in a sample and the filtration of the stock sample solution are key elements of the experimental procedure described in Exhibit 2.1. The active amount of polymer was assumed to be 100% after drying the sample to constant weight. Approximately 10% of an original polymer sample was removed during the drying process. The filtration procedure was developed to remove dust and extraneous material without affecting the measured molar mass and rms radius. The filtration method selected was the filtration of only the stock polymer solution using a screen-type filter membrane (Nuclepore® Polycarbonate Track-Etch Membranes). A 5.0 μm pore size was suitable for Alcoflood 935, the commercial polymer used in this work.

The last step of the procedure is the processing of the light-scattering data using various extrapolation techniques. It was determined that the Berry formalism using a linear extrapolation for concentration and a second-order polynomial extrapolation for the angle was the best method to determine molar masses and rms radii for the polyacrylamide and gel aggregates studied.

Exhibit 2.1

Standard Procedure for Measurement of the Weight-Average Molar Mass and RMS Radius of Polyacrylamide Samples

These procedures were developed for measuring the weight-average molar mass and rms radius of polyacrylamide samples that have molar masses on the order of 5 million Dalton. The light scattering measurements were conducted with a Dawn EOS multi-angle light scattering detector that is configured to run in batch mode.

Drying of polyacrylamide sample

- Dry polyacrylamide sample in a vacuum oven at 100°C and –17.5 inches of mercury until the weight of the polymer remains constant. Typically, this process will take 24 hours to two weeks.
- Store the dried polymer sample at 50°C and –17.5 inch vacuum mercury until use.
- Non-dried samples can be used if the active amount of polymer in the sample is known.

Glassware cleaning

- Wash glassware with water using detergent.
- Rinse glassware thoroughly with water followed by distilled water.
- Air-dry glassware upside down on lint free tissues.

Solvent preparation

- Dissolve KCl and sodium azide in laboratory -grade water to obtain a solution with 1% KCl and 100 ppm sodium azide.
- Filter the solution through a 0.02 μm filter membrane.

Refractive index of solvent

- Measure the refractive index of solvent using a refractometer.

Stock solution preparation

Stock solutions are usually prepared with polyacrylamide concentrations of 500 ppm.

- Weigh polyacrylamide sample on an analytical balance.
- Weigh the appropriate amount of solvent in a beaker or jar.
- Stir the solvent with a magnetic stirrer to produce a deep vortex.
- Add the polyacrylamide sample onto the shoulder of the vortex to wet each granule/bead of polyacrylamide.
- Stir the stock solution for 24 hours to ensure complete dissolution. Take steps to eliminate evaporation.

Filtration

- Filter polyacrylamide stock solution twice using a screen-type filter membrane. A 5.0 μm filter was used for Alcoflood 935. The size of the filter was determined by measuring the molar mass of a series of stock samples that were filtered by a range of filter sizes. The smallest filter size that did not reduce the molar mass was selected.

Diluted solution preparation

- Prepare six samples at polymer conc. between 20 and 100 ppm by diluting the stock solution.
- Shake the vials to ensure uniform concentrations.
- Measure the density of each diluted samples, and convert the concentration to g/mL.

dn/dc measurements

This procedure is conducted once for each type of polymer sample and solvent pair. For example, Alcoflood 935, Lot 7158V in the 1.0% KCl, 100 ppm sodium azide solvent represents a pair. A measurement is required for a change in the polymer lot number or when the solvent is changed.

- Prepare six samples at polymer concentrations between 100 and 1000 ppm.
- Measure the dn/dc value using the Optilab DSP differential refractometer.

Molar mass and RMS radius measurement

- Measure the light scattering data with DAWN EOS.
- Repeat the measurements several times to ensure reproducibility.

Data processing

The measured data are the amount of light scattered as functions of the angle to which it is scattered and the polymer concentration. These data are fitted to polynomials and extrapolated to zero concentration and to zero angle in order to determine the weight-average molar mass and the RMS radius. The method used to perform the extrapolations for this work was the Berry formalism using a linear relationship to extrapolate the concentration to zero and a second-order polynomial to extrapolate the angle to zero. Detectors 4 (38 degrees) through 12 (99 degrees) were used in the extrapolation.

• • •

Gelant Preparation The gel system selected for study contained Alcoflood 935 polyacrylamide (Ciba Chemical Co., Lots 3243A, 7158V and A2247BOV) and chromium acetate. (McGean and Rhoco, Inc.). Stock polymer solutions containing KCl were filtered through a 5.0 μm screen filter membrane. Polymer used for light-scattering experiments was dried before weighing. Drying reduced the weight of the polymer by 8 to 10 %. Non-dried polymer was used for the FFFF experiments. The chromium acetate was diluted in lab-grade water and filtered through a 0.02 μm membrane.

A gelant was made by adding freshly prepared chromium acetate solution into the polymer solution such that the gel solution contained 5000 ppm polymer and 1.0% KCl. Chromium(III) concentrations in the gelants were usually 100 ppm. The reaction was conducted at 25°C by keeping the glass bottles that contained the reacting mixture in a temperature-controlled water bath. The viscosity of the reacting gelant was measured periodically using a cone-and-plate microviscometer.

Results and Discussion

Flow Field-Flow Fractionation Technique

Fractionation of Alcoflood 935 polyacrylamide. The size distribution of Alcoflood 935 polyacrylamide (Lot 7158V) was determined by flow field-flow fractionation (FFFF). Detector responses verses time, or fractograms, for several runs using two concentrations of polymer and three sample loop volumes are shown in Figure 2.5. The peaks at approximately one minute are typical void peaks and do not represent polymer in the sample. The peaks centered at an elution time of 21 minutes represent the Alcoflood 935 polyacrylamide. The peaks are similar for the different amounts of injected polymer which indicated the channel was not overloaded at these conditions. Peak areas, and approximately the peak heights, were proportional to the amount of polymer in the injected sample.

Different detector responses were expected and observed for Alcoflood 935 when using different crossflow rates as shown in Figure 2.6. The fractograms of this figure were converted to size distributions by the software using the mathematical flow model and are shown in Figure 2.7. The size distributions were similar for these runs that were conducted at different experimental conditions and indicate that the mathematical flow model described well the polymer transport through the fractionator.

The size distributions in Figure 2.7 illustrate the polydispersity of Alcoflood 935 with a mean diameter of about 150 nm. Additional runs with FFFF channel as well as other measurements were conducted to verify that the size distributions calculated with the mathematical flow model for *normal* flow through the channel were appropriate [Willhite, 2001]. That is, Alcoflood 935 polymer eluted the FFFF channel in the manner described by *normal* FFFF flow and did not exhibit steric flow in the channel. There were some differences between the measured size distributions for polymer stock solutions prepared at different times and the cause was possibly changes in sample preparation procedures and the age/history of the membrane in the FFFF channel. However, distributions from a single stock solution were consistent and the *peak* (mean) size was within the range between 150 and 170 nm.

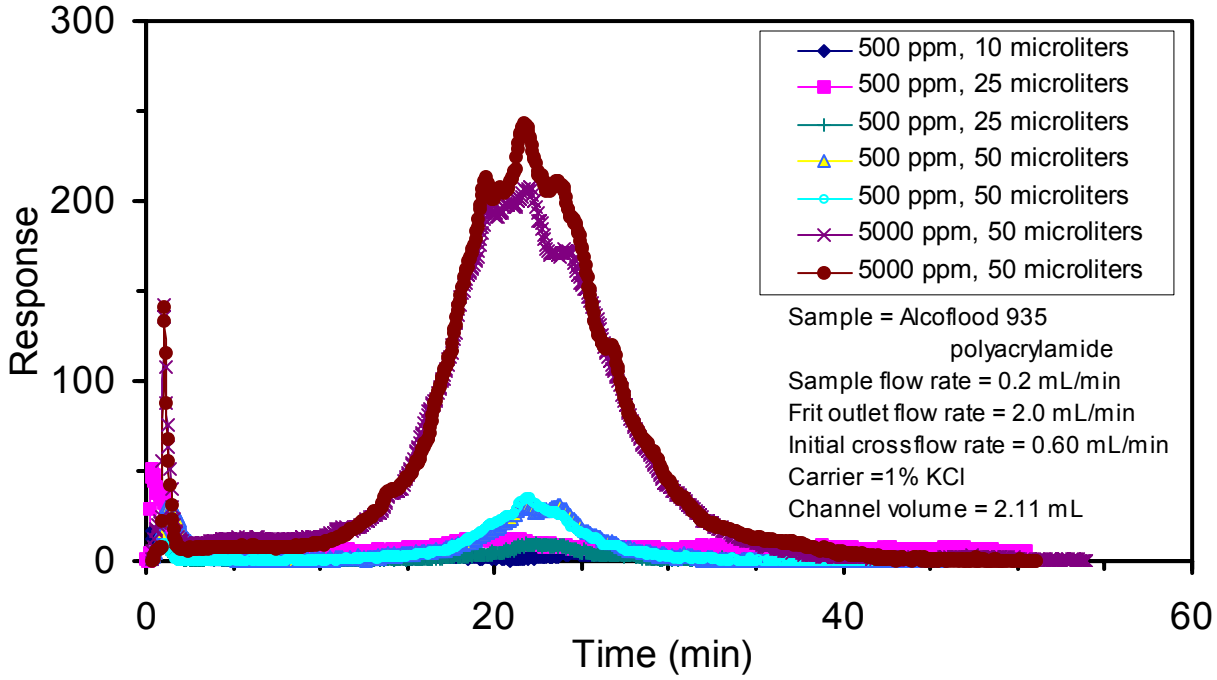

Figure 2.5 - Elution profiles of Alcoflood 935 polyacrylamide for several amounts of injection mass.

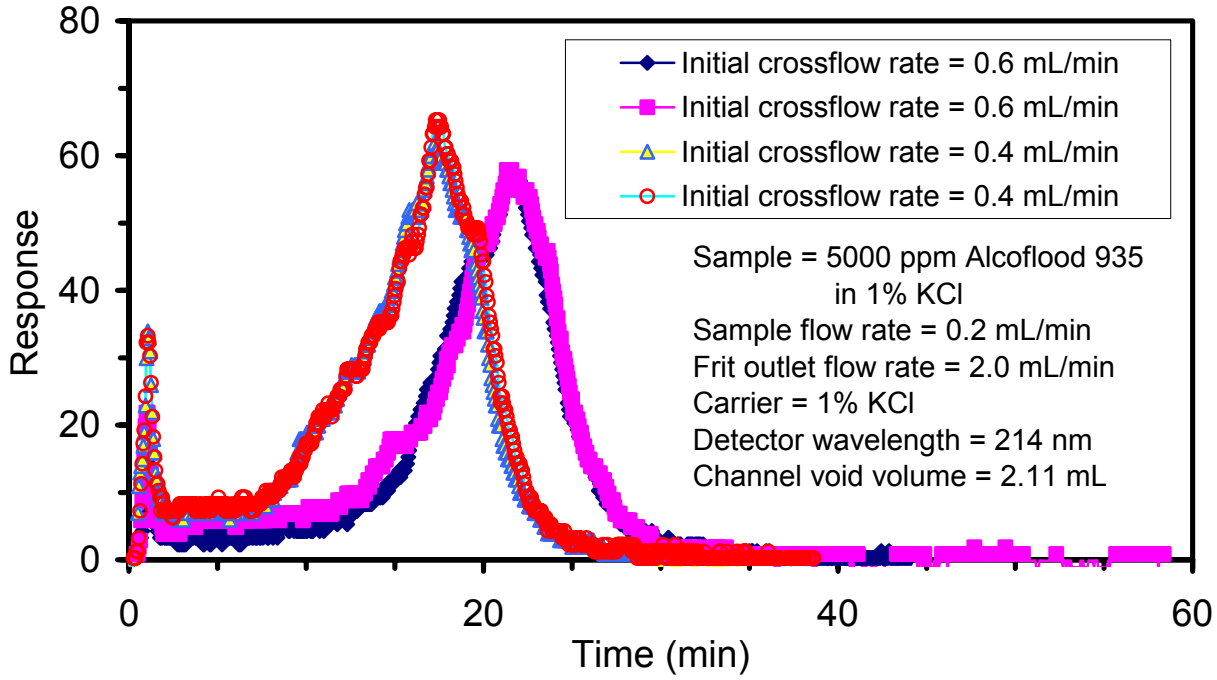

Figure 2.6 – Effect of crossflow rate on the elution profiles of Alcoflood 935.

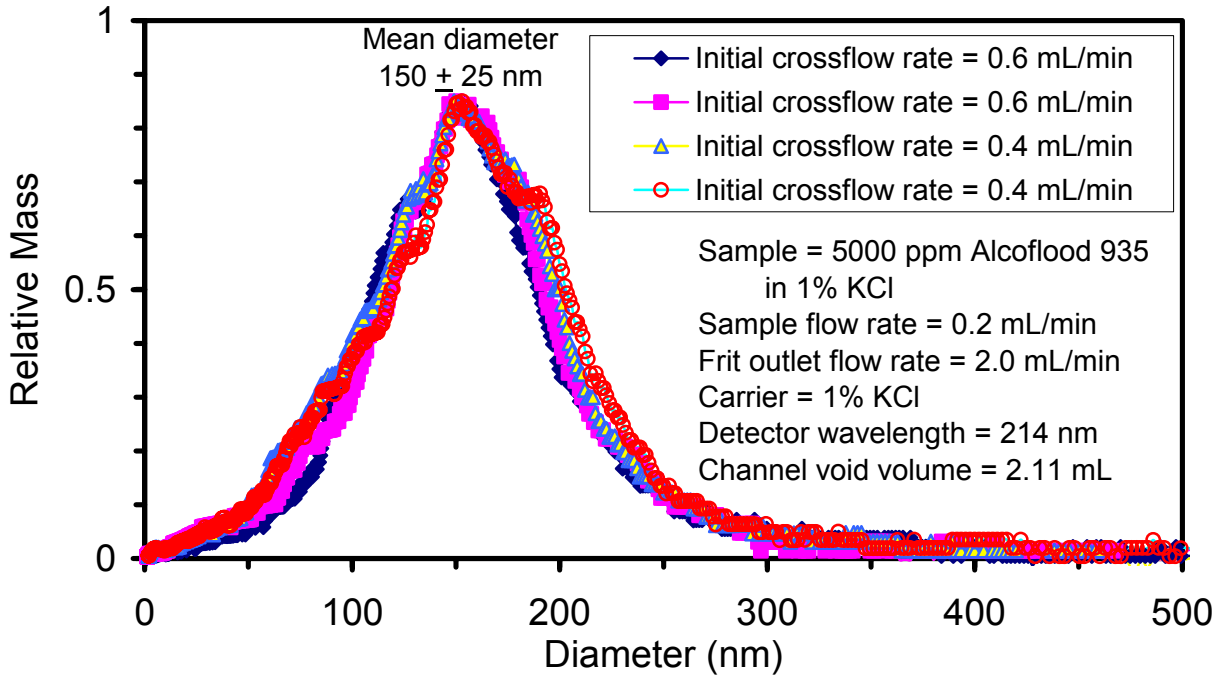

Figure 2.7 – Size distributions of Alcoflood 935 that were measured by flow-field-flow fractionation at different conditions.

A size distribution of Alcoflood 935 determined using FFFF was compared to a size distribution determined by equilibrium dialysis [Willhite 2001] in Figure 2.8. The distributions are reasonable similar in view of the different techniques that were used. (Equilibrium dialysis relies on the diffusion of the smaller molecules through a membrane that have holes in narrow diameter range. The amount of polymer larger and smaller than the hole diameter is determined by measuring the polymer concentration on each side of the membrane at equilibrium. A size distribution is established using a series of membranes with different hole diameters.)

Fractionation of reacting gelant. Size distributions of the polymer molecules/aggregates in the Alcoflood 935 polyacrylamide-chromium(III) acetate system during the gelation process were determined by FFFF. Elution profiles at different reaction times are shown in Figure 2.9. Shifting of the elution profiles to lower retention times as a function of reaction time was observed. Smaller molecules/aggregates elute sooner than larger molecules/aggregates when fractionation in the channel occurs under *normal* FFFF conditions, that is, when the size of the molecules/aggregates are less than about 600 nm. Based on the *normal* FFFF theory, the shifting to lower retention times with reaction time indicated that the molecules/aggregates were becoming smaller as the gelation reactions proceed. This result was unexpected and contrary to data obtained from equilibrium dialysis experiments [Chong] and light scattering experiments (next section) where the size of the molecules/aggregates grew with reaction time.

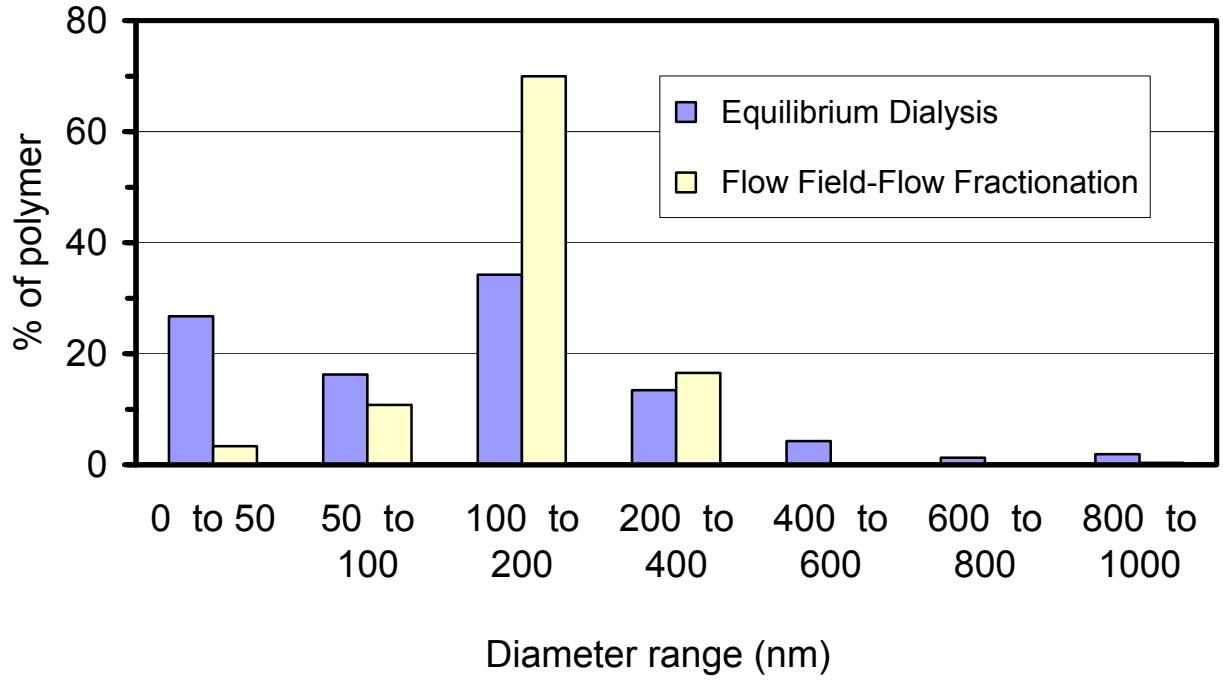

Figure 2.8 – Comparison of the size distributions for Alcoflood 935 obtained by flow field-flow fractionation and by equilibrium dialysis.

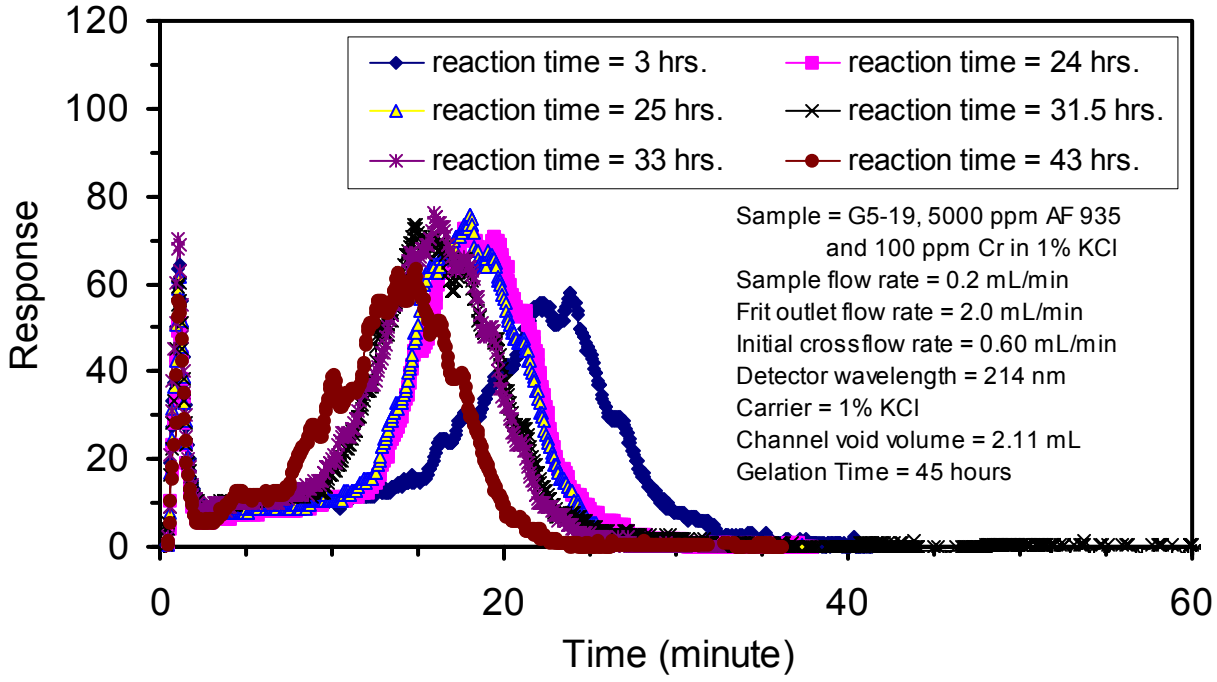

Figure 2.9 - Elution profiles of 5000 ppm Alcoflood 935 polyacrylamide and chromium(III) crosslinking gelant at several reaction times.

Work was conducted to verify that the data from the FFFF runs were accurate and reproducible. In addition, samples of polymer without crosslinker were injected between runs conducted on the reacting gel system. Elution times for runs conducted on polymer solutions without crosslinker were consistent and were comparable to runs conducted on the freshly prepared gel system as shown in Figure 2.10.

The elution profiles from the FFFF on the reacting gel system can be interpreted several ways. During *normal* FFFF, molecules/aggregates elute at later times as their size increases up to about 600 nm in diameter. As the size increase above 600 nm, steric flow occurs and the elution time decreases. Thus, two diameters are represented at a particular elution time, one for *normal* flow and one for steric flow. The diameter based on *normal* flow is predicted by theory and is calculated by software that accompanies the FFFF equipment. Diameters based on steric flow are determined by calibration with particles of known diameters. Work conducted on the polymer without crosslinker and described in the previous section showed that the polymer molecules were fractionated under *normal* flow conditions and the average diameter of the polymer molecules was between 150 and 170 nm. The diameter of the molecules/aggregates of the freshly-prepared gel system was also about 170 nm since the elution times for runs on the freshly-prepared gel system were comparable to runs conducted on polymer solutions without crosslinker. It is unlikely that the addition of crosslinker to the polymer increased immediately the diameters of the molecules/aggregates to the 2000 – 5000 nm range (as determined by calibration during steric flow) and that the elution times just happened to coincide. It is much more likely that the reacting gel system was fractionated under *normal* flow conditions and that the initial average diameter of the molecules/aggregates was between 150 and 170 nm. This is supported by the elution profiles for a reacting gelant at short reaction times that is shown in Figure 2.11**.** The elution profiles move slowly to earlier times with reaction time.

The data strongly indicate that the polymer and the reacting gel system flow through the channel under *normal* flow conditions. Size distributions of the gelant at selected reaction times using *normal* flow theory is shown in Figure 2.12. It is possible, but unlikely, that the aggregates become more compact due to intra-molecular crosslinks and that at some point intermolecular crosslinks become significant to bond the aggregates together and form a three-dimensional gel. The FFFF runs were conducted on samples at reactions times less than the nominal gel time where the gelant is still relatively fluid and several more hours are required for significant development of gel structure. Other measurements of size distribution of reaction gel systems [McCool et al.] do not support this interpretation.

An alternate interpretation of data takes into account the changing ionic character of the polymer molecules/aggregates during the gelation reactions. Alcoflood 935 is a hydrolysed polyacrylamide where approximately 8% of the monomer groups have negatively charged carboxyl groups. During gelation, a positively charged Cr(III) complex (+1 to +3 charge) reacts with a carboxyl group on the polymer (-1 charge). This reduces the negative charge on the polymer and possibly introducing a positive charge at the reaction site. Modification of the charge on the molecule can alter (1) the configuration and size of the molecule, (2) the interactions between molecules and (3) the interaction between the molecule and the membrane in the flow channel. These changes can affect the propagation of the molecule through the

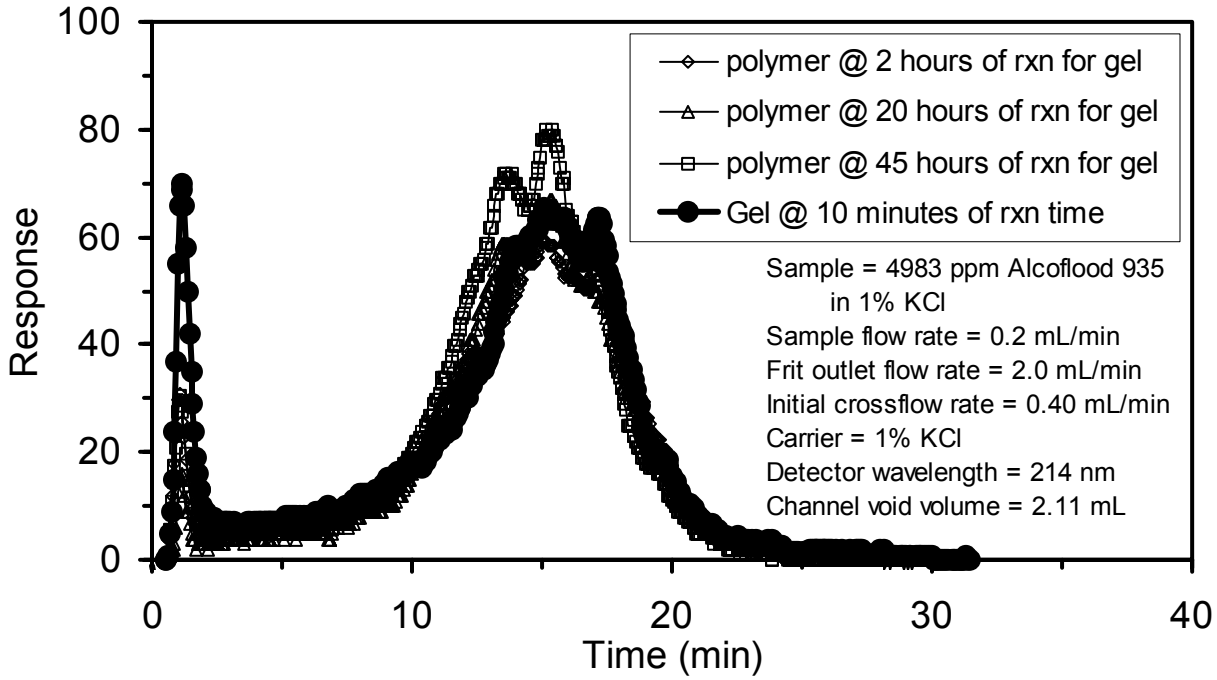

Figure 2.10 – Comparison of elution times for the freshly prepared gelant and the polymer solution without crosslinker.

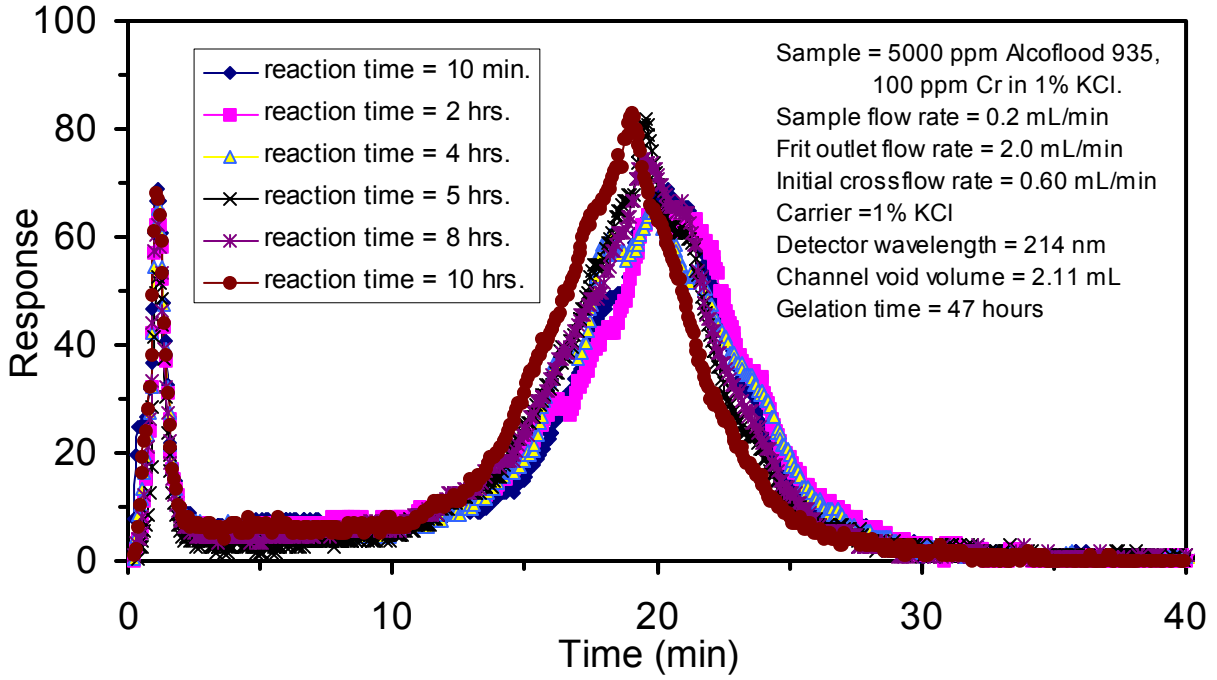

Figure 2.11 – Elution profiles of the gelant at short reaction times.

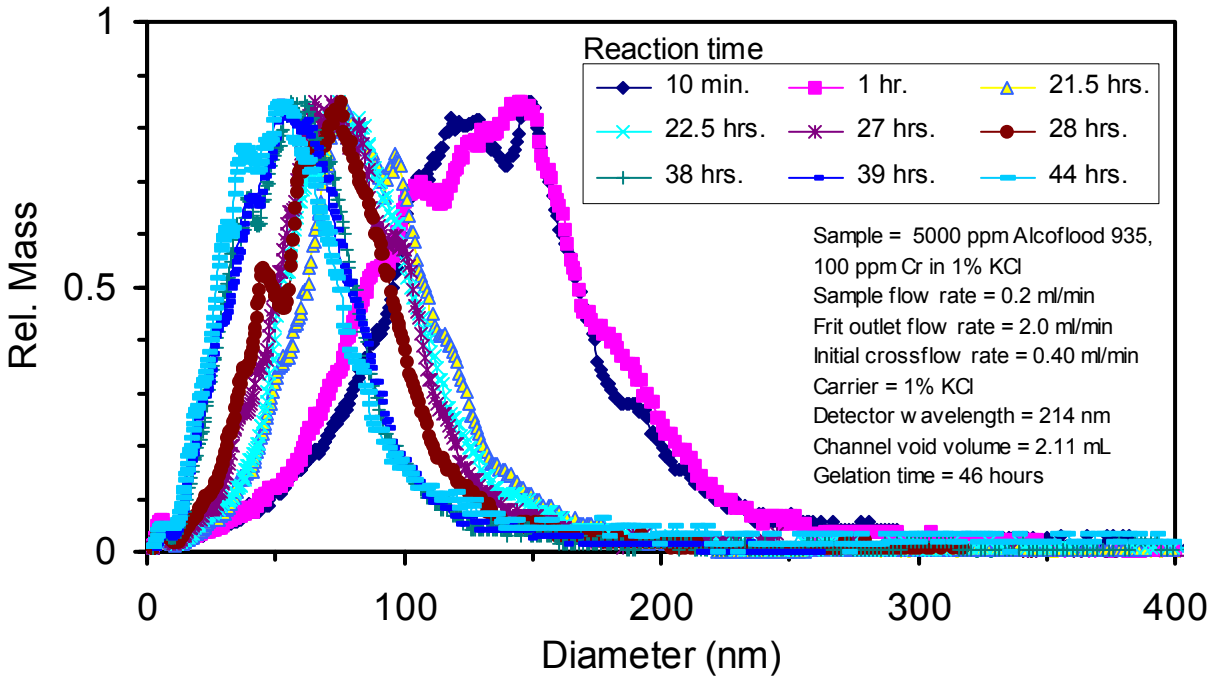

Figure 2.12 – Size distributions of the gelant at selected reaction times.

channel resulting in different elution times. This interpretation of charge modification was acknowledged as a probable explanation by the world's experts on FFFF at the Ninth International Symposium on Field-Flow Fractionation, 26-29 June 2001 in Golden Colorado. It was decided not to investigate the cause of this behavior at this time due to the resources that would be required. Alternatively, it was decided to verify the size of the eluting polymer and aggregates from the FFFF channel using the multi-angle light scattering detector. This effort was not accomplished during the contract period of this project, in part, due to the malfunction of the FFFF channel and delayed repair by the manufacture. We plan to accomplish this plan in future work.

Multi-Angle Laser Light Scattering Technique

A significant effort was required to develop a standard procedure for determining the molar mass and the root-mean-square (rms) radius of aqueous polyacrylamide solutions using the multi-angle light scattering detector. The procedure is detailed in the Experimental Techniques and Materials section above and supporting data were given in previous reports [Willhite et al., 2001, 2002]. This section describes the results of measurements on polyacrylamide solutions and polyacrylamide-chromium acetate gelants.

The weight-average molar mass and z-average rms radius of two lots of Alcoflood 935 polyacrylamide were determined numerous times using the standard procedure. The results are given in Table 2.1 and represent measurements that were conducted a few times on several of the same prepared aqueous samples as well as many samples that were prepared from the dried

polymer. The standard deviations are reasonable for these types of measurements. The weight-average molar mass and z-average rms radius for Lot A2247BOV was larger than for Lot 7158V and this correlated with higher viscosity and faster gel times for system prepared with Lot A2247BOV.

Table 2.1 – Weight-average molar mass and z-average rms radius of Alcoflood 935.

	Weight-average molar mass		Z-average rms radius	
Lot #; researcher; # of measurements	Average (Daltons)	Relative standard deviation (%)	Average (nm)	Relative standard deviation (%)
Lot 7158V				
T.Wang; 23 runs	5.39×10^6	5.0	183.6	2.9
C.Wang; 22 runs	5.26×10^6	11	181.7	3.4
Lot A2247BOV				
C.Wang; 9 runs	6.64×10^6	13	216.8	6.2

A test was conducted to determine if the application of a high shear stress would reduce the molar mass and rms radius of an Alcoflood 935 sample. A 2000 ppm Alcoflood 935 stock sample that had been filtered through a 5.0 μm membrane was stirred at high speed for 15 minutes in a Osterizer blender. The sheared sample was then diluted and the light scattering measurements were conducted six times. The molar mass and the rms radius of the degraded sample are presented in Table 2.2. The average molar mass of the sheared Alcoflood 935 sample was 1.96×10^6 Daltons and the average rms radius was 95 nm. Shearing in the blender reduced the weight-averaged molar mass by 58% and reduced the rms radius by about 36%.

Table 2.2 - Molar mass and the rms radius of Alcoflood 935 (Lot 7158v) after shearing in an Osterizer blender at high stir speed for 15 minutes.

Run	1	2	3	4	5	6
Molar mass (10^6 daltons)	1.96	1.95	1.96	1.98	1.95	1.97
RMS radius (nm)	98	92	94	96	95	95

Alcoflood 935 Polyacrylamide - Chromium Acetate Gelant. The effects of chromium concentration and acetate concentration on the growth of pre-gel aggregates were determined using the multi-angle light scattering detector. The results presented here are for gelants prepared with Lot A2247BOV of Alcoflood 935 at a concentration of 5000 ppm. Measurements were also made on a low-concentration system that contained 100 ppm polymer and 2 ppm chromium(III). Additional results for Lot 7158V of Alcoflood 935 were similar and were presented in a previous report [Willhite 2002].

Gelants were prepared at chromium concentrations of 20, 50 and 100 ppm. The gelants contained 5000 ppm polyacrylamide and 1.0% KCl. The initial pH values were 5.0, 5.5 and 5.7 for the gelants with 1000, 50 and 20 ppm chromium, respectively. Viscosity was measured as a function of time and is shown in Figure 2.13. The measurements were conducted at a shear rate of 11.25/sec for viscosity values less than 200 cp and at a shear rate of 4.5/sec for viscosity values greater than 205 cp. The viscosity of the reacting gelants increased gradually initially as the crosslinking reaction proceeded, followed by an abrupt increase over a short time period. The gel time was defined as the time at which the viscosity of the gelant increased to a value greater than 200 cp. Gel times decreased with increased chromium concentration. The physical nature of the gelant changes considerably during the time period of the abrupt viscosity change which represents approximately 10% of the measured gel time. During this period, the gelant becomes much more elastic and stringy which makes it difficult to separate an aliquot from the gelant for analytical measurements. The samples continued to develop stronger gel characteristics after the defined gel time.

Gelants containing 100 and 20 ppm chromium were selected for study using the light scattering equipment. The gel times were about 30 hours for the gelant containing 100 ppm chromium(III) and 166 hours for the 20 ppm chromium(III) gel. The weight average molar masses and the z-average rms radii of the polymer/aggregates as a function of time for the gelants at the two chromium(III) concentrations are shown in Figures 2.14 and 2.15, respectively. These data show that as the gelling reactions proceed, the molar mass and rms radius of the polymer aggregates increased moderately up to the gel time when the viscosity of the gelants increased abruptly. The relative increase of the molar mass and rms radius are much less than the relative increase in the viscosity value in the vicinity of the gel time. It is unclear how the gelant forms a gel so quickly after this time with such little increase in size or molecular weight.

The effect of acetate concentration on the gel time and the growth of aggregates was investigated. The gelants contained 5000 ppm Alcoflood 935, 100 ppm chromium and 1.0% KCl and had an initial pH of 5.0. Increased acetate concentration delayed gelation as shown in Figure 2.16 for gelants at selected acetate-to-chromium ratios. An acetate-to-chromium ratio of 40 increased the gel time by about six times as compared to the gel time of the gelant that contained no added acetate (acetate-to-chromium ratio of 3). The weight-average molar masses and z-average rms radii for the gelants that contained added acetate are shown in Figures 2.17 and 2.18, respectively. The molar masses increased by a factor of about three and rms radius increased by about 50% at the gel time for the acetate-to-chromium ratios of 10:1 and 20:1. Similar increases were observed for the gelants prepared at an acetate-to-chromium ratio of 3:1 shown in Figures 2.14 and 2.15. The molar mass and size of the gelant containing an acetate-to-chromium ratio of 40:1 increased to somewhat larger values at the gel time.

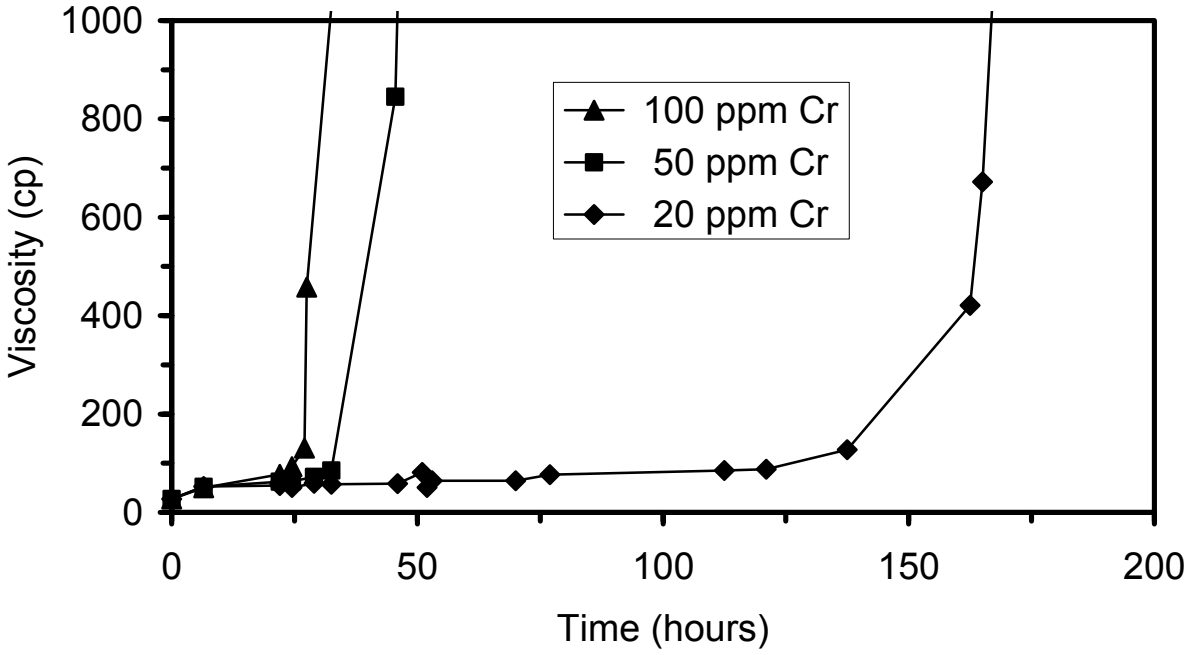

Figure 2.13 – Viscosity development of gelants as a function of chromium concentration.

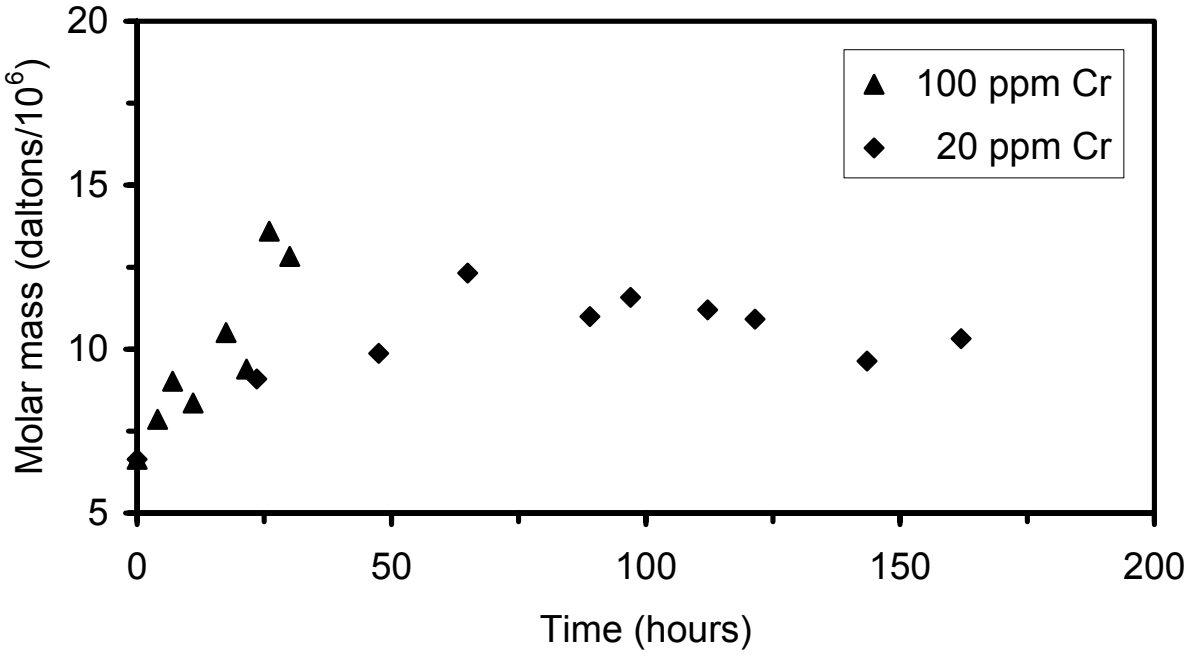

Figure 2.14 – Molar mass of aggregates as a function of time for gelants containing 100 and 20 ppm chromium.

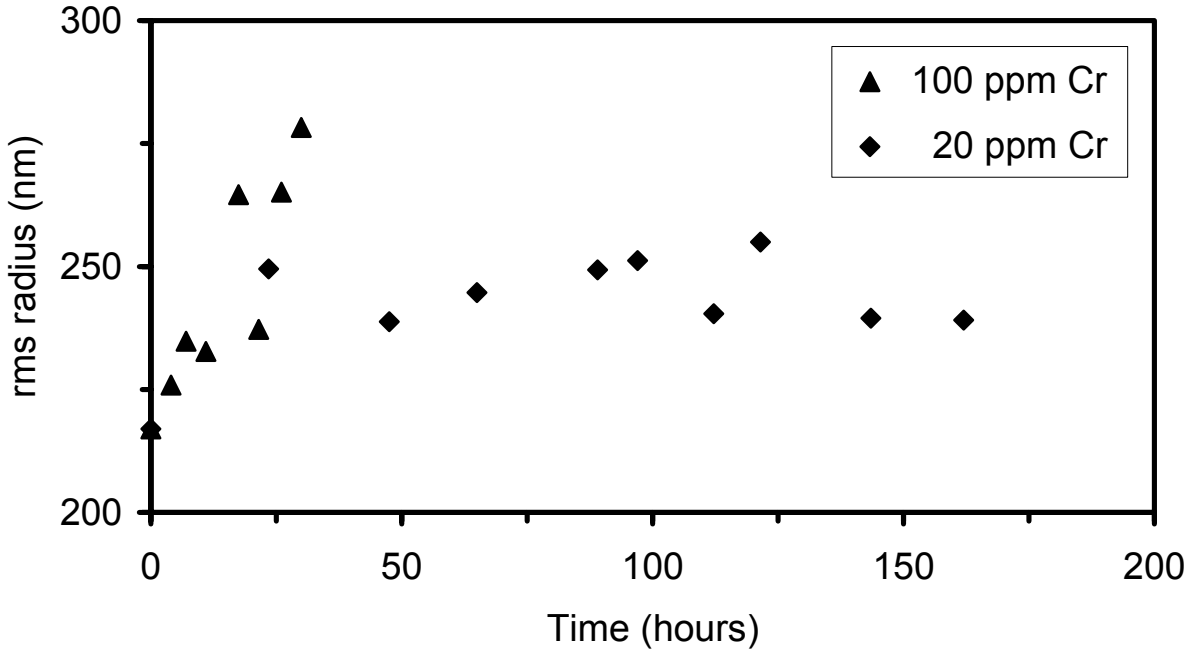

Figure 2.15 – Size of aggregates as a function of time for gelants containing 100 and 20 ppm chromium.

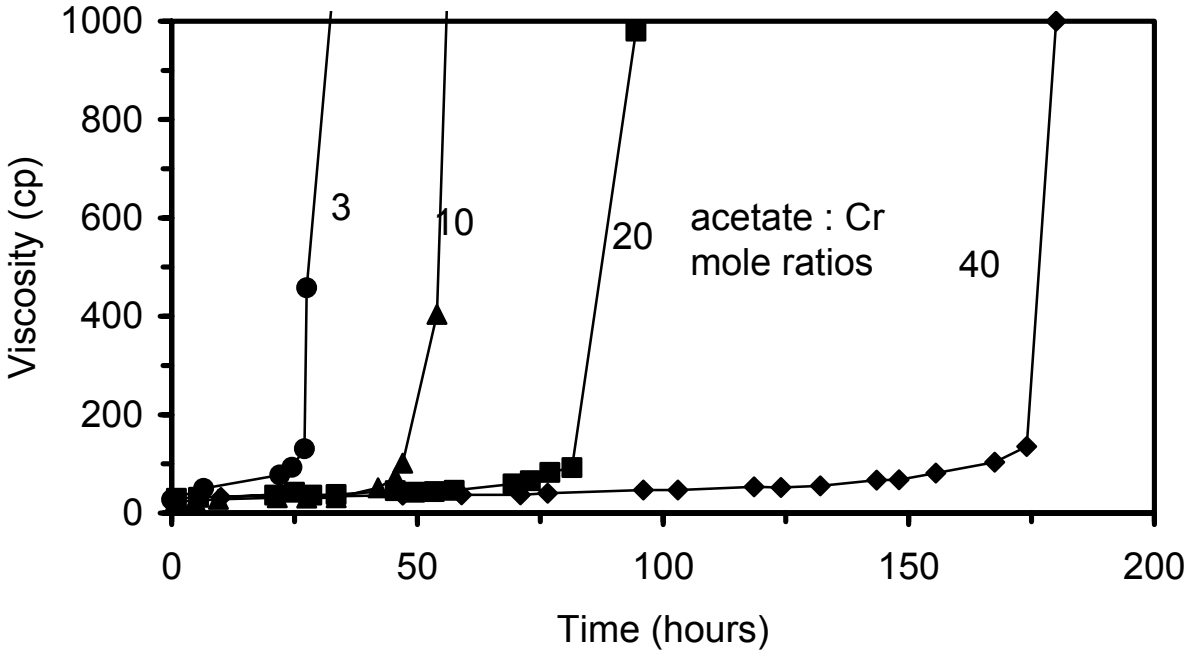

Figure 2.16 – Viscosity development of gelants as a function of acetate concentration.

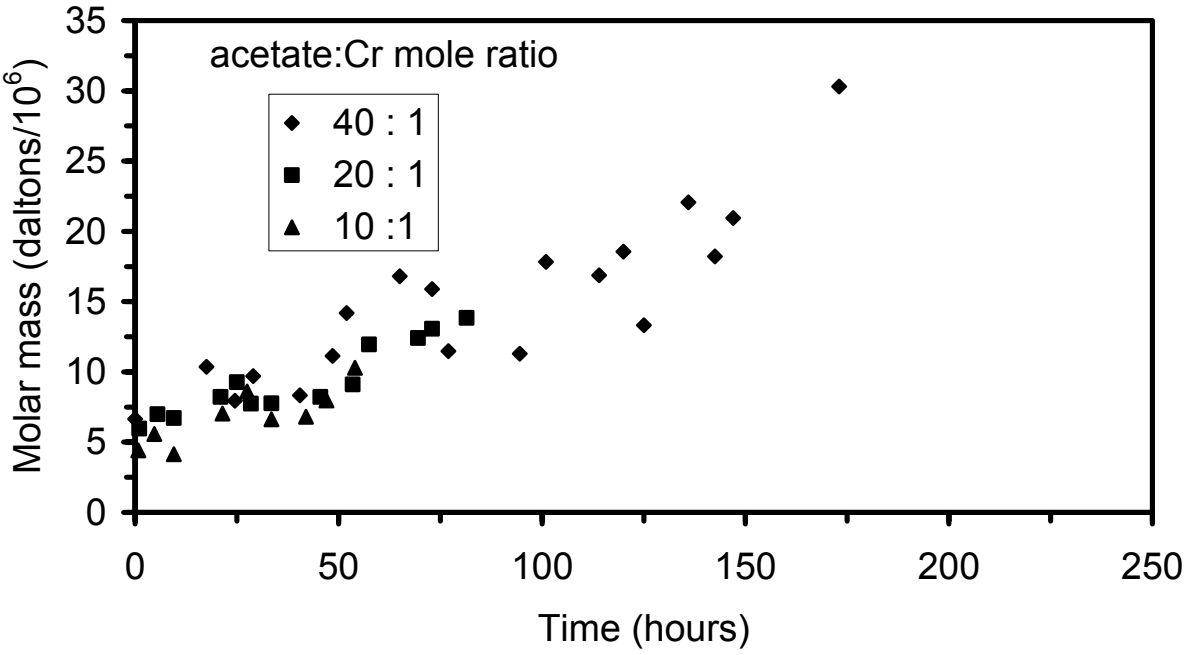

Figure 2.17 – Molar mass of aggregates as a function of time and acetate concentration.

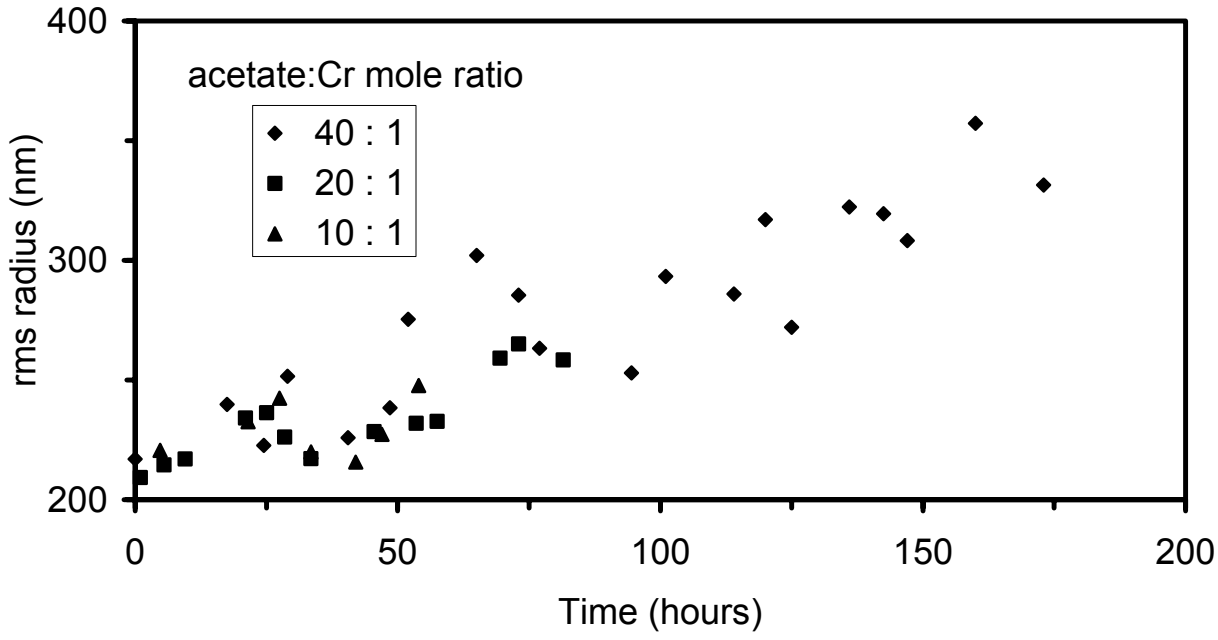

Figure 2.18 – Size of aggregates as a function of time and acetate concentration.

The trend of the light-scattering measurements was a relatively slow increase in the molar mass and rms radius up to the gel time. The trend was apparent but there was significant scatter in the data. Data scatter is usual for these types of measurements. Possible causes of scatter in our data were heterogeneous gelant samples and the large values of molar mass and size that are being measured, which were at the upper limit of the range for the equipment and the mathematical theory.

The weight average molar mass increased at a faster rate than did the size (as measured by the z-average rms radius) of the aggregates. Polymer sizes, in this case rms radii, are correlated with molar masses for monodispersed polymers according to the relationship

$$< r_g^{\,2} >^{1/2} = K \times M^{a} \qquad \text{Eq. 2.3}$$

where

r_g = rms radius
M = molar mass
K, a = fitting paramters

The data from the polydispersed gelant systems were correlated with this equation as shown in Figure 2.19. Also shown in this figure are data and the correlating equation obtained for several polyacrylamide samples or standards (no crosslinker) that were measured. The parameter, a, is a measure of the conformation of the polymer/aggregate in solution. The value of a for a random coil polymer is between 0.5 and 0.6, which is expected for the polyacrylamide samples. Values of a below 0.5 indicate a tighter coil that results from branching. The value of a for the aggregate is 0.30 and shows that the aggregates are more compact as a result of the crosslinking process that creates branches. These correlations and interpretations appear consistent with concepts of crosslinking even though the data were collected on polydispersed systems.

Molar mass and size measurements on a gelant composed of 100 ppm Alcoflood 935 polyacrylamide and 2 ppm chromium were conducted to determine if aggregate growth would occur in a dilute system. The polymer concentration of 100 ppm was well below the critical overlap concentration. The weight-average molar mass and the z-average rms radius for the dilute system is shown as a function of time in Figures 2.20 and 2.21, respectively. The uncertainty of the data increased to about 50 % at 187 and 218 hours and the experiment was terminated. These results show that intermolecular crosslinking occurred in a system that was below the critical overlap concentration. The increase in molar mass and rms radius was similar to data for the 5000 ppm polymer, 100 ppm chromium system although it occurred at a slower rate.

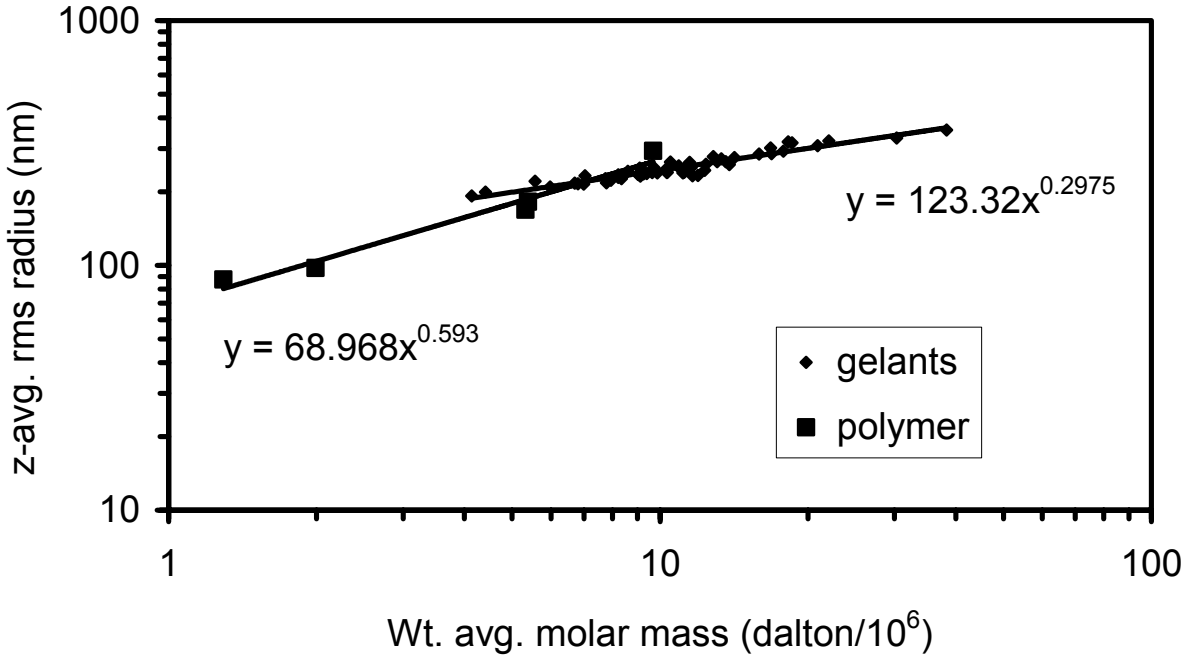

Figure 2.19 – Correlation between rms radius and molar mass for polymer samples and gelant samples.

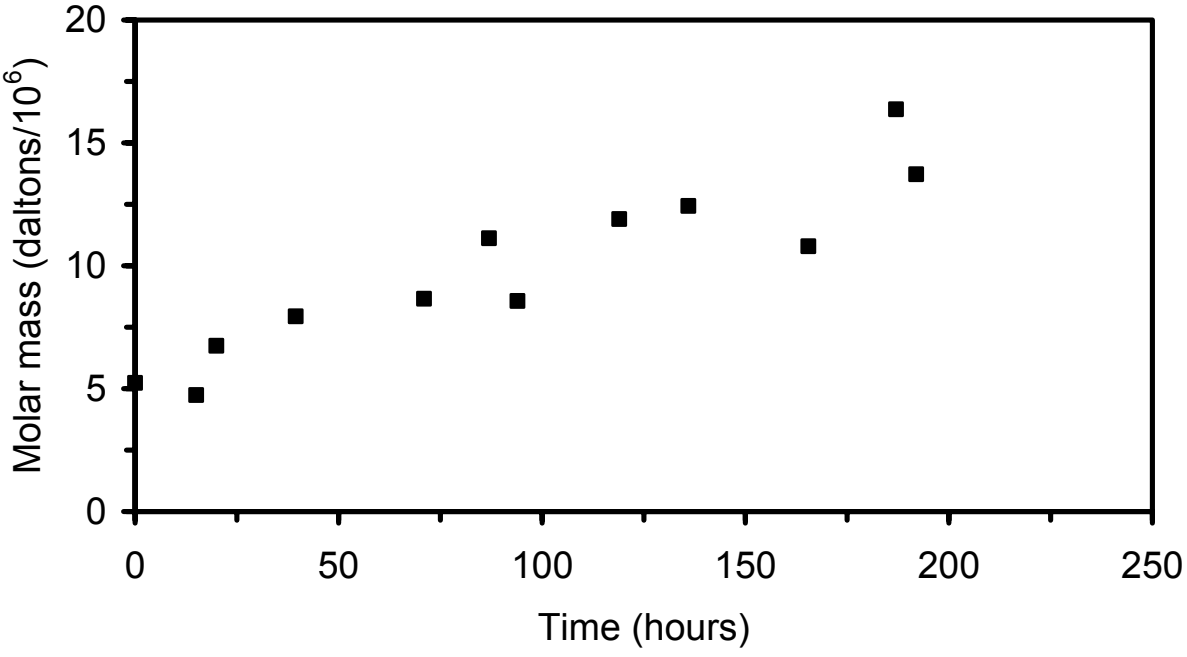

Figure 2.20 – Molar mass of aggregates as a function of time for a low-concentration system; 100 ppm polymer and 2 ppm chromium.

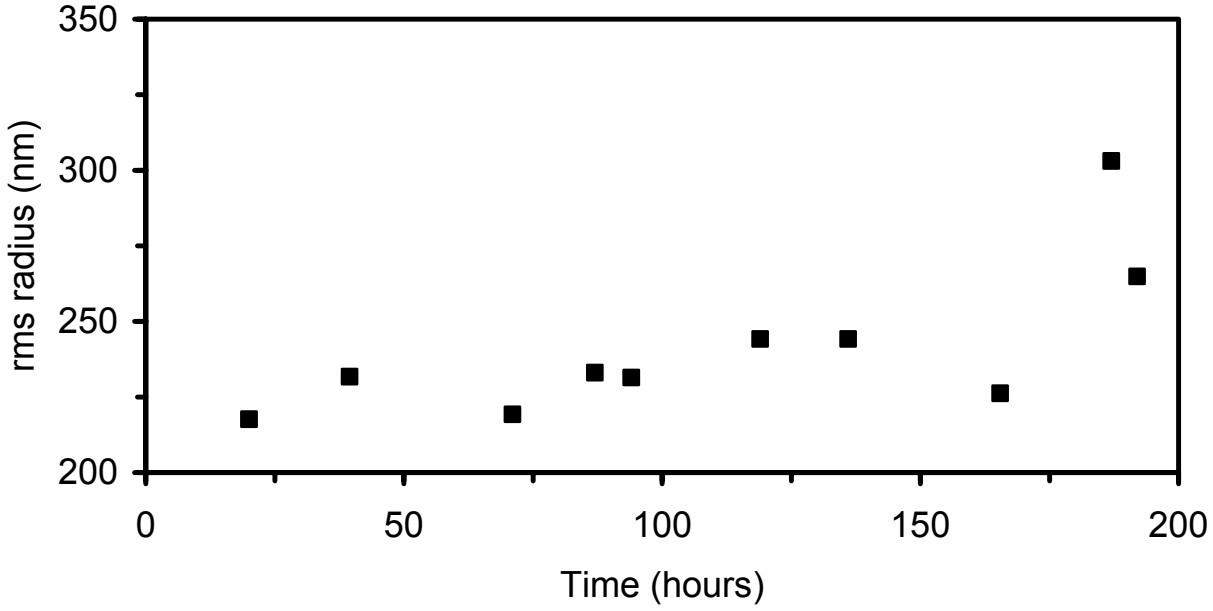

Figure 2.21 – Size of aggregates as a function of time for a low-concentration system; 100 ppm polymer and 2 ppm chromium.

Summary

The flow field-flow fractionation (FFFF) technique was capable of determining size distributions for polyacrylamide polymers. FFFF results for size distributions of aggregates in gelants indicated that the size of aggregates decrease during the gelation reactions up to the gel time of the systems. The FFFF results for gelants were not in agreement with data from other techniques. Further work is required to evaluate the use of FFFF for the measurement of size distributions of pre-gel aggregates.

A standard procedure using light-scattering measurements was developed for the determination of the weight-average molar mass and the z-average rms radius of polyacrylamide samples that are used in oilfield operations. Light scattering measurements on a polyacrylamide-chromium acetate gelant showed moderate increases in the molar mass and rms radius up to the time when the viscosity of the gelant increases rapidly (gel time). At the gel time, the molar mass approximately tripled in value and the rms radius increased on the order of 50%.

References

1. Benincasa, Maria Anna and Giddings, J.Calvin, "Separation and Molecular Weight Distribution of Anionic and Cationic water soluble polymers by Flow Field Fractionation," *Anal. Chem., **64*** (1992) 790-798.
2. Chong, Pau Ying, "An Experimental Study of the Aggregate Size Distributions of a Polyacrylamide-Chromium(III) Gel During Gelation," MS thesis, University of Kansas (2000).

3. Giddings, J.C., Yang, F.J., Myers, M.N.: "Theoretical and Experimental Characterization of Flow Field-Flow Fractionation," *Analytical Chemistry*, **48** (1976) 1126-1132.
4. Giddings, J.C., Wahlund, Karl-Gustav, Winegarner, Helen S., and Caldwell, Karin D.: "Improved Flow Field-Flow Fractionation System Applied to Water-Soluble Polymers: Programming, Outlet Stream Splitting, and Flow Optimization," *Analytical Chemistry*, **58** (1986) 573-578.
5. Giddings, J.C.: "Hydrodynamic Relaxation and Sample Concentration in Field-Flow Fractionation Using Permeable Wall Elements," *Anal. Chem.,* **62** (1990) 2306-2312.
6. Hansen, Marcia, Giddings, J.C., and Li, Ping: "Advances in Frit-Inlet and Frit-Outlet Flow Field-Flow Fractionation," *J. Microcolumn Separations*, **10** (1997) 7-18.
7. Hecker, R, Fawell, P.D., Fefferson, A. and Farrow, J.B., "Flow Field-Flow Fractionation of High-Molecular-Mass Polyacrylamide," *Journal of Chromatography A*, **837** (1999) 139-151.
8. Huglin, M.B. (ed), *Light Scattering from Polymer Solutions*, Academic Press, London, (1972).
9. Kurata, M. and Tsunashima, Y.: "Viscosity-Molecular Weight Relationships and unperturbed Dimensions of linear Chain Molecules," *Polymer Handbook* J. Brandrup, E.H. Immergut, and E.A. Grulke (eds), John Wiley & Sons, New York City (1999) Section VII/1, 1-83
10. Lewis, Robert D., "An experimental study of gel aggregate formation in a polyacrylamide-aluminium system," M.S. thesis, University of Kansas (1996).
11. McCool, C.S., Green D.W. and Willhite, G.P.,"Permeability Reduction Mechanisms Involved in In Situ Gelation of a Polyacrylamide/Chromium(VI)/Thiourea System in Porous Media," *SPE Reservoir Engineering,* **6** (Feb. 1991) 77-83.
12. Meyers, M.N., Overview of Field-Flow Fractionation," *J. Micro Seperations,* **9** (1997) 151-162.
13. Taylor, Kevin C. and Nasr-El-Din, Hisham A., "Acrylamide copolymers: A review of methods for determination of concentration and degree of hydrolysis in acrylamide copolymers," *Journal of Petroleum Science and Engineering,* **12** (1994) 9-23.
14. Thielking, H and Kulicke, W-M., "Determination of the Structural Parameters of Aqueous Polymer Solutions in the Molecular, Partially Aggregated, and Particulate States by Means of FFFF/MALLS," *J. Microcolumn Separations*, **10**, (1998) 51-56.
15. Willhite, G.P., Green, D.W. and McCool, C.S., "Increased Oil Recovery from Mature oil Fields using Gelled Polymer Treatments," Annual Report for June,1999-June, 2000, Report No. DOE/BC/15209-2, Contract No. DE-AC26-99BC15209, US DOE (2001).
16. Willhite G.P., Green, D.W. and McCool, C.S., "Increased Oil Recovery from Mature oil Fields using Gelled Polymer Treatments," Annual Report for June,2000-June, 2001, Report No. DOE/BC/15209-2, Contract No. DE-AC26-99BC15209, US DOE (2002).
17. Wyatt, P.J., "Light Scattering and the Absolute Characterization of Macromolecules," *Analytica Chimica Acta*, **272** (1993) 1-40.
18. Ying, H., Wu, G. and Chu, B., "Laser Light Scattering of Polyacrylamide in 1 M NaCl Aqueous Solution," *Macromolecules*, **29** (1996) 4646-4654.

Chapter 3

Effect of Acetate Concentration on In-Depth Penetration of a Polyacrylamide-Chromium Gel System

Graduate Research Assistant: Lingyun Du
Research Associate: Michael Michnick

Introduction

Polyacrylamide–chromium (III) gel systems have proven to be effective for flow control in petroleum reservoirs. However, a disadvantage of these systems has been the confinement of treatments to near wellbore volumes in the reservoir. A relatively rapid crosslinking reaction and the formation of gel aggregates prevent in-depth penetration of a gel system before build up of flow resistance. While near-wellbore treatments can be effective, this effectiveness can be diminished if there is significant layer-to-layer cross flow. Fluids can simply "flow around" a gel-treated volume and back into the high permeability thief zone or water producing zone. Based on this, it would be desirable to develop a system with which greater penetration into the reservoir around the treated well could be achieved before gelation occurs.

The specific objective of this project was to investigate in situ gelation behavior of a chromium acetate-polyacrylamide gel system as a function of the relative acetate concentration. It is known from bulk gelation studies that added acetate increases the gel time. It was an objective to investigate whether this behavior could be used to advantage to increase penetration into a reservoir. The porous medium used for the experimental work was unconsolidated sand.

Tackett [1989] conducted a comprehensive study on the possible species and structures of chromium acetate in solution via FT-IR, NMR, FAB spectrometry and ion exchange chromatography. He concluded that chromium acetate exists in several complex forms depending on the source, acetate-to-chromium ratio and pH. At pH below 4.5, an aqueous chromium acetate solution contains primarily the green cyclic trimer and some free ionic acetate/acetic acid. As the pH of the solution is increased using a base and the solution becomes aged, hydroxyl groups gradually substitute the bridging acetate ligands leading to a solution containing primarily acetate-hydroxyl bridges, free acetate ions and some bidentate acetates. Extensive hydroxyl substitution results in the formation of a purple linear trimer with two bridging acetate groups, four bridging hydroxyl groups and a bidentate acetate group in the end, as shown in Figure 3.1.

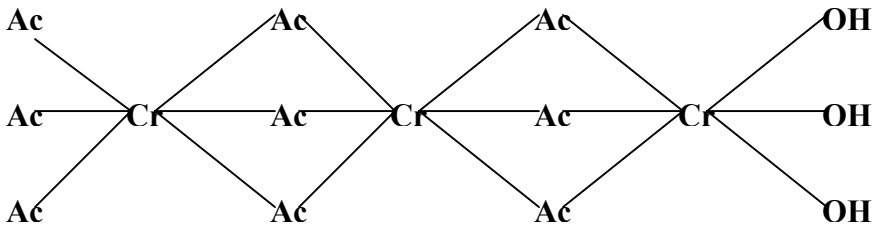

Figure 3.1 - Linear structure of chromium acetate trimer [Tackett. 1989].

The amide group and the carboxyl group are the potential direct attachment sites on the polyacrylamide for the Cr(III) species. Many studies have indicated that the Cr(III) species attaches to the carboxyl group rather than the amide group. Gelation studies conducted by Sydansk [1997] suggest that the rate of gelation increases with the degree of hydrolysis, which can also serve as a measure of the carboxyl content of the polymer.

Several researchers have viewed the chromium–polyacrylamide reaction as a ligand exchange reaction. Equation 3.1 is a simple representation of this reaction.

$$Cr(L)_n + m\ P\text{–}CO_2^- \Leftrightarrow Cr\text{-}(P\text{-}CO_2)_m\ (L)_{n-m} + m\ L \qquad \text{Eq. 3.1}$$

L in the equation represents any possible ligand that may form a coordinate bond with the chromium complex, a water molecule or a hydroxyl group, for instance. $P\text{-}CO_2$ represents a carboxyl group on a polymer molecule that may complex with chromium. This equation has been used by Burrafato et al. [1990] to justify the different rates of gelation with different ligands as discussed later. They also used inorganic Cr(III) salt sources to determine the possible Cr(III) species involved in crosslinking the polymer. It was shown that gelation occurs where Cr(III) is present exclusively in soluble molecular forms at pH values below 5.3. For pH >7, Cr(III) forms an insoluble colloid and the polymer solution remains fluid indicating no gelation. Gel samples in the pH range of 6.1 – 6.6 showed signs of turbidity and gelation. Based on these results, Burrafato et al. concluded that molecular forms of chromium caused gelation. In the pH range of 6.1 to 6.6, an equilibrium was hypothesized as shown in Equation 3.2.

$$Cr + OH + P\text{–}CO_2 \begin{cases} \leftrightarrow Cr\text{-}CO_2\text{-}P & \text{(favorable reaction)} \\ \text{or} & \\ \leftrightarrow Cr(OH)_3 & \text{(precipitation)} \end{cases} \qquad \text{Eq. 3.2}$$

In all the studies described above, inorganic salts of chromium were used as the crosslinking sources. Bottle tests conducted by Burrafato et al. [1990] showed significant difference in the gelation characteristics between chromium acetate and inorganic chromium salts. They were able to demonstrate that gelation times of samples prepared from chromium acetate had a weaker pH dependence than those prepared from inorganic chromium sources. Gelation was observed at pH greater than 8 for chromium acetate samples while samples made from inorganic sources did not gel beyond a pH of 6.6 due to colloid formation.

Burrafato et al. [1990] also concluded that gels formed with chromium acetate exhibit good kinetic stability of the crosslinked product. Turbidity studies indicated that the rate of chromium precipitation as insoluble colloids in chromium acetate solutions was much slower at higher pH. They hypothesized that this may be due to the step-wise dissociation of acetate from the coordinate complexes.

Burrafato et al. [1990] conducted bottle tests to evaluate the performance of various ligands as gelation delaying agents. Gelation delay was affected by the concentration of the added ligand. They viewed the delaying effect as a result of competition between the reaction of hydrated Cr(III) (formed by substitution of the inorganic ligand by water molecules upon the dissolution

of the inorganic salt of Cr(III) in an aqueous solution) with the organic ligand and with the polymer functional groups.

Green et al. [1993] studied the effect of various ligands like acetate, nitrate, chloride etc. and their concentrations as free ligands in solution on the gel times of the polyacrylamide-chromium (III) system. The studies showed that the use of chromium acetate and the presence of free acetate in solution could delay gelation significantly at 25°C.

The works described all support the idea of viewing the gelation reaction as a ligand exchange reaction. The rate and the extent to which ligand exchange occurs depends on the relative displacement tendencies of the entering and leaving ligands, their concentrations and duration of reaction time allowed. The anion type in the gelant and/or its concentration will affect the Cr(III)–carboxyl gelation reaction rates by the extent to which the anion competes with the HPAAm carboxyl groups for Cr(III).Gelation can be further delayed by the presence of uncomplexed ligands in the gelling solution.

In situ gelation characteristics of gels in porous media were studied by McCool [1988] and Natarajan et al. [1998] with HPAAm –Cr(III) gels and other gel systems. Their work showed that the buildup of apparent viscosity (a measure of flow resistance) during flow experiments of gelling solutions in porous medium was much faster than the corresponding gelation in the bulk. They hypothesize that pre-gel aggregates formed during the gelation reaction and some of these aggregates are filtered from the solution during transport, thus building up high flow resistance and limiting the depth of penetration into the porous medium. Furthermore, Natarajan et al. [1998] also demonstrated from displacement experiments in sandpacks of one foot in length that increased acetate concentration delayed the development of flow resistance during gelant injection in porous media.

Selection and concentration of various ligands can delay the in situ gelation of systems as they flow through sand-packs. Nonetheless, it is not known how the extension of the bulk gel time translates to the time/distance that a gel can be injected into a porous medium before high flow resistance develops. The feasibility of formulating the HPAAm-Cr(III) gel system with added acetate for in-depth propagation into porous media needs to be further tested.

Experimental Materials and Procedures

Bottle Gelation Tests. Bottle tests were conducted to study the effect of added acetate ions on the bulk gelation times of an HPAAm-Cr(III) gel system. A relationship between the bulk gel times and acetate-to-chromium ratios was desired for the design of displacement experiments to be conducted.

Polymer Stock Solution. Polymer stock solutions were prepared from the polyacrylamide source of Alcoflood 935, batch # 8033 VVR. The stock solutions were prepared at a concentration of 8333 ppm on a weight basis to four significant figures. The solution container was put on a magnetic stir plate and a magnetic stir bar was used to stir the solution during preparation. The speed of the stirrer was carefully adjusted and the pre-weighed amount of polymer was slowly added to the vortex of the stirred solution. The container was securely sealed

to minimize evaporation and was stirred until polymer particles were completely dissolved and were not detectable from visual observation.

Chromium Stock Preparation. Chromium stock solutions were prepared from the chromium(III) acetate source of McGeane-Rocho, Inc. (lots # 4001480 and 40086816). The chromium content in the chromium acetate source was measured on a Perkin Elmer Atomic Absorption apparatus prior to stock preparation. The required amount of chromium source was weighed on the HM-202 electronic balance in a plastic container to an accuracy of four significant figures. Fresh distilled water was added to the chromium source until the desired chromium concentration was achieved. The chromium solution was shaken vigorously and allowed to settle for an hour for optimum dissolution before use. The exact chromium concentration of the stock was later calculated from the values measured during the weighing process.

Sodium Acetate and Acetic Acid Stock Preparation. Acetic acid stock is required to adjust the pH of the gel solutions to 5.0±0.1. The sodium acetate stocks were prepared from anhydrous sodium acetate S 210-2 by Fisher scientific at a concentration of 10.96% (wt %). Acetic acid stocks were prepared from glacial acetic acid, $A38^{C}$-212 by Fisher scientific at a concentration of 4.56% (wt %) to four significant figures. The required amount of sodium acetate was weighed on the SC Fairbanks balance in a beaker. Fresh distilled water was added to a beaker until the desired acetate concentration was achieved. The solution was shaken vigorously and allowed to settle for complete dissolution before use. Acetic acid stocks were prepared using the same procedure.

Gel Preparation. A consistent gel solution preparation procedure was adopted (Figure 3.2). The required amounts of polymer and Cr(III) stock were weighed and mixed in 60mL beaker bottles on the SC Fairbanks balance. The required equal amounts of sodium acetate stock and acetic acid stocks were added to the polymer-Cr(III) mixture. An additional amount of water was added when needed to bring the final weight of gel solution to 50 grams. The gel solutions were then stirred on a magnetic stir plate for about three minutes and their pH measured by a calibrated Accumet Basic pH meter from Fisher Scientific. The final gel solutions prepared were of 5000 ppm Alcoflood 935, batch 8033 VVR, 125 ppm McGeane-Rocho Cr(III) with acetate-to-chromium ratios ranging from 8:1 to 153:1 at a pH of 4.95±0.05. At the end, the gel solutions were allowed to gel in a constant temperature water bath at 30°C.

Gelation Monitoring. A Brookfield digital viscometer, model DV-1+, was used to monitor the viscosity development and hence bulk gelation times. The temperature of the viscometer was controlled at 25±0.1°C and the viscometer was calibrated with Cannon Certified Viscosity Standard (Lot 98301) before each viscometer measurement to ensure accuracy.

Viscosities were generally measured at a shear rate of 11.25 s^{-1}, which allowed for the observation of the onset of rapid viscosity increase at one consistent shear rate. The gel solutions were assumed to have gelled when the viscosity increased beyond the upper range of the viscometer, which was 1028 cP at a shear rate of 2.25 s^{-1}.

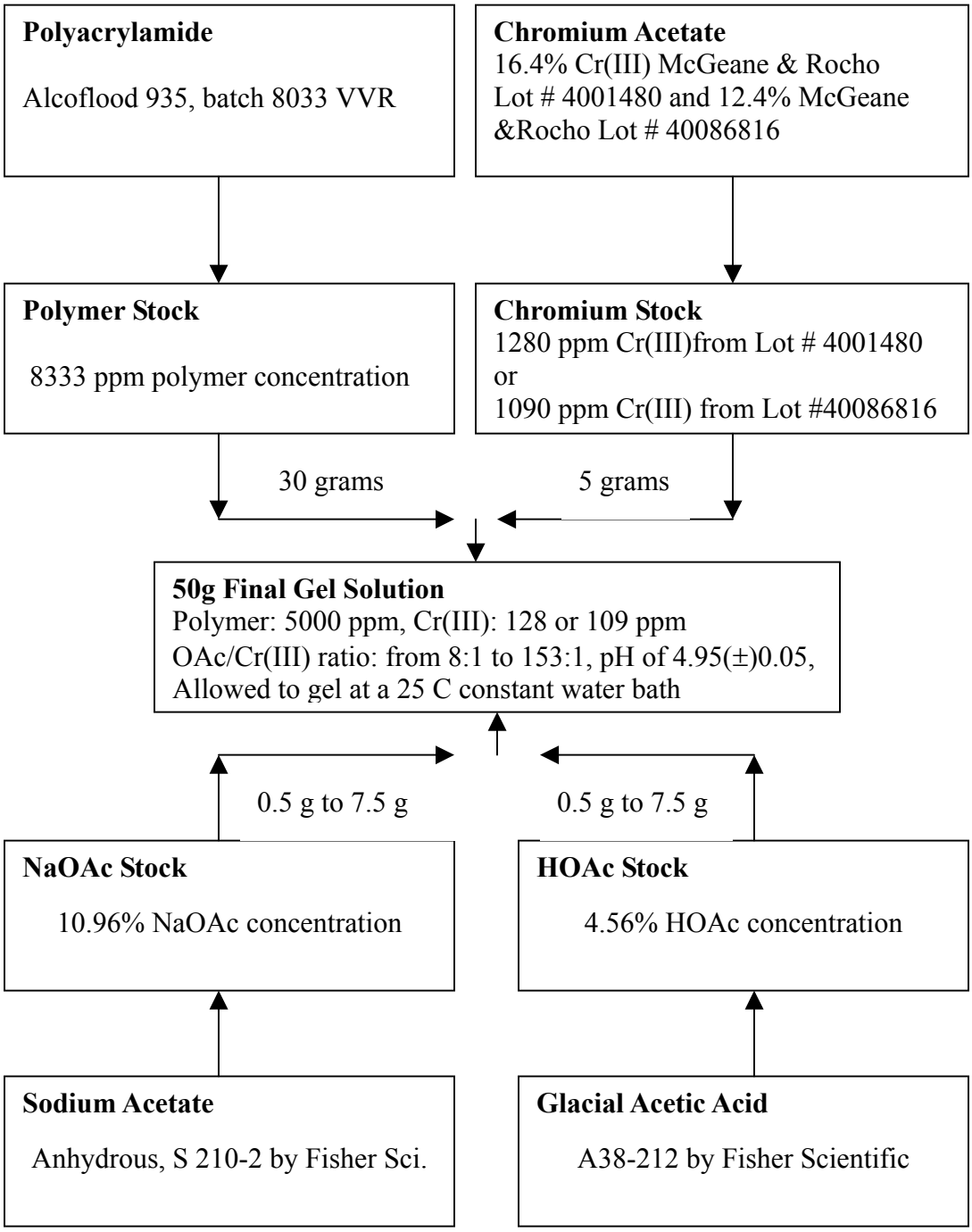

Figure 3.2 Schematic of the gel preparation procedure.

Displacement Experiments. ***Sandpack Holders.*** The sandpack holders were fabricated from schedule 80, nominal ID 1.5" transparent PVC tubes. All the sandpack holders were 6 inches in length. Both end caps to the holders had grooves cut on the inner faces to allow uniform distribution of the fluids injected. Size 37 mesh screens were held onto the inner faces of both ends with washers to avoid sand washout. The sandpack holders were hydrostatically tested to withhold a pressure differential of up to 350 psi.

For pressure differential measurement, two ports were secured to each sand-pack holder at an equal distance of 2 inches along the length of the holder. Thus, each sandpack holder was divided into 3 sections with each section 2 inches in length. Screens were also placed in the pressure ports to prevent sand particles from entering the transducer tubing. The empty volume of the sandpack holders was obtained from the difference between the tare weight and weight after water saturation. The holders were then dried and ready for use.

Sand filtering, Washing and Drying. F-110 silica sand obtained from Ottawa, Illinois was used in the packing of all the 6-inch sand packs. Both coarse sand of 20 to 30 mesh and fine sand of 140 mesh were used in the packing process. The fine F-110 Ottawa sand was filtered through a 50 mesh sieve to remove the debris in the sand. Sand washing was performed on the filtered sand to eliminate the unwanted metallic particles such as ferric iron that may interfere with the gelation process. Sand was added into technical grade concentrated hydrochloric acid and left submerged in capped glass containers under the hood for a few days. The excessive amount of acid was then removed by decantation followed by the addition of a small amount of 1 molar technical grade sodium hydroxide. After about three or four washes with distilled water to a pH of about 5, the sand was ready to be dried in a 100°C oven for a few days before use.

Sandpacking. The sandpack holders were packed with fine F-110 Ottawa sand in the middle and coarse sand in the ends to minimize sand washout. The bulk densities of both types of sands were carefully measured so that the exact amount of sand needed was obtained. About 20 grams of coarse F-110 Ottawa sand was added to the sandpack holder first, which gave a layer of about 1 cm thick of coarse sand at the bottom of the holder. Acid washed, dried fine sand was then added on top of the coarse sand until a level about 1 cm from the top of the holder. The addition of another 20 grams of coarse sand filled the pack holder. Throughout the packing process, the sandpack holder was vibrated with a magnetic vibrator to allow for maximum sand settlement. Finally, the top end fitting was secured to the packed holder with a pipe wrench. A detailed illustration of the sand packs is given in Figure 3.3.

Saturation and Porosity Estimation. Porosities of the sand packs were determined from the weight difference before and after saturation with water. The pack was mounted vertically and the bottom end was connected to the water source through a gear pump. Fresh distilled water was injected into the pack at a rate of 380 mL/min and the effluent water was collected at regular intervals. The absorbance of the effluent water measured on a Perkin Elmer UV/Vis spectrometer reflected the amount of extra-fine sand particles being washed out. Meanwhile, the bleed volume of water from occasional interruption of water injection indicated the residual air content in the pack. After negligible absorbance of the effluent in the spectrophotometer and a bleed volume of less than 0.2 mL, water injection was terminated with an optimum flush out of the extra fine sand

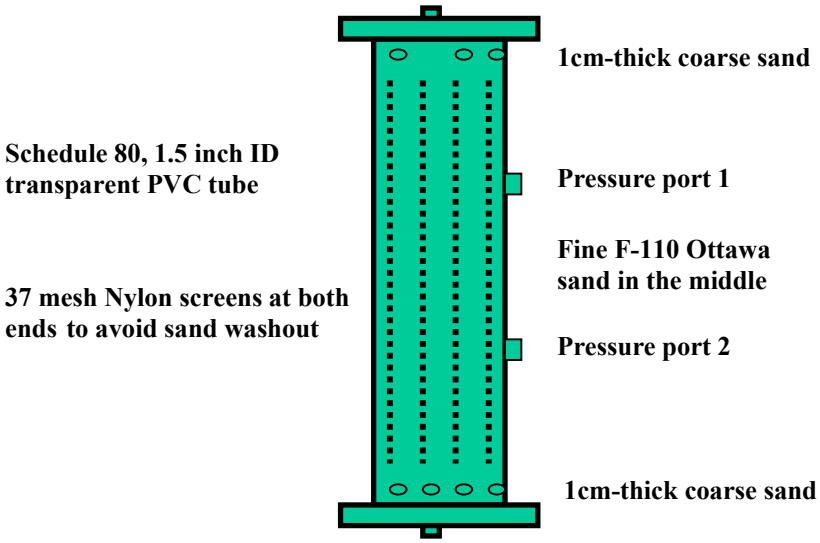

Figure 3.3 - Schematic of the configuration of the 6-inch sand packs.

particles and residual air in the packs. The water-saturated sandpack was then weighed on the SC Fairbanks electronic balance and porosity of the pack was calculated.

Dispersion Tests. When a step change of the influent concentration is introduced and the effluent concentration is plotted against the volume injected into a porous medium, an S- shaped curve can be obtained that represents the flow front response to the step change in concentration. The S-shape of the plot is due to the mixing across the flow front and its sharpness indicates the absence (or presence) of significant dispersion in the porous medium. Dispersion tests were conducted on all the water-saturated sand packs to verify their homogeneity. The dispersion curves obtained for all the packs, if plotted in one graph, would also help to verify the consistency of properties of the packs prepared.

A schematic of the experimental arrangement for dispersion tests is provided in Figure 3.4. Freshly prepared 1% KNO_3 tracer solution and fresh distilled water were injected through the 4-way switching valve into the vertically mounted water-saturated packs alternately at a steady rate of 3.00 mL/min. At least three cycles of tracer-water alternating injections were conducted on each pack to verify reproducibility. The absorbance of the effluent, measured through an in-line UV spectrophotometer, was plotted against the volume injected for each dispersion test performed on one particular pack. The homogeneity of the packs is confirmed by the standard "S" shape of the dispersion curves obtained. The uniformity of the packs was verified by the superimposability of the dispersion curves on one another as illustrated in Figure 3.5.

Permeability Measurement. A set of pressure transducers was connected through a valve system to the pressure ports on the packs using 1/8-inch tubes filled with dyed light mineral oil. Distilled water was injected at measured flow rates through the sand packs using a gear pump.

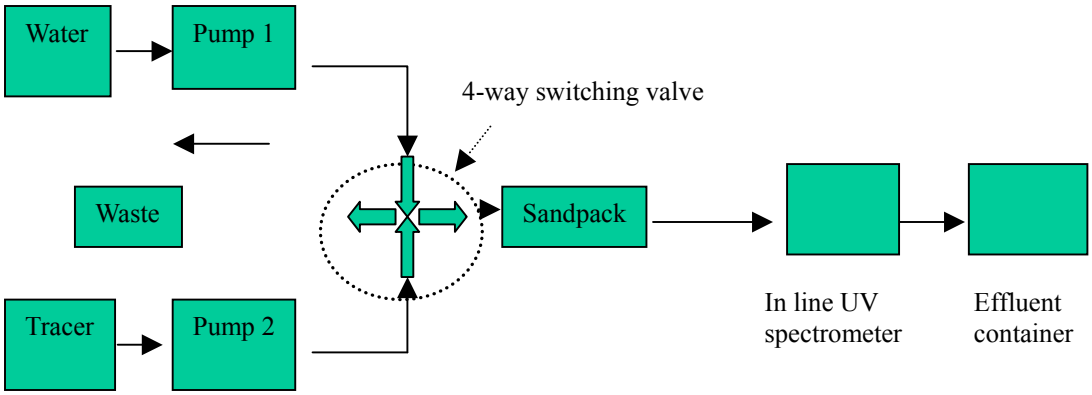

Figure 3.4 - Schematic of experimental set-up for dispersion tests.

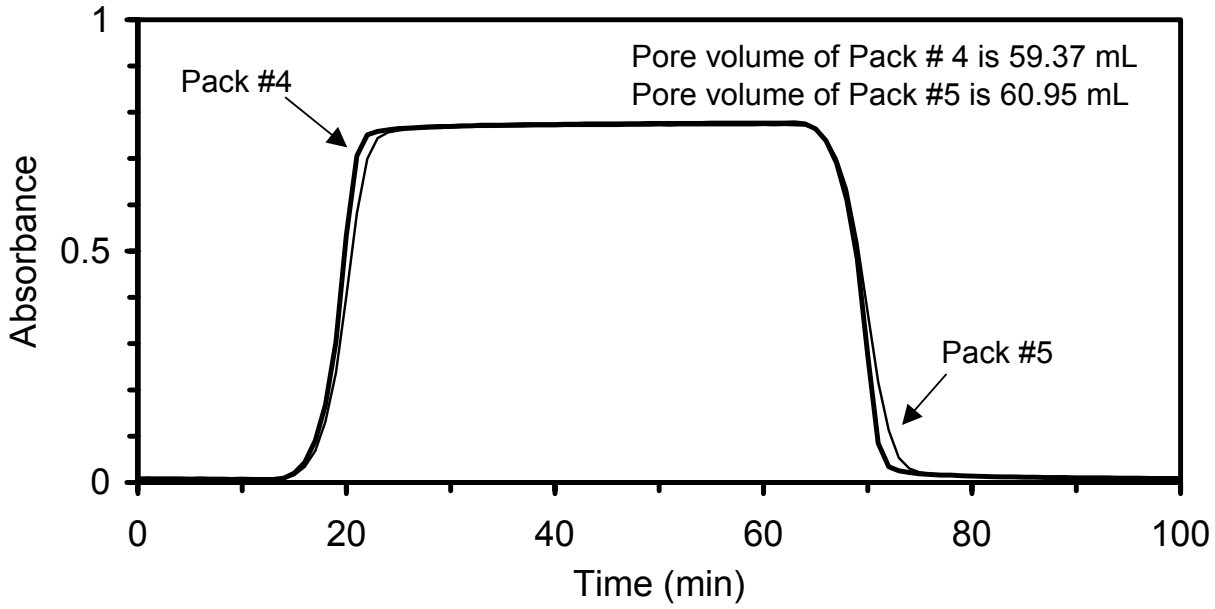

Figure 3.5 - Examples of dispersion curves for two sandpacks.

Pressure differentials measured across the individual sections and the entire length of the pack were measured via a transducer set-up and recorded by a computer. Pressure data across the pack were collected for at least five different flow rates of water injection. The pressure and flow rate data were used to determine permeabilities of the individual sections and the overall pack for different flow rates using Darcy's Law.

A sandpack was accepted as being well packed if a linear relationship was obtained between the measured pressure differentials and water flow rates. For all the packs used in displacement

experiments, there was very little variation (within 6%) of permeability values with respect to flow rates within a single pack or among different packs. Permeability values for the different packs are listed in Table 3.1.

Table 3.1 - Summary of the properties of the six-inch long sandpacks.

Sandpack #	Acetate:Cr Ratio	Porosity (%)	Permeability (Darcies)			
			Section1	Section 2	Section 3	Overall
1	38:1	36.5	5.45	5.26	5.53	5.41
2	44:1	36.4	5.58	5.28	5.26	5.34
3	56:1	37.0	5.58	5.46	5.57	5.52
4	90:1	37.1	5.64	5.58	5.55	5.55
5	103:1 (Run #1)	36.6	5.73	5.35	5.14	5.42
6	103:1 (Run #2)	36.9	5.65	5.35	5.39	5.47
7	103:1 (Run #3)	36.6	5.57	5.30	5.37	5.41
8	153:1	36.6	5.70	5.39	5.30	5.44

Gel Displacement Experiments in the Packs. A schematic of the displacement experimental set-up is presented in Figure 3.6. Bulk gelling solutions were placed in the bottom of the transfer cylinder in a constant 30°C water bath, gradually aged, while being displaced into the 6-inch packs by light mineral oil. Effluent samples from the packs were collected in 20 mL vials on an automatic sample collector at an interval of 250 minutes. A random selection of effluent samples was placed in another 30°C water bath for viscosity and pH monitoring.

The gel solutions used in the displacement experiments were prepared from the same polymer, chromium, sodium acetate and acetic acid sources and at the same procedure as previously described. The composition of the gel solutions injected were of 5000 ppm polymer, 110, or 125, ppm chromium and different acetate-to-chromium ratios ranging from 34:1 to 153:1 at a pH of 4.95±0.02. The injection rate was measured to be constant at 0.08 mL/min, equivalent to an interstitial velocity of approximately 0.91 ft/D. Both the gel solution and the pack were placed in a constant temperature water bath at 30°C for all the displacement experiments conducted.

Pressure differential data across the individual sections and the overall sandpack during gel injection were collected via the transducer setup in the computer based Camile data acquisition system. The displacement experiments conducted were terminated when the pressure differential across any individual section of the pack exceeded 25 psi. Pressure data were extracted and processed in a spreadsheet after the experiment was completed.

Post Displacement Experimental Analysis. Bulk gel samples and effluent from the displacement experiments were selectively analyzed to further interpret the gel displacement process. The pH, viscosity, and chromium concentration were measured. Atomic Absorption spectrometry was adopted to measure the chromium concentrations in the gels. Gel samples were pre treated to destroy the crosslinked polymer that would interfere in the analysis. About 0.5

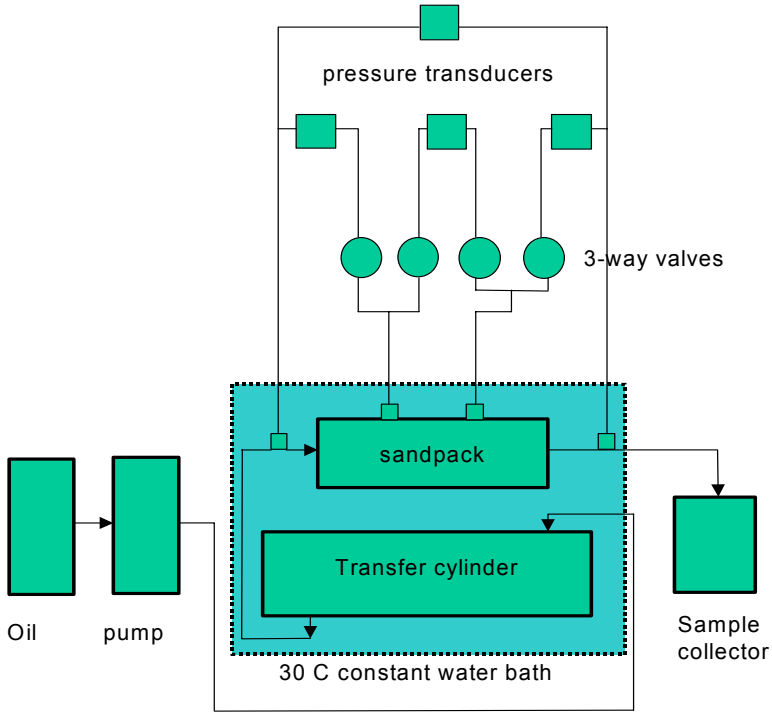

Figure 3.6 - Schematic of the experimental set-up for displacement experiments.

gram of each gel sample was weighed on the SC Fairbanks electronic balance in a Nalgene P.M.P. container and the weight was recorded. Approximately 1mL of hydrogen peroxide and 1mL of sodium hydroxide were added to the samples and they were then allowed to set in a 50°C oven for 3 hours to destroy the crosslinked polymer and oxidize Cr(III) to Cr(VI). Finally, the digested samples were diluted about 40 fold by distilled water so that their chromium contents were within the linear measurable range of the spectrometer.

During analysis, 1 ppm, 3 ppm, and 5 ppm chromium (VI) standards were freshly prepared with their absorbencies measured on the spectrometer to construct a calibration curve. The spectrometer was designed so as to directly give the chromium concentrations by fitting the measured absorbencies of the samples to the calibration curve. Chromium concentrations in the original untreated gel samples were obtained by multiplying the measured value by the dilution factors. The accuracy of the measurement was within 1%.

Results and Discussion

The experimental results are presented in two series of experiments. The first series consisted of bulk gel time measurements to characterize the gels for the design of displacement experiments. In the second series, in situ gelation times were measured during flow of the gel systems through sandpacks. Experiments at different acetate/chromium ratios were conducted. In situ gel times were conducted. In situ gel times were correlated as a function of bulk gel time and acetate/chromium ratio in the gel solutions.

Bulk Gelation Measurements. Bulk gelation tests were conducted to characterize the HPAAm-Cr(III) gel systems for the design of displacement experiments. In the bulk gel time experiments, the effect of added acetate on gelation time was investigated by monitoring the viscosity development of the gel solutions maintained under static conditions in a 30°C constant temperature water bath. The gel solutions prepared differ from each other only in terms of acetate concentration, or acetate-to-chromium ratio. Figure 3.7 shows typical viscosity development data for four gels of different acetate-to-chromium ratios, all at a chromium concentration of 125 ppm. The onset of gelation can be identified from the figure as a sharp increase in measured viscosity and gelation time is herein defined as the time required for the viscosity to reach 1028 cP at a shear rate of $2.25s^{-1}$, the maximum measurable viscosity of the viscometer. Gelation times at different acetate to chromium ratios are shown in Table 3.2.

Table 3.2 - Bulk gelation times for gelant with a chromium concentration of 125ppm.

Acetate-to-chromium mole ratio	Bulk gelation time (days)
7	1.25
12	1.25
16	2.5
20	2.5
29	2.5
37	6.5
44	12
46	12
54	14
63	17
80	26
88	28
103	52
105	52
131	112

In addition to the gels as described above, bulk gelation measurements gels at a different chromium concentration of 110 ppm. Test results are tabulated in Table 3.3. Figure 3.8 shows a plot of bulk gelation time versus acetate-to-chromium ratio of the gels. Added acetate has a significant delaying effect on gelation times for the gels studied. Increase in the acetate-to-chromium ratio from 7:1 to 153:1 increased the gelation time from about one day to approximately five months.

Though the exact mechanism of the gelation reactions is not totally understood, the gelation delay capability of acetate on the gels is largely attributed to its stronger affinity towards the Cr(III) ion than the carboxyl groups of the polymer as a ligand. Excess acetate ligands, added to the gel system in this study as sodium acetate, compete with the carboxyl group of the polymer molecule for Cr(III), thus reducing the rate of crosslink formation.

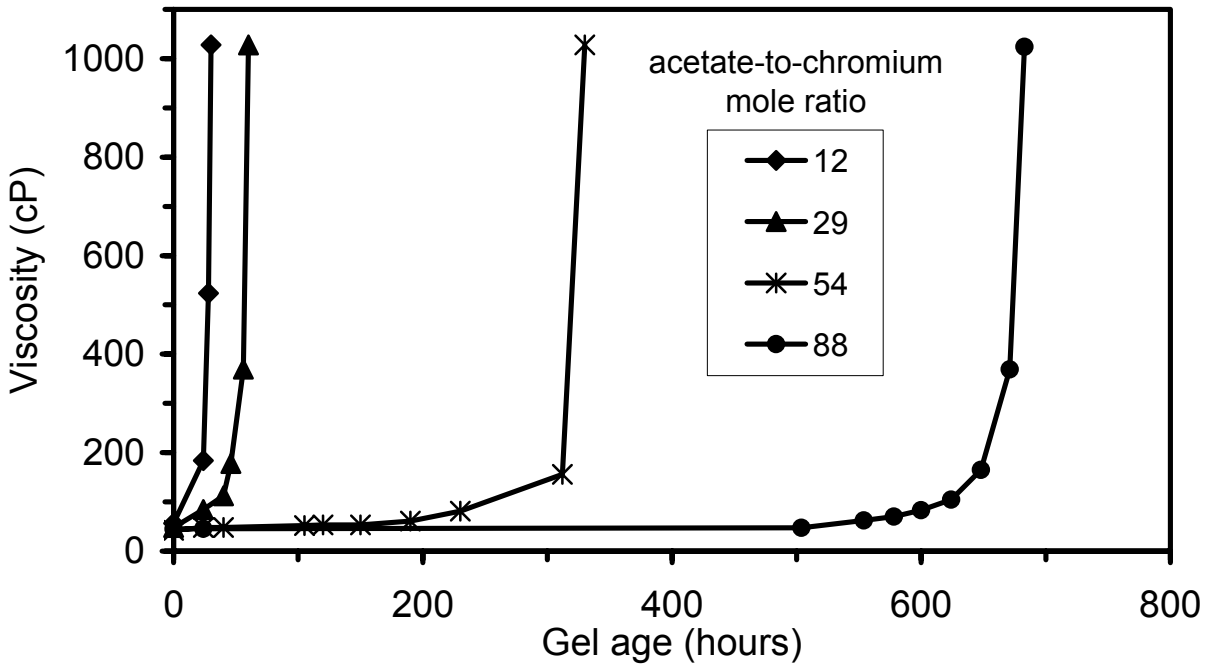

Figure 3.7 – Examples of viscosity development as a function of acetate-to-chromium mole ratio.

Table 3.3 - Bulk gelation times for a chromium concentration of 110 ppm.

Acetate-to-chromium mole ratio	Bulk gelation time (days)
38	9
56	17
90	30
103	51, 55
153	163

A second set of bulk gelation tests was performed after the completion of gel displacement experiments. The different concentrations of chromium used for displacement experiments necessitated that the effect of chromium concentration on bulk gelation time be studied for data interpretation. Gels in this set of tests differ from each other only in terms of chromium concentration for each particular acetate-to-chromium ratio studied. The test conditions are the same as those for the first set of bottle tests described above.

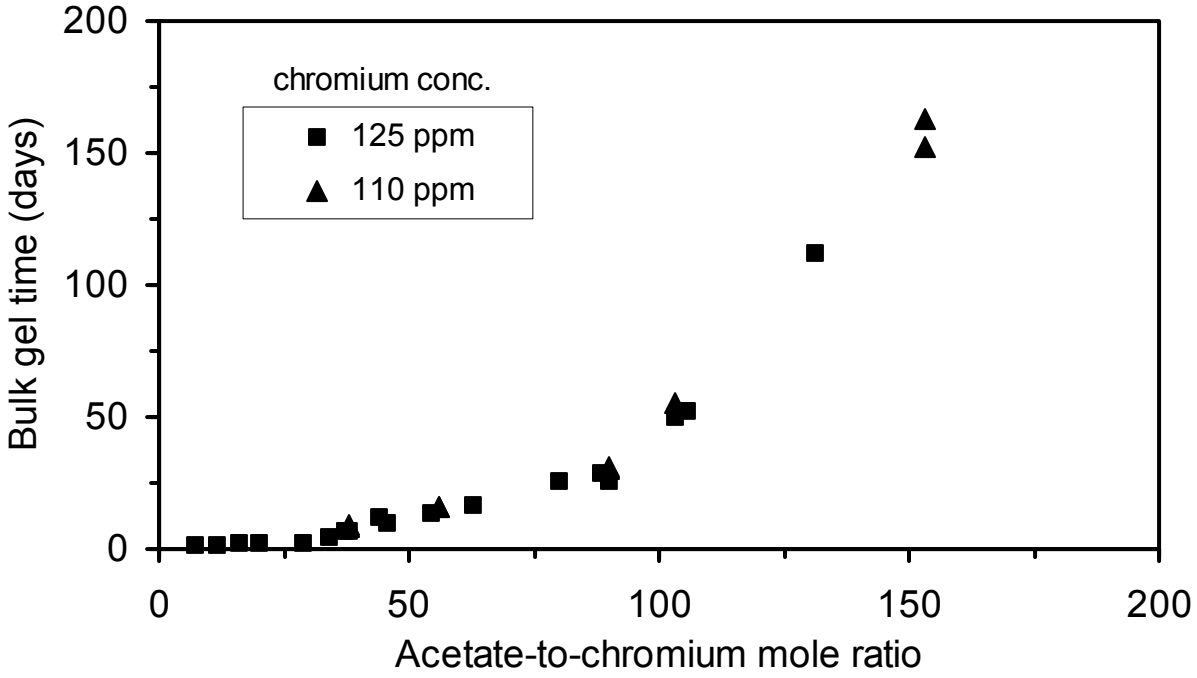

Figure 3.8 – Bulk gel time as a function of acetate-to-chromium mole ratio.

Four representative chromium concentrations of 100, 110, 120, and 130 ppm were selected for testing. Four acetate-to-chromium ratios of 38:1, 46:1, 56:1, and 90:1 were selected to determine if the effect of chromium concentration on bulk gelation times is consistent among gels of different acetate concentrations.

The effect of chromium concentration on gelation at different acetate-to-chromium ratios is presented in Figure 3.9. At the lowest acetate-to-chromium ratio studied of 38:1, the maximum difference resulting from varying chromium concentrations on bulk gelation times was one day out of a total gelation time of 7 days (roughly 14%). For the highest OAc to Cr(III) ratio of 90:1 studied, the maximum difference is 3 days out of a total gelation time of 27 days (roughly 11%).

In summary, increasing the chromium concentration from 100 ppm to 130 ppm led to 10%~15% decreases in bulk gelation times for all the gels prepared. This suggests that a small degree of variation in chromium concentration does not have a significant impact on the bulk gelation times for the gel system studied.

In Situ Gelation. The objectives of the displacement experiments were to: (1) evaluate the injection and transport characteristics of an HPAAm–Cr(III) gelling system in unconsolidated sandpacks; (2) determine whether the use of excess acetate would delay in situ gelation in unconsolidated sandpacks; (3) relate in situ gelation times to the corresponding gelation times in the bulk, and (4) examine the feasibility of using excess acetate in the gelling solution to achieve greater in-depth propagation and hence permeability modification in a porous medium.

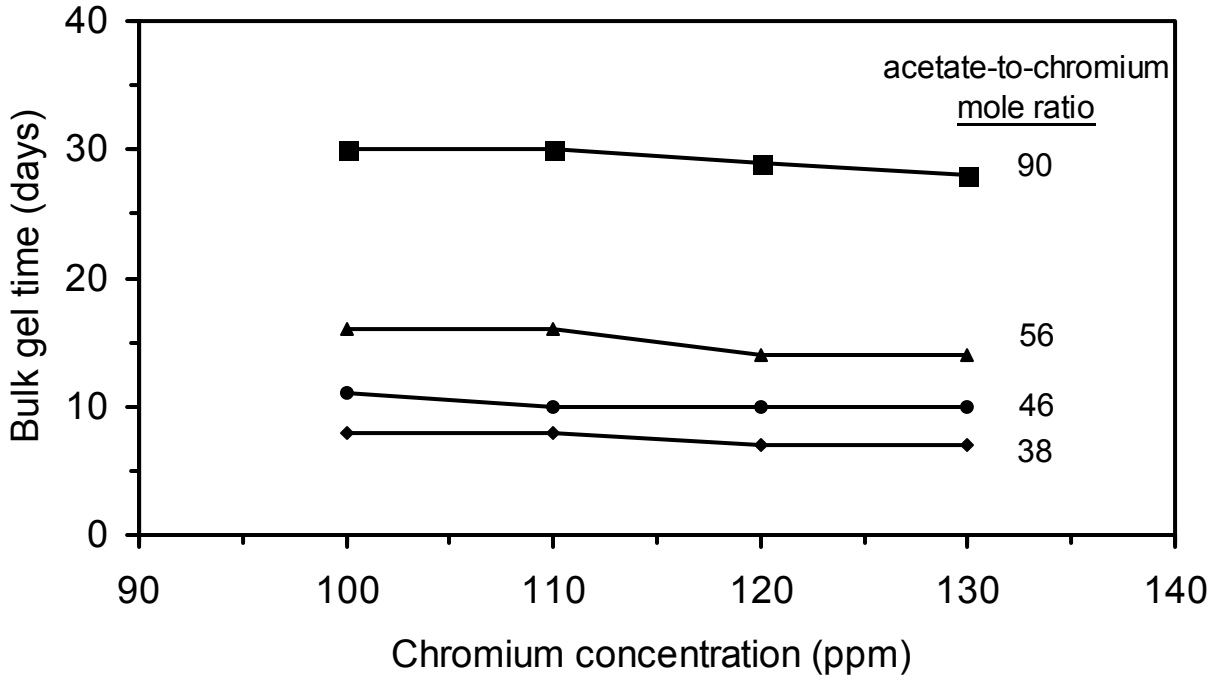

Figure 3.9 – Effect of chromium concentration on bulk gel time.

Eight displacement experiments were conducted in which bulk gelling solutions were flowed through 6-inch-long unconsolidated sandpacks under the experimental conditions described earlier. The displacement experiments are denoted by the acetate-to-chromium ratio of the gelant injected during each particular run. Briefly, selected acetate-to-chromium ratios of the gelant gave a wide range of bulk gel times. As the gelling solutions aged in the transfer cylinder, crosslinking took place and some pre gel aggregates were formed. When injected into the short sand-packs, as the pre gel aggregates became of sufficient size and/or reactivity, they were filtered out and started to accumulate in a sandpack. A significant increase in flow resistance, indicating in situ gelation, developed in the packs eventually. At the completion of the eight displacement experiments, the continuous injection times till the significant increase in flow resistance in the pack were related to the gelation times of the gelant in the bulk. Results of the eight runs are presented both in terms of apparent viscosity and pressure differentials in the sandpacks versus gel solution injection times. Pressure differentials and apparent viscosities are both direct measures of flow resistance or in situ gelation in the pack. For consistency, in situ gelation time is herein defined quantitatively as the cumulative injection time at which the pressure differential across a certain section of the pack reached twenty five psi, which was the upper limit of the measuring pressure transducers. A twenty-five psi pressure differential can be translated into an apparent viscosity value of 15,000 cP (or a mobility value 0.37mD/cP) across a two–inch–long segment of 5.5 Darcies′ permeability typical of the sandpacks used. Both values indicate large flow resistance in the sandpack indicative of in situ gelation.

Relationship between In situ Gelation and Bulk Gelation Times. The eight displacement experiments in short sandpacks confirmed that in situ gelation, i.e., the build-up of flow

resistance in the pack due to pre-gel aggregate formation, filtration and accumulation during gelant injection was much faster than the corresponding gelation in the bulk. Furthermore, results also demonstrated that in situ gelation was delayed by increasing the acetate concentration in the gelant.

In situ gelation times for the series of experiments are summarized in Table 3.4 along with the corresponding bulk gelation times. A plot of in situ gelation time versus bulk gelation time is shown in Figure 3.10. Figure 3.11 is a graph of the in situ gelation time versus acetate-to-chromium ratio of the gelants. A linear relationship between in situ gelation time and bulk gelation time was obtained as:

$$Y = 4.73\ X + 16 \qquad \text{Eq. 3.3}$$

where Y denotes in situ gelation time in hours
X denotes bulk gelation time in days.

Table 3.4 - Summary of gel times for gel displacement experiments.

Acetate-to-chromium mole ratio	Chromium conc. (ppm)	Bulk gel time (days)	Insitu gel time (hours)
38	110	8	44
44	125	12	20
56	110	17	120
90	110	30	200
103-#1	125	52	280
103-#2	110	55	285
103-#3	110	51	240
153	110	163	780

In situ gelation time can be considered as a measure of practical continuous injection times of a gelant without encountering significant flow resistance in the field for permeability modification purposes. Combined with interstitial velocity, continuous injection times will give the distance that the gelant will penetrate into a porous medium. As a result, the significance of this relationship is that it validates the feasibility of formulating the HPAAm-Cr(III) gel system with added acetate to achieve a desired in situ gelation time, hence a certain depth of penetration without the development of significant flow resistance in a porous medium.

Characteristics of Gel Solution Effluents, Viscosity and pH Measurements. The pH of the effluent measured after gelant breakthrough remained stable at a value of 4.95 ±0.05, the same as that of the solution injected. Viscosity of the effluent, however, behaved differently. A typical

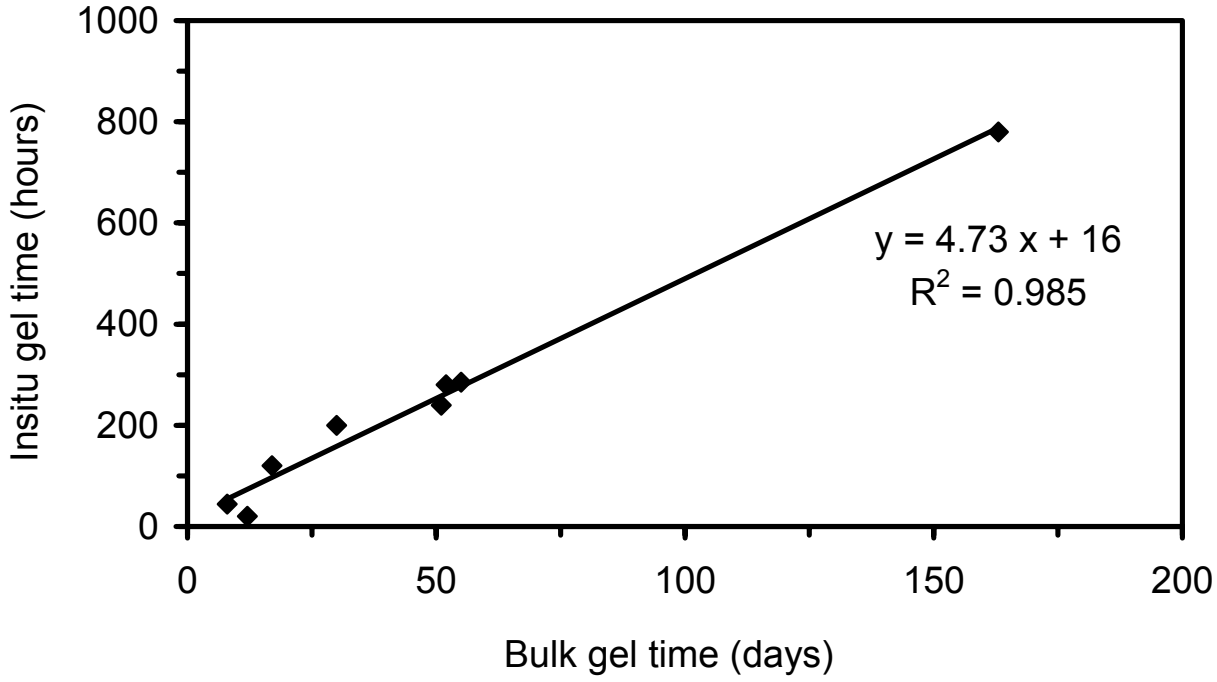

Figure 3.10 – Relationship between insitu and bulk gel times.

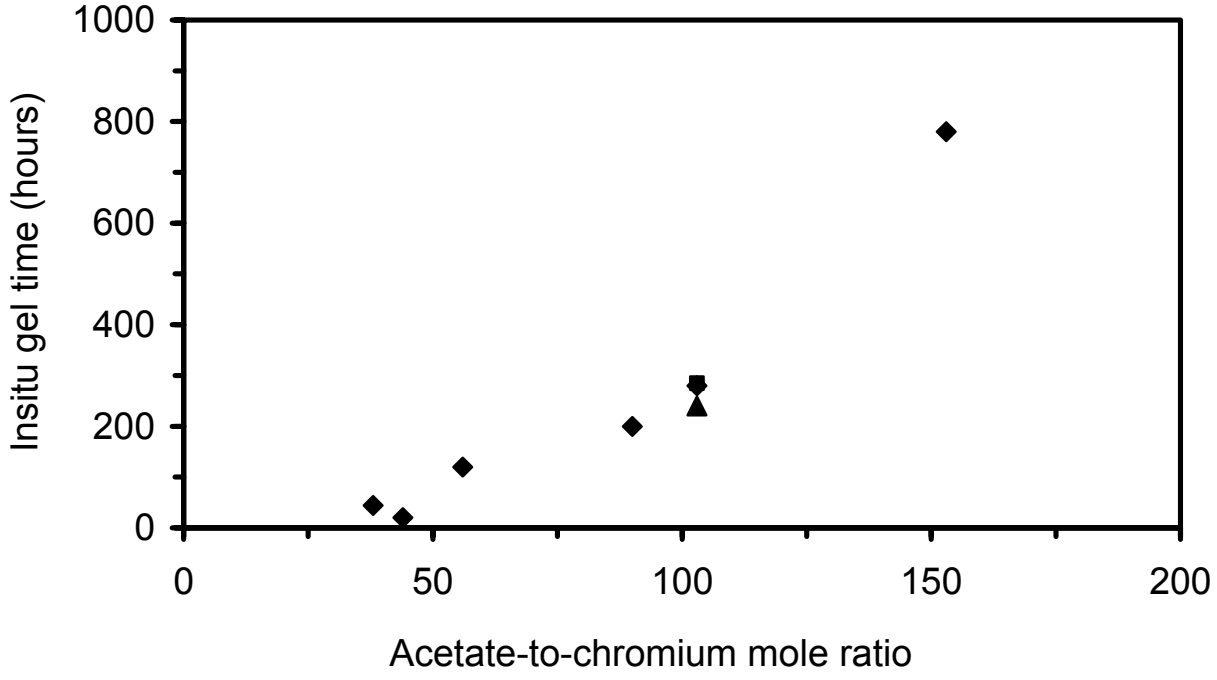

Figure 3.11 – Insitu gel time as a function of acetate-to chromium mole ratio.

profile of effluent viscosity versus injection time is illustrated for the 153:1 gel run in Figure 3.12. Because the sandpack was initially saturated with water, viscosity of the effluent was close to that of water at about 1cP during the first 10 hours of the injection experiment. A sharp increase in effluent viscosity to the injected value of about 33 cP was observed for the effluent collected after the breakthrough of the gelant front. The viscosity of effluent remained essentially the same as that of the bulk (about 33 cP) during the time period corresponding to the time before development of flow resistance in the pack. Viscosity of the effluent gradually dropped after the build-up of pressure differential (flow resistance) in section 1 of the pack. At the end of the experiment, the viscosity of the effluent was only at about 65% of the injected value. The drop in effluent viscosity is believed to have resulted from the stripping of the polymer content during gelant flow through the zone of high flow.

Chromium Analysis of Effluent. Chromium concentrations of the bulk gels injected for each displacement experiment were measured and are shown in Table 3.4. Chromium concentration in the effluent as a function of injection time was analyzed for the 153:1 gel run to detect possible chromium retention in the sandpack during gelant injection. The result is shown in Figure 3.13. Minor fluctuations in the effluent chromium concentration were within the noise level of the measuring equipment. It is apparent the effluent chromium concentration stabilized after gelant breakthrough at a value corresponding to that of the chromium in the gel solution injected, despite the development of flow resistance during the injection process. It is concluded that chromium retention in the pack was negligible for the series of gel displacement experiments conducted.

Conclusions

The following conclusion can be drawn from this work for the gel system and sandpacks used:

1. Bulk gelation of a partially hydrolyzed polyacrylamide-chromium(III) acetate gel system was delayed by added acetate, i.e., increased acetate-to-chromium ratio, at 30°C. Bulk gel times in the range of one day to about five months were achieved by increasing the acetate-to-chromium ratio from 7:1 to 153:1 in gelling solutions containing 5000 ppm polymer and 125 ppm chromium.
2. In situ gelation, indicated by the build-up of pressure differential within the pack during gelant propagation, was much faster than the corresponding gelation in the bulk in bottle tests.
3. Increasing the acetate-to-chromium ratio effectively delayed the development of flow resistance during gel injection in unconsolidated sand-packs. Increasing the acetate-to-chromium ratio from 38:1 to 153:1 delayed development of flow resistance in the sandpacks from 40 hours to as long as 33 days.
4. A linear relationship was obtained between in situ gelation time and bulk gelation times. This relationship suggests that the HPAAm-Cr(III) gel system can be formulated with added acetate to achieve a desired in situ gelation time hence a certain depth of penetration without the development of significant flow resistance unconsolidated sand.

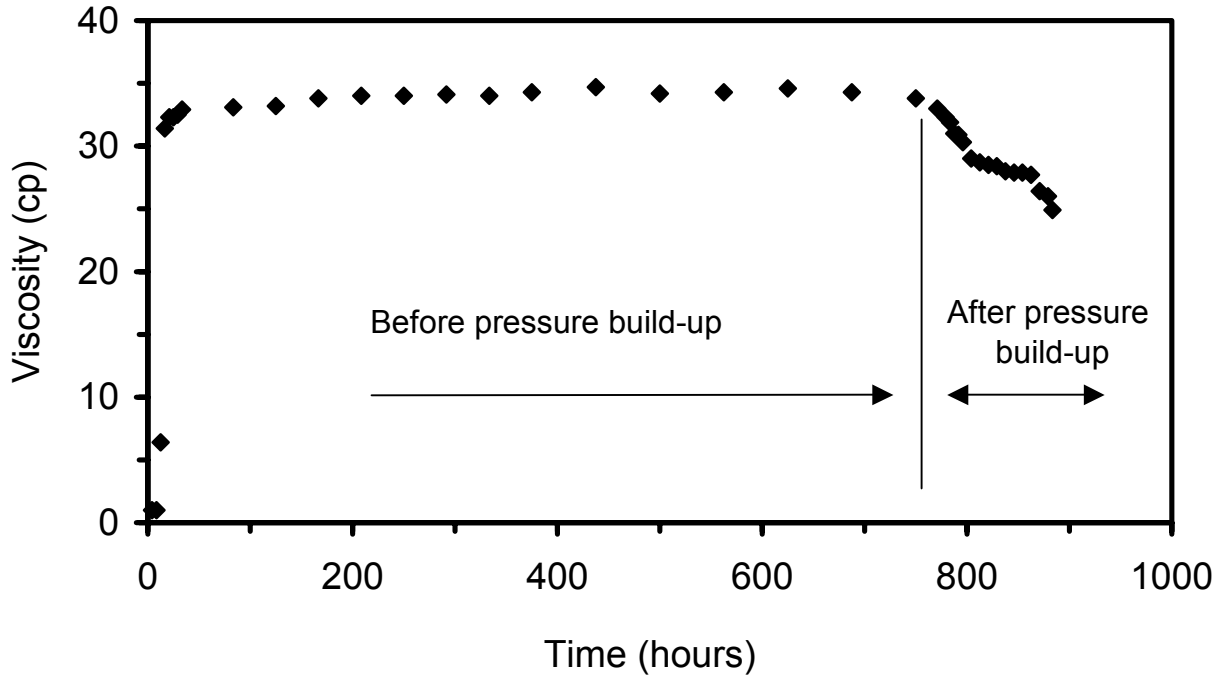

Figure 3.12 – Viscosity of the effluent during the gel displacement using the gelant with a mole ratio of acetate-to-chromium of 153.

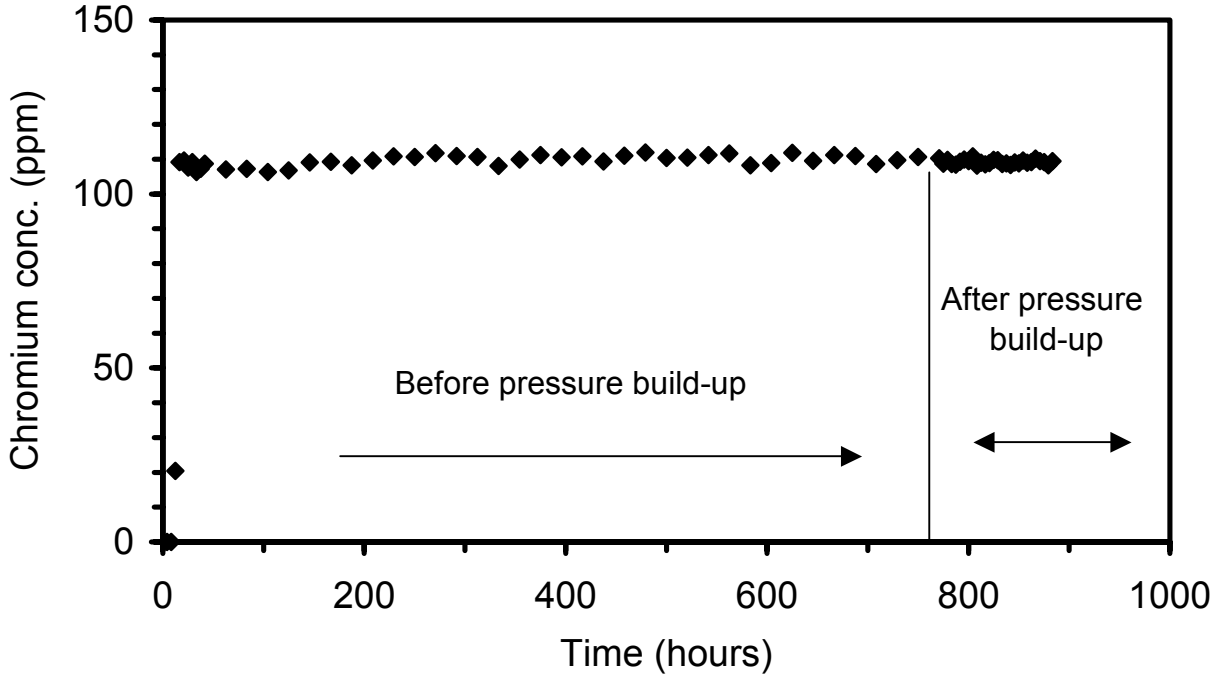

Figure 3.13 – Chromium concentration in the effluent during the gel displacement using the gelant with a mole ratio of acetate-to-chromium of 153.

References

1. Burrafato, G. Albonico, P., Bucci, S. and Lockhart, T.P., "Ligand –Exchange Chemistry of Cr+3-Polyacrylamide Gels," *Makromolec. Chem.,Macromol, Symposium,* **39** (1990) 137-141.
2. Green, D.W., Willhite,G. P., McCool, C. S. and McGuire, M., "Improving Reservior Conformance Using Gelled Polymer Systems," Annual report for the period September 25 1992 to September 24 1993, DOE contract No. DE-AC22-92BC14881, Report No. DOE/BC/14881-5, Chapter 5, The University of Kansas.
3. McCool, C.S. "An Experimental Study of the In situ Gelation of a Polyacrylamide-Chromium(VI) – Thiourea System in a Porous Medium," Doctoral Dissertation, The University of Kansas (1988).
4. Natarajan, D., McCool, C.S., Green, D.W. and Willhite, G.P., "Control of In-Situ Gelation Time for HPAAM-Chromium Acetate Systems," paper SPE 39696 presented at the 1998 SPE/DOE Improved Oil Recovery Symposium, Tulsa, OK (19-22 April).
5. Sydansk, R. D., "pH Dependent Process for Retarding the Gelation rate of a Polymer Gel Utilized to Reduce Permeability in or Near a Subterranean Hydrocarbon-Bearing Formation," U.S. Patent 5,609,208 (March. 11, 1997).
6. Tackett, J.E., "Characterization of Chromium(III) Acetate in Aqueous Solution," *Applied Spectroscopy*, **43** (1989) 490-499.

Chapter 4

Propagation of Chromium(III) Acetate Solutions Through Dolomite Rock

Graduate Research Assistant: Hong Jin
Research Associate: Michael Michnick

Introduction

Poor sweep efficiency is a problem in oil reservoirs due to the heterogeneous flow properties of reservoir rocks. Preferential fluid movements during oil-recovery processes result in bypassed oil. Application of gelled polymer treatments is one method to modify and/or reduce the permeability in zones of the reservoir in order to redirect injected fluids to flow through previously unswept portions of the reservoir.

Aqueous polymer systems composed of high molecular weight, partially hydrolyzed polyacrylamide (HPAM) and xanthan polymers that are crosslinked by chromium(III) have been used for treatments. However, *in-depth* treatment of matrix rock using these systems may be limited by the poor propagation of the chromium crosslinker, particularly in reservoirs containing carbonate.

When a solution containing chromium acetate and partially hydrolyzed polyacrylamide is injected into a porous matrix, two competitive reactions occur. These are: (1) the reaction between chromium acetate and polymer in which an acetate ligand is displaced by the carboxyl group to form a chromium acetate-polymer bond and (2) precipitation of chromium from solution due to the hydrolysis of chromium acetate when acetate ligands are displaced by hydroxide groups decreasing the solubility of the chromium acetate complex. The hydrolysis of chromium acetate is affected by the pH of the solution. In dolomite rocks, the pH of the solution is determined by the chemical composition of the aqueous solution. Aqueous solutions that are not highly buffered by dissolved salts have values of pH in the order of 9-10 when displaced through the dolomite porous matrix.

Chromium may also be retained by ion exchange or adsorption. Since the loss of chromium in previous studies in porous rocks exceeded the estimated ion exchange capacity of the rocks, the primary mechanism for loss of chromium is believed to be precipitation.

Further reaction of the chromium acetate-polymer complex leads to the formation of the gel structure. The importance of precipitation on this process depends upon the relative rate of chromium uptake by the polymer to the rate that chromium precipitates from solution in the porous matrix when exposed to the pH environment within the pore space. The kinetics of the chromium acetate-polymer reaction is not known. Consequently, it is not possible to determine at this time which reaction controls the transport of chromium acetate in a porous matrix during the gelation process.

A number of research groups have investigated the transport of chromium(III) and chromium(III)-crosslinked gel systems in porous cores containing carbonate minerals and in

carbonate rocks. Garver et al.[1989] measured the retention in Berea sandstone cores of chromium(III) from chromium chloride solutions, with and without xanthan polymer, during displacement experiments conducted with continuous flow and with shut-in periods. Significant retention was observed in all cases. Effluent chromium concentration and pH profiles were simulated with the UTChem simulator using a cation-exchange mechanism for chromium retention. The results indicated that cation exchange was not sufficient to describe the entire loss of chromium during its transport through the cores. The authors concluded that the "loss" of chromium to clays is detrimental to the in-depth placement of gelants that use chromium chloride for the crosslinker.

McCool et al.[2000] studied the interaction between dolomite rocks and a xanthan-chromium(III) gel system. Transport of both chromium(III) chloride and chromium(III) acetate solutions was studied at 35^{o}C. At the injected chromium(III) concentration of 50ppm (by weight), only 50% was recovered in the effluent after 4 pore volume (PV) of chromium acetate injection, while essentially no chromium was recovered when the same amount of chromium chloride was injected. Chromium was retained faster when chloride was the counter ion. The authors suggested that chromium was removed from solution by precipitation.

Bryant et al.[1996] studied chromium(III) retention in Berea sandstone cores. The cores were shut-in for 24 hours after injecting 4 PV of chromium solution. Chromium retention was a function of the injected pH, temperature, core lithology, and the chromium ligand. Bryant et al.[1996] pointed out that chromium retention was mainly due to a precipitation process, but reversible adsorption and ion exchange processes might be involved as well.

Stavland et al.[1993] studied chromium retention in Berea and Brent sandstone. They concluded that irreversible chemical adsorption is not the mechanism for chromium retention in the sandstone cores. Stavland et al.[1993] also observed that, given long periods of chromium injection, long-term retention occurred so that the effluent chromium concentration at steady state continued to be lower than the injected values. Retention of chromium exceeded the ion exchange capacity of the cores. Further study revealed that the retention rate of chromium(III) was lower when less carbonate was present in the cores. The authors suggested that precipitation is the major factor for chromium retention in the cores, which was likely caused by the elevated pH due to dissolution of the carbonates.

Seright [1992] studied the transport of chromium chloride in Berea and Indiana limestone cores. Chromium propagated more effectively when acetate was added as a counter ion. Solutions containing chromium acetate with and without polymer were propagated through Berea sandstone. Propagation of chromium was faster in Berea sandstone than in Indiana limestone.

The work reported in this paper is a continuation of previous research by Zou et al.[2000] who studied precipitation of chromium from chromium acetate solutions as a function of pH, temperature, salinity, and acetate concentration in the absence of dolomite. Figure 4.1 [Zou et al., 2000] shows the effect of pH on chromium concentration as a function of time. In bulk solutions, an induction period occurred before precipitation of chromium began. Increase in pH, temperature, and salinity decreased the induction period and increased the precipitation rate. Increase in acetate concentration moderately reduced the chromium precipitation rate over the concentration range studied.

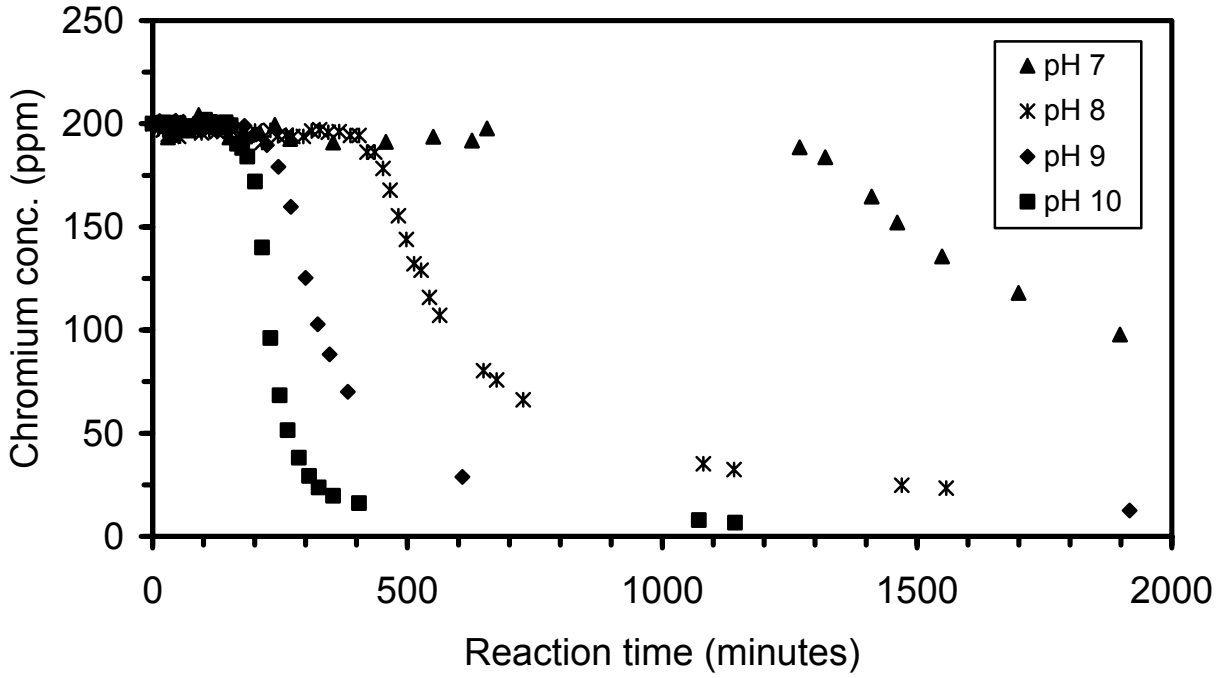

Figure 4.1 – Chromium concentration remaining in a chromium(III) acetate solution after precipitation at various pH values [Zou, 2000b].

An empirical kinetic model was developed by Zou et al.[2000] to describe the rate of chromium precipitation from solutions at 25°C with 1% KCl. Parameters include initial pH, chromium concentration, and OAc/Cr mole ratio. The model simulates the induction period and the chromium concentration in batch experiments as a function of time. The model also predicted the pH and chromium concentration as a function of time for experiments where ground dolomite was added to the chromium acetate solution.

The objectives of this work were to determine chromium retention when chromium acetate solutions were injected into dolomite cores in the absence of polymer and to compare retention with results predicted from the study of Zou et al.[2000]. Results of these studies provide insight into the transport of chromium in a porous matrix where flow occurs either from direct injection or by leakoff from a fracture treatment. In field applications, chromium acetate is injected simultaneously with polymer. Consequently, these results are not directly applicable to field situations without considering the effect of chromium-polymer reactions that occur simultaneously.

Experimental Details

Two types of displacement experiments, continuous-flow and shut-in, were conducted. In continuous-flow experiments, chromium(III) acetate solutions were injected into dolomite cores at selected flow rates and potassium chloride concentrations to determine chromium retention. In shut-in experiments, a chromium(III) acetate solution was injected into a dolomite core at a high rate until the effluent concentration was equal to the injected concentration, after which the core

was shut in for a selected time period. This was followed by a second high-rate injection of the chromium solution to displace the resident chromium(III) acetate solution from the core. This procedure was repeated for selected time intervals between the injections. The shut-in experiments resembled chromium precipitation in bottle tests except that the reaction occurred in porous dolomite cores. All experiments were conducted at room temperature.

Materials. The rock material used was Baker dolomite from Millersville, Ohio. Two cylindrical cores were cut from the same block, washed with water and dried in an oven at about 100°C. Plastic endplates that allowed for distribution of fluids across the face were attached to both ends of the cores and the core was encapsulated with an epoxy coating. The cores were saturated with water and the porosities and permeabilities were determined. Core properties are listed in Table 4.1. Two virgin cores were used in displacement experiments. A small core, with 1.9 cm diameter and 4.8 cm length, was used in most runs. A larger core, with 3.7 cm diameter and 11.7 cm length was used in one experiment.

Table 4.1 – Properties of dolomite cores.

	Core 1	Core 2
Diameter (cm)	1.9	3.7
Length (cm)	4.8	11.7
Weight (g)	28.4	265
Porosity (fraction)	0.21	0.22
Pore volume (mL)	2.86	27.7
Permeability (md)	25	19

Chromium solutions were prepared by dissolving chromium(III) acetate into potassium chloride solutions, degassing with vacuum for about 15 minutes, and aging for seven days before usage. The chromium(III) acetate was obtained from Alfa Chemicals in the form of a dark green powder with an empirical formula $Cr(OAc)_3.H_2O$. Concentration of chromium(III) was 200ppm by weight. Concentrations of potassium chloride were 0, 0.5 and 1.0% by weight. The pH of aged chromium solutions was around 4.5 and the pH of potassium chloride solutions was about 6.5.

Tracer tests were conducted prior to chromium injections in each run to characterize the cores. The tracer was a 0.1 mole/liter potassium nitrate solution and was selected due to its chemical inertness with the dolomite cores.

Displacement Experiments. A schematic of the experimental apparatus used for the displacement experiments is presented in Figure 4.2. Solutions were pumped through the cores with two ConstaMetric 2000 pumps. A four-way valve was used to switch between injected fluids. An in-line UV-Visible spectrophotometer was used to monitor chromium(III) and tracer concentrations in the effluent at wavelengths of 414 nm (Vis) and 301 nm (UV), respectively.

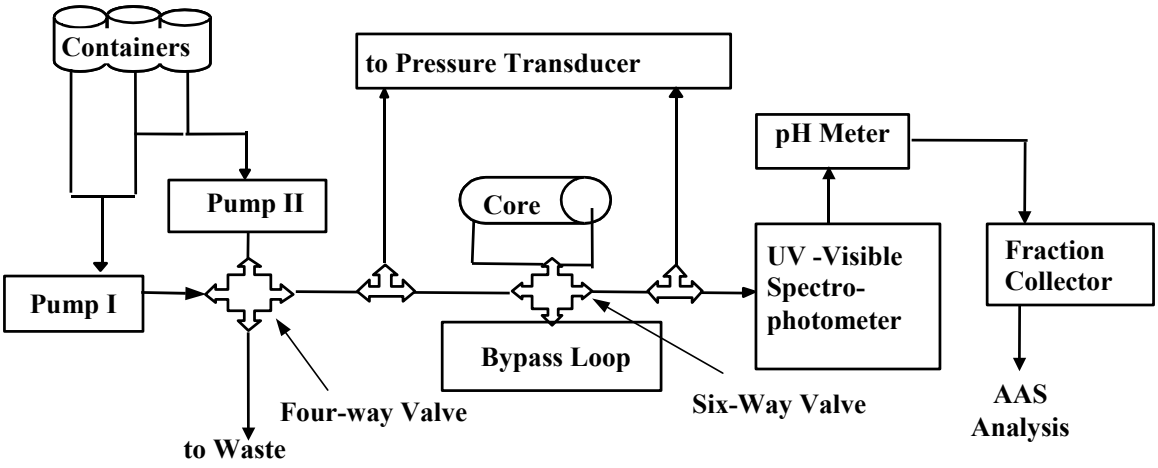

Figure 4.2 – Schematic of equipment used for displacement experiments.

Effluent pH was monitored in-line. A pressure transducer measured pressure drop across the core. An automated collector collected effluent fractions. Chromium concentrations in the effluent samples were determined using an atomic absorption (AA) spectrophotometer. A six-way valve and a bypass loop were used to divert injected fluids past the core for calibrations.

Continuous-flow experiments were conducted by injecting a chromium(III) acetate solution into the dolomite core at constant rate. Three different injection rates, 0.02, 0.10 and 1.00 mL/min, and two potassium chloride concentrations, 0.5% and 1% by weight were tested in the small-sized Core 1. A flow rate of 0.02 mL/min and a chromium acetate solution containing no potassium chloride were used in Core 2 followed by the injection of brine to displace the resident solution from the core.

Shut-in experiments were conducted using the same experimental set-up as for the continuous-flow runs. In these experiments, chromium acetate solutions that contained 200 ppm chromium(III) were flowed through a core at a high rate so that the residence time was too short (less than 3 minutes for Core 1) for significant loss to occur. The effluent chromium concentration was at its injected value when the core was shut in. The chromium solution in the inlet and outlet tubing was removed immediately after injection was completed. After selected time periods, ranging from 0.5 to 48 hours, the core was flushed with the same chromium acetate solution at the same flow rate. Chromium concentrations and pH in the effluent were measured before and after the shut-in periods. Effect of salt content was tested using two parallel runs conducted with and without the presence of potassium chloride.

Results and Discussion

Continuous-Flow Experiments. Five continuous-flow displacements were conducted. Flow rates, steady state effluent pH, residence time and potassium chloride concentrations in the chromium(III) acetate solutions (200ppm chromium) are given in Table 4.2.

Normalized concentrations of chromium and tracer in the effluent for Runs 1 and 2 of Table 4.2 are shown in Figure 4.3 as a function of pore volumes of fluid injected. The injected chromium

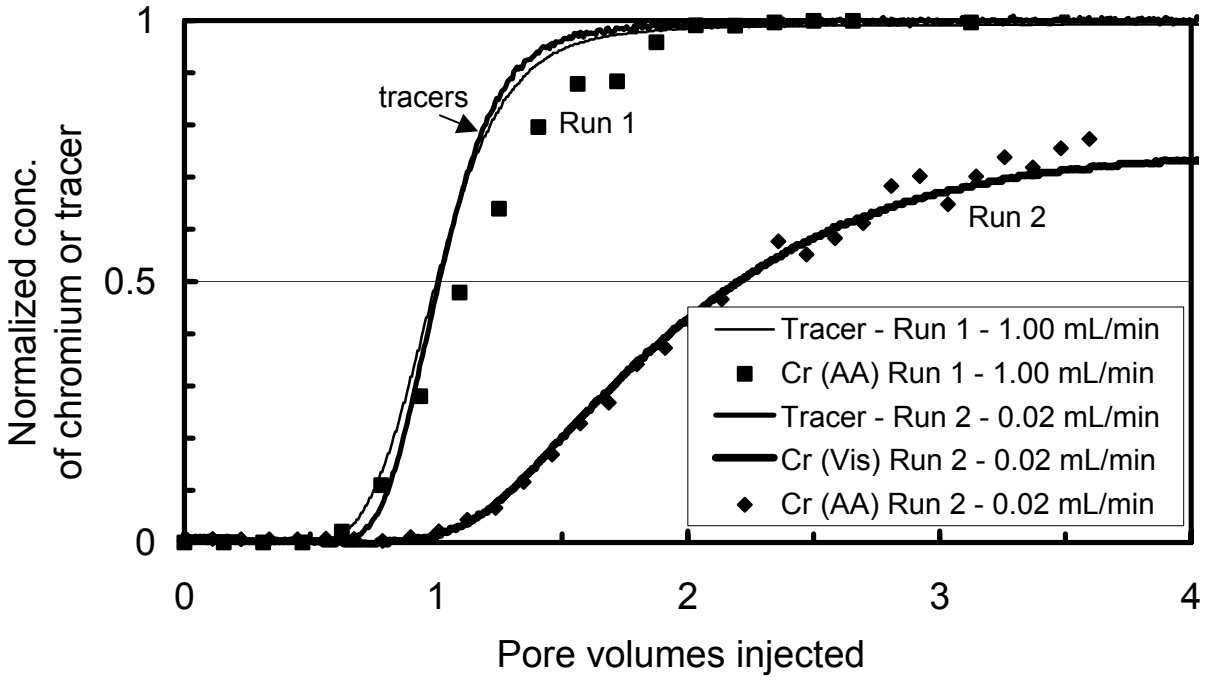

Figure 4.3 – Rate effect on the concentration profiles of chromium(III) and tracer in the effluent during continuous-flow experiments; 1.0% KCl, Core 1.

Table 4.2 – Summary of continuous-flow experiments.

Run #	KCl Conc. (%)	Injection Rate (mL/min)	Residence time (minutes)	Effluent values at 4 PV injection		Chromium retained* (μg/g of rock)	
				Normalized chromium conc.**	pH	Visible data	AA data
1	1	1.00	2.9	1.00	7.6	N/A	5.0
2	1	0.02	143	0.73	7.0	33	33
3	0.5	0.10	28.6	0.99	7.4	1.2	2.6
4	0.5	0.02	143	0.82	7.3	N/A	21
5***	0	0.02	1380	0.35	6.7	52	52

* Retention was calculated at four pore-volumes of chromium solution injected.
** AA data.
*** Run 5 conducted in Core 2, Runs 1 to 4 in Core 1.
All chromium acetate solutions contained 200ppm Cr(III).

solutions contained 1.0% potassium chloride and the flow rates were 1.00 and 0.02 mL/min for Runs 1 and 2, respectively.

The difference between the normalized concentration curves of chromium(III) and tracer is a measure of the amount of chromium retained. A material balance was calculated at four pore volumes of chromium solution injected with the assumption that the chromium solution at that time saturated the pore space and was at a concentration that was an average of the injected concentration and the effluent concentration at 4 PV injection. Estimates of chromium retention are given in Table 4.2 and range from 2.6 to 52 μg/g of rock.

The chromium front in Run 1 was slightly delayed with respect to the tracer curve. Thereafter, the chromium concentration in the effluent approached the injected concentration of 200 ppm due to the short residence time of around 3 minutes. This showed that chromium was retained at the front of the chromium solution bank as it flowed through the core with insignificant retention thereafter. Much greater amounts of chromium were retained in Run 2 at a flow rate of 0.02 mL/min and a residence time of 143 minutes. Retention of chromium also occurred at the front of the chromium solution bank in Run 2. The chromium concentration then approached a steady value after about 4 PV injected, which indicated that chromium would be retained indefinitely. These data are consistent with previous work [Bryant et al., 1996; McCool et al., 2000; Stavland et al. 1993] and show that chromium retention was a kinetic process.

Similar results were observed for the injection of the chromium(III) acetate solutions with 0.5 % KCl at injection rates of 0.10 and 0.02 mL/min (Runs 3 and 4).

The potassium chloride concentration in the injected chromium solution affected the retention of chromium in the dolomite core. Normalized chromium concentrations in the effluent are shown in Figure 4.4 for Runs 2 and 4 which were conducted at the same flow rate (0.02 mL/min) and at potassium chloride concentration in the injected solutions of 1.0 and 0.5%, respectively. More chromium(III) was retained at the higher salt concentration. This trend is consistent with previous research by Zou et al.[2000] on the precipitation of chromium from bulk chromium(III) acetate solutions. The mechanism responsible for this effect is not understood.

Run 5 was conducted to determine chromium retention in the dolomite core at a long residence time of about 23 hours. About 6 PV of chromium(III) acetate solution (0.0% potassium chloride) was injected into the larger Core 2 at 0.02 mL/min. Experimental data are shown in Figure 4.5. Effluent pH stabilized at about 6.6 after 3 PV injected. A substantial amount of chromium retention was observed. After 4 PV of injection of chromium solution, around 35% of the injected 200ppm chromium(III) concentration was detected in the effluent and the effluent concentration was stable. The retention of chromium calculated by material balance was 52 μg/g of rock at 4 PV injected. The rate of retention was constant. Thus, it appeared that retention of chromium would continue indefinitely.

Shut-In Experiments. Shut-in experiments were conducted by alternating the high-rate injection of a chromium solution with shut-in time periods to allow the chromium solution to soak in the core. The shut-in periods ranged from 0.5 to 48 hours. The composition of the injected chromium solution was 200ppm chromium(III). Two runs were conducted with the

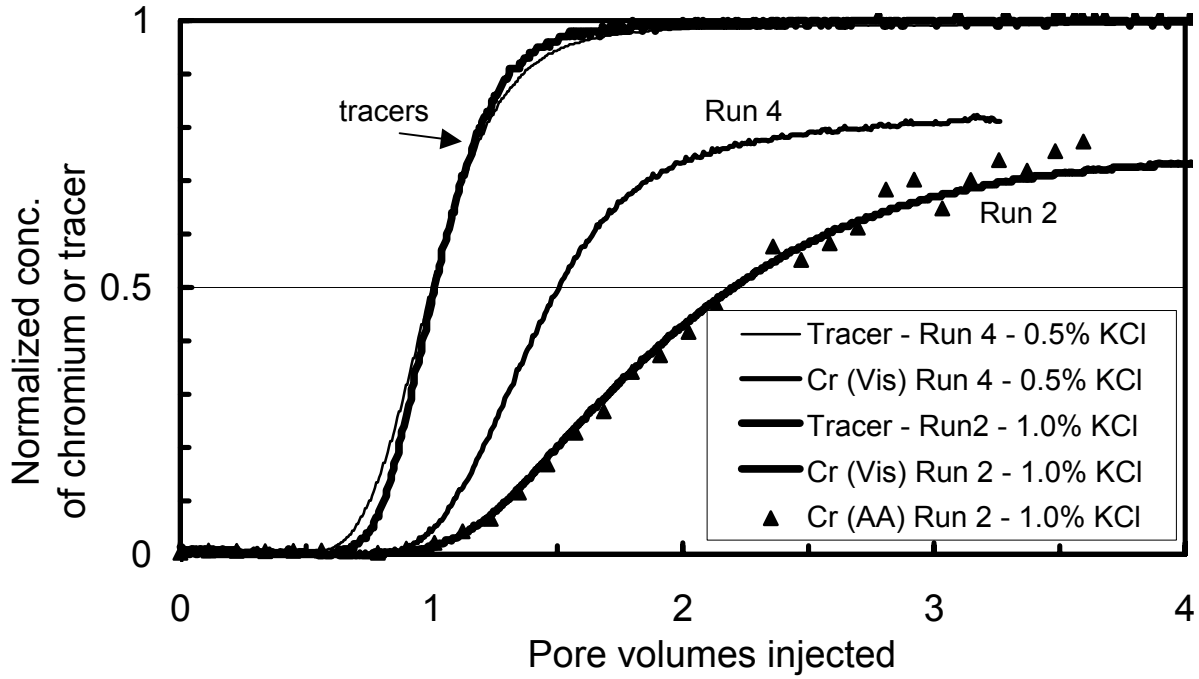

Figure 4.4 – Effect of salt concentration on the concentration profiles of chromium(III) and tracer in the effluent during continuous-flow experiments; Flow rate = 0.02 mL/min, Core 1.

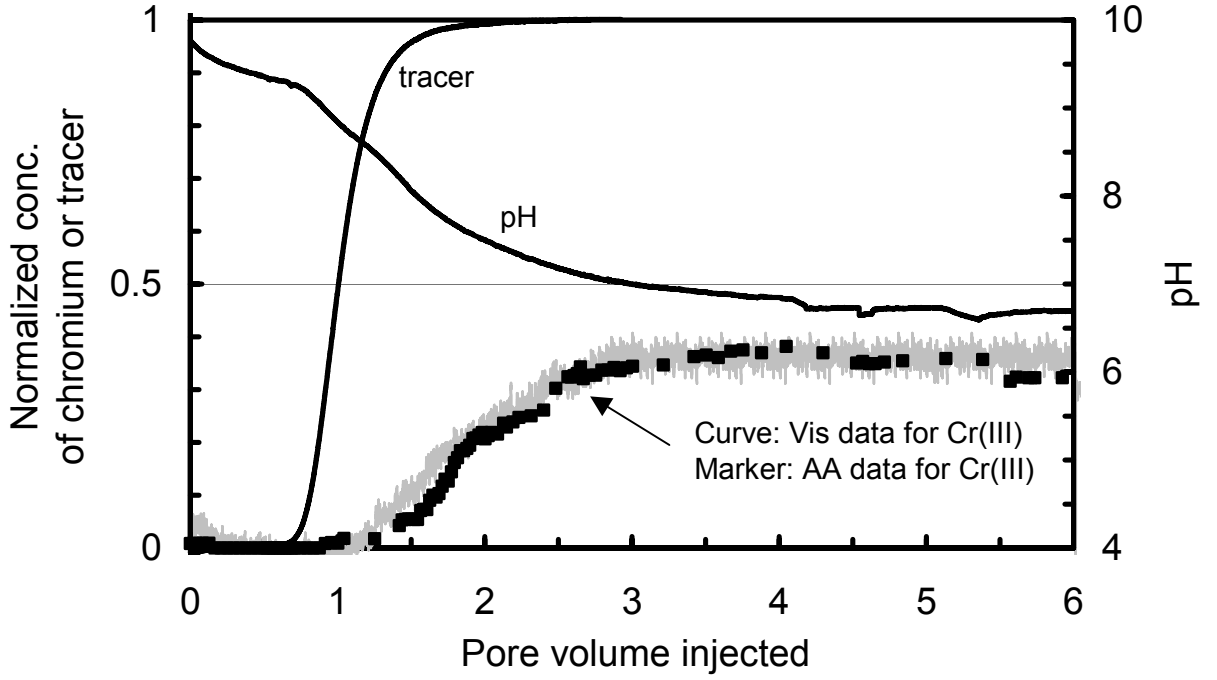

Figure 4.5 – Concentration profiles of chromium(III) and tracer in the effluent during continuous-flow experiment No. 5; Flow rate = 0.02 mL/min, 0.0% KCl, Core 2.

concentrations of potassium chloride in the chromium solution of 0.0 and 1.0% to study the effect of salt concentration on chromium precipitation.

Normalized chromium(III) concentrations in the effluent are shown in Figure 4.6 as a function of the pore volume of fluid injected for each injection for a chromium solution containing 0.0% potassium chloride in Core 1. The chromium concentration in the effluent during the initial injection represents the concentration of chromium in the core. The chromium concentration increased to the injected value after the resident solution was displaced. As noted earlier, the injected concentration was measured in the effluent after the resident solutions was displaced rapidly using a displacement rate that gave a residence time of about 3 minutes. The data show greater retention of chromium with longer shut-in times.

The first measured effluent concentration for each run after the shut-in period is plotted as a function of the shut-in time in Figure 4.7. Chromium retention was rapid in the dolomite cores after shut-in. More than 20% chromium(III) was lost in the core within one-half an hour for the case of 1% KCl. About 80% of the chromium(III) was retained in the core for a 24-hour shut-in period and more than 90% of the chromium was retained after a 48-hour shut-in period. Similar behavior was observed for the shut-in experiment conducted with a salt concentration of 0% KCl as shown in Figure 4.7. More chromium was retained when the chromium solution contained 1.0% KCl. Details of the two series of shut-in experiments are summarized in Table 4.3. The pH of the injected chromium acetate solution was 4.5. Effluent pH remained between 6.5 and 7.3 for most of the shut-in periods, indicating that the pH of the injected fluid was buffered by interactions with the dolomite core as chromium was retained.

Table 4.3 – Summary of the results for the shut-in experiments.

Shut-in period (hours)	1% KCl			0% KCl		
	Normalized chromium concentration		pH	Normalized chromium concentration		pH
	Vis Data	AA Data		Vis Data	AA Data	
0.5	0.73	0.75	7.3	0.80	0.80	7.7
1	0.72	0.75	7.0	0.80	0.79	7.6
2	0.72	0.74	6.8	0.78	0.78	7.2
3	0.58	0.60	6.8	0.75	0.75	7.0
6	0.44	0.43	6.8	0.70	0.68	6.9
12	0.37	0.37	6.8	0.45	0.45	7.0
24	0.23	0.22	6.7	0.32	0.36	7.0
36	0.12	0.12	6.6	0.26	0.25	6.9
48	0.08	0.11	6.5	0.22	0.16	---

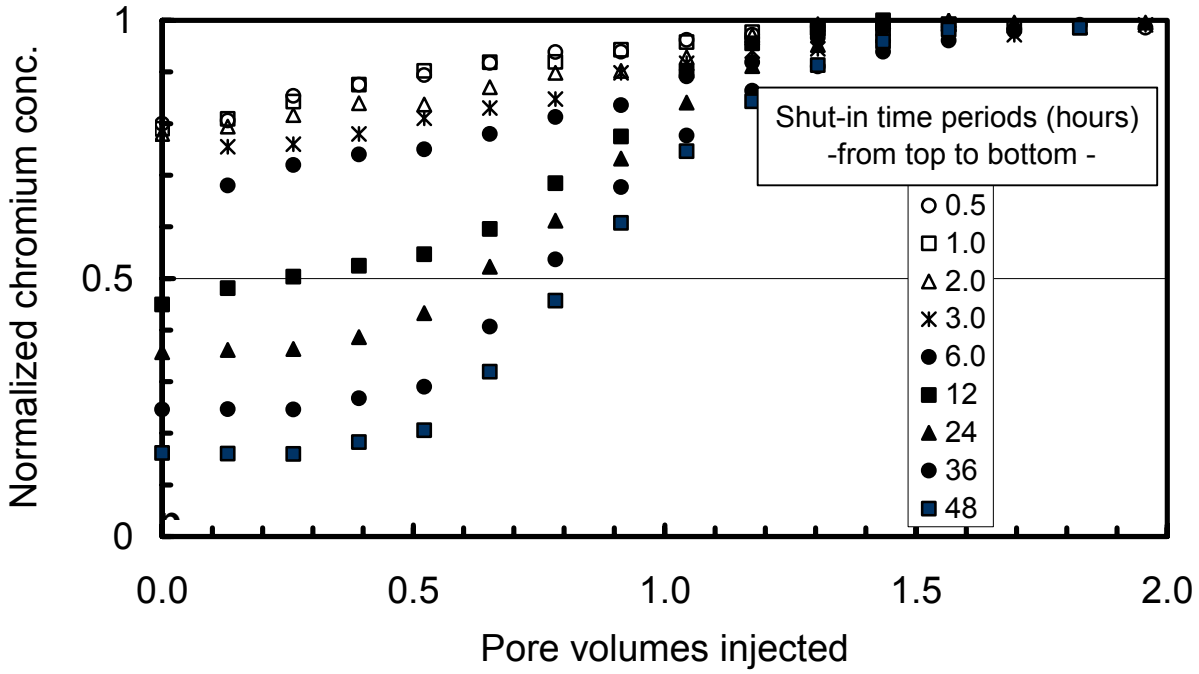

Figure 4.6 – Concentration profiles of chromium(III) in the effluent during injections of the shut-in experiments; 0.0% KCl, Flow rate = 1.00 mL/min, Core 1.

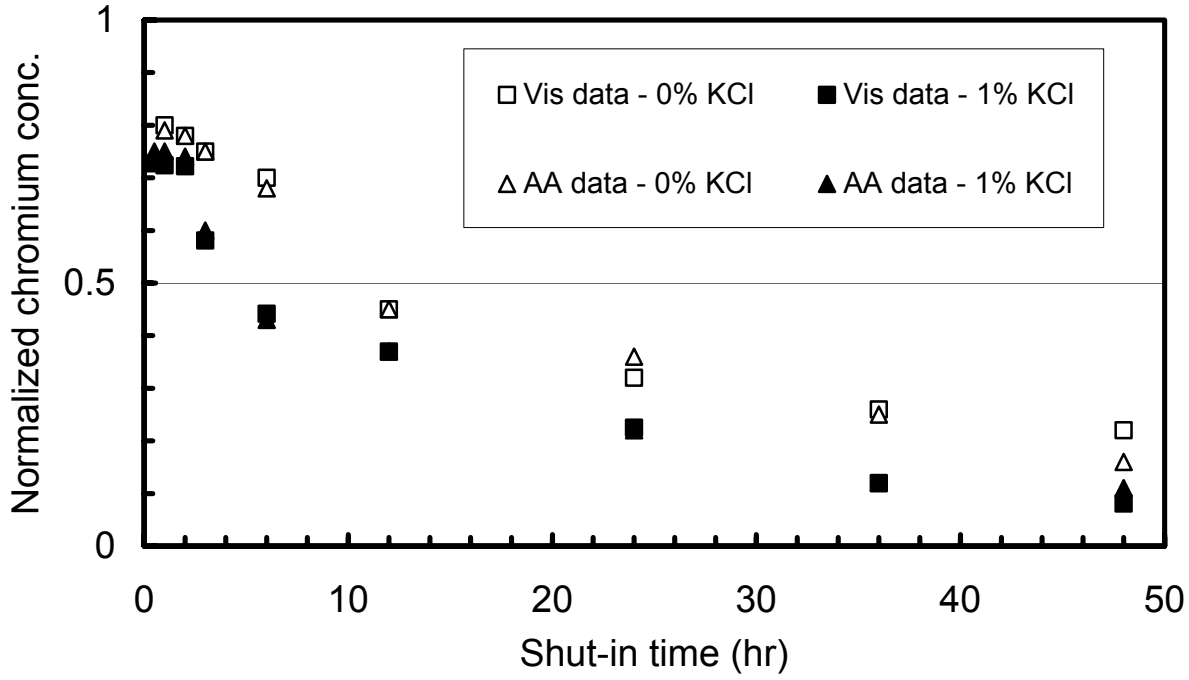

Figure 4.7 – Concentration of chromium(III) in the core as a function of shut-in time; Core 1.

Discussion. Chromium(III) retention data for the shut-in experiments were compared with the kinetic model developed by Zou et al.[2000] which describes the precipitation of chromium(III) from bulk chromium(III) acetate solutions containing 1.0% KCl at 25°C. The model has two parts, an induction period where no precipitation occurs followed by the kinetic precipitation of chromium. Both parts are a function of the pH value. The pH values of the initial effluent during the shut-in experiments with 1.0% KCl were between 6.5 and 7.3 as listed in Table 4.3. The model was run using a pH value of 7. Equation 1 is the empirical expression for the rate that chromium concentration changes due to precipitation of chromium from chromium acetate solutions after the induction period.

$$\frac{dC^*}{dt'} = -k_0 C^* C_{OH^{-1}}^{\gamma} C_{OAc}^{\beta} \qquad \text{Eq. 4.1}$$

where,

$k_0 = 2.6\text{x}10^{-3}/(\text{min } M^{\gamma+\beta})^{-1}$;

$\gamma = 0.37$;

$\beta = 1.2$;

t' = the elapsed time from the end of the induction period.

Results of simulation using the model are presented along with shut-in data in Figure 4.8. The model predicts an induction period of 19 hours that did not occur in shut-in runs. However, when the induction period of the model is neglected, the model gives a reasonable prediction of chromium retention in the core. This indicates that the kinetic model developed for chromium precipitation in bulk solution describes chromium retention during shut-in experiments in cores and suggests that precipitation might be the principal mechanism of chromium retention in dolomite cores. The reason that an induction period is observed in bulk solutions but not in porous dolomite rocks is not understood.

The experimental data indicate that effluent chromium(III) concentrations for the continuous-flow experiments approach stable values after 4 PV injection, and the values appear to be a function of residence time. For example, in Core 1 the effluent concentration was about 75% of the injected chromium(III) concentration at a flow rate of 0.02 mL/min, or residence time of 2.38 hours. The normalized chromium(III) concentration after 2-hour shut-in was 74%. Similar agreement was found for the 0%-KCl case. In Run 5 (Core 2), the effluent chromium concentration at steady state reached 35% of the injected value for a residence time of 23 hours, while the normalized effluent chromium concentration for the 24-hour shut-in run at 0% KCl in Core 1 was 34% after shut-in.

Additional data were obtained in Run 5. Figure 4.9 shows the normalized effluent concentration when water (0% KCl) was injected into Core 2 at 1.00 mL/min (residence time = 27.7 min) following the 6 PV injection of chromium acetate solution. The effluent chromium(III) concentration increased during the first half pore-volume of water injection peaking at about 0.52 of the injected concentration. The data demonstrate that the chromium concentration in the resident fluid increased with distance measured from the outlet of the core towards the inlet, i.e., there was a concentration gradient of chromium(III) along the direction of flow in the core during chromium solution injection. At the moment of water flush, the concentration of chromium(III) was higher inside the core than at the exit.

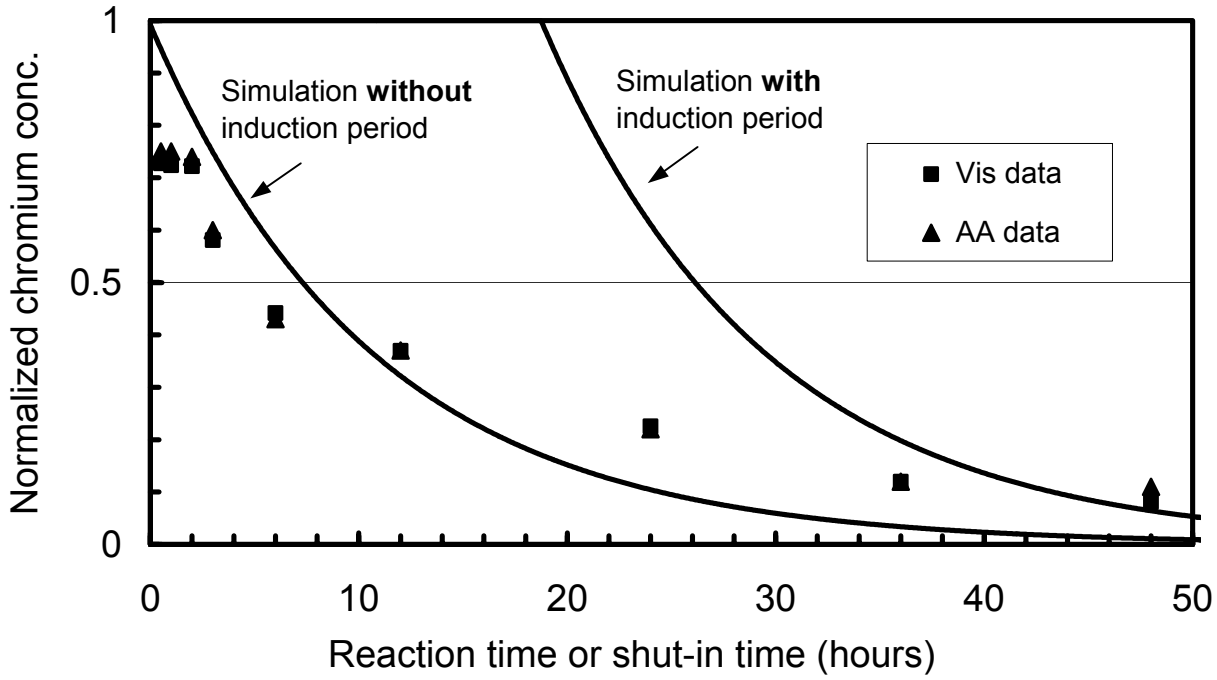

Figure 4.8 – Comparison between the results of the shut-in experiments and the chromium precipitation model [Zou, 2000b]; 1.0% KCl.

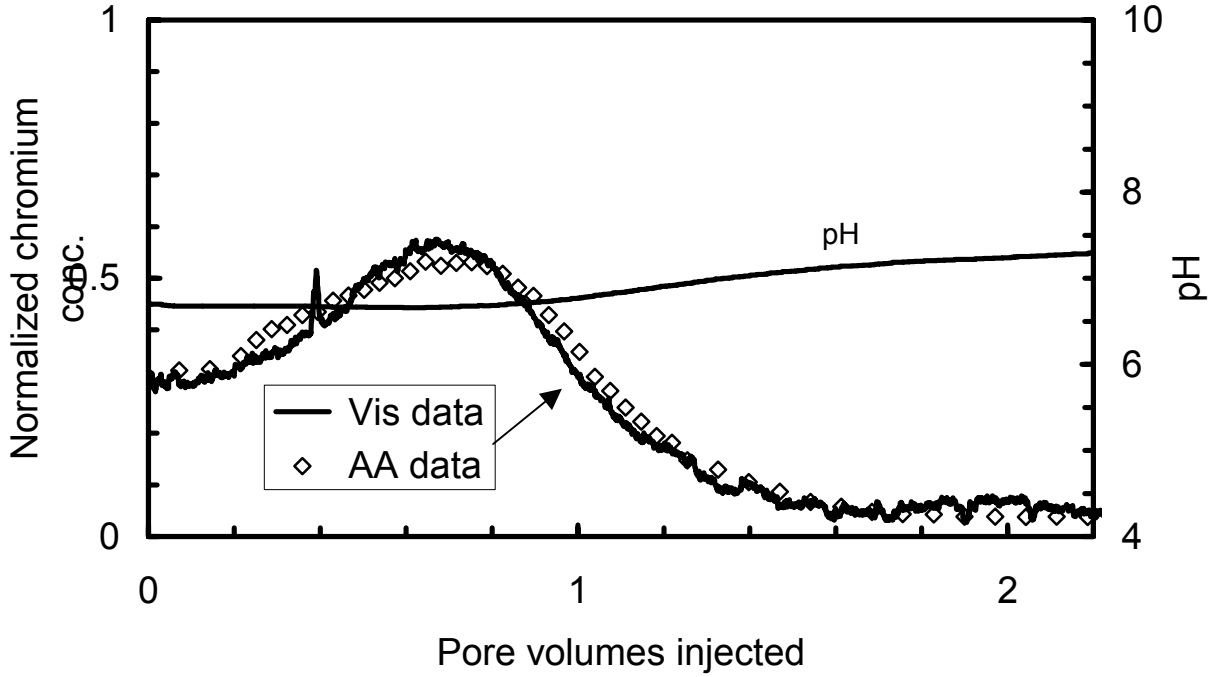

Figure 4.9 – Concentration of chromium(III) and pH in the effluent during water injection for continuous-flow experiment No. 5; Flow rate = 1.00 mL/min, 0.0% KCl, Core 2.

Effluent data collected in the first 0.6 pore-volume of brine injection were converted to equivalent residence time and compared with the retention rate represented by shut-in data from Core 1 (0% KCl in the chromium solution) in Figure 4.10. The first 0.6 pore-volume data were selected to remove effects of dispersive mixing between the water and the displaced fluid on the concentration profiles. Details of the conversion are given in the Appendix. Good agreement was found between these two sets of data, which established that there was a chromium concentration profile along the direction of flow during a displacement.

These data provide further evidence that chromium retention during the flow of chromium acetate through dolomite cores is a kinetic process that depends upon the residence time that a specified solution remains in the core. As discussed earlier, the effect of chromium retention on gel placement is determined by the competitive reactions between chromium and the polymer in addition to precipitation. Research on the kinetics of the chromium acetate-polymer reactions is needed to discriminate between these two mechanisms and to determine the impact of chromium retention during gelant placement in field applications.

Conclusions

The conclusions are limited to the chromium(III) acetate retention in 19-25 md dolomite matrix rock studied at room temperature and in the absence of polymer with chromium(III) concentration of 200ppm and an OAc/Cr mole ratio of 3.

1. Significant retention of chromium occurred during transport of chromium acetate solutions through dolomite cores.
2. The rate of chromium retention in dolomite cores is consistent with a precipitation model developed from precipitation in bulk solutions and demonstrates that precipitation is the principal mechanism for chromium retention from chromium acetate solutions in dolomite rock.
3. Precipitation of chromium in dolomite rock is a rate-dependent process. The amount of chromium retained varied with the injection rate, or the residence time of chromium in the dolomite cores. Longer residence times resulted in larger amounts of chromium retention. Given enough residence time, a chromium concentration distribution will be established along the direction of flow in the core.
4. Chromium precipitation was affected by salinity. The presence of potassium chloride enhanced chromium retention in dolomite rock in the range studied. The observation is consistent with that from previous research by Zou et al.[2000].
5. Chromium precipitated faster in the cores than in the batch-scale experiments. The induction period observed in precipitation experiments using bulk solutions was not observed in dolomite cores.
6. Effluent pH remained stable around 7 during continuous chromium injections, indicating that a buffer was formed in the system from chromium acetate-dolomite interactions.

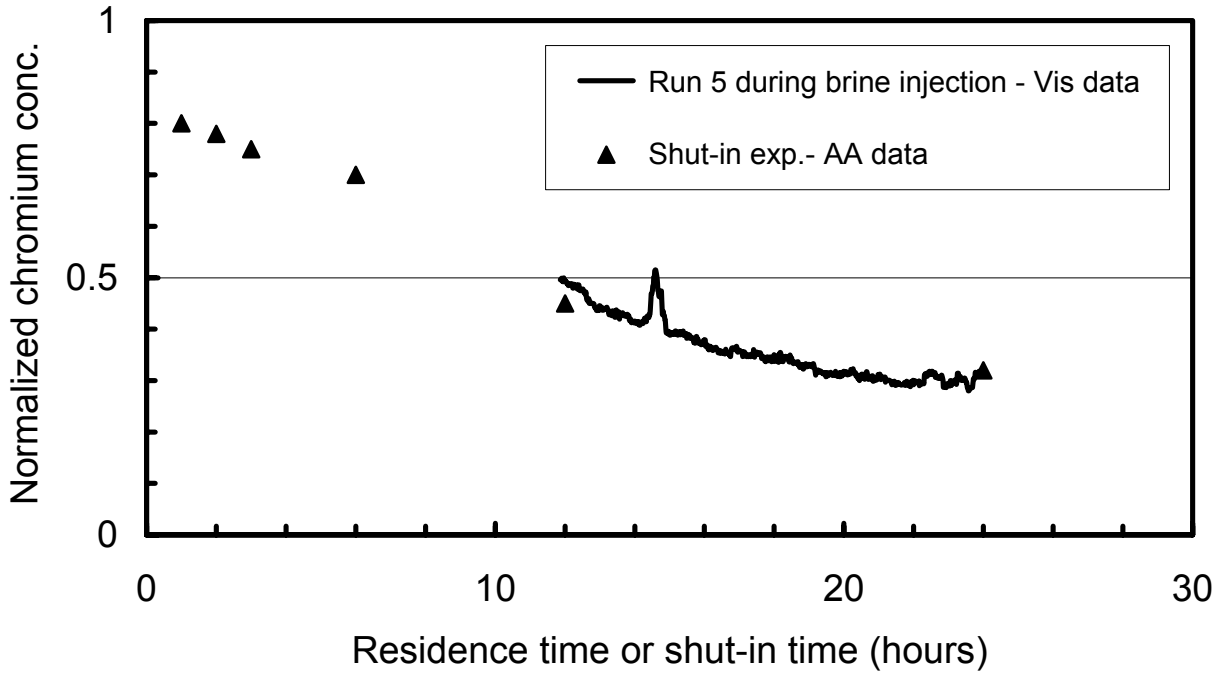

Figure 4.10 – Comparison between the results of the shut-in experiments and the data obtained during the brine injection after Run 5 (Figure 9); 0% KCl.

Nomenclature

$C^*_{t'} = \dfrac{C_{t'} - C_{eq}}{C_0 - C_{eq}}$ = Dimensionless chromium conc.

$C_{t'}$ = Chromium concentration at time t′, ppm

C_{eq} = Calculated chromium concentration at equilibrium using solubility constants of Rai et al.[1987], ppm

C_0 = Chromium concentration at time t′ = 0, ppm

C_{OH^-} = Hydroxide ion concentration, M

C_{OAc^-} = Total acetate concentration, M

β, γ = Fitting parameters, dimensionless.

t' = Time from onset of precipitation (after induction period), min

Acknowledgement

Material in this chapter is substantially unchanged from a copyrighted paper published by the Society of Petroleum Engineers. The paper is in SPE 75159, SPE/DOE Thirteenth Symposium on Improved Oil Recovery, Tulsa, OK April 13-17, 2002 and published in the June 2003 issue of the *SPE Journal*. The SPE copyright release form grants authority to authors the "nonexclusive right to incorporate all or part of the work in future writings or presentations."

References

1. Bryant, S.L., Bartosek, M., and Lockhart, T.P.: "Propagation of Cr(III) in porous media and its effect on polymer gelant performance," *Journal of Petroleum Sciences and Engineering,* **16** (1996) 1-13.
2. Garver, F.J., Sharma, M.M., and Pope, G.A.: "The competition for chromium between Xanthan biopolymer and resident clays in sandstone," paper SPE 19632, presented in 64th Annual Technical Conference and Exhibition, San Antonio, 8-11 Oct. (1989).
3. McCool, C.S., Green, D.W., and Willhite, G.P.: "Fluid-rock interactions between Xanthan-chromium(III) gel polymer systems and dolomite core materials," *SPE Production and Facilities* **15**, 3 (2000) 159-167.
4. Rai, D., Sass B.M., and Moore, D.A., "Chromium(III) hydrolysis constants and solubility of chromium(III) hydroxide," *Inorganic Chemistry* **26** (1987) 345-349.
5. Seright, R.S., "Impact of Permeability and Lithology on Gel Performance," paper SPE/DOE 24190 presented at Eighth Symposium on Enhanced Oil Recovery, Tulsa,OK (22-24 April 1992).
6. Stavland, A., Ersdal, T., Kvanvik, B., and Lohne, A., "Evaluation of xanthan-Cr(III) gels for deep emplacement: retention of Cr(III) in north sea sandstone reservoirs," Seventh European Symposium on Improved Oil Recovery, 27-29 October, Moscow, Russia (1993).
7. Zou, B., McCool, C.S., Green, D.W., and Willhite, G.P., "A study of the chemical interactions between brine solutions and dolomite," *SPE Reservoir Evaluation and Engineering* **3**, 3 (2000a) 209-215.
8. Zou, B., McCool, C.S., Green, D.W., Willhite, G.P., and Michnick, M.J.: "Precipitation of chromium acetate solutions," *SPE Journal,* **5,** 3, (2000b) 324-330.

Appendix

The following describes the calculation of the residence time for the effluent from Core 2 when the fluid was displaced through the core at a two different flow rates. Effluent chromium concentrations were plotted as a function of this resident time in Figure 4.10.

Piston-like displacement of resident fluid with no dispersion was assumed. The following variables were defined.

- t_r: Residence time of chromium(III) solution in the core at a position X during the slow injection of chromium acetate solution. This is equivalent to the time for chromium(III) to travel from entrance of core to position X when the chromium acetate injection rate is Q_1.
- t_e: The time for chromium(III) at position X to be displaced to the end of the core and be detected in the effluent during the fast injection rate for water, Q_2.

Applying material balance concepts, the distance that the chromium(III) solution traveled in the core was expressed as follows:

$$X = Q_1 t_r / (A\varphi) \qquad \text{Eq. A-1}$$

$$L - X = Q_2 t_e / (A\varphi) \qquad \text{Eq. A-2}$$

where

X	=	Distance from the inlet at the time water was injected, cm,
Q_1	=	Injection rate for chromium solution, 0.02 mL/min,
Q_2	=	Injection rate for water, 1.00 mL/min,
A	=	Cross-sectional area of core, cm^2,
V_0	=	Pore volume of the dolomite Core 2, cm^3, $V_0 = A\varphi L$,
L	=	Total length of core; cm,
Φ	=	Porosity of core, fraction.

Adding Equations A-1 and A-2 gives:

$$A\varphi L = V_0 = Q_1 t_r + Q_2 t_e \qquad \text{Eq. A-3}$$

Rearranging Equation A-3 gives:

$$t_r = (V_0 - Q_2 t_e) / Q_1 \qquad \text{Eq. A-4}$$

Equation A-4 was used to estimate the residence time for chromium(III) in the dolomite core at position X before water was injected to displace chromium(III) acetate solution in the core.

Chapter 5

Pressure Distribution in and Fluid Displacement ThroughGels in Tubes

Graduate Research Assistant: Xiaofang Suo
Research Associates: Somenath Ganguly and Michael Michnick

Introduction

Gelled polymer treatments are applied in oil reservoirs to improve fluid flow characteristics such that oil production is increased and/or water production is reduced. After placement, the gel is subjected to pressure gradients by flows of oil and water. Injected water imparts a pressure gradient on the gel after placement in an injection well. In applications adjacent to a production well, both oil and water flowing to the well subject the gel to a pressure gradient. Pressure gradients imparted by water and/or oil will eventually create flow paths through the gel that is placed in fractures and/or matrix rock. The development of flow paths through gels affects the persistence of a gel treatment and provides conduits for oil production.

The objectives of this study were to identify phenomena/mechanisms that occur when confined gels are subjected to a pressure gradient and to determine the effect of critical parameters on those mechanisms. This was accomplished by using water and oil to pressurize one end of a tube in which a gelant was placed and allowed to mature. Three general types of experiments were conducted. In Failure Pressure Experiments, the outlet of the tube was open to atmosphere and the pressure of the oil or water at the inlet was increased until the gel failed and flow was established. In Pressure Distribution Experiments, the pressure of the oil or water at the inlet was held constant for a period of time at a value less than the failure pressure and the outlet was either open or closed. Pressure distribution along the gel was measured and fluid movement was monitored when the outlet was open. A third type of experiment was conducted to determine the permeability of a gel to brine flow.

Experimental Materials, Equipment and Procedures

Gel System

Experiments were conducted with a gel system composed of polyacrylamide and chromium acetate. Gelants were prepared by mixing a stock polymer solution and a stock chromium solution in a 3:1 weight ratio. The polymer solution was prepared from Alcoflood 935 (Ciba Specialty Chemicals, Lots 7158Vand 3243A) and contained potassium chloride salt. Solid polymer beads were added to a salt solution and stirred slowly for 24 hours before gelant preparation. The chromium solution was prepared from a 50% chromium-acetate solution (McGean-Rohco, Inc., Lot. 40014806) just prior to gelant mixing. A typical gelant contained 7500 ppm polymer, 150 ppm chromium (661 ppm chromium triacetate) and 1% KCl. The initial pH of this gelant composition was about 4.8 and was adjusted to a pH of 5.0 using potassium hydroxide immediately after mixing. The gel time was approximately 15 hours at room temperature (about 22^{o}C). The gel time was determined by measuring viscosity of a gelant sample as a function of time and was defined as the time when the viscosity increased to a value of 200 cp. Other compositions for gelants were used and are identified in the text and figures.

Compositions were adjusted to give similar gel times for different lots of polymer. Gel times for all gelant compositions ranged from 12 to 23 hours.

Failure Pressure Experiments

A schematic of equipment used to determine failure pressure is shown in Figure 5.1. Pressure at the inlet of the gel-filled tube was increased with time by injecting oil or water with a positive-displacement pump. An air filled reservoir was connected to the injection system in some runs to slow the pressure increase and to provide increased flow capacity after the maximum, or rupture, pressure occurred. In other runs, the air reservoir was not used and the injection flow rate was held constant. Pressure at the inlet of the tube increased steadily with time until failure occurred after an elapsed time between 4 and 15 minutes.

Gels were placed in tubes constructed of several materials. Glass tubes and a portion of the polypropylene tubes were pretreated before use. Glass tubes were washed with chromic acid and then water. Polypropylene tubes were used as received and after being washed with acetone and water and then dried. Other tube types were used as received. Four to ten tube-volumes of gelant were displaced through a tube, the tube was sealed and the gelant was allowed to mature for a period of time. The failure pressure experiments were conducted at room temperature, about 22°C.

Pressure Distribution Experiments

The equipment setup for pressure-distribution experiments that used oil as the pressurizing fluid in 6-foot long tubes is shown in Figure 5.2(a). An additional section was added for 8-foot long tubes. A QUIZIX QL-700 pump was used to apply mineral oil (viscosity 39 cP) at constant pressure to the gel tube system. The 6-foot long tube was divided into four 2-foot long sections that were separated by tee fittings. The gel tube outlet was closed or opened and placed in a beaker of 1% KCl brine to prevent evaporation of the solvent from the gel. The pressure of the gel was measured at several positions along the tube using pressure transducers that were hydraulically connected to the tube with mineral oil. The gel tube was place in a constant-temperature water bath and the pump and pressure measuring equipment in a constant-temperature air bath, both at 30°C.

The equipment setup for the experiment using brine to exert pressure on a gel in a 5-foot long tube is shown in Figure 5.2(b). A transfer vessel containing brine was connected to the gel tube. The headspace of the transfer vessel was pressurized with nitrogen gas. Pressures were measured as described above.

Gel Permeability Experiments

The experimental setup to determine the permeabilities of the bulk gel and the filter cake, which formed during the flow experiment, is shown in Figure 5.3. The ID of the tube was 1 cm. Brine was flowed through the gel, filter cake and constraining Teflon frit in series. Pressure drops were measured across the bulk gel (three pressure ports) and across the entire system. Several hours were required for the system to reach steady state due to the dehydration of the gel and development of a filter cake.

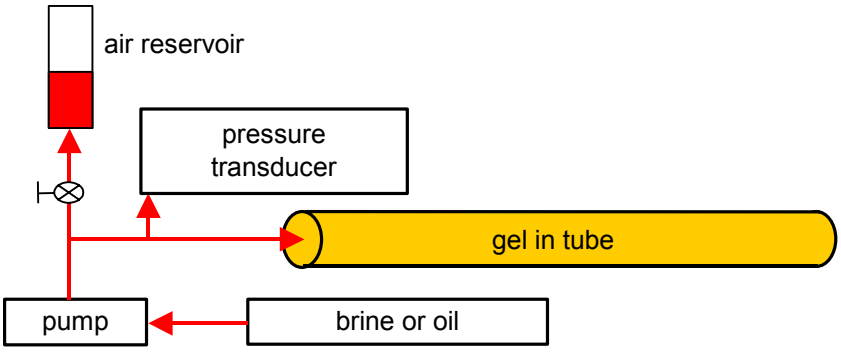

Figure 5.1 – Diagram of experimental apparatus for measurement of rupture pressure.

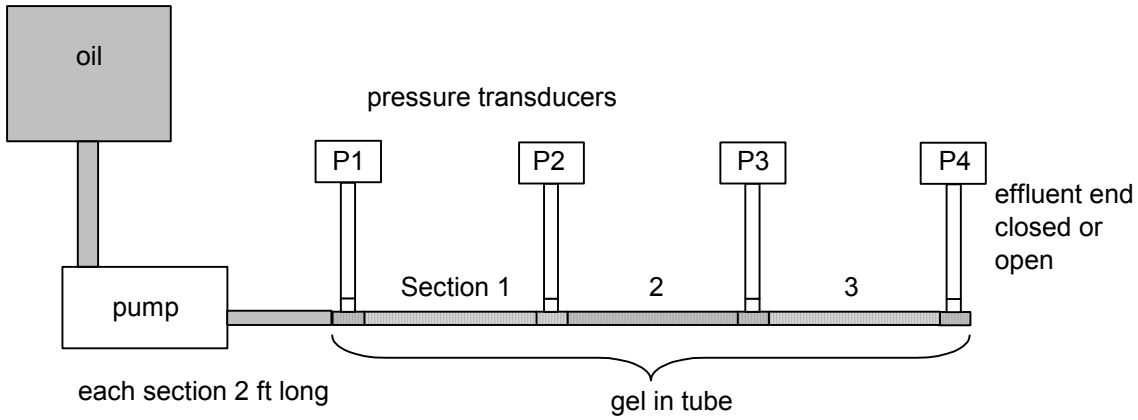

(a) oil as pressurizing fluid.

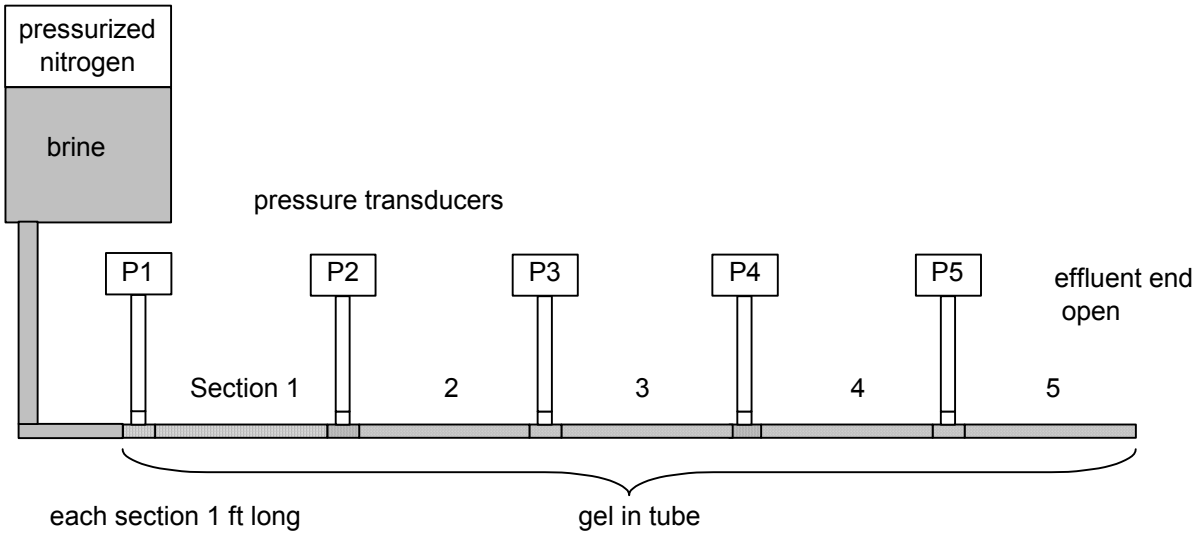

(b) brine as pressurizing fluid.

Figure 5.2 – Diagrams of apparatus for pressure distribution experiments.

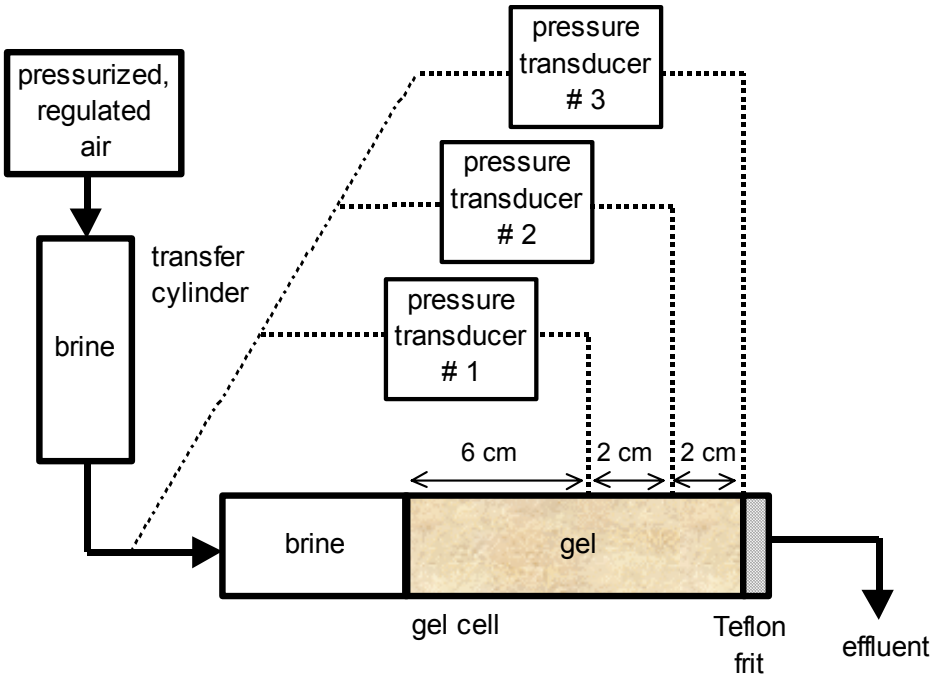

Figure 5.3 – Diagram of apparatus for gel permeability experiments.

Results and Discussion

Failure Pressure Experiments

Parameters investigated to determine their effect on failure pressure were the tube material and pre-treatment of the tube, inside diameter and length of the tube, gel age and injection rate, flow capacity and type of the pressurizing fluid. Examples of the pressure behavior are shown in Figure 5.4 for runs conducted in glass and polypropylene tubes. The pressures increased to a maximum and then decreased rapidly when the gel failed. Failure pressure was defined as the maximum pressure.

Two general types of gel failure were observed during the tests that depended on tube type and possibly the injection system. The two types of failures were termed *center-rupture* and *wall-rupture*. Center-rupture occurred when the injection fluid created a path down the centerline of the gel. Oil or water that was injected following rupture flowed through a path in the center of the gel. The gel-tube bond was intact and a sizeable portion of the gel remained in the tube. Wall-rupture occurred when the gel detached from the tube and a significant amount of the gel was displaced from the tube with continued injection.

A constant flow-rate injection system and a high-capacity injection system, that utilized the air reservoir, were used for the failure pressure experiments (see Figure 5.1). Results are presented for each injection system separately. Lines on the figures that present the results represent least-squares regressions of the rupture pressures as a function of the abscissa value.

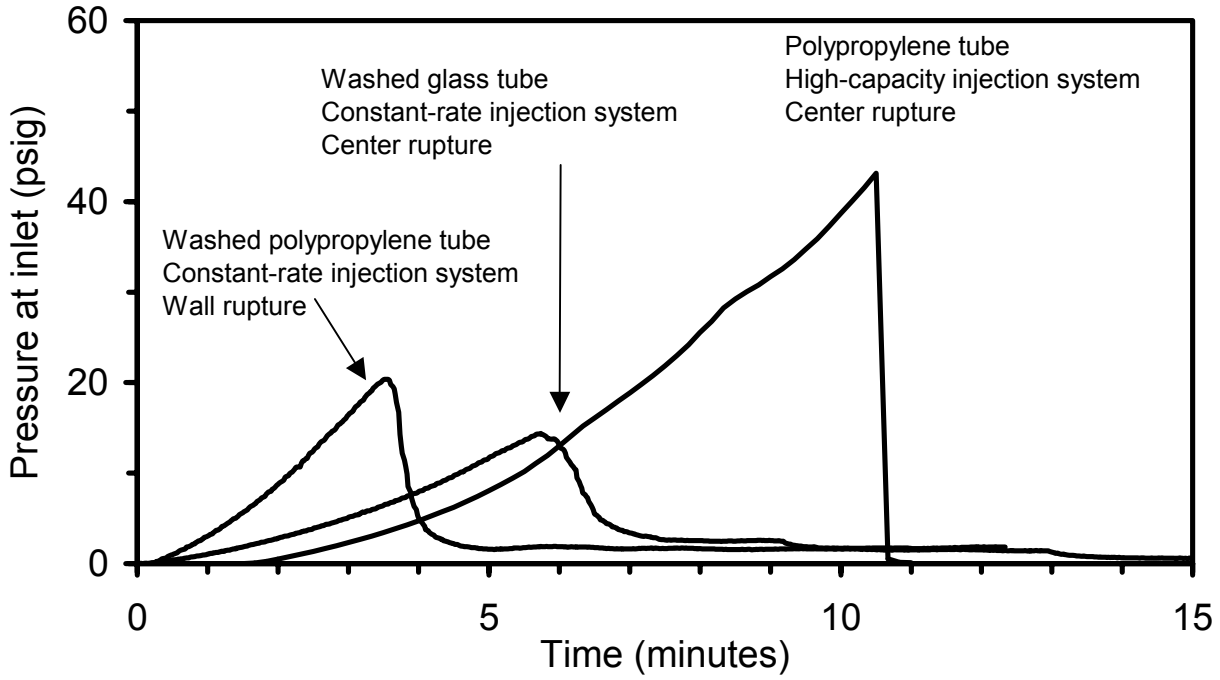

Figure 5.4 – Examples of pressure behavior during rupture pressure experiments.

High-capacity injection system. Center-rupture always occurred in experiments that utilized the high-capacity injection system. The injected fluid fingered rapidly through the gel and inflated a gel balloon out the end of the tube until the balloon burst. The rapid displacement of oil/brine through the gel tube after rupture (high flow capacity) was caused by the expansion of the air and displacement of oil/brine that had accumulated in the reservoir.

Rupture pressures (center-rupture) that were measured with the air reservoir in the injection system were measured in unwashed polypropylene (Batch A) and nylon tubes. Rupture pressures in 0.188-inch ID polypropylene tubes using oil and brine as the injection fluid are plotted as a function of tube length in Figure 5.5. Rupture pressures increased with tube length and no significant differences were observed between oil and water as the injection fluid. A series of runs was conducted in polypropylene tubes over a range of internal diameters and lengths. The rupture pressures increased linearly and correlated with a ratio of the length-to-diameter as shown in Figure 5.6. A similar correlation was obtained for runs conducted in nylon tubes as shown in Figure 5.7. The amount of time the gel was allowed to mature, or age, in nylon tubes increased the rupture pressure at a given length-to-diameter ratio as shown in Figure 5.8. Rupture pressures were much higher for gels aged three weeks in comparison to gels aged four days.

Constant flow-rate injection system. The constant flow-rate injection system, without the air reservoir, was used to measure rupture pressures in glass, polypropylene (Batch B) and 890 Teflon FEP (fluorinated ethylene propylene) tubes. Rupture pressures for runs conducted in unwashed polypropylene and FEP tubes varied widely at the same experimental conditions.

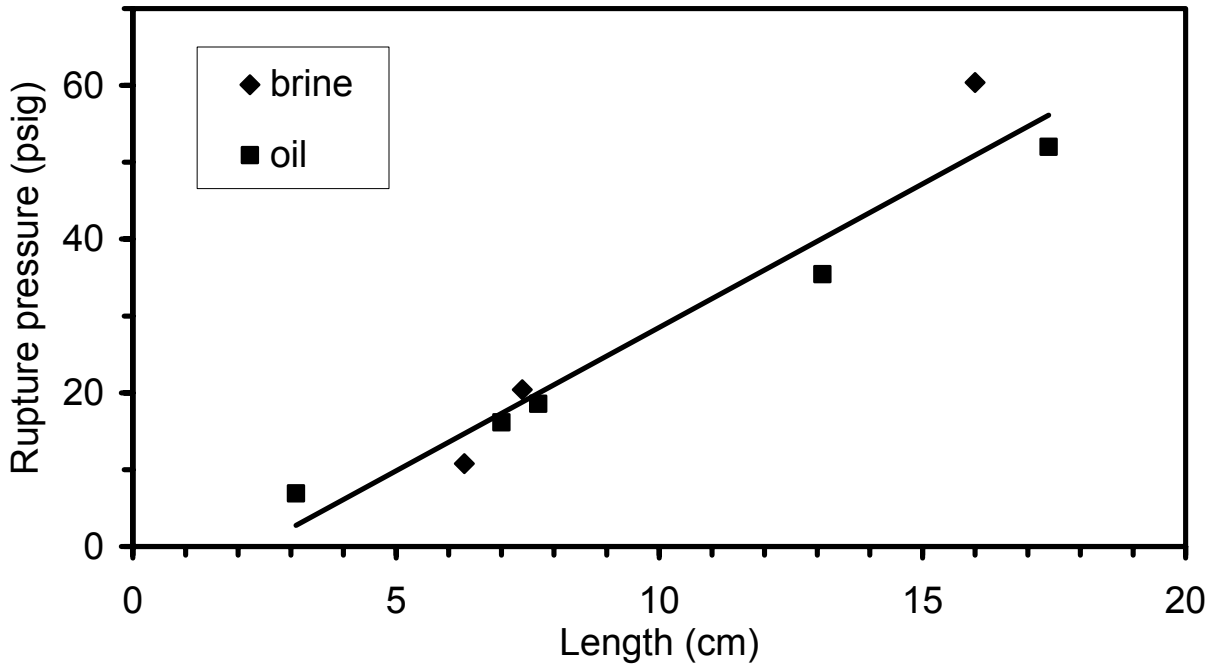

Figure 5.5 – Rupture pressure as a function of length in 0.188-inch ID polypropylene tubes; High-capacity injection system using oil and brine; 7500 ppm polymer, 150 ppm Cr, 1.0% KCl, pH=5.0, gel time = 15 hours; Gel was aged one month.

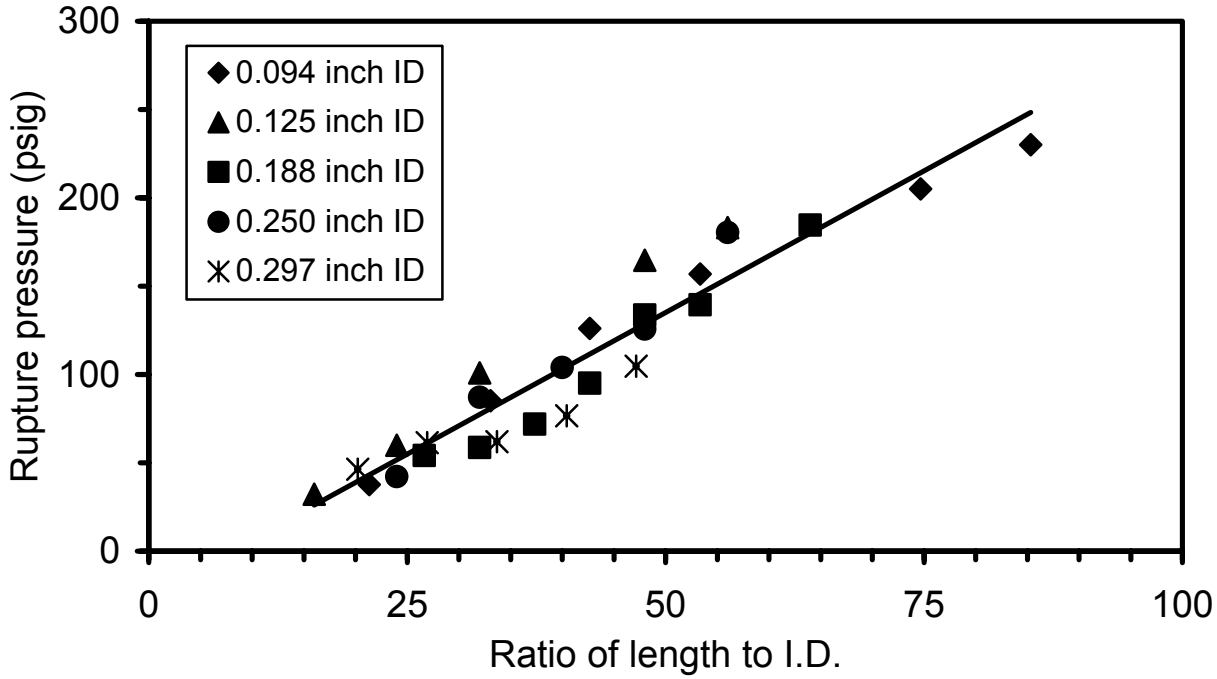

Figure 5.6 – Rupture pressure as a function of length-to-diameter ratio in polypropylene tubes; High-capacity injection system using brine; 7500 ppm polymer, 94 ppm Cr, 1.0% KCl, pH=5.0, gel time = 12 hours; Gel was aged 6 to 8 days.

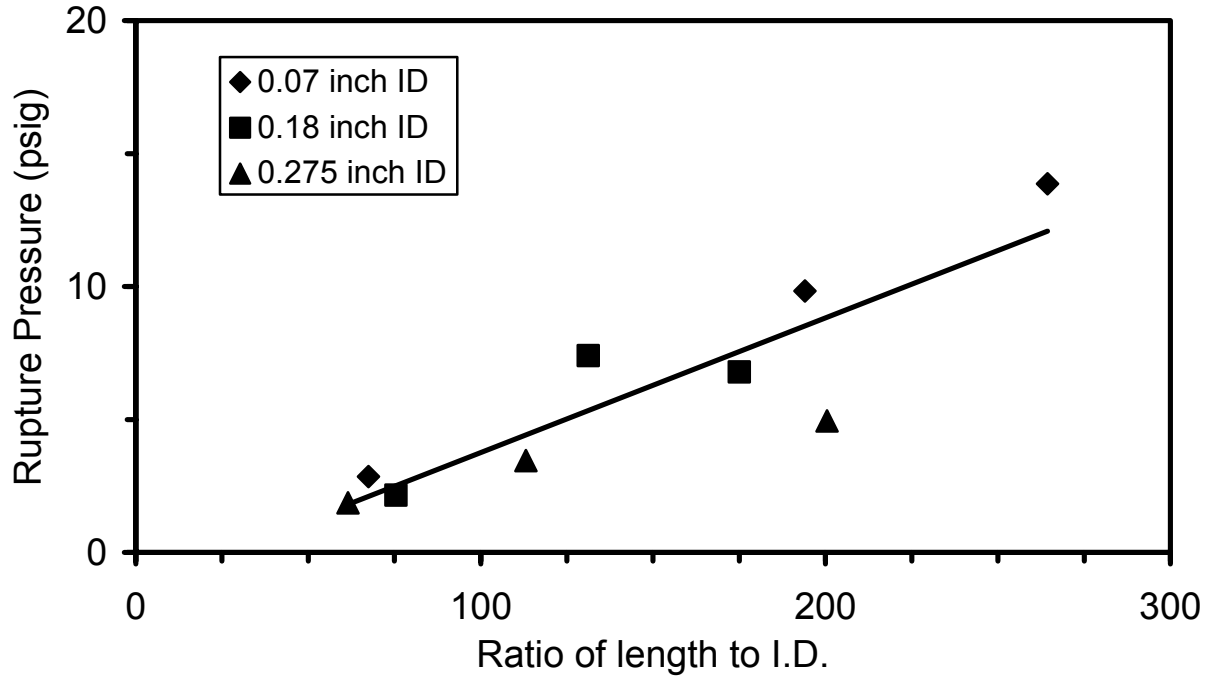

Figure 5.7 – Rupture pressure as a function of length-to-diameter ratio in nylon tubes; High-capacity injection system using brine; 6667 ppm polymer, 94 ppm Cr, 1.0% KCl, pH=5.0, gel time = 12 hours Gel was aged 5 days.

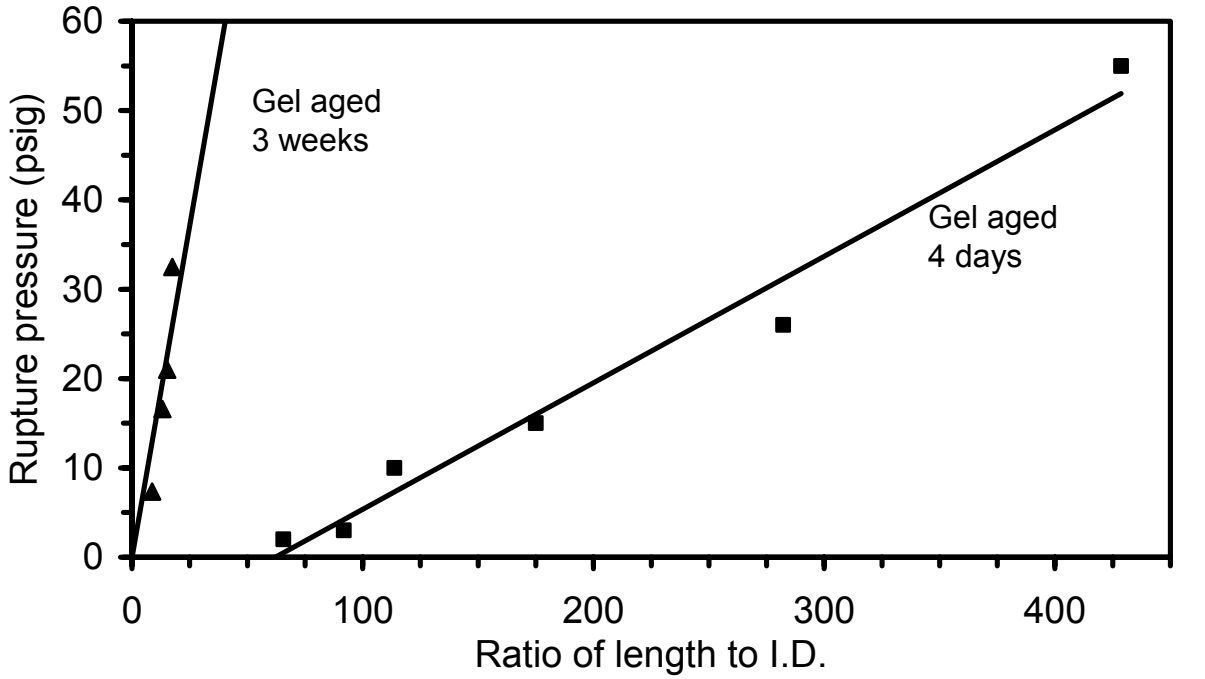

Figure 5.8 – Rupture pressure as a function of length-to-diameter ratio and age in 0.018 inch ID nylon tubes; High-capacity injection system using brine; 5000 ppm polymer, 94 ppm Cr, 1.0% KCl, pH=5.0, gel time = 12 hours.

Varied surface properties of the tubes were suspected as the cause. The results of these runs can be found elsewhere [Suo, 2002]. Runs in washed glass and washed polypropylene tubes were more consistent and a summary of these runs is given in Table 5.1. Oil was the injected fluid in these runs. Movement of oil through the gel after rupture occurred at a slower rate with the constant-rate injection system which allowed observation of the displacement process. Center-rupture occurred in runs conducted with glass tubes and wall-rupture occurred in runs conducted in the polypropylene and FEP tubes.

Table 5.1 – Summary of rupture pressure experiments using the constant flow-rate injection system and washed polypropylene and glass tubes.

Tube material	Tube ID (inch)	Gel age (days)	Oil flux (mL/min/cm^2)	Tube length (ft)	Times Repeated*
polypropylene	0.1875	11	0.224	1	3
	0.1875	11	0.224	2, 3, 4	3, 3, 2
	0.1875	21	0.224	1, 2	4, 3
	0.1875	32	0.224	1, 2, 3, 4	4, 3, 3, 2
	0.1875	42	0.224	1, 2, 3, 4	5, 3, 3,3
	0.0937	11	0.224	1, 3, 4	3, 3, 2
	0.0937	21	0.224	1, 2	4, 3
	0.0937	32	0.224	1, 2, 3, 4	3, 3, 3, 3
	0.0937	42	0.224	1, 2, 3, 4	2, 3, 3, 2
	0.1875	20	0.0561, 0.449	2	2, 2
glass	0.151	11	0.173	2, 4	4, 3
	0.254		0.173	1, 2, 4	2, 2, 2
	0.151		0.043, 0.086, 0.173	1	2, 2, 2
	0.151		0.346, 0.69, 1.39	1	2, 2, 2
	0.151		2.77, 11.1	1	2, 1

* Repeated runs at same tube length or at same oil flux.

Displacement of oil through the gel in glass tubes occurred as a center-rupture. A finger of oil formed in the center of the gel next to the inlet. The finger grew in diameter and then suddenly penetrated a short distance, usually a few centimeters, at the rupture pressure. The oil drop would usually have an hourglass shape after the rupture occurred and the front of the drop would move backwards to the original neck position of the hourglass, displacing gel forward. Further displacement down the center of the gel continued at a lower pressure drop as shown in Figure 5.4. Movement of the oil drops through the gel most often occurred by a snap-off process. Small drops of oil would snap off at the front of the oil drop and penetrated the gel ahead where they would coalesce into another large oil drop. The snap-off and coalesce process repeated down the center of the gel until oil reached the end of the tube.

Rupture pressures were measured for gels in glass tubes having two diameters and lengths of 1, 2 and 4 feet. The injected oil flux was the same for each diameter. The rupture pressures correlated with the length-to-diameter ratio as shown in Figure 5.9. A series of runs was also conducted in the 0.151-inch ID glass tubes at several values of oil flux. The rupture pressure increased significantly with oil flux below about 1 mL/min/cm^2, and above that value, the rupture pressure increased slightly with injected oil flux as shown in Figure 5.10.

Gel failures in the washed polypropylene tubes (Batch B) were complex, not as uniform and occurred at positions next to the tube wall. A thin oil film formed along the tube wall or an oil drop penetrated the center of the gel structure during the initial pressure increase up to the rupture pressure. The thin oil film broke the adhesion between the gel and the tube wall and large segments gel were displaced from the tube with continued oil injection. In cases where the oil initially penetrated the gel at the inlet, the tail of the oil drop was distorted and touched the tube wall. The maximum pressure (rupture pressure) occurred when the oil drop in the center of the gel moved to a thin film along the tube wall, breaking the adhesion between the gel and tube wall. Continued oil injection displaced most of the gel from the tube.

The behavior described in the proceeding paragraph (Batch B tubes) was different than that observed in polypropylene tubes (Batch A) using the high-capacity injection system where center-rupture occurred with injection of oil or brine. The polypropylene tubes used for the two injection systems were purchased at different times. A comparison of the rupture pressures for the two cases at similar conditions is shown in Figure 5.11. The adhesion between the gel and the tube was much stronger in the experiments using the high-capacity injection system, probably caused by different surface properties of the different batches of tubing or possibly an effect caused by the different injection systems.

Runs were conducted in washed polypropylene tubes (Batch B) as a function of gel age, tube diameter and length, and injected oil flux (Table 5.1) The series of runs conducted at the same injected oil flux of 0.224 mL/min/cm^2 was correlated with length-to-diameter ratio and gel age. Rupture pressures increased linearly with length-to-diameter ratio as shown in Figure 5.12 for gels that were allowed to mature in the tube for 11 days. Similar results are shown in Figures 5.13, 5.14 and 5.15 for gels with ages of 21, 32 and 42 days, respectively. Rupture pressures increased moderately with age at a given length-to diameter ratio as shown in Figure 5.16.The effect of injected oil flux on the rupture pressure in washed polypropylene tubes is shown in Figure 5.17. Rupture pressures increased with oil flux over the limited range of fluxes that were tested.

Pressure Distribution Experiments

Experiments were conducted to determine the pressure distribution along a gel confined in a tube when one end of the tube (inlet) was subjected to a pressurized fluid. Runs were conducted with the other end of the tube (outlet) either closed or opened to atmospheric pressure. Pressures were measured at positions along the length of the gel for both closed and opened outlets. Fluid displacements occurred and were monitored for runs conducted with the tube outlet open.

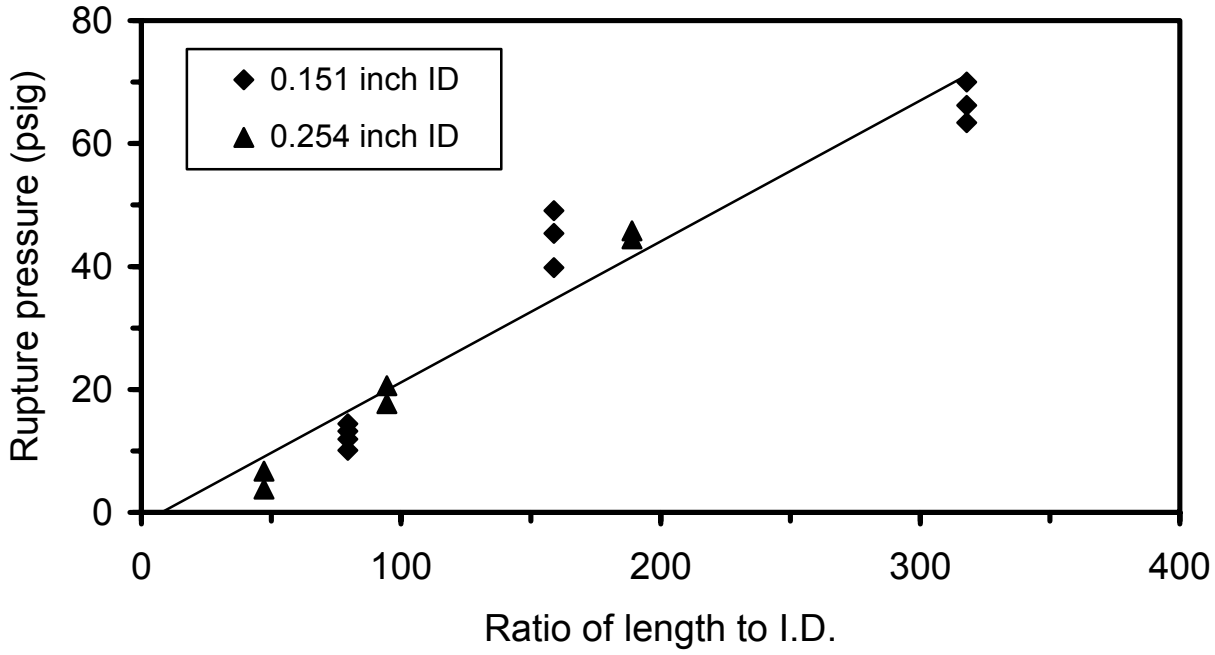

Figure 5.9 – Rupture pressure as a function of length-to-diameter ratio in glass tubes; Constant flow-rate injection system.

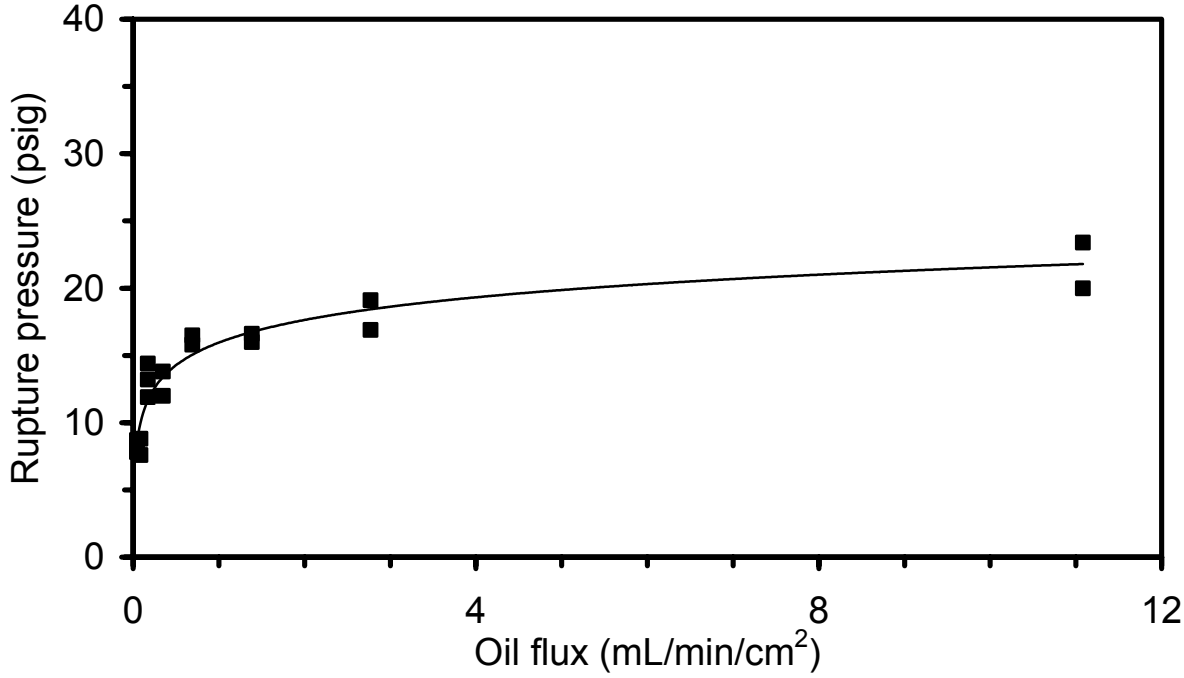

Figure 5.10 – Rupture pressure as a function of oil flux in glass tubes; Constant flow-rate injection system.

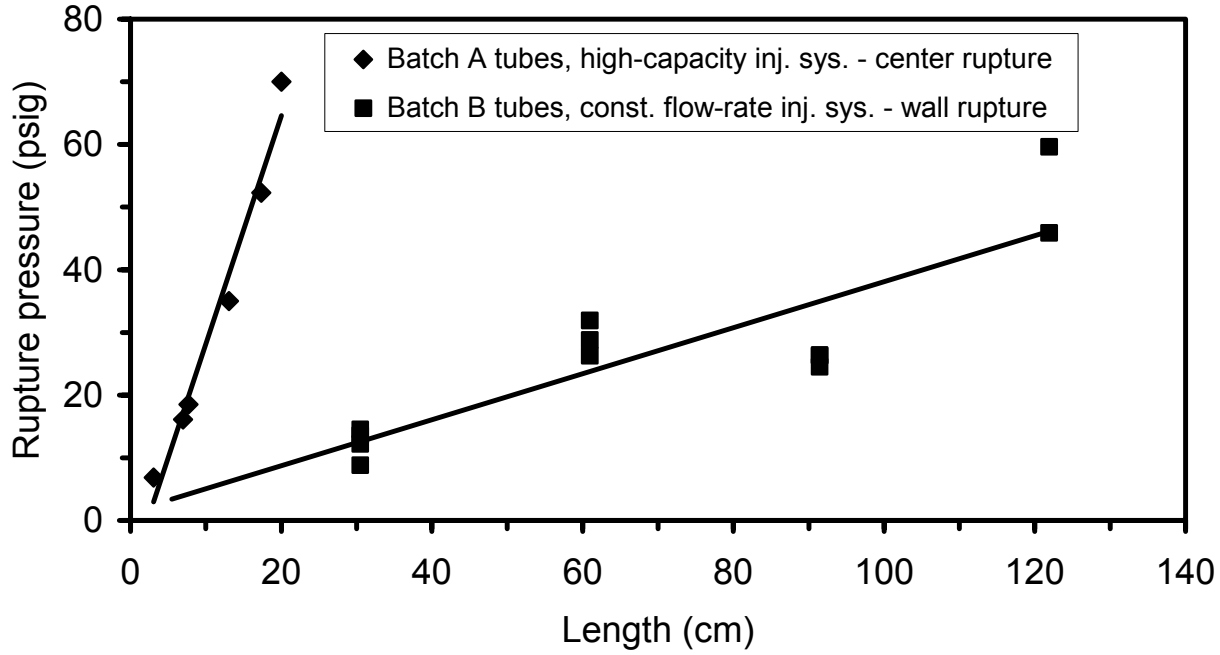

Figure 5.11 – Comparison of rupture pressures for different injection systems and different batches of polypropylene tubes.

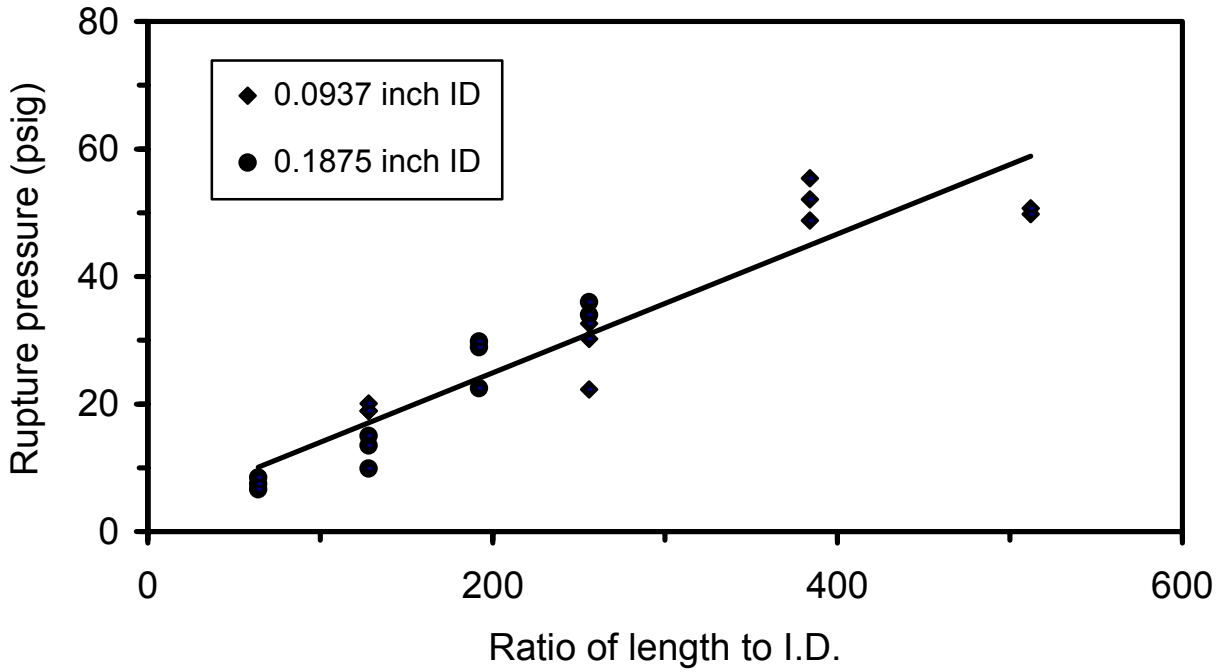

Figure 5.12 – Rupture pressure as a function of length-to diameter ratio in polypropylene tubes; Gel matured for 11 days; Constant flow-rate injection system.

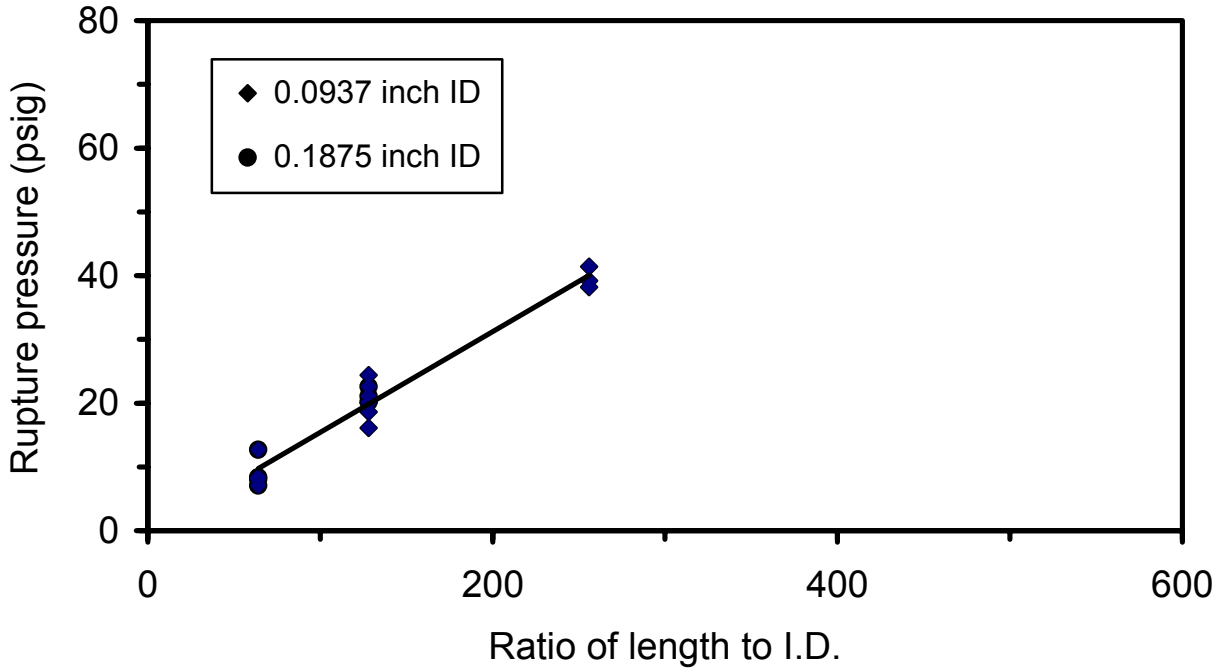

Figure 5.13 – Rupture pressure as a function of length-to diameter ratio in polypropylene tubes; Gel matured for 21 days; Constant flow-rate injection system.

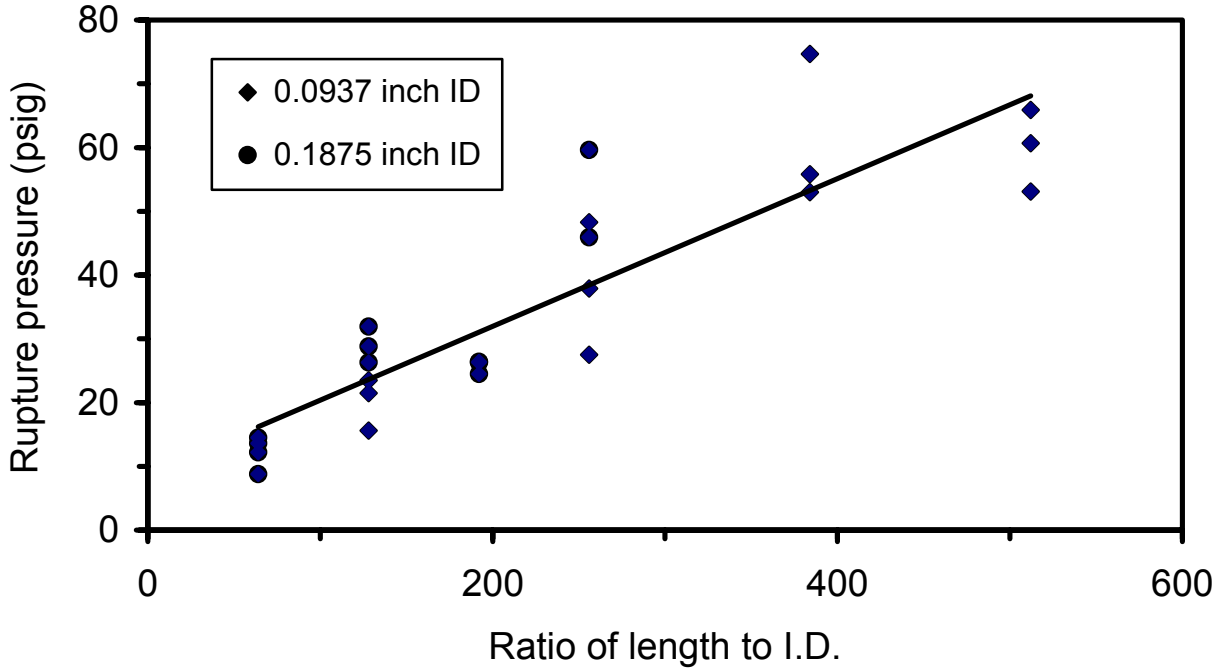

Figure 5.14 – Rupture pressure as a function of length-to diameter ratio in polypropylene tubes; Gel matured for 32 days; Constant flow-rate injection system.

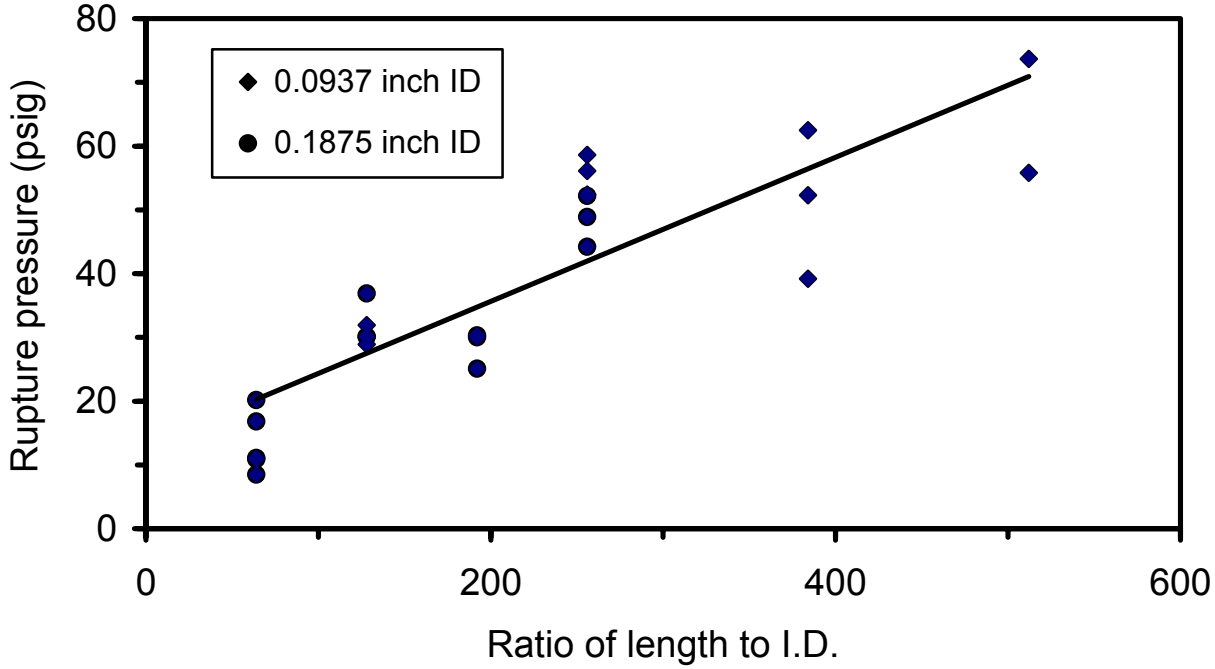

Figure 5.15 – Rupture pressure as a function of length-to diameter ratio in polypropylene tubes; Gel matured for 42 days; Constant flow-rate injection system.

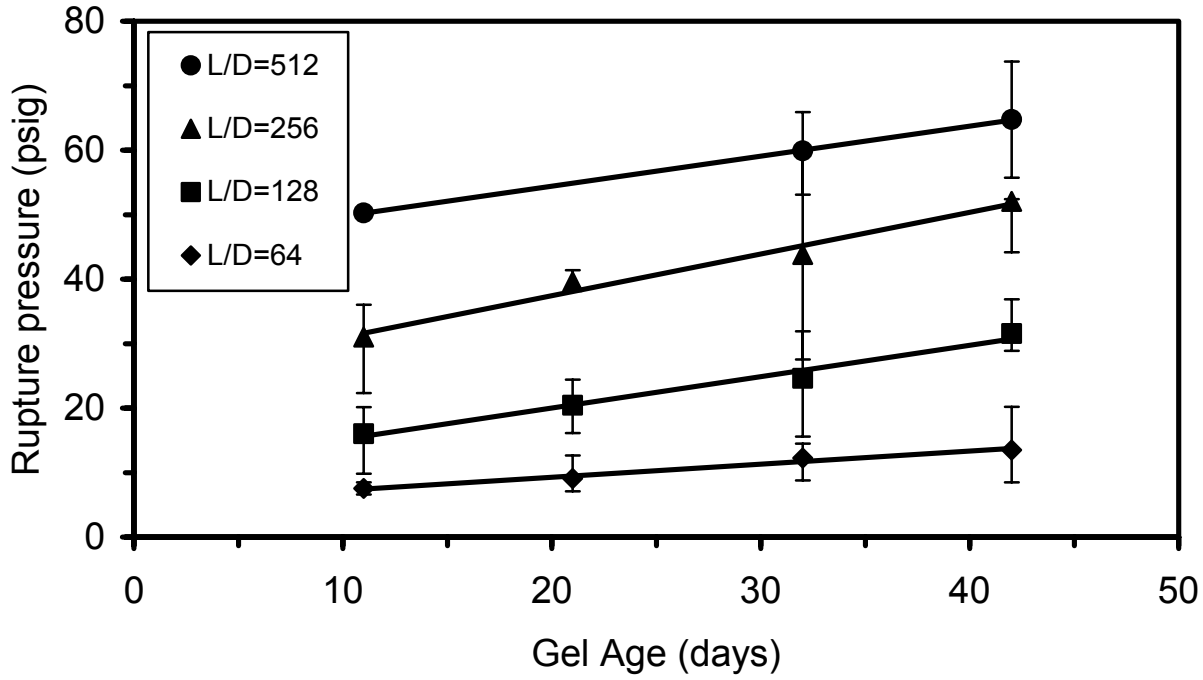

Figure 5.16 – Rupture pressure in polypropylene tubes as a function of gel age and length-to diameter ratio; Constant flow-rate injection system.

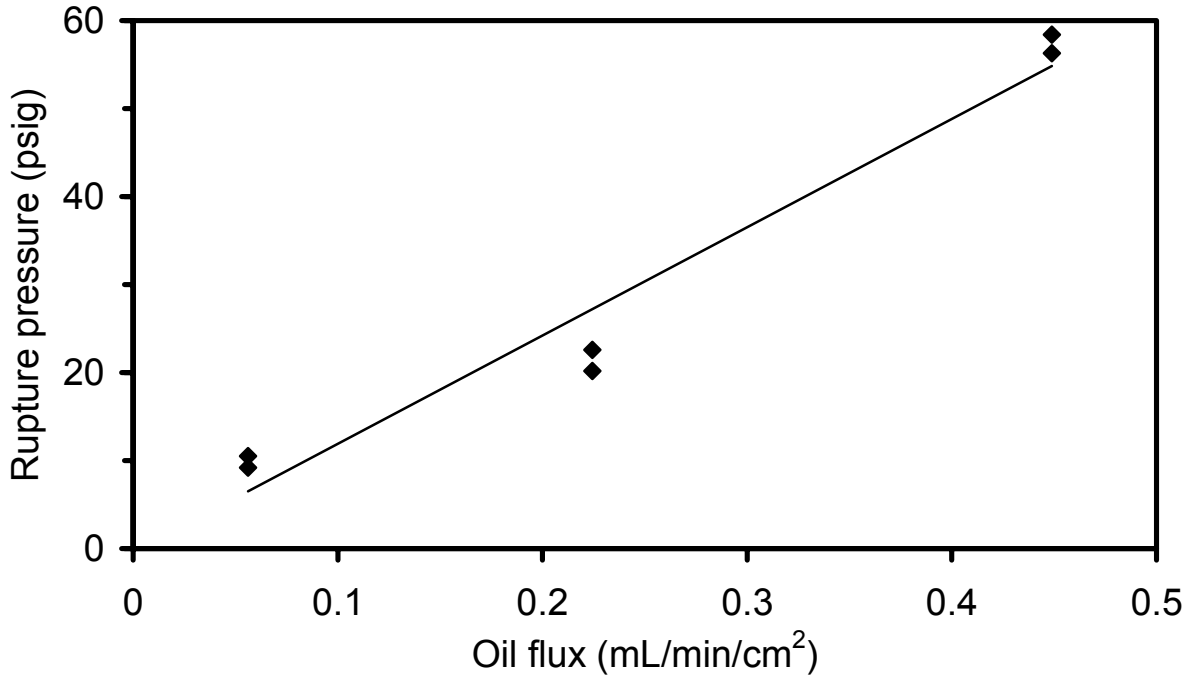

Figure 5.17 – Rupture pressure as a function of oil flux in polypropylene tubes; Constant flow-rate injection system.

Closed outlet. Tube dimensions for runs conducted in closed-end tubes are listed in Table 5.2. Gels were allowed to mature for 5 to 6 days before each run. Pressurized oil at 50 psig was applied to the tube inlet.

Table 5.2 – Tube dimensions for pressure distribution experiments with closed outlets.

Tube #	Tube ID (inches)	Tube length (ft)	Number of sections
C1	0.438	6	3
C2	0.188	6	3
C3	0.0625	8	4

Pressure distributions for the three runs with three different inside diameters are shown in Figures 5.18, 5.19 and 5.20. The extra length of the 0.0625 inch ID tube should not preclude comparisons of the three runs, particularly since little pressure was transmitted to the last section. It is noted that the initial small pressures measured at the down stream ports in the 0.0625 ID tube (Figure 5.20) were the result of the procedure to connect the pressure transducers, which is supported by the fact that the pressures at the 6 and 8 ft positions decreased prior to the influence of the pressurized fluid that increased their values. During each of the experiments, two tests

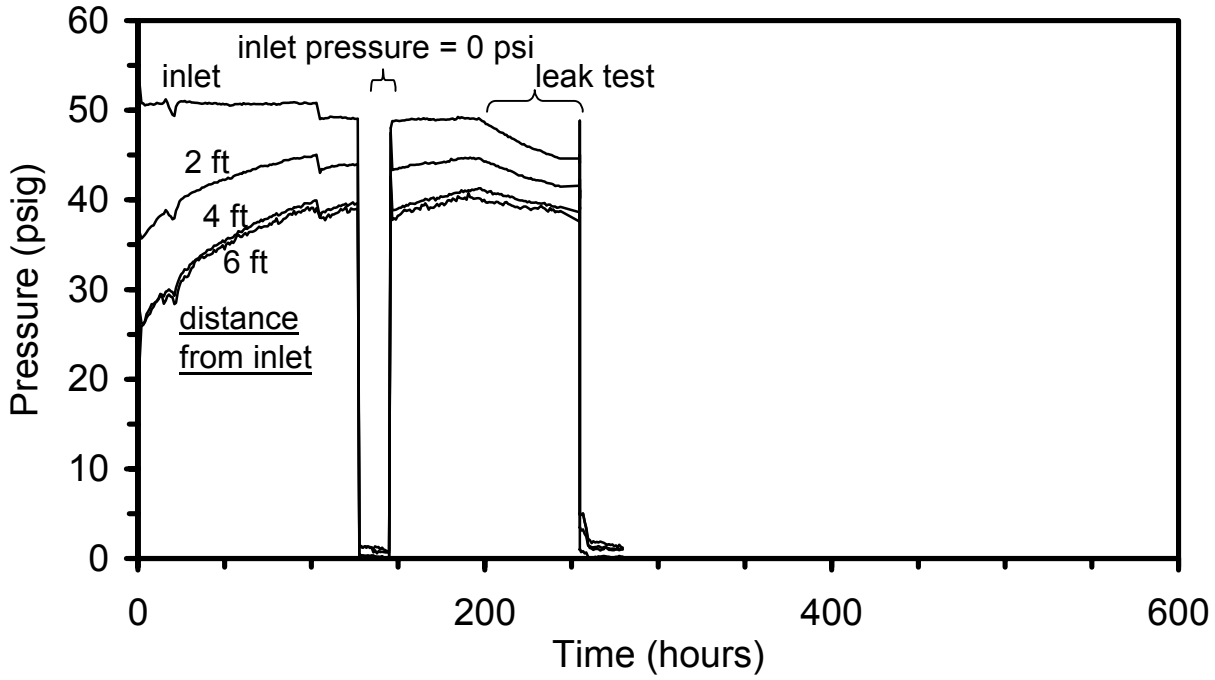

Figure 5.18 – Pressure distributions in Tube C1 (0.438-inch ID) with outlet closed.

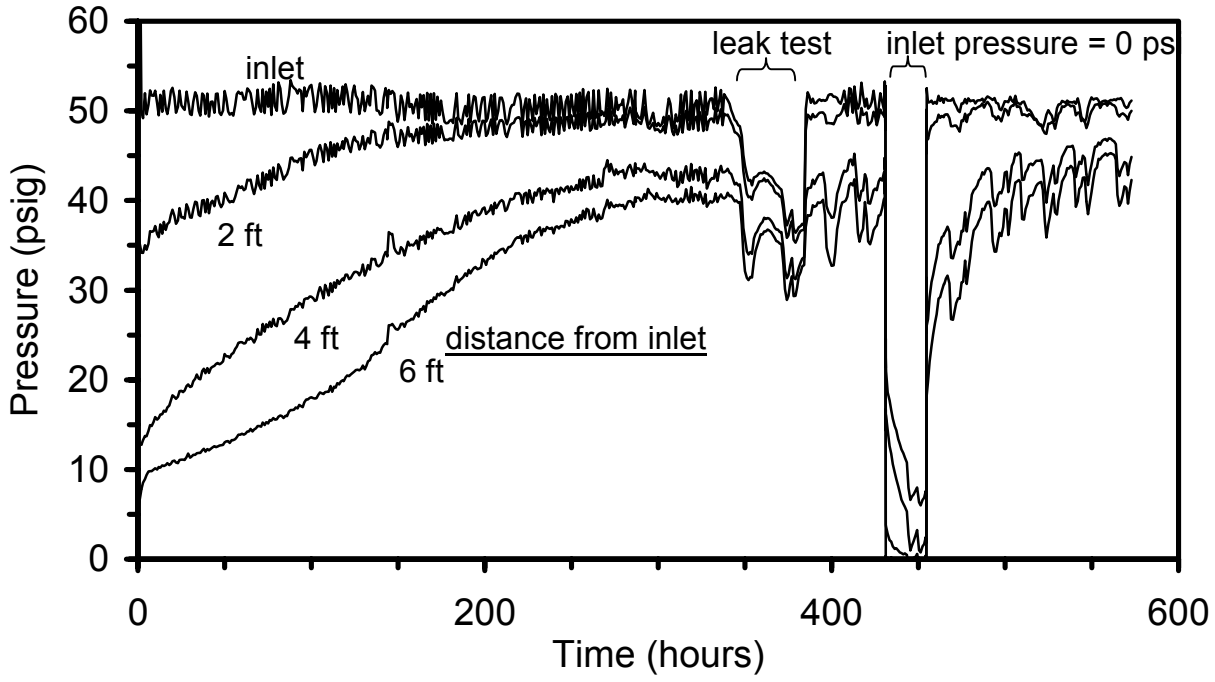

Figure 5.19 – Pressure distributions in Tube C2 (0.188-inch ID) with outlet closed.

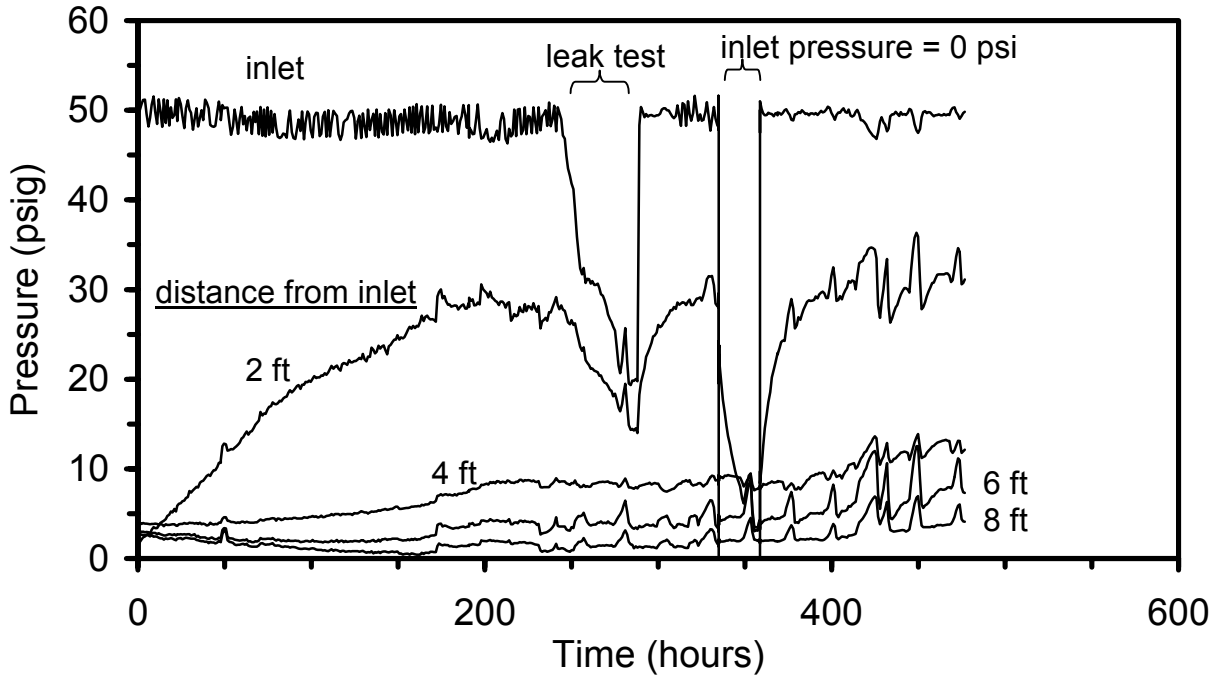

Figure 5.20 – Pressure distributions in Tube C3 (0.0625-inch ID) with outlet closed.

were performed. The inlet valve was closed to test for leaks. Although the pressures decreased to some extent, the leakage was considered negligible for a liquid-filled system. A second test was conducted to observe the pressure responses at downstream positions when the inlet pressure was reduced to 0 psig for a period of time, followed by re-pressurization to 50 psig.

Inspection of Figures 5.18, 5.19 and 5.20 shows a fraction of the inlet pressure was transmitted immediately down the gels confined in the 0.188 and 0.438 ID tubes. The initial pressure transmission at a position down the gel increased with tube diameter. Pressure along the length of the gels increased with time in each of the runs as the gel slowly responded to stress applied at the inlet. Although affected by the leak and 0-psig tests, less than 20% of the inlet pressure was transmitted past 4 feet in the 0.0625 ID tube at 20 days. Pressure transmission was clearly a function of the ID of the tube.

Pressure responses to the reduction of the inlet pressure to 0 psig for a period of time was also a function of the tube ID. Pressures responded quickly to the decrease and increase of inlet pressure in the 0.438 inch ID tube, while negligible response was observed at positions of 4 feet and beyond in the 0.0625-inch ID tube. Pressures increased to the pre-test values faster after the test than after the initial application of 50 psig at time zero, that is, the pre-stressed gel responded quicker to pressure transmission.

Open outlet. Runs were conducted to determine pressure behavior and fluid movements in gels confined in tubes when the inlet was subjected to a pressurized fluid and the outlet of the tube was opened to atmospheric pressure. The runs were exploratory and conducted at various

conditions, some of which are listed in Table 5.3. Oil was the injected fluid in all of the experiments except in Tube 4, where brine was used.

Table 5.3 – Experimental conditions for pressure distribution experiments conducted with the outlet open.

Tube #	Applied pressures (psig)	Tube ID (in)	Tube length (ft)	Number of sections	Section length (ft)
O1	80	0.438	6	3	2
O2	20, 50	0.188	6	3	2
O3	60	0.0625	8	4	2
4	90, 170	0.0625	5	5	1

Runs O1, O2 and O3 were conducted on the same gel tubes that were used for the closed-end experiments described above. The gels were 15 to 30 days old and had been stressed during the closed-end runs. Application of oil at 80 psig in the largest ID tube, O1, exceeded the rupture pressure of the system and resulted in the immediate displacement of most of the gel from the tube. A lower pressure of 20 psig was applied initially to Tube O2 (0.188 inch ID) as shown in Figure 5.21. Part of the inlet pressure was transmitted down the gel immediately followed by an increase and leveling off of the pressure at the position 4 ft from the inlet. During this time, oil penetrated less than an inch into the inlet section with a small protrusion of gel at the outlet. At about 24.5 hours, the inlet pressure was increased to 50 psi and the pressure distribution adjusted as shown in Figure 5.22. At about 25 hours, oil drops quickly moved about a foot into the tube and the pressures measured at 2 and 4 ft down the tube increased abruptly. At about 25.5 hours, the gel ruptured and was displaced from the tube. A small amount of gel was left along the tube wall.

The pressure behavior and fluid movements were more remarkable in the small diameter tube. Pressurized oil at 80 psig was applied at the inlet of the 8-foot long Tube O3 for 270 hours before rupture occurred. A large pressure gradient occurred over a short length of gel and this gradient progressed down the tube a short distance ahead of the injected oil front. The initial applied pressure of 80 psig was confined over the 2-foot long first section as shown Figure 5.23. Pressure at the 2-foot position increased sharply as oil penetrated about 1.5 feet into the gel. Similar behavior occurred downstream at the 4- and 6-foot positions. As the oil front advanced to within about six inches from the pressure port, the pressure would increase abruptly, indicating a large pressure gradient across the gel ahead of the oil front. (A fluctuation of the injection pressure occurred at 118 hours and coincided with the abrupt increase in the pressure at the 6-foot position.) The oil front was at the 5.5 ft position at 118 hours and moved forward gradually towards the 6-foot position over the time period between 118 and 270 hours. The gel ruptured at 270 hours, displacing most of the gel from the tube by a steady flow of oil.

The gel in Tube 4 was not pre-stressed and the injection pressure was applied with red-colored brine. Pressures measured along the five-foot long gel at one-foot intervals are shown in Figure 5.24. A pressure of 90 psig was applied for about 21 hours and then increased to 170 psig for

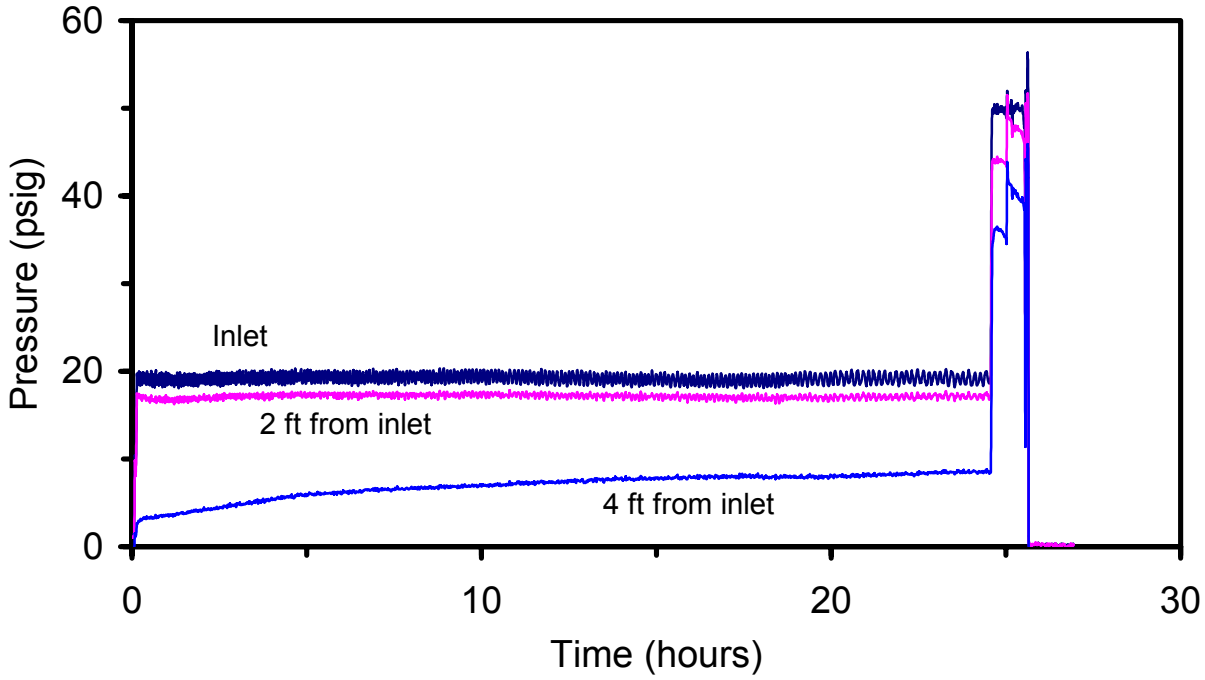

Figure 5.21 – Pressure distributions in Tube O2 (0.188-inch ID) with outlet opened to atmospheric pressure.

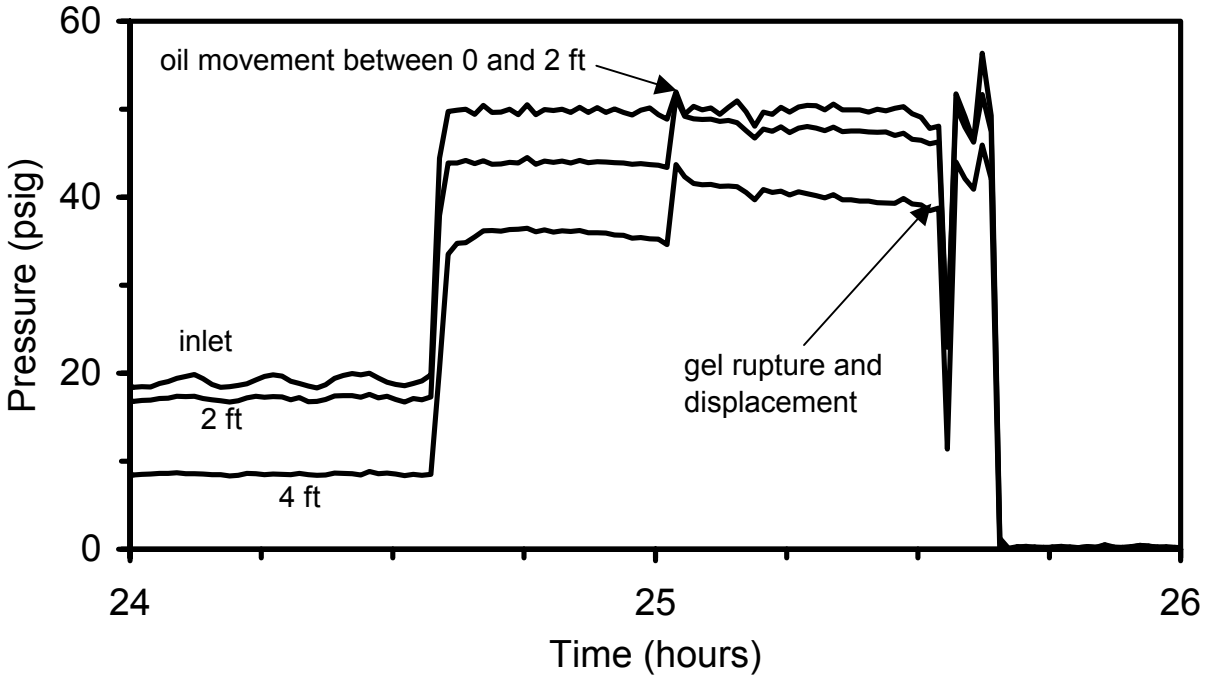

Figure 5.22 – Pressure distributions for two-hour period in Tube O2 (0.188-inch ID) with outlet opened to atmospheric pressure.

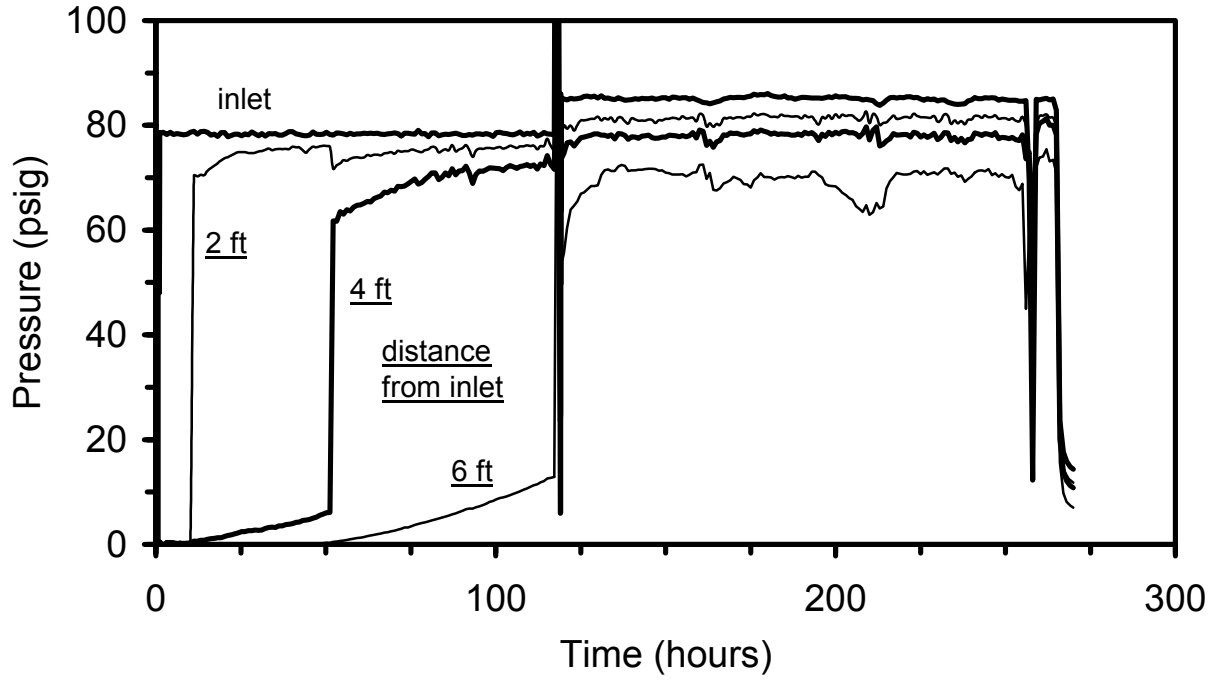

Figure 5.23 – Pressure distributions in Tube O3 (0.0625-inch ID) with outlet opened to atmospheric pressure.

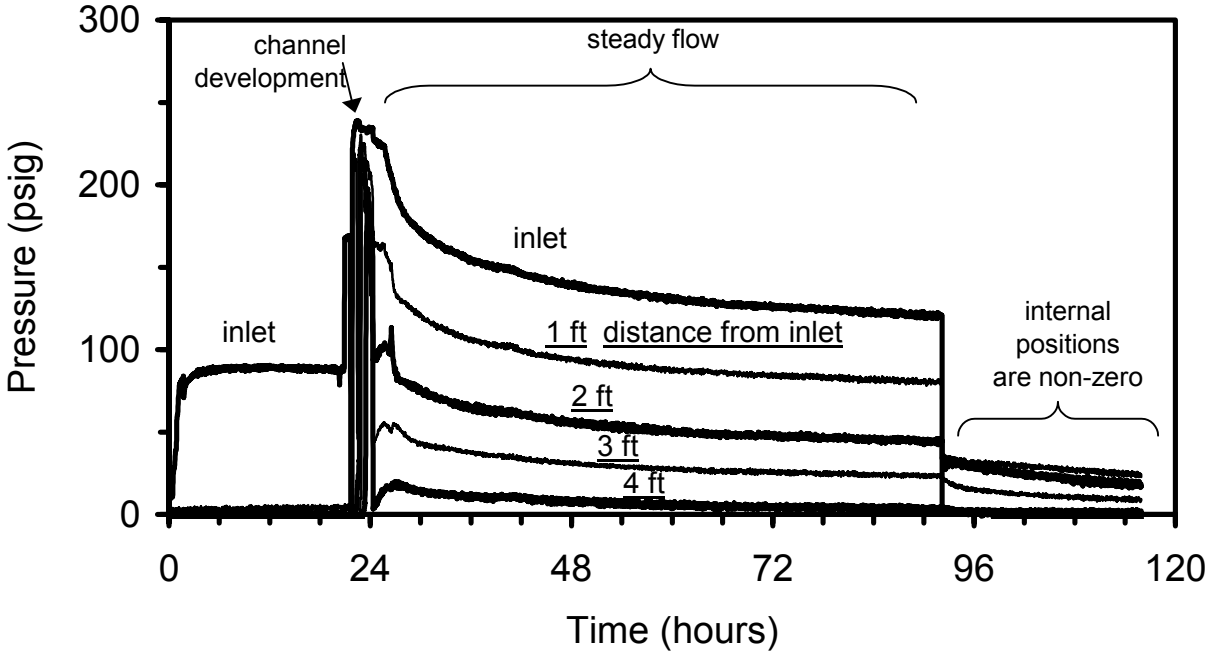

Figure 5.24 – Pressure distributions in Tube 4 (00625-inch ID) with outlet opened to atmospheric pressure; brine was pressurizing fluid.

about 40 minutes. The applied pressure was not transmitted along the gel during the application of these pressures as indicated by the near zero values of the downstream pressures. Brine penetrated about six inches into the gel during this time period. The brine formed a couple of "drops" in the center of the tube, enclosed by gel. The brine was dyed red in order to differentiate between brine and gel. The brine pressure was released for about five minutes (0 psig), followed by a pressurization to 240 psig. Brine penetrated the gel at this pressure and developed a channel through the entire length over the next 75 minutes between 22 and 24 hours. Pressures measured along the gel changed abruptly during channel development. After the channel was formed, brine steadily flowed through the tube at an average flow rate of about 0.7 mL/hr during the time period between 25 and 92 hours (Figure 5.24). An approximately linear pressure gradient along the tube was observed during the steady flow of brine. The applied pressure decreased during this period as the pressurizing gas in the transfer vessel expanded to displace brine through the tube. At 92 hours, the injection pressure was reduced to zero (no flow) and residual pressures were measured at the internal pressure ports.

The pressure data during the time period when the brine penetrated the gel and developed channels are shown in Figure 5.25. When the pressure on the brine was increased to 240 psig at 21.8 hours, a brine "drop" that was in Section 1 at a six-inch position quickly penetrated and stopped in Section 2. This movement corresponded to the abrupt increase of the pressure at the 1-foot position. The pressure at the one-foot position decreased, possibly due to the gel disrupting the fluid connection to the inlet. Movement of brine drops through the remaining length of the tube correlated with the abrupt increases observed in pressures measured at the 2, 3 and 4-foot positions (Figure 5.25). The furthest penetrating brine drop was about 3 to 5 inches from the each pressure port when the abrupt pressure increase occurred. That is, a significant portion of the pressure drop applied to the tube is localized at a point just ahead of the furthest position that the pressurizing fluid had advanced. The localized pressure gradient in some manner altered the gel structure, which then allowed the pressurizing fluid to advance. This observation may indicate that the length of the gel downstream of this zone may not have a significant influence on the process.

Permeability of Gel to Brine

Results are shown in Table 5.4 for three replicate experiments. Permeability of the 10-micron Teflon frits were measured by injecting brine through the frit at a pressure drop of 50 psi after the flow experiment. The pressure drop across the frit was calculated using the measured flow rate, final permeability of the frit and the dimensions of the frit. The pressure drop across the filter cake was then determined by the difference between the total pressure drop and the pressure drops of the gel and the frit. The permeability of the filter cake was calculated using this pressure drop and the measured flow rate. The permeability of the filter cake was less than one microdarcy.

The permeability of the gel was determined using the pressure drop across two adjacent pressure ports and are shown in Table 5.4. Permeability of the gel made from 7500 ppm AlcoFlood 935 and 300 ppm chromium(III) used in this experiment varied between 0.3 and 0.8 md. The permeability in the gel between the first and second pressure ports was about 10% higher than gel permeability between the second and third transducers.

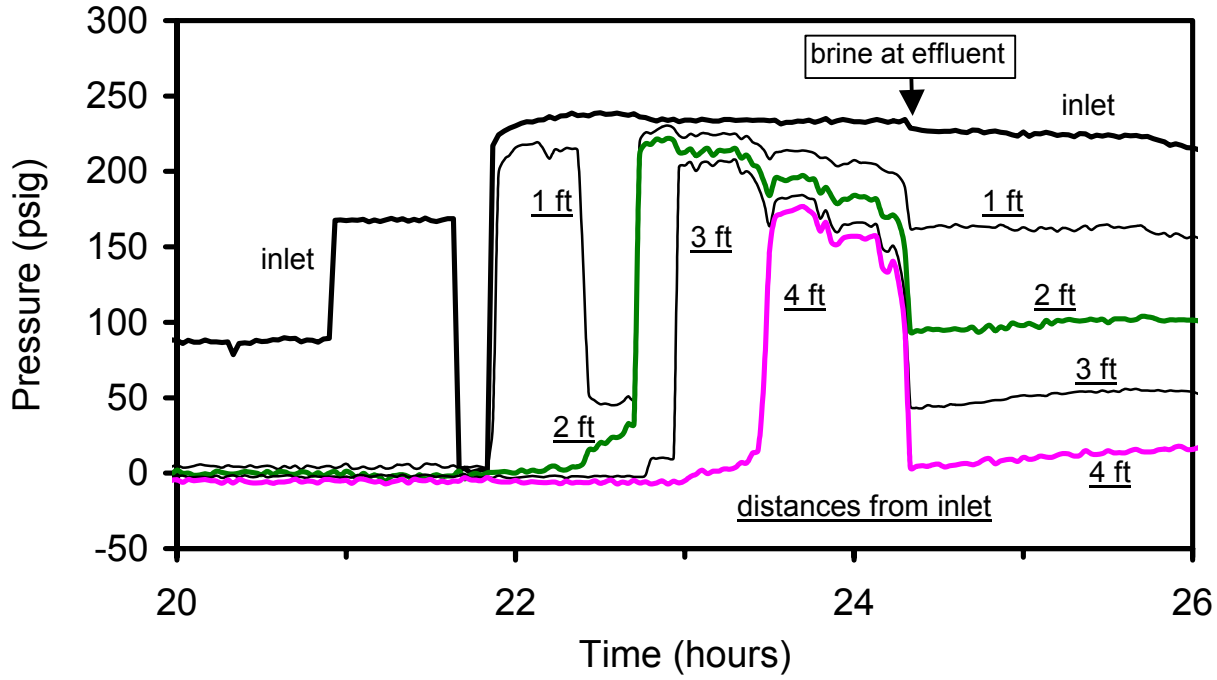

Figure 5.25 – Pressure distributions during channel development in Tube 4 (00625-inch ID) with outlet opened to atmospheric pressure; brine was pressurizing fluid.

Table 5.4 - Permeabilities of the gel and the filter cake; Gel composition: 7500 polymer, 300ppm chromium and 1% KCl.

	units	Run #1	Run #2	Run #3
Pressure drop across gel*	psi	2.24	1.76	2.64
Permeability of Teflon frit after run	md	0.08	0.07	0.02
Flow rate	mL/min	0.00045	0.00036	0.00067
Pressure drop across frit	psi	0.37	0.34	2.2
Pressure drop across filter cake	psi	47.39	47.9	45.16
Pressure drop between ports #1 and #2	psi	0.760	0.356	0.57
Pressure drop between ports #2 and #3	psi	0.844	0.456	0.70
Permeability of gel between ports #1 and #2	md	**0.37**	**0.63**	**0.73**
Permeability of gel between ports #2 and#3	md	**0.33**	**0.49**	**0.60**
Permeability of the filter cake	md	0.0006	0.0005	0.0010

* Obtained from transducer #3 in Figure 5.3.

Permeabilities of the bulk gel measured by our method were an order of magnitude greater than the value of 0.042 md reported by Seright and Martin [1991] for a similar system that contained approximately twice the polymer concentration. Al-Sharji et al. [1999] reported a bulk gel permeability of 0.021 md for a 1.8% polyacrylamide (molar mass of 500,000 daltons) -chromium acetate system. The difference between our values of permeability and those by other investigators was probably due to the different gel systems.

Summary

The experiments conducted in this study revealed some characteristics of how gels respond to pressure gradients. The physical structure of the gels fails when the pressure gradient exceeds a critical value, termed the rupture pressure. Two types of gel failure were observed, termed *center-rupture* and *wall-rupture*. Center-rupture occurred when the injection fluid created a path down the centerline of the gel. The gel-tube bond was intact and a sizeable portion of the gel remained in the tube with subsequent oil or brine flow. Wall-rupture occurred when the gel detached from the tube and a significant amount of the gel was displaced from the tube with continued injection. The tube material and condition affected the adhesion strength of the gel to the tube wall. Rupture pressures increased linearly with the ratio of the tube length to tube ID and moderately increased with the time period the gel was allowed to mature.

Response of the gel to an applied pressure gradient that is below a value where rupture occurs depended on time and how well the gel is confined. Part of the pressure was transmitted down the length of the gel immediately followed by a smooth increase in pressure transmission when the gel was well confined (outlet end closed). The pressure transmission was relatively slow and decreased with the ID of the tube.

Different behavior was observed when the tube outlet was open which allowed greater deformation of the gel under the applied pressure gradient. Both oil and brine developed channels and flowed through or pass the gel. The movement of oil and brine through the gel occurred intermittently. Small pressure gradients were observed along the length of the gel where the brine or oil had penetrated. Most of the applied pressure gradient was across a short section of gel downstream of the position where the oil or brine had advanced. The oil or brine eventually penetrated the entire length of the gel.

Channel development through gels has implications on the performance of gelled polymer treatments. In production wells, injected brine can develop channels through the placed gel, possibly reducing the effectiveness of the treatment. In production wells, the relative development of channels by oil and water could affect the treatment's ability to reduce water production while sustaining oil production.

The work reported here was conducted to explore the response of gels to applied pressure gradients. General behavior of gel failure and of the development of flow channels through the gel by oil and brine were observed and reported. Adhesion of the gel to surfaces as well as the deformation properties of the gel appeared to be key to further investigation of how gels that are confined in porous rocks and fractures will respond to pressure gradients.

Acknowledgement

A portion of the material in this chapter is substantially unchanged from a copyrighted paper published by the Society of Petroleum Engineers. The paper is in the *Soc. of Pet. Engrs Journal*, September, 2002, pp. 309 – 315. The SPE copyright release form grants authority to authors the "nonexclusive right to incorporate all or part of the work in future writings or presentations."

References

1. Al-Sharji et al.("Pore-Scale Study of the Flow of Oil and Water Through Polymer Gels," SPE paper 56738, 1999 SPE annual Technical Conference and Exhibition.
2. Seright, R.S. and Martin, "Fluid Diversion and Sweep Improvement with Chemical Gels in Oil Recovery Prosesses," Second Annual Report, DOE Contract No. DE-FG22-89BC14447, report no. DOE/BC/14447-10 (Nov 1991).
3. Suo, Xiaofang, "An Experimental Study of Pressure Distribution in Gel-Filled Tubes and the Measurement and Discussion of Gel Displacement Pressures," MS thesis, The University of Kansas, Lawrence, KS (2002).

Chapter 6

The Effect of Fluid Leakoff on Gel Placement and Gel Stability in Fractures

Research Associate: Somenath Ganguly

Introduction

Fractures occur in hydrocarbon reservoirs due to various reasons and at a variety of scales. In addition to natural fractures, the reservoir around oil wells may be hydraulically fractured to improve production. Over pressuring and thermal stresses during water injection also cause fractures. During waterflooding of a fractured reservoir, most of the water may bypass the matrix and preferentially flow through channels consisting of a single fracture or an interconnected network of fractures. The consequence is additional cost for handling of excess water, and an incomplete recovery of oil from the reservoir. One remedy is injection of a gelant into the fracture that reacts to form an immobile gel. The immobile gel then diverts injected water to previously unswept portions of the reservoir.

Investigators have studied the application of gelled polymer treatments to fractured systems. Sydansk [1990] presented detailed laboratory testing and evaluation of a Cr(III)-partially hydrolyzed polyacrylamide gel system for fracture applications. Seright [1995] studied the performance of several immature, preformed and mechanically degraded gels by displacing them through fractured cores. Immediate breakthrough of tracer after treatment of the core with immature gel was observed indicating poor performance of the gel to divert flow into the matrix. Similar experiments with mature gel resulted in delayed breakthrough of tracer indicating sweep improvement. Seright [1995] concluded that superior diversion can be obtained by injecting mature gel (rather than gelant) in the fracture.

Seright [1997] also studied the placement of preformed Cr(III)-partially hydrolyzed polyacrylamide gel in fractured Berea core. He investigated the pressure drop, the gel dehydration and the delay in gel propagation that occur during the flow of preformed gel through fractured cores. Dehydration and leakoff of water concentrated the gel in the fracture. The gel injected at a later stage of extrusion made wormholes through the thickened gel to reach the fracture outlet.

During placement of an immature gel (referred to here as a gelant) through a fracture, some of the gelant leaks off to the adjoining matrix. The effect of leakoff on the strength of gel placed in a fracture was not studied previously. The objectives of this research were to study (a) the role of leakoff on the performance of a gel placed in a fracture and (b) the ability of a gel formed within a fracture to resist failure when subjected to an imposed brine pressure.

Experimental Details

Fracture Models. Three types of fracture models were used for displacement experiments: fractured slabs, fractured cores and slots. The slabs and cores contained one fracture and were constructed to provide for leakoff from both sides of the fracture to the adjoining matrix. The slot was constructed from a saw-cut rock and an acrylic wall.

A schematic of the fractured slab and associated fluid ports is shown in Figure 6.1. Slabs cut from Berea sandstone were 10 inches long, 2 ft wide, and 1 inch thick. Each slab was fractured along the 10 inch length using a Hydrasplit® (Park Industries, Inc.) rock splitter. Spacers were placed between the two symmetric halves to establish a fracture aperture of known width. The top and bottom of the fracture were then sealed with an epoxy coating. Acrylic fluid ports were installed across the fracture aperture at the front and back faces to allow flow through the fracture. Acrylic side plates were installed on each side of the matrix opposite the fracture. The side plates were milled to provide an aperture between the plate and the smooth face of the slab. Ports at each end of the side plates provided for fluid withdrawal from each side of the slab. The slab was sealed by coating the top, bottom, front and back surfaces with epoxy. Pressure ports were installed at the inlet and outlet end of the fracture. Details of the slab preparation process are given by Ganguly [2000].

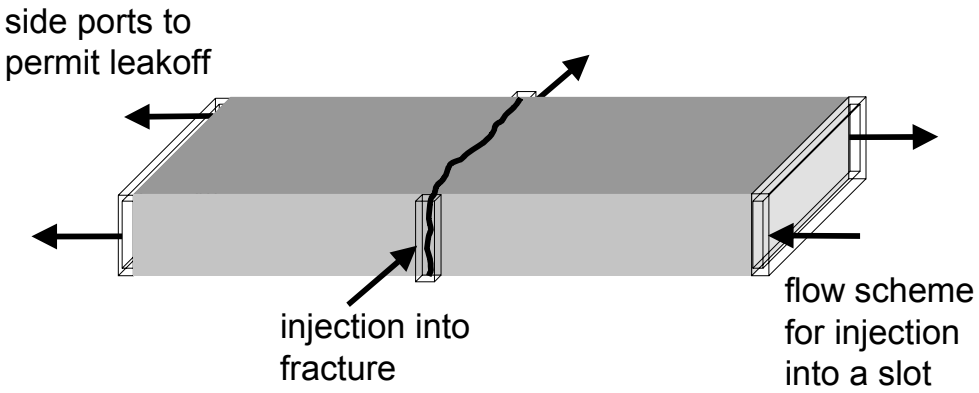

Figure 6. 1 - Schematic description of a fractured slab.

Each slab was initially saturated with 1% NaCl brine. Permeability of the fracture was determined by flowing brine at constant flow rates through the fracture with the side outlets closed. Aperture width was estimated utilizing theory of flow between two parallel plates. Matrix permeability was determined by injecting brine into the fracture and measuring the flow rate at the matrix (side) outlets and pressure differentials across the matrix sections. Pore volume of the matrix was determined from tracer runs. A step change in concentration of potassium iodide was introduced into the fracture and the effluent concentrations from the matrix (side) outlets were monitored using a UV spectrophotometer. The slabs had permeabilities of about 200 md and an average porosity of 0.17. Some slabs were cleaned and reused in other runs.

Flow experiments were also conducted in slots using an alternate flow configuration from the slabs. The side plates were constructed and installed on the slab to provide an aperture between the matrix and the plate. Fluid ports at the front and back of the plate allowed for displacement of gelant through the aperture between the saw-cut Berea matrix and the smooth-cut acrylic plate.

This configuration is referred to as a slot. Closing all other fluid ports in the slab minimized leakoff from the "fracture" into the Berea matrix during runs using slots.

Fractured cores were also used in flow experiments. A schematic of the fractured core is shown in Figure 6.2. The cores had 2-inch square cross-sections and were fractured along their lengths with the Hydrasplit® rock splitter. The two halves were secured together with epoxy using spacers to define the fracture aperture. Acrylic plates were attached to the ends of the fractured cores with epoxy. The endplates sealed the ends of the cores except for a slit to allow for fluids to enter or exit the fracture. The top, bottom and sides of the core were then sealed with epoxy. Fluid ports along the sides of the core were constructed to provide an exit for fluid to leak off from the fracture and through the matrix. Holes were drilled on the sides at one-inch intervals along the length. Tubing of 0.125-inch OD was secured in each hole with epoxy. The Berea cores had nominal permeabilities of 500 md before they were fractured.

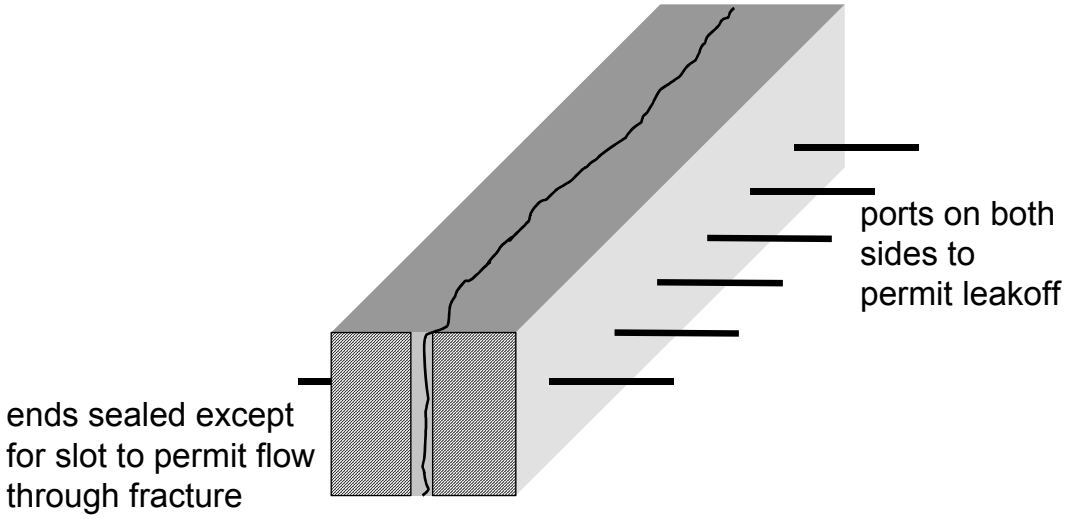

Figure 6. 2 - Schematic description of a fractured core.

Gel System. The composition of the gelant in most of the experiments was 5000 ppm polymer, 417 ppm chromium triacetate, and 1% NaCl in water. The initial pH of the mixture was 4.78 and was not adjusted. Stock solutions of polymer and chromium acetate contained 1% NaCl and were mixed in the ratio of 2:1, respectively, to prepare a gelant. The polymer was a partially hydrolyzed polyacrylamide (Alcoflood 935; molecular weight 5×10^6 daltons; degree of hydrolysis 5-10%; Allied Colloids now Ciba). Two lots of polymer (3243A and 7158V) were used. The polymer concentration was increased in a few runs and these runs are appropriately identified. Chromium acetate stock solutions were prepared from a 50% chromium acetate solution (McGean Rhoco Lot No. 40014806). The gel time varied from 12 to 32 hours depending on the polymer lot and polymer concentration.

Procedures. Two types of experiments, designated as Series 1 and Series 2, were conducted in the fracture models. Series 1 experiments were conducted to determine the effect of leakoff on the performance of the gel in terms of increasing flow resistance in a fracture. It was determined that leakoff was required for the gel to mature in a fracture and develop flow resistance. Series 2 experiments were conducted to determine the reason for the poor performance of the gel when it was placed in a fracture without leakoff.

Series 1 experiments were conducted in fractured slabs and fractured cores to determine the effect of leakoff on the performance of the gel. Descriptions of the fractured slabs and fractured cores are given in Table 6.1. Cr(III)-PHPA gelant was prepared by mixing the polymer and the crosslinker in bulk. The gelant was aged for three hours and then injected into the fracture inlet. The gelant was aged to simulate the time delay between the mixing on the surface and the injection into reservoir rock at the bottom of a well. The amount of leakoff into the matrix was controlled. The condition of no leakoff was accomplished in Slab 1 by closing valves at the matrix (side) outlets, opening the valve at the fracture outlet and injecting five fracture pore volumes of gelant. Different penetrations of leakoff were accomplished by closing the fracture outlet valve and opening the matrix (side) outlets. Gelant that was injected into the fracture was forced to penetrate the matrix. The distance of leakoff was determined by the amount of gelant that was injected. The entire matrix was penetrated by leakoff for several runs. All injections took less than one hour. The gel time for the system used in all runs (except one) was 12 hours. The slabs and cores were shut-in for time periods ranging from 5 to 30 days to allow the gel to mature. The performance of the gel was then determined by subjecting the inlet of the fracture to brine and increasing the pressure of the brine until displacement of gel and brine occurred in the fracture. The fracture outlet was open and the matrix (side) outlets were closed during this procedure.

Series 2 experiments were conducted in fractured slabs and slots to determine the reason for the poor performance of the gel when it was placed in a fracture without leakoff. Three runs were conducted with leakoff and three runs were conducted without leakoff. The fracture was one inch high and ten inches long. Apertures of fractures and other experimental parameters are given in Table 6.2. Cr(III)-PHPA gelant was prepared by mixing the polymer and the crosslinker in bulk. The gelant was aged before injection into a fracture or slot. In-line mixing of the gelant was used in one experiment. Five to six fracture volumes were then injected through the fracture or slot in the experiments without leakoff. Leakoff was minimized in these runs by closing all fluid outlets except at the end of the fracture or slot. Runs with leakoff were conducted in fractured slabs with the outlet of the fracture closed and the matrix (side) outlets open. Gelant was injected into the fracture and forced to penetrate the matrix. The depth of leakoff into the matrix was determined by the amount of gelant injected. The time period to inject gelant in these runs was less than 10 minutes for Runs 8, 9 and 10 and less than 1.5 hours for Runs 11 and 13. Gelant that was mixed in-line in Run 12 was injected for 15 hours. After placement, the media were shut in until the time just before the gel time. For most cases, this was 29 hours after mixing the gelant for a gelant with a gel time of 30 to 32 hours. At this time, gelant that was left from the placement procedure (and reacting in the transfer reservoir) was displaced through the fracture or slot.

During the original placement and subsequent displacement of gelant, the effluent was collected in small fractions for measurement of pH and chromium concentration. The pH of the effluent

fractions was measured immediately after the collection. The polymer/gel in the effluent samples was digested by addition of sodium hypochlorite for a day. The digested samples were diluted with water to reduce the chromium concentration below 10 ppm. Chromium concentrations were determined by atomic absorption spectrophotometry.

Results and Discussion

Formation and Displacement of a Gel in a Fracture. Series 1 experiments were conducted to determine how the performance of a gel is affected by the leakoff that occurs during placement of the gelant in a fracture. Runs were conducted in fractured slabs and fractured cores. The depth of leakoff into the matrix during placement of the gelant was varied in these runs from 0 to 30 cm as a shown in Table 6.1. The results of Runs 1 and 2 are described in what follows.

Table 6.1 – Summary of Series 1 experiments for determining the formation and displacement of a gel in a fracture.

Run #	Fracture model and #	Fracture height and length (cm × cm)	Fracture aperture (cm)	Leakoff distance (cm)	Shut-in time (days)	Rupture pressure (psig)
1	Slab 1A	2.5 × 25	0.10	0	5	1
2	Slab 1B	2.5 × 25	0.10	1	5	5.5
3	Slab 1C	2.5 × 25	0.10	10	5	6.4
4	Slab 2	2.5 × 25	0.030	30	7	12
5	Core 1	5.1 × 30	0.039	2.5*	30	18
6	Core 2	5.1 × 45	0.029	2.5*	7	40
7	Core 3**	5.1 × 61	0.10	2.5*	5	10

* Entire matrix filled with leak-off by injection of about three pore volumes of gelant.
** Gel time of 30 - 32 hours.(Gel time was 12 hours for Runs 1 through 6).

Slab 1 was used to study gel performance in a fracture when the gelant is placed in the fracture without leakoff (Run 1) and with leakoff (Run 2). The gelant used in Runs 1 and 2 had a bulk gel time of 12 hours and was aged three hours before injection into the fracture. Flow experiments were conducted in the following sequence:

Run 1

- Five fracture volumes of gelant were flowed through the fracture without leakoff. The fracture outlet was open and the matrix outlets were closed.
- The slab was shut-in for five days to allow the gelant to mature.
- Brine was injected into the fracture to determine the pressure that was required to initiate fluid displacement through the fracture. The matrix outlets were closed during brine injection.

Run 2

- A large volume of brine was injected to clean the fracture and matrix.
- Gelant was injected into the fracture with the fracture outlet closed and the matrix outlets open. The amount of gelant injected corresponded to the volume contained in the fracture plus 1 cm of matrix on each side of the fracture.

- The slab was shut-in for five days to allow the gelant to mature.
- Brine was injected into the fracture to determine the pressure that was required to initiate fluid displacement through the fracture. The matrix outlets were closed during brine injection.

Pressures of the brine during injection into the fracture are shown in Figure 6.3 for Runs 1 and 2. When the gelant was placed without leakoff (Run 1), the gelant was displaced from the fracture at a differential pressure of less than 1 psi. A gel did not form in the fracture. This is consistent with experiments reported by Seright [1995] who found that this gel system did not reduce the permeability of a fracture in a Berea core when injected as an immature gelant.

When the placement was conducted with leakoff into the matrix (Run 2), a gel formed in the fracture. Fluid displacement occurred in the following manner. As pressure increased, a gel blob appeared at the fracture outlet. The blob expanded rapidly which corresponded to the sharp drop in brine injection pressure at the inlet. Brine then broke through from the interior of the gel blob. Brine occupied most of the volume of the expanded gel blob. Run 2 demonstrated that the gel formed within the fracture had limited resistance to displacement when subjected to an imposed pressure using brine. The rapid displacement of brine through the fracture at the limiting pressure indicated that the gel ruptured.

Additional tests were conducted to obtain a visual account of the rupture process and to determine the pressure gradient required for rupture of gel inside a fracture. Gelants were placed in the fractures with leakoff and the rock was shut-in to allow the gel to mature inside the fracture. The results are summarized in Table 6.1. In all experiments conducted with leakoff, a consistent rupture process was observed. Pressure at which rupture occurred ranged from 5.5 to 40 psig. The rupture pressure presumably depends on the fracture aperture and length as well as the strength of the gel.

Permeability of the fracture to brine after rupture of the gel was determined for Run 7 using Core 3 with a fracture aperture of 0.1 cm. The gel time of the system was 30 to 32 hours. The placement was conducted three hours after mixing the gelant and the rupture experiment was conducted after five days of shut-in time. The rupture took place at a pressure of 10 psig. After the gel ruptured, brine pressure at the fracture inlet was held constant at 8.5 psig, and the cumulative flow was measured at the fracture outlet.

Figure 6.4 presents the cumulative flow through the fracture outlet with time when the pressure drop was kept constant across the fracture. Cumulative flow increased rapidly with time. The cumulative flow-time data were fitted to a polynomial expression as a function of time and the expression was differentiated to obtain the flow rate as a function of time. Values of k_fh for the fracture as a function of time were calculated using Darcy's law and are shown in Figure 6.4. The value of k_fh increased continuously, indicating that the brine constantly eroded the gel layer that was adhering to the fracture face. The value of k_fh prior to the gel placement was 8000 Darcy-cm. At the end of this experiment, the k_fh value was 140 Darcy-cm and was rapidly increasing. Brine flow was eroding the gel treatment after the rupture occurred.

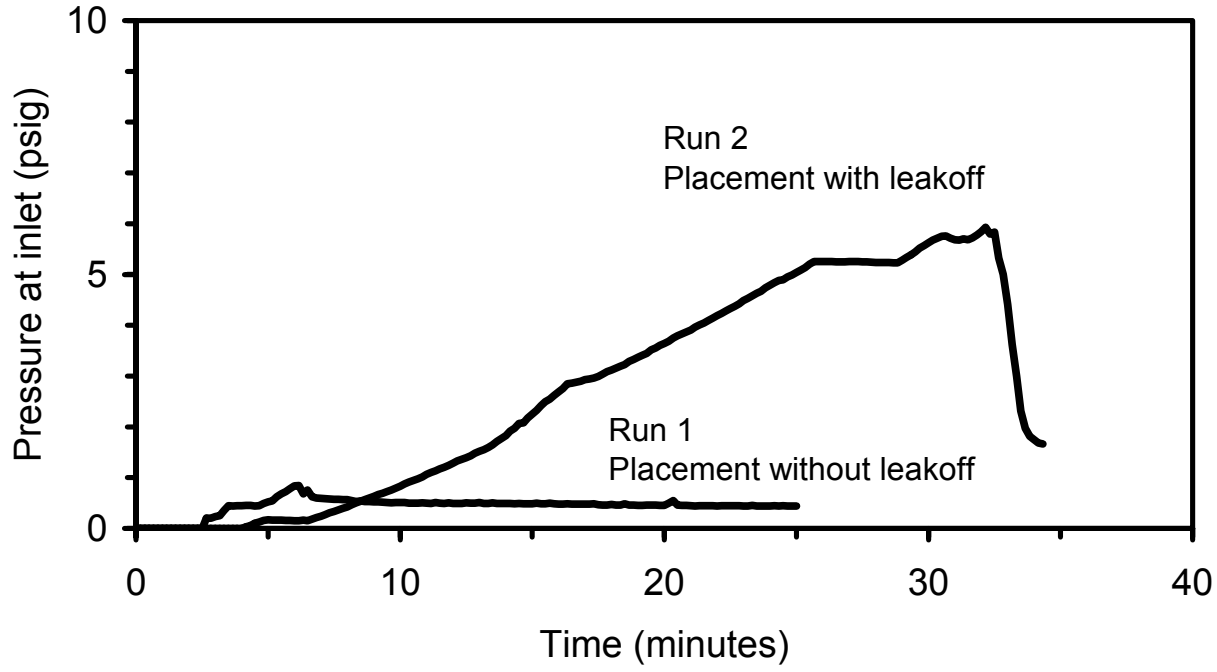

Figure 6. 3 - Pressure at the fracture inlet before and during displacement of brine.

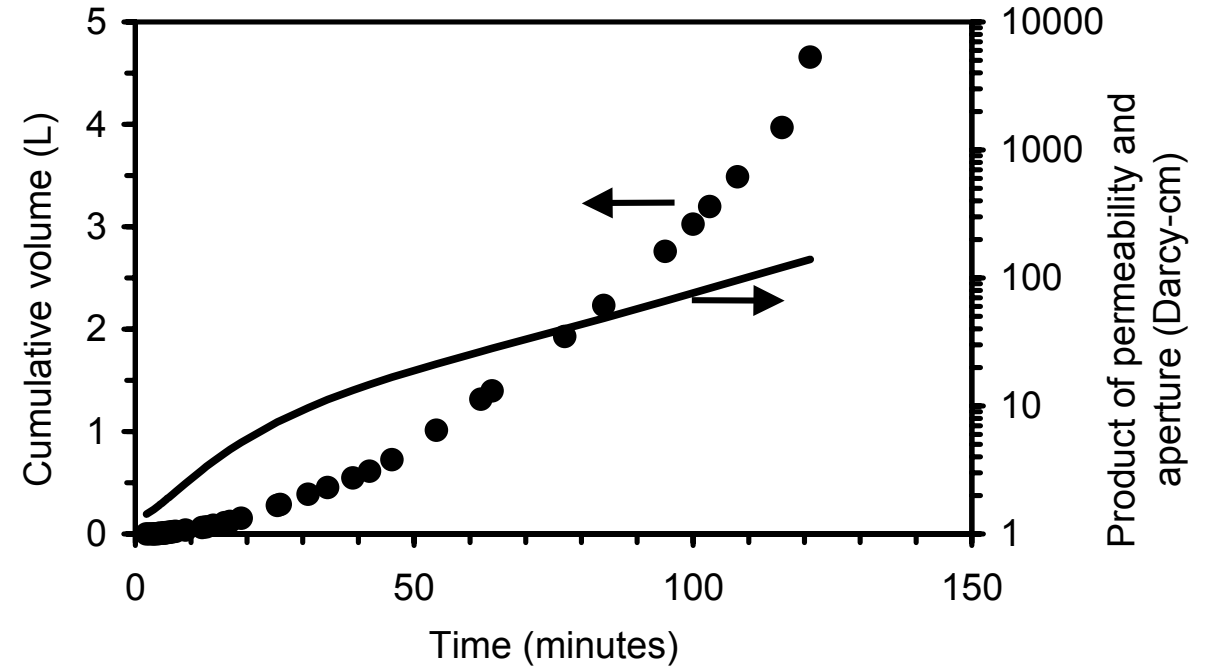

Figure 6.4 - Volume injected and flow resistance in the fracture during brine flow after gel rupture.

Series 1 experiments demonstrate that gelation did not occur in the fracture when there was no leakoff of gelant into the matrix. Gelation in the fracture was observed when there was leakoff of the gelant into the matrix. Gels that formed in the fracture were ruptured when brine that was applied at one end exceeded a threshold pressure. The threshold pressure is referred to as a rupture pressure and was found for each experiment. Substantial flow resistance was observed in the fracture even after the gel ruptured.

Failure of Gelation in Fractures. Series 2 experiments were conducted to investigate why gelants placed without leakoff did not form gels in the fracture. These experiments are summarized in Table 6.2. In each experiment, the gelant was displaced into the fracture with or without leakoff into the matrix. After placement, the media was shut-in until the time just before the bulk gel time. The fluid in the fracture was then displaced with gelant of the same age. The fluid displaced from the fracture was analyzed for pH and chromium concentration.

Table 6.2 – Summary of Series 2 experiments for determining the cause for gels not to mature in fractures when they were placed without leakoff.

Run #	Slab #	Fracture model	Fracture aperture (cm)	Leakoff distance (cm)	Age of gelant when placed in fracture (hours)	Age of gelant when displaced from fracture (hours)
8	Slab 3	fracture	0.08	0	12	29
9	Slab 3	slot	0.04	0	12	29
10	Slab 4	slot	0.05	0	9	29
11	Slab 3	fracture	0.08	7.6	12	29
12	Slab 4	fracture	0.11	30*	3**	25
13	Slab 5	fracture	0.11	30	3	11***

* Entire matrix filled with leak-off by injection of about two pore volumes of gelant.
** Gelant mixed in-line and with delay loop before injection into fracture.
*** Gel time was 12 hours (Gel time for Runs 8 through 12 was about 31 hours)

Changes in chromium concentration and pH during the placement of gelant in the fracture without leakoff for Slab 3A (Run 8 in Table 6.2) are shown in Figure 6.5. Results are similar for other placements. As the gelant displaced the resident brine from the fracture, the pH decreased from 8 to 5 and the chromium concentration changed from zero to one on a normalized scale. The viscous gelant broke through after injection of one fracture pore-volume and reached the injected concentration after about 2 fracture volumes of gelant were injected. Thus, when the slab was shut in after placement of gelant, the concentration of the gelant in the fracture was the same as injected gelant.

Figure 6.6 shows the change in pH in the fluid displaced from the fracture by gelant after the shut-in period for Runs 8 through 13. Although the pH of the displacing gelant remained less than 5 in the transfer cylinder, the pH of the fluid displaced from the fracture was around 7. There is little difference between effluent pH values in experiments with and without leakoff.

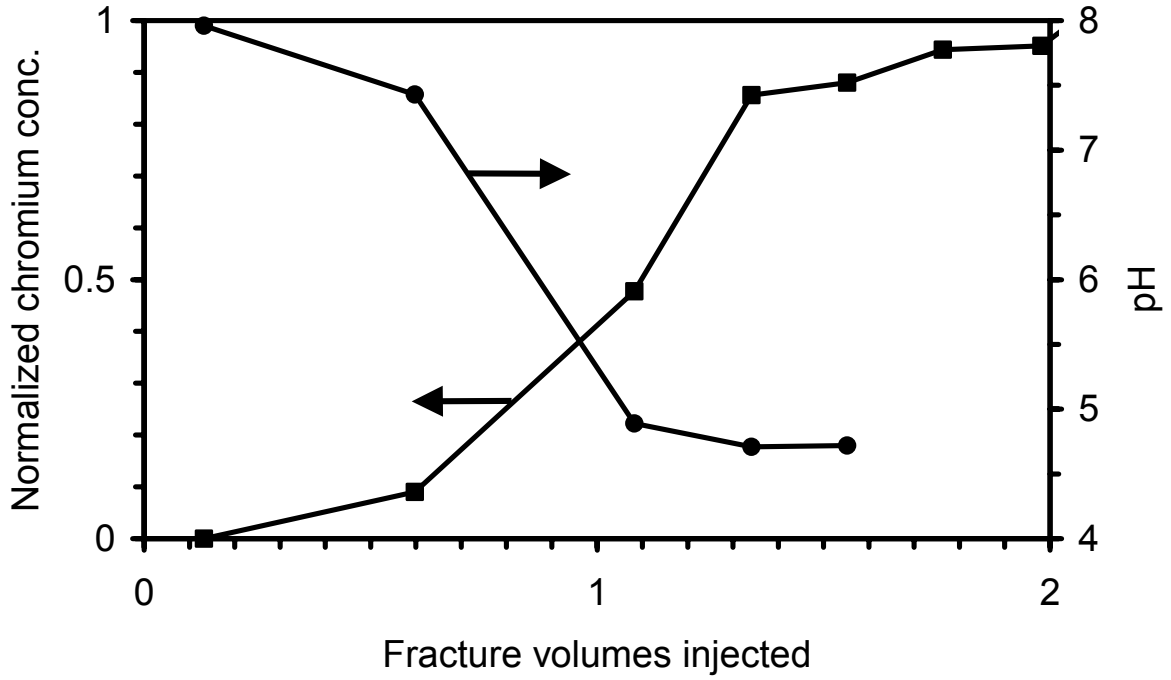

Figure 6.5 - Chromium concentration and pH of effluent during injection of gelant in Run 1.

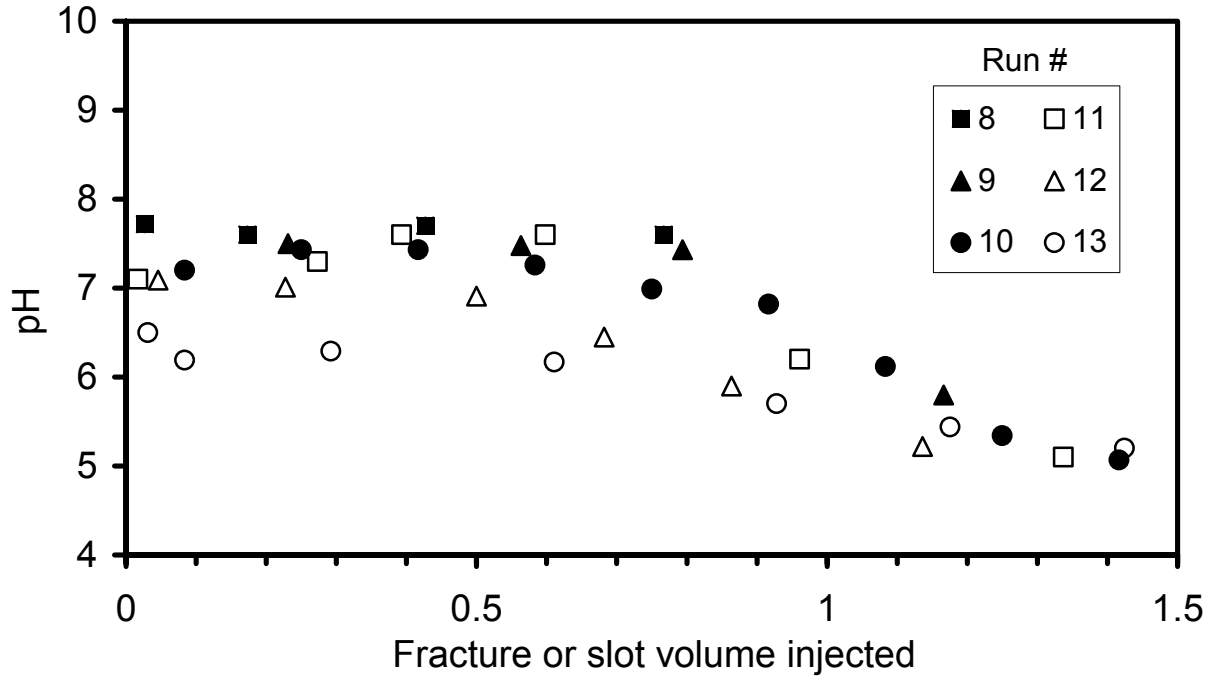

Figure 6.6 - pH of the effluent during displacement of gelant from the fracture after the shut-in period.

Figure 6.7 describes the chromium concentration in the displaced fluid. The chromium concentration is normalized against the concentration of the chromium in the injected gelant. When the displacement was conducted with leakoff, the chromium concentration remained at 80-90% of the injected concentration when displaced from the fracture. When the gelant was injected into the fracture without leakoff, the chromium concentration in the displaced gelant was 20-40% of the initial concentration. These data suggest that a gel did not form in the fracture when there was no leakoff because the chromium concentration in the gelant after placement decreased to values where gelation would not occur. The loss of chromium was larger in the fracture than in the smooth slot of equivalent aperture.

There are at least two explanations for this behavior. Increase in the gelant pH due to fluid-rock interaction, and the consequent precipitation of chromium are known to occur. Gelants that were placed with leakoff in fractured slabs experienced a similar increase in pH after similar shut-in periods but formed gels in situ. Gelation would not have occurred if significant amounts of chromium had precipitated within the time frame of the experiments. Therefore, precipitation of chromium from the gelant in the fracture due to an increase in pH does not appear to explain the early loss of chromium when the gelant was placed without leakoff.

Zou et al.[2000] studied the precipitation of chromium from bulk chromium (III) - acetate solutions at constant pH. Precipitation of chromium from bulk solutions was preceded by an induction period where there was no change in concentration. For a chromium acetate solution with chromium content of 200 ppm at a pH of 7, and at 25 deg C, the induction period was on the order of 20 hours. The experiments, described in Table 6.2, involve a shut-in period of up to 17 hours for gelant inside the fractured Berea slabs. During this period, the pH of the gelant increased from 4.8 to 7.1 and the chromium content of the gelant in the fracture decreased from 100 ppm to about 20 ppm. The bulk precipitation data of Zou indicate that precipitation was not the principal mechanism for chromium loss in the fracture. Recent data in dolomite rocks without fractures[6] show no induction period for chromium precipitation and chromium losses on the order that were observed here. However, the extrapolation of data from dolomite matrix to fractures in Berea sandstone is questionable. Chromium losses by precipitation must be considered for placement of gels in reservoir rocks where interactions, particularly carbonate dissolution, can increase the pH of the gelant.

A second mechanism for chromium loss from gelants in fractures is the diffusion of chromium into the adjoining matrix. Placement without leakoff leaves a thin layer of gelant confined in the fracture adjoining the porous matrix that is saturated with brine. Chromium can diffuse from the fracture into the adjacent matrix during the shut-in period, reducing the chromium concentration to values where gelation is not possible. Figure 6.8 shows chromium concentration profiles calculated for diffusion from a fracture when there is no leakoff. Diffusion calculations show that the chromium concentration in the fracture drops rapidly during the shut-in period. When leakoff occurs, a region of high chromium concentration penetrates into the matrix. Additional calculations of chromium diffusion for gelants placed with leakoff (0.5 cm into the adjoining matrix) showed much smaller decreases in chromium concentration in the fracture. That is, there is sufficient chromium in the fracture for gelation when leakoff occurs for the gel system studied here. Placement of gelants in a fracture in a reservoir is almost always associated with some extent of leakoff and chromium losses due to diffusion would often be minimal. Experiments

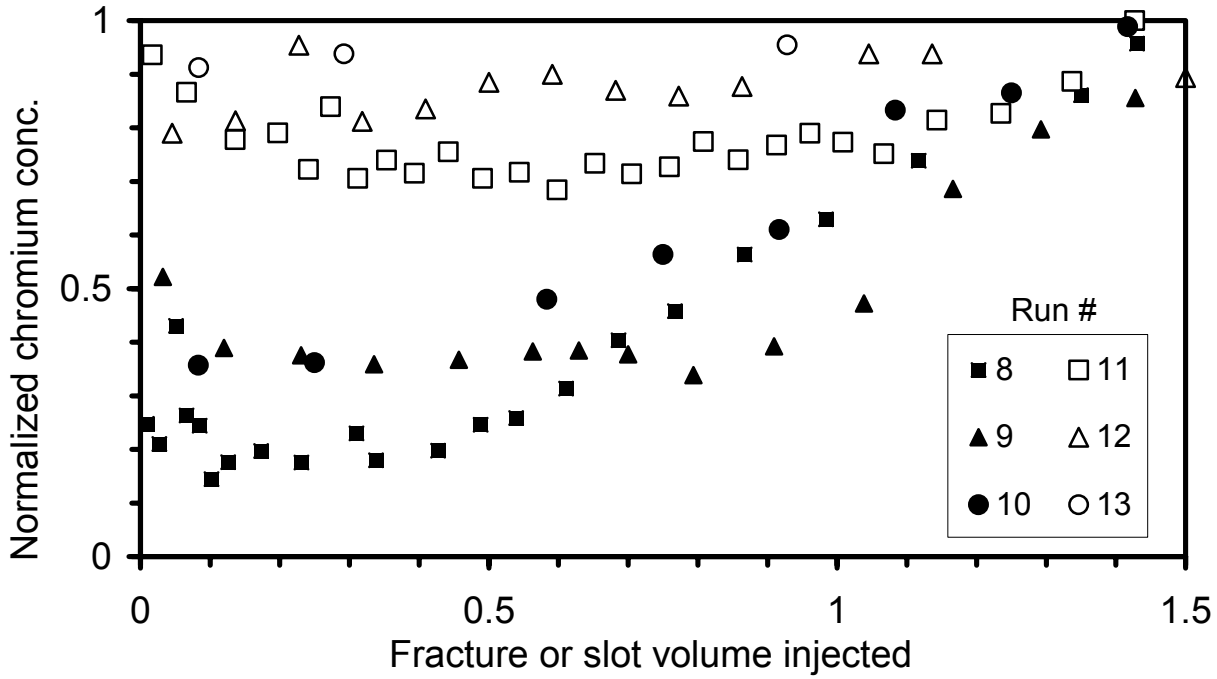

Figure 6.7 - Chromium concentration in the effluent during displacement of gelant from the fracture after the shut-in period.

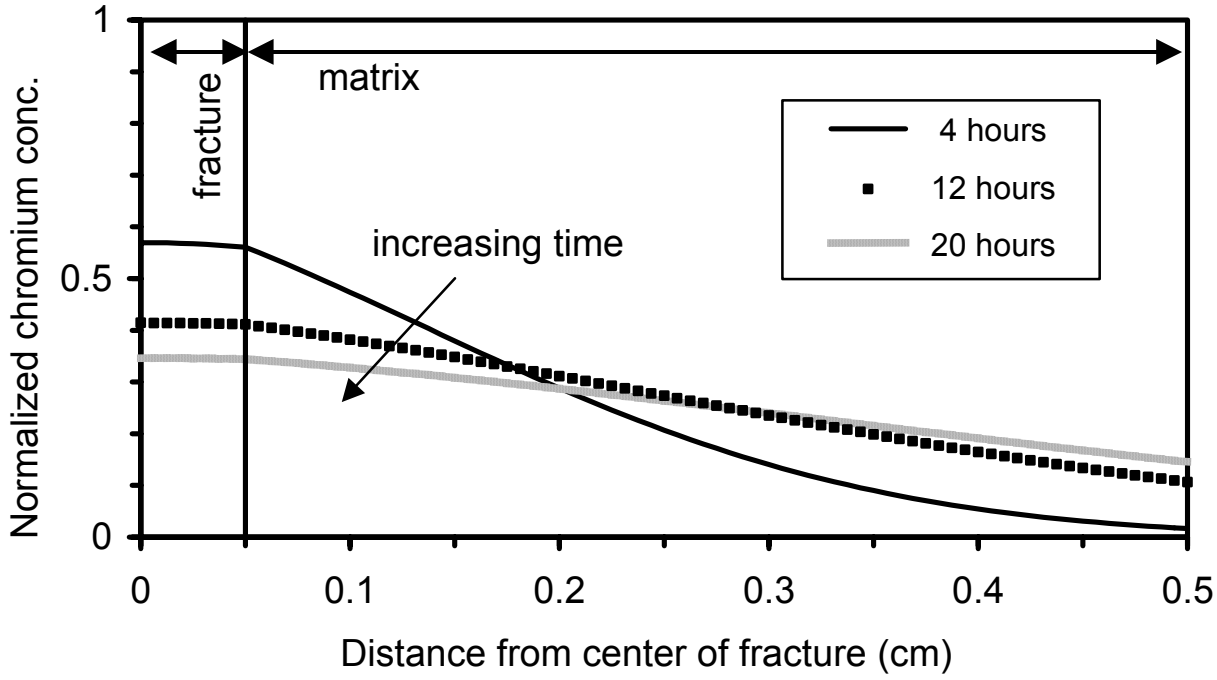

Figure 6.8 - Simulation of chromium concentration in the fracture and matrix after placement of gelant without leakoff.

with no leakoff were conducted in this work to ascertain the effect of leakoff on the availability of chromium in the fracture.

Sufficient chromium must be available for crosslinking the polymer for gelation to occur in a fracture. Precipitation of chromium and diffusion of chromium from the fracture are potential mechanisms that can reduce the chromium that is available for reaction with the polymer (uptake reaction). Presumably, increasing the chromium concentration in the gelant could offset chromium losses that occur by diffusion and precipitation.

Conclusions

The following conclusions can be drawn for the gel system and porous medium used in this study.

1. When Cr(III)-partially hydrolyzed polyacrylamide gelant was placed in the fracture without leakoff, extrusion of the gelant after a shut-in period took place on application of a relatively small pressure gradient. The formation of a gel structure in the fracture was not evident.
2. When Cr(III)-partially hydrolyzed polyacrylamide gelant was placed in the fracture with leakoff and a brine pressure was imposed on one end of the fracture, brine ruptured the gel structure once a threshold pressure was reached. Formation of gel structure was evident in the fracture.
3. After placement without leakoff the pH of the gelant in fracture increased from 4.8 to 7.0 and the concentration of chromium decreased from 100 ppm to 20 ppm before the gel time was reached.
4. After placement with leakoff, the pH of the gelant in the fracture increased by a similar amount as occurred after placement without leakoff. However, decrease in chromium concentration was not significant.
5. Diffusion of chromium into the brine in the adjoining matrix is hypothesized to account for the loss of chromium after placement without leakoff.
6. After gel rupture, continued flow of brine (due to a constant pressure gradient being imposed along the fracture) eroded the gel layer adhering to the fracture wall and displaced gel fragments from the fracture. Substantial resistance to fluid flow remained after the gel was ruptured, but this resistance was eroded by continuous brine injection.

Nomenclature

k_f = fracture permeability, L^2, Darcy
h = fracture aperture, L, cm

Acknowledgement

Material in this chapter is substantially unchanged from a copyrighted paper published by the Society of Petroleum Engineers. The paper is in the *Soc. of Pet. Engrs Journal*, September, 2002, pp. 309 – 315. The SPE copyright release form grants authority to authors the "nonexclusive right to incorporate all or part of the work in future writings or presentations."

References

1. Ganguly, S.: "Effect of Leak-Off on Behavior of Cr(III)-PHPA Gel in Fractured Media," PhD dissertation, University of Kansas, Lawrence, KS (2000).
2. Jin, Hong, "Transport of Chromium(III) Acetate through Dolomite Rock," MS thesis, University of Kansas (2001).
3. Seright, R.S.: "Gel Placement in Fractured Systems," SPEPF (November 1995) 241.
4. Seright, R.S.: "Use of Preformed Gels for Conformance Control in Fractured Systems," SPEPF (February 1997) 59.
5. Sydansk, R.D.: "A Newly Developed Chromium (III) Gel Technology," SPERE (August 1990) 346.
6. Zou, B., McCool, C.S., Green, D.W., Willhite, G.P. and Michnick, M.J.: "Precipitation of Chromium Acetate Solutions", SPEJ (September 2000) 324.

Chapter 7

Development of a Conceptual Model for Disproportionate Permeability Reduction

Graduate Research Assistant: Dilip Natarajan
Research Associate: H. Zhu

Abstract

It is well established that treatment of porous rocks with gelled polymer systems can cause the permeability of water at residual oil saturation to be reduced by one to three orders of magnitude more than the permeability of oil at the water saturation that is immobile after treatment. This phenomenon is called disproportionate permeability reduction and is of interest because application of gel treatments in production wells has potential to reduce water production.

The mechanisms that cause this phenomenon are not well understood. This paper describes how permeability to oil and water is developed in pore space that is filled with a chromium acetate/partially hydrolyzed polyacrylamide (HPAM) gel and proposes a mechanism for disproportionate permeability reduction based on the interpretation of the experimental data. Experimental data for the flow of oil and brine were obtained in unconsolidated sandpacks and in Berea sandstone cores with and without residual oil saturation after a chromium acetate/Alcoflood 935 gelant was injected and gelled in situ.

Interpretation of the experimental data suggests that oil permeability develops as oil penetrates into the gel-filled pore space, dehydrating the gel by displacing brine from the gel structure and creating "new flow" channels within or around the gel. The "*new pore space*" is a fraction of the original porosity, and the permeability to oil is reduced substantially from its value before placement and in situ gelation of the gelant. Subsequent brine injection displaces oil from these flow channels but traps some of the oil in the "*new pore space*" as a residual saturation. The trapping of residual oil in the "*new pore space*" causes the disproportionate reduction in brine permeability because the brine flows primarily in the pore channels created by dehydration of the gel even though the gel has some brine permeability. When gelant is placed in matrix containing residual oil, dehydration of the gel reconnects some of the trapped oil and the oil permeability increases. Subsequent brine displacement experiments conducted at the same pressure drop showed that initial brine permeability was reduced by factors of 100-1000 more than the oil permeability, verifying the existence of disproportionate permeability reduction.

Introduction

Increased water production is a worldwide problem in mature fields produced by natural water drive or active waterflood. There are economic and environmental incentives to develop methods that reduce water production without significantly affecting oil production. During the past 15 years, a number of polymer systems have been developed that when placed in a porous matrix reduce the permeability to water at residual oil saturation significantly more than the permeability to oil at the saturation where water is immobile. This phenomenon is termed disproportionate permeability reduction (DPR). Systems that exhibit this behavior are called relative permeability modifiers (RPM).

There are extensive investigations [Liang et al.,1992; Dawe and Zhang,1994;, Liang and Seright, 1997; Thompson and Fogler, 1997; Nilsson et al.,1998 and Al-Sharji et al., 1999] on the mechanisms that cause disproportionate permeability reduction. Proposed mechanisms include segregated flow paths on a microscopic level, wall effects caused by a polymer/gel film that covers the pore walls, restriction of pore throats due to adsorption of polymer or precipitation of hydrophilic components of the gel system , changes in wettability, lubrication effects, swelling and shrinking of gels and polymer films, and change in pore morphology. Of the proposed mechanisms, research continues on the microscopic segregated flow path model, wall effect models, restricted pore throat model and effects of changes in pore morphology. None of these proposed mechanisms has been unequivocally demonstrated to be the primary cause of DPR.

This paper describes an experimental study of chromium acetate polyacrylamide gels which demonstrate DPR when placed in sandpacks and Berea sandstone core material. The research was stimulated by experiments conducted by Dawe and Zhang [1994] who used microscale models to observe mechanisms of oil and water flow through a gel placed in a porous medium made by etching pore structure on a glass plate. They observed that oil flowed through the micromodel by fingering through the gel. Water flowed through the gel by diffusing into the gel structure. A subsequent paper by Al-Sharji et al. [1999] provides additional support for the pore level mechanisms observed by Dawe and Zhang [1994].

Thompson and Fogler [1997] studied pore level mechanisms by altering the permeability of a porous matrix following a gel treatment. In their studies, the interstitial water saturation was gelled in situ by introducing an organic orthosilicate in the hydrocarbon phase after the interstitial water saturation was attained. The orthosilicate reacted with the interstitial water to form a silica gel, effectively immobilizing the initial interstitial water saturation. In subsequent two-phase flow experiments, trapping of a residual hydrocarbon phase and a "new", residual water phase altered the endpoint saturations as well as the endpoint values of both water and oil permeabilities. The presence of the "new" residual water phase reduced the oil phase permeability, while the trapping of residual oil in the "new" pore space reduced the water phase permeability at residual oil saturation. Disproportionate permeability reduction was observed. However, the permeabilities of both oil and water phases at endpoint saturations were reduced significantly.

Krishnan et al [2000] demonstrate that chromium acetate polyacrylamide gels dehydrate when subjected to pressure gradients by either oil or water phases. When gels dehydrate, some of the water is squeezed out of the gel as the gel structure adjusts to the applied pressure gradient. Figure 7.1 shows the percentage of the water that leaves a typical chromium acetate polyacrylamide gel when it dehydrates, as a function of pressure gradient and time. An oil phase was used to apply pressure to the gel. Dehydration differs from gel rupture in that when a gel ruptures, fragments of gel are produced which have a volume equivalent to the pore space filled by the injected fluid. Dehydration is dewatering of the gel. When a gel is dehydrated in a porous matrix, the brine is displaced from the gel structure leaving most of the polymer in the porous matrix. Uncrosslinked polymer may also be produced when a gel is dehydrated. In this paper, dehydration was investigated after placement and in situ gelation of the gelant.

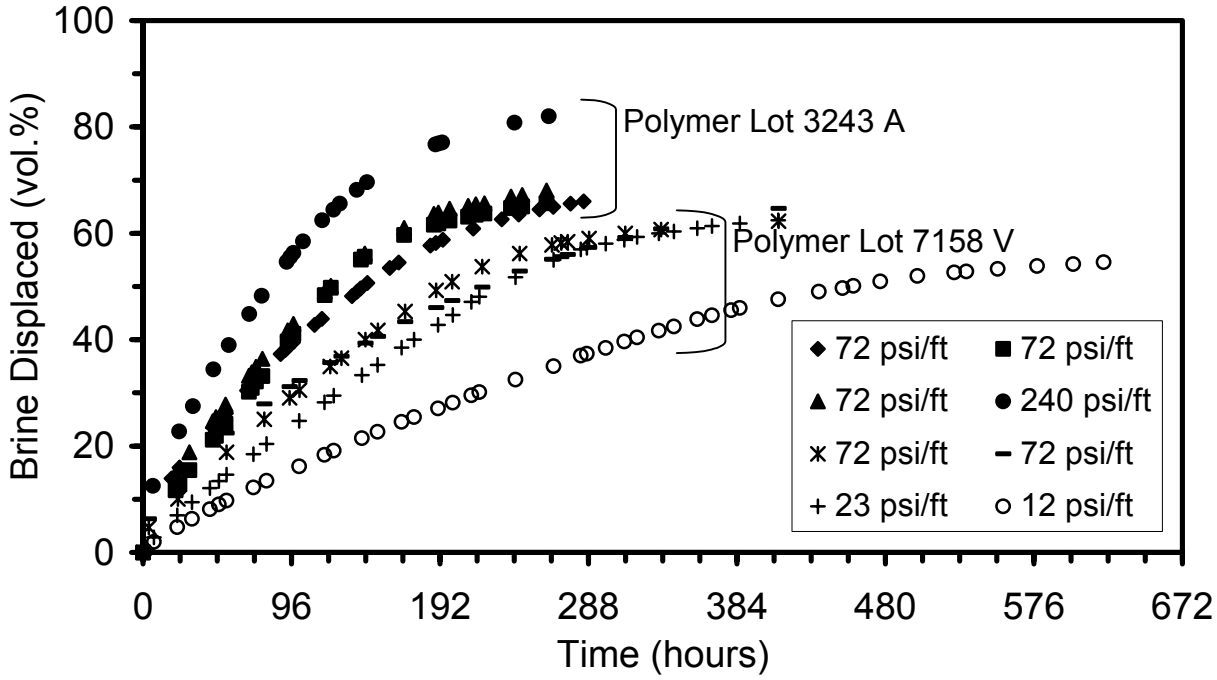

Figure 7.1 – Percentage of brine displaced as a function of time when using oil to dehydrate gel; 7500 ppm polymer, 300 ppm chromium and 10,000 ppm KCl [Krishnan, 2000].

These observations suggest the following explanation for the flow behavior of oil and water following a gel treatment. When an aqueous gelant is placed in a porous matrix such as a sandpack, the gelant displaces the entire aqueous phase except where the pore size is of the same order of magnitude as the largest polymer molecule in the gelant or in dead-end pores. In most cases, the volume not contacted by the gelant will be small. After the gel forms, the fraction of the pore space filled by the gelant is essentially immobile. If the porous matrix contains a residual hydrocarbon saturation during placement, the gelant initially encapsulates the residual hydrocarbon [Liang et al.,1992]. Although the water content of most aqueous gels is on the order of 95-99%, the permeability of a gel to brine is on the order of tens to a few hundred microdarcies [Dawe and Zhang,1994; Krishnan et al.,2002; Seright and Martin, 1990-1991 and Al-Sharji et.al. 1999]. The gel is impermeable to oil under low-pressure gradients. Thus, the effective porosity available for two-phase flow of oil and water is essentially zero after a gel treatment.

In order to develop substantial permeability and effective porosity to either brine or oil phases, it is necessary to disrupt the gel structure by increasing the pressure on the injected phase. Rigid gels used for casing leak repair or complete water shutoff [Sydansk and Southwell, 1998] are essentially impermeable to both water and oil and are not used for DPR. When the injected phase is oil, the oil fingers through the gel structure [Dawe and Zhang, 1994]. Oil cannot finger through the gelled porous matrix without displacing gel or brine. If the pressure gradient is sufficient, the gel should dehydrate and water will be displaced from the matrix. Oil injection is continued until brine production is negligible. The dehydrated gel is impermeable to oil and occupies a reduced volume within the pore space. In some cases, a small amount of polymer may

be displaced during dehydration. The amount of dehydration at a given pressure gradient can be estimated by measuring the volume of brine displaced during oil injection. Since most of the polymer remains in the dehydrated gel, the polymer concentration of this gel increases in proportion to the amount of dehydration, and the permeability of the dehydrated gel to brine decreases.

Dehydration experiments [Krishnan et al., 2000] show that injection of brine at high-pressure gradients also causes fingering through the gel structure and dehydration. Brine injection at high-pressure gradients should also create permeability and effective porosity in a porous matrix that is gelled with an aqueous gelant. Dehydration of the gel structure due to brine injection may be overlooked because it is difficult to perform accurate material balances when brine is used to create effective porosity. Aqueous tracers have been used to estimate the volume occupied by the aqueous phase in a gelled porous matrix [Liang et al., 1992]. Since the gel is 95-99% water, aqueous tracers also exchange with water bound in the gel structure. Thus, it is difficult to discriminate between free water in a pore space and water bound in the gel structure, because use of aqueous tracers to determine effective pore volume becomes insensitive at high mass transfer rates where the water soluble tracer exchanges rapidly with the water within the gel structure [Mennella et al., 1997].

The experimental program consisted of two sets of experiments. The first series of experiments was conducted on sandpacks to verify that the phenomena of gel dehydration observed in bulk tests also occurred in porous media as hypothesized. The second series of experiments was conducted in Berea sandstone cores with and without the presence of a residual hydrocarbon saturation. This series of experiments was designed to investigate DPR when the gel structure was dehydrated by injection of oil at successively increasing pressure gradients. All experiments were conducted at room temperature (~25°C). Although these experiments and the resulting conclusions were based on the chromium acetate/HPAM gel system over a limited range of concentrations, the inferred mechanisms are likely to occur in other gel systems that dehydrate under applied pressure gradients. The polymer used in this study was Alcoflood 935 with molar mass of about 5 million daltons, and a degree of hydrolysis 5-10%.

Dehydration of Chromium Acetate Polyacrylamide Gels after Placement in Sandpacks. A series of experiments was designed to determine if the phenomena of gel dehydration observed in bulk tests also occurred in porous media. Four sandpacks (SP11, SP12, SP19 and SP20) were prepared and treated with gelant. The experimental procedures for preparation of sandpacks and placement of the gelant are summarized in references [Natarajan et al., 1998; Willhite et al., 1996-1998 and Green et al., 1997-1998]. SP11 and SP12 were saturated with brine and displaced with a chromium-acetate gelant consisting of 5000 ppm Alcoflood 935 (Batch 3243A), 109 ppm Cr^{+3}, with an Ac/Cr ratio of 91. In SP11, 2 PV of gelant were injected. Five PV of gelant were injected into SP12. The pH of the gelant was adjusted to 5.0 by adding acetic acid. Nominal gelation time was 17-18 days. Samples of the injected gelant and the effluent collected during gelant placement formed stable gels and did not exhibit syneresis (*i.e. expel brine spontaneously on aging*) so that gels remained intact. Thus, at the beginning of the experiment, the amount of "free" water in the sandpack was considered negligible.

Dehydration of each sandpack was done by injection of oil at a constant pressure. The dehydration experiments began by connecting the inlet of the sandpack to a transfer cylinder containing mineral oil (baby oil) where the pressure was maintained at 80 psi by air injection. The viscosity of the oil was 18 cp. The pressure gradient across the sandpack was 80 psi/ft. The oil was dyed red so that the progression of the oil zone could be observed through the transparent walls of the sandpack holder. The oil fingered slowly into the gelled sandpack, dehydrating the gel. Brine was collected continuously at the effluent and measured to enable material balance calculations. Material balances on the effluent were used to determine the pore volume occupied by the mobile fluid phases. Pressure drops were measured to determine the permeability of the fluid during dehydration and subsequent fluid injection experiments. In one experiment, the gelant was injected into the sandpack in the presence of a waterflood residual oil saturation.

Run SP12. The initial experiments were conducted in sandpack SP12, a one-foot long sandpack (1.5" ID). Following gelation, the permeability of the gelled sandpack to brine was estimated to be about 30-40 μd based on experimental data from sandpacks treated with similar gel systems followed by injection of brine [Natarajan, 1998]. In SP12, dehydration of the gel occurred at a slow rate. Oil broke through about 70 hours after the oil pressure was applied at the entrance of the sandpack. A mixture of oil and brine was produced and after 200 hours of oil injection, the brine volume had decreased to levels where one drop of brine (0.05 mL) was produced over 24 hours. Volume of brine produced was 41.8 mL, which is 37% of the initial pore volume of the sandpack (112 mL). The rate that brine was produced was not measured in this experiment. However, the average rate that brine was produced during the 200 hours that oil was injected was about 0.0035 mL/min. At this flow rate, the estimated permeability to brine at a pressure gradient of 80 psi/ft is about 29 microdarcies for the sandpack. Brine permeability of the gelled sandpack is sufficient to permit dehydrated brine to flow from dehydration sites through the gel structure to the end of the sandpack. This estimate supports the proposed mechanism of gel dehydration.

The produced brine was not viscous, and was not slippery to the touch, indicating that the amount of polymer "squeezed" out of the gel was small. Neither viscosity nor polymer concentration were measured because the produced effluent appeared to have little dissolved polymer. The remainder of the pore space (63%) was considered filled with gel that had been dehydrated. Average polymer concentration of the "dehydrated gel" was estimated to be 8100 ppm. If the pore space filled by the dehydrated gel is considered as part of the matrix, the initial porosity of the sandpack was reduced from 32% to an effective porosity of 12%. Permeability of the core to oil was 8.2 md at 80 psi/ft and 6.88 md at 40 psi/ft. Oil permeabilities were measured with the flow not quite at steady state. The increase in oil permeability with pressure gradient is consistent with data reported by Yan et al.[1999] and is attributed to the deformation of the gel structure with increased pressure gradient.

The second stage of this experiment was to inject brine at a constant pressure drop until no further oil was produced and to determine permeability to brine at "S_{or}". The waterflood displaced 11.4 mL of oil. The oil remaining in the pore space was 30.4 mL, which is equivalent to a residual oil saturation of 73% and a brine saturation of 27% in the *"new pore space"* created by the dehydration of the gel. Permeability to brine at residual oil saturation in the *"new pore space"* was 6.4 μd. This low permeability coupled with high oil saturation in the *"new pore space"* suggests that the brine phase flows in thin films and channels around the trapped oil

phase, which occupies a large fraction of the pore space in the *"new pore space"* as well as through the remaining gel. Thus, part of the brine flows in the same flow channels as the oil phase when oil is the continuous phase.

The final stage of this experiment was an oilflood at 80 psi/ft to determine the amount of brine that could be displaced from the "*new pore space"* as well as to determine the interstitial brine saturation. The amount of brine displaced was 7.8 mL. That left an interstitial brine saturation of about 9% in the effective pore volume of the sandpack. Experimental data are presented in the original paper [Willhite, 2000]. Results from this series of displacement experiments are summarized in Table 7.1. Brine and oil permeabilities determined in this sequence of experiments are shown in Figure 7.2.

Table 7.1 - Dehydration of chromium acetate-polyacrylamide gel in Sandpack SP12.

Run	Displacement	S_w (%)	S_{gel} (%)	S_o (%)	ϕ_{eff} (%)	S_w* (%)	S_o* (%)	k_o (md)	k_w (md)
1	Brine injection before gel treatment	100	0	0	32	100	0		4000
2	Gel treatment	0	100	0	0	0	0		
2a	Brine injection after gel treatment		100	0	0	0	0		~0.03-0.04
3	Dehydration with oil @80 psi/ft	0	62.7	37.3	12	0	100	8.2	
4	Brine flood at 80 psi/ft	10.2	62.7	27.1	12	27.3	72.7	0	0.0064
5	Oil flood at 80 psi/ft	3.21	62.7	34.1	12	8.9	91.1	34.3	

* Based on effective porosity

SP11. The second dehydration experiment was conducted in SP11, a four-foot long sandpack studied previously [Natarajan et al., 1998]. Following gelation, the permeability of the gelled sandpack to brine was 108 μd. This sandpack had been kept in a constant temperature bath for six months following completion of gelation experiments [Natarajan, 1998].

Oil breakthrough during dehydration of the gelled sandpack occurred after 18 days of injection. Water production became insignificant at 65 days of oil injection. The volume of water dehydrated from the sandpack was 133 mL, which is about 29% of the pore volume of 460 mL. Thus, the effective porosity of the sandpack was reduced from an initial value of ~33% to 9.6% by the gel treatment followed by dehydration of the gel. Permeability of the dehydrated sandpack to oil was 3.7 md compared to the initial permeability of 3600 md. Brine was not injected into this sandpack after dehydration by oil.

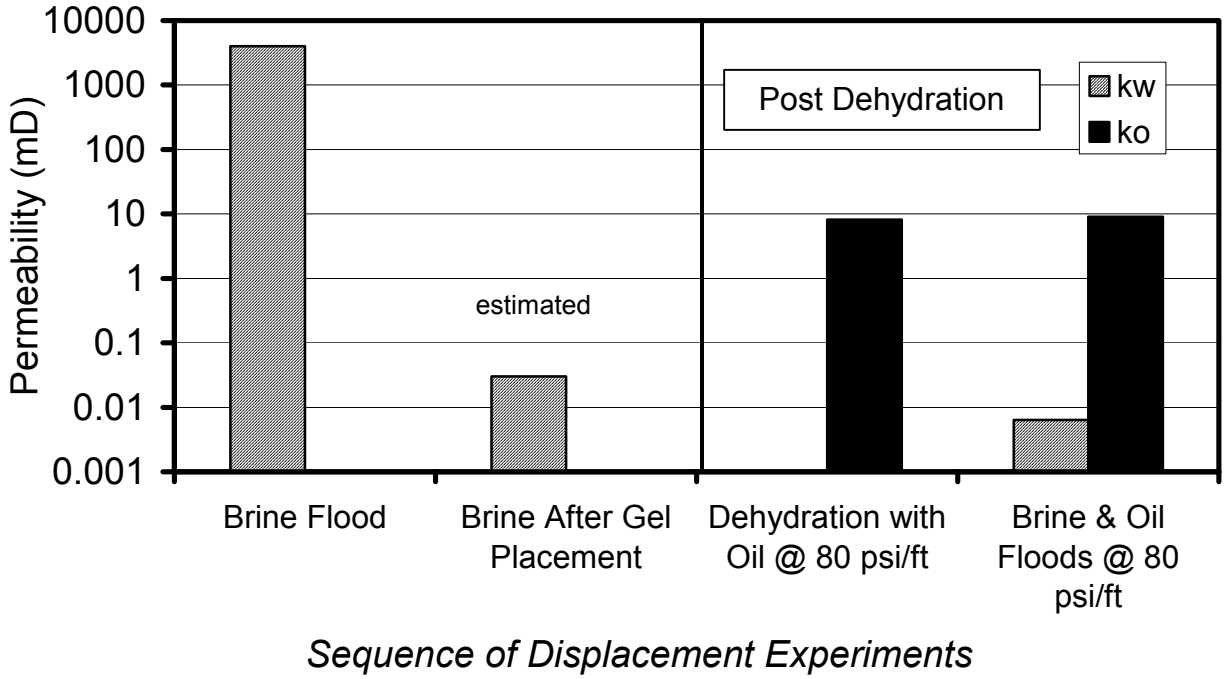

Figure 7.2 – Permeabilities obtained from dehydration of the gel in Sandpack SP12.

SP20/SP19. An experiment (SP20) was conducted in a six-inch long sandpack to compare dehydration of a gelled sandpack that contained waterflood residual oil saturation with a sandpack without residual oil saturation. SP20 was saturated with brine, oilflooded and then waterflooded to residual oil saturation before placement of the gelant. Properties of the sandpack are summarized in Table 7.2. The pH of the sandpack was adjusted to 5.0 using an acetic acid/sodium acetate buffer. A gel solution containing 5000 ppm Alcoflood 935, 109 ppm chromium (as chromium acetate) in 10,000 ppm NaCl was injected into the sandpack. There was no added acetate. Gel time was about 11 hours at 25°C. The gelant was bulk mixed and about three pore volumes were injected into the sandpack at a rate of about 5 mL/min. The sandpack was shut-in for 2.5 days to permit gelation before beginning oil injection at a pressure of 80 psi, which is equivalent to a pressure gradient of 160 psi/ft.

In SP20, the injected oil displaced 13 mL of brine. During the dehydration of SP20, oil broke through rapidly and the entire volume of oil in the transfer cylinder (700 mL) was displaced through the sandpack along with some air. Interpretation of the permeability measurements was flawed by the fact that some air entered the sandpack. SP20 was flushed with oil to displace air from the system prior to oil and water permeability measurements. The permeability to oil was 280 md while the permeability to brine at "residual oil saturation" was 10 md. Residual oil saturation was not determined. Permeabilities for SP20 are presented in Figure 7.3. The permeability to oil at S_{iw} was estimated as $0.9k_w$ at S_w=100%. The permeability to oil at S_{iw} was reduced by a factor of 13.9 while the permeability to water at S_{or} was reduced by a factor of 138.5. Disproportionate permeability is clearly evident in SP20. In a parallel treatment in SP19

Table 7.2 - Dehydration of chromium acetate-polyacrylamide gel in Sandpack SP20.

Run	Displacement	S_w (%)	S_{gel} (%)	S_o (%)	k_o (md)	k_w (md)
1	Brine injection before gel treatment	100	0	0		4324
2	Oil flood	21	0	79	3900*	0
3	Waterflood	62	0	38	0	1485
4	Gel treatment	0	62	38	0	
5	Dehydration with oil @160 psi/ft	0	39.6	60.4	280	0
6	Brine flood @160 psi/ft	-		-	0	10

* Estimated as 0.9 k_w at S_w=100%

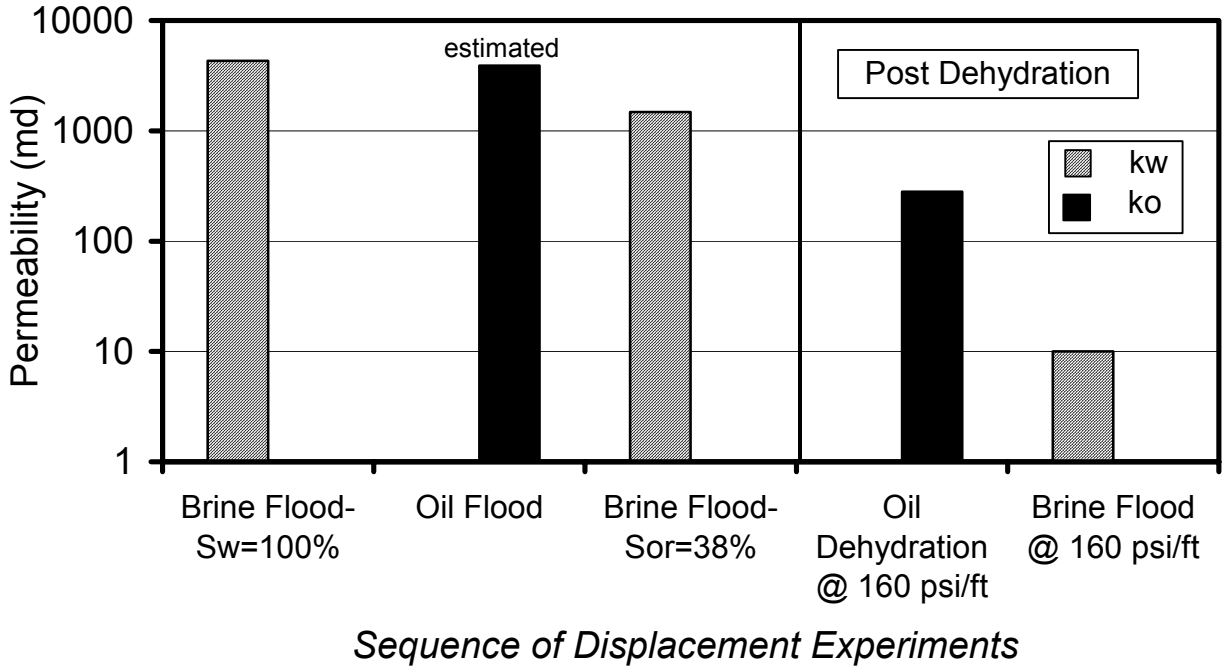

Figure 7.3 – Permeabilities obtained from dehydration of the gel in Sandpack SP20.

without an initial oil saturation, the oil permeability after gel dehydration was 50 md [Willhite, 2000]. We believe the high oil permeability in SP20 occurred because the injected oil became hydraulically connected with the residual oil from the previous waterflood.

Disproportionate Permeability Reduction in Berea Cores. The second set of experiments was conducted in Berea cores. Experiments in Berea were designed to determine permeability to oil and water at end-point saturations before and after gel treatment. Saturations were determined

by material balance at each endpoint. Results of two experiments are presented. In the first experiment (Core B5), a residual hydrocarbon saturation was established prior to injection of gelant. In the second experiment (Core B6), the core was saturated with brine prior to the gel treatment.

Experimental Data

The polymer used in this study was Alcoflood 935 (Batch 7158V). The brine contained 20,000 ppm NaCl. The gelant contained 5000 ppm HPAAM, 110 ppm Cr(III) and 5200 ppm NaOAc and had a solution pH of 6.00. An OAc/Cr ratio of 30 moles OAc:mole Cr was chosen to delay the gelation sufficiently to permit placement of the gelant before a significant viscosity increase occurred in the bulk solution and to compensate for the increase of solution pH from dissolution of carbonates. Berea cores with a nominal absolute permeability to brine of around 500 md were used in the core experiments. Each core was 1" square by 6" in length. Berea cores were fitted with endcaps and wrapped with an epoxy/fiberglass wrap. Pressure drop was measured across the core using a Validyne transducer monitored by a data acquisition system. Dodecane was used for the oil phase.

In each coreflood, the core was saturated with brine and the porosity was determined by material balance. A dispersion test was conducted with tracer (40 ppm KI, wavelength = 226.5 nm) to characterize the core and to verify porosity. Permeability to brine was determined. The oil (dodecane) used in experiments had a viscosity of 1.336 cp and a density of 0.7451 g/mL, and the brine had a viscosity of 1.023 cp, a density of 1.0115 g/mL and a pH of 5.95 at 25°C.

Core B5 was prepared for gel treatment by oilflooding to interstitial water saturation, followed by waterflooding to a residual oil saturation. Stilbene (200 ppm was added to the oil as a tracer during the initial oilflood. Stilbene is an oil soluble compound and has been used as an effective oil phase tracer by Liang et al. [1992] and Thompson and Fogler [1997]. Since the residual oil saturation contained 200 ppm stilbene, appearance of the tracer during the displacement tests indicated connection of the oil phase with the residual oil saturation that had been encapsulated within the gel. Analysis of the oil phase from flooding experiments for stilbene was used to estimate the amount of waterflood residual oil that became connected to the continuous oil phase when the gel was dehydrated by injection of oil. Endpoint oil and water permeabilities were determined at the interstitial water saturation after the oilflood and at the residual oil saturation after the waterflood, respectively. Endpoint permeabilities were determined at three constant injection rates (1 mL/min, 3 mL/min and 5 mL/min). Core B6 did not contain residual oil.

Berea core contains carbonates that dissolve in brine and increase the solution pH. Gelation of chromium acetate polyacrylamide systems is affected by pH. Therefore, each core was treated with a buffer solution to adjust pH to approximately 4.7 prior to gelant injection. About four pore volumes of acetic acid-sodium acetate buffer ([HAc] = 0.0374M, [NaAc] = 0.0635M) were injected into the core. The gelant was bulk mixed and injected at a rate of 0.1 mL/min. About 6.5 pore volumes of gelant were injected into the core. The pH of the effluent varied from 6.3 to 6.4 while the injected pH was about 6.0. The effluent was collected to measure the gel properties of effluents and concentrations of Cr (III) and Fe(III). The first part of gelant effluent (between 1 and 1.5 pore volumes injected) was a light yellow solution with a viscosity of 3.1 cp for Core B5 and a viscosity of 6.2 cp for Core B6. Cr (III) concentration was less than half of the original

concentration of 110 ppm. These effluent samples did not form gels. Samples collected after three pore volumes were injected formed gels and contained chromium concentrations at approximately the injected values. The gel time for the injected gelant was about 55 hours. The light yellow color of the initial effluent was due to small concentrations (~1-2 ppm) of Fe(III) dissolved from the core.

In Core B5, oil and brine were injected at increasing pressure drops to determine endpoint permeabilities and saturations. Flow experiments were started after a 5-7 day shut-in period following placement of the gelant. In all experiments, either oil or brine was injected at a constant pressure drop. The amount of oil or brine displaced was determined volumetrically or by weighing the effluent using an electronic balance that was connected to a data acquisition system. Experiments were carried out over a long time period because permeability developed slowly in the treated cores. The sequence of flow experiments is summarized in Table 7.3. It was not possible to inject oil into Core B5 when a pressure drop of 10 psi was applied across the core for a period of 168 hours. The initial dehydration was achieved by increasing the oil pressure drop to 20 psi.

Table 7.3 - Sequence of Injections in Core B5.

1. Saturate with brine and determine porosity and permeability to brine.
2. Conduct aqueous tracer test to verify porosity and characterize the core
3. Inject oil until brine displacement was negligible, measure volume of displaced brine and permeability to oil at interstitial water saturation.
4. Inject brine until oil displacement was negligible, measure volume of displaced oil and permeability to brine at residual oil saturation.
5. Inject acetic acid-sodium acetate buffer system and measure permeabilility to the solution at residual oil saturation.
6. Inject about 6.5 pore volumes of gelant and shut-in for 5-7 days to allow for in situ gelation.
7. Inject oil at a pressure drop of 20 psi until no brine is produced, measure volumes of oil and brine produced, measure steady state flow rate and analyze oil for stilbene
8. Inject brine at a pressure drop of 20 psi until no oil is produced, measure volumes of oil and brine produced, measure steady state flow rate, analyze oil for stilbene.
9. Inject oil at a pressure drop of 20 psi until no brine is produced, measure volumes of oil and brine produced, measure steady state flow rate, analyze oil for stilbene.

** Repeat Steps 8 & 9 at 30,40 and 50 psi pressure drops for Steps 10-15.

16. Inject oil containing stilbene tracer at a constant rate to determine volume occupied by connected oil in the dehydrated gel.

Oil and brine injections were done in the opposite direction to the direction used during gelant placement. The storage modulus and viscosity of the aqueous phases displaced by oil in the dehydration experiment were measured to determine if polymer or gel was displaced from the treated core. The stilbene concentration in dodecane was measured with a Perkin Elmer UV/VIS spectrophotometer (Lambda 20) in the manual mode at 296 nm. The dispersion test in Core B5

(Step 16) was also conducted with oil tracer (10 ppm stilbene, wavelength = 296nm) using an inline V4 Absorbance Detector (UV) to verify the volume of mobile fluid in Core B5 after gel treatment and numerous dehydration experiments.

Core B6 was not flooded with oil prior to gelant injection. Treatment of this core was done to simulate disproportionate permeability reduction in a water zone, which did not have an initial oil saturation. The sequence of experiments was the same as in Table 7.3 except Steps 3-4 and 9-16 were omitted. All experiments were performed at 25^{o}C.

Results and Analysis of Data. Results of dispersion tests confirmed that the Berea cores did not contain high permeability streaks such as hairline fractures. Pore volumes determined by material balance during brine saturation and the dispersion test were in good agreement. In contrast to experiments in the sandpacks, the aqueous phase displaced in the first oil dehydration experiment at 20 psi in Core B5 (1.1 mL) had a viscosity of 22.3 cp, indicating that some polymer or gel was displaced during dehydration. The concentration of polymer in this sample was not determined. Subsequent brine samples in the remaining dehydration runs had the same viscosity as the injected brine, indicating negligible amount of polymer or gel was displaced following the initial dehydration. Saturations, porosities and effective saturations based *"new pore space"* are summarized in Table 7.4 and Table 7.5 (next page) for Cores B5 and B6, respectively. Supporting data were presented in the reference by Willhite [2000].

Table 7.5 - Results of Berea Core B6 runs.

Experiment Procedure	S_w (%)	S_{gel} (%)	S_o (%)	Effective porosity (%)	S_w^* (%)	S_o^* (%)	k_w (md)	k_o (md)
Brine saturation	100	0	0	18.1	100	0	494	
Gel placement	0	100	0	0.	0	0		
Post gelation		100	0	0.	0	0	~0.02	
Oil dehydration 1 at 20psi	0	65.2	34.8	6.3	0	100	~0.02	103.
Brine flood 1 at 20psi	24.7	65.2	10.1	6.3	70.1	29.9	29.8	

* Based on effective porosity

An endpoint permeability was calculated from the data for each run. Values of k_w and k_o are summarized in the last two columns of Tables 7.4 and 7.5. Permeabilities from all runs are compared in Figure 7.4 for Core B5. Both brine and oil permeabilities increased as the pressure drop across the core increased. These changes are due to additional dehydration at higher pressures and the elasticity of the gel. Core B5 exhibited disproportionate permeability reduction after the gel treatment. However, permeability to oil at interstitial water saturation was reduced substantially.

Table 7.4 – Results from Berea Core B5 runs.

Experiment Procedure	S_w (%)	S_{gel} (%)	S_{ot} Encapsulated by gel (%)	S_o Not encapsulated by gel (%)	Effective Porosity** (%)	S_w* (%)	S_o* (%)	k_w (mD)	k_o (mD)
Brine saturation	100	0	0	0	19.2	100	0	520	
Oil flooding	33	0	0	66.6	19.2	33	66.6	0	420.6
Brine flooding	69	0	0	31.2	19.2	69	31.2	57.85	0
Buffer solution injection	69	0	0	31.2	19.2	69	31.2	57.85	0
Gel placement	0	68.8	31.2	0	0	0	0	57.85	0
Post gelation	0	68.8	31.2	0	0	0	0	~0	0
Oil dehydration 1 at 20psi	0	63	24.9	12.1	2.3	0	100		4.62
Brine flood 1 at 20psi	9.0	63	24.7	3.3	2.4	73.2	26.8	0.0061	0
Oil dehydration 2 at 20psi	0	61.8	21.3	16.9	3.2	0	100	0	5.69
Brine flood 2 at 30psi	11.6	61.8	21.3	5.3	3.3	68.6	31.4	0.0064	0
Oil dehydration 3 at 30psi	0	61.8	19.0	19.2	3.7	0	100	0	13.08
Brine flood 3 at 40psi	6.9	61.8	19.0	12.3	3.7	65.1	34.9	0.0104	0
Oil dehydration 4 at 40psi	0	57	17.6	25.4	4.9	0	100	0	26.7
Brine flood 4 at 50psi	12.7	57	17.6	12.7	4.9	50	50	0.033	0
Oil dehydration 5 at 50psi	0	57	16.5	26.5	5.1	0	100	0	36.75

* Based on effective porosity
**Effective porosity does not include oil trapped in the gel

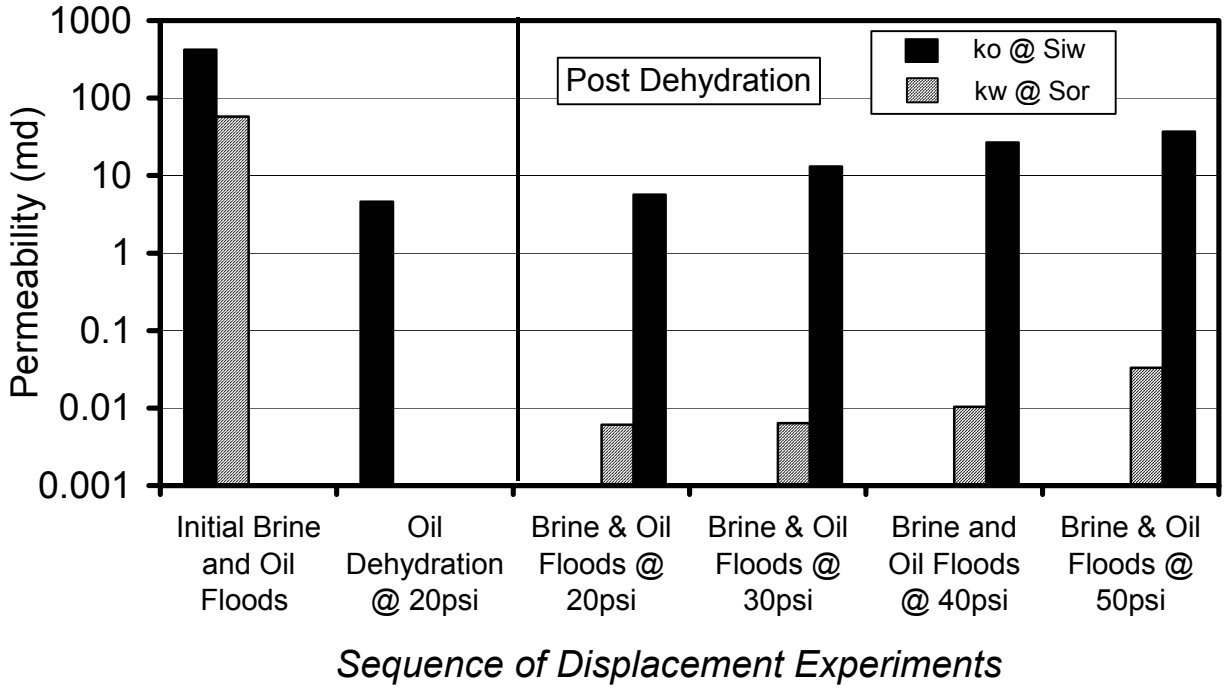

Figure 7.4 – Development of brine and oil permeabilities following dehydration of Core B5 after gel placement.

Insight into the causes of DPR in Core B5 can be obtained by estimating endpoint saturations as well as saturations of the immobile and trapped phases calculated from the data collected for each displacement experiment in Table 7.4. Endpoint saturations were determined by material balance. We assumed that the initial aqueous phase was displaced by the gelant so that this volume was filled with immobile gel upon gelation. The volume occupied by the gel was assumed to be the same as the volume of the gelant with no change of volume upon gelation. When the gel was initially dehydrated by the injection of oil, the pore space created by dehydration of the gel was filled with oil. Water produced by dehydration of the gel structure was assumed to be displaced from the core. The effective pore volume for the core is defined as the pore space not containing a gel or oil encapsulated by gel. The effective pore volume was calculated by subtracting the volume occupied by the remaining gel and the encapsulated waterflood residual oil from the initial pore volume. Volumetric data were presented in the preprint of this paper [Willhite, 2000].

The effective porosity of the core following the initial dehydration of the gel was estimated to be 2.3% compared to an effective porosity of 13.2% following brine flooding (Step 4, Table 7.3) and an initial porosity of 19.2%. Reduction of the effective porosity caused substantial reduction in permeability of the core as observed in experiments in both sandpacks and Berea core. Although the gel treatment reduces the water permeability preferentially, the absolute permeability of each phase is reduced substantially from the original values.

Stilbene was found in the displaced oil during every oilflood in which the pressure drop was increased. With the exception of the first brine flood, small concentrations of stilbene were found in the oil displaced by brine floods. Oil flooding at increased pressure drop caused additional dehydration of the gel structure, connecting some of the original waterflood residual oil saturation to oil flow paths. This is reflected in the increase in oil permeability with increasing pressure drop shown in Table 7.4. Some of the increase in oil permeability may be due to the effect of flowrate on oil permeability observed by Yan et al. [1999] and Al-Sharji et al. [1999].

Stilbene concentration data were used to estimate the amount of trapped residual waterflood oil that became connected (mobile) following dehydration by injecting oil. Saturations of the trapped oil in Table 7.4 are based on the total porosity. The "reconnected" residual oil was calculated by assuming the total stilbene produced during a run was released by connecting the flowing fluid to the volume of residual oil containing the same amount of stilbene at the initial concentration of 200 ppm. To check the overall material balance, no stilbene was found in the oil during oil injection prior to injecting stilbene as a tracer in Step 16, suggesting that the remaining trapped oil saturation (16.5%) was not in contact with the oil phase after the completion of the oilflood in Step 15. The volume of the mobile oil phase based on material balance calculations was 6.9% less than the value determined from the stilbene tracer experiment. The agreement between these two values is within experimental error and validates the methods used to determine the saturations of both brine and oil phases by material balance.

There is an additional consequence that contributes to the mechanisms causing DPR in a porous matrix treated with a gelant that forms a dehydratable gel. If we consider only the volumes of the oil and brine phases in the porous matrix, we note that the saturations of brine and oil in the effective pore space are quite different from the initial saturations. Material balance calculations suggest that the volume of water remaining in the effective pore space is small at the end of the oil dehydration cycle. There was no evidence of rehydration of the gel with time as the volume occupied by mobile fluids (oil and brine) did not decrease with time.

Results from floods in Core B6 are summarized in Table 7.5. Core B6 did not contain residual oil and the volume of gel dehydrated by the oilflood was substantially higher than in Core B5. The effective porosity following dehydration by oil at 20 psi was 6.3% and the permeability to oil was 103 md. After the waterflood at 20 psi, the residual oil saturation in the pore space created by dehydration of the gel was 29.9% and the water saturation was 70.1%. Permeability to water was 29.8 md. These permeabilities are much higher than the permeabilities observed in Core B5 under the same pressure gradient. In Core B5, the residual oil saturation in the effective pore volume after the first brine flood is 26.8% but the brine permeability was 6.1 μd.

The principal difference between these runs is the presence of residual oil saturation in Core B5 prior to the gel treatment. Berea sandstone is strongly water wet. The residual oil saturation in Berea sandstone occupies the largest pores and reduces the permeability to water by a factor of about 10. Thus, the treatment of Core B5 can be viewed as the treatment of a core which had an effective permeability of 57.8 md and an effective porosity of 13.2% at the time the gelant was placed. Since residual oil occupies the largest pores in Core B5, the inferred morphology of the flow paths created by dehydration of gel in Core B5 is much different than in Core B6. Since endpoint permeabilities were not available in Core B6, it is not possible to compare

disproportionate permeability reduction in the same manner as can be done for Core B5. However, two conclusions can be drawn. First, the permeability to both oil and water are reduced by the gel treatment. Second, the presence of a residual oil saturation either before gel placement or after gel placement is a major contributor to disproportionate permeability reduction.

Discussion

These experiments provide insight into the mechanism of disproportionate permeability reduction when a porous matrix is treated with a chromium acetate-polyacrylamide gelant that is dehydratable. Dehydration of the gel observed in bulk experiments occurs in unconsolidated sandpacks and Berea sandstone cores. Dehydration with oil creates a "*new pore space"* for fluid flow as the gelled polymer is squeezed into a smaller volume. The effective polymer concentration increases in the remaining gel, further strengthening its resistance to deformation. Since the permeability of gelled polymer is quite low, flow of fluids occurs primarily in the pore structure created by the dehydration of the gel. The "*new pore space"* is a fraction of the original porosity and the permeability to oil is reduced substantially from its initial value. Subsequent brine injection displaces oil from these flow channels but traps some of the oil in the "*new pore space"* as a residual saturation.

We believe that dehydration is irreversible and that the gel does not rehydrate when contacted with excess solvent. The trapping of residual oil in the "*new pore space*" causes the disproportionate reduction in brine permeability because the brine flows primarily in the pore channels created by dehydration of the gel even though the gel has some brine permeability. The result suggests that both brine and oil flow through the same path, but the brine phase must flow in thin films and channels around the trapped oil phase, which can occupy a large fraction of the *"new pore space"* created by dehydration of the gel. Some brine can flow through the dehydrated gel structure but the permeability of the dehydrated gel is on the order of tens to hundreds of microdarcies. The trapped oil phase in the "*new pore space"* is a significant contributor to disproportionate permeability reduction.

Figures 7.5a-d illustrate the proposed mechanisms causing DPR in a porous matrix containing a residual oil saturation. Figure 7.5a shows residual oil ganglia from a previous waterflood encapsulated by the gel, which is assumed to fill the entire pore space in this illustration. Figure 7.5b shows the *"new pore space"*, created when oil is injected into the porous media, dehydrating the gel. Water and uncrosslinked polymer in the dehydrated gel are displaced as the oil invades the gelled matrix. Some residual oil ganglia are reconnected as the injected oil generates the *"new pore space".* It is not known whether the process of reconnection involves rupture of the gel-oil interface as observed by Miller and Fogler [1995] for foam gels or progressive thinning of the gel-oil interface leading to rupture. In any case, part of the oil flow path prior to gel treatment is reconnected and is incorporated into the *"new pore space".* Since the gel is hydrophilic, water produced by additional dehydration after formation of the initial flow path can flow in thin films at the gel-oil interface as well as through the gel structure when the pressure gradient is increased during the initial oil injection. Figure 7.5c illustrates the fluid distribution when water is injected into the porous medium after creation of the *"new pore space"*. Oil is displaced from the *"new pore space"*, but a residual oil saturation remains. The residual oil saturation in the *"new pore space"* creates substantial flow resistance to water in the *"new pore space"* and is a major contributor to DPR. Figure 7.5d illustrates the fluid distribution when oil is injected after the first

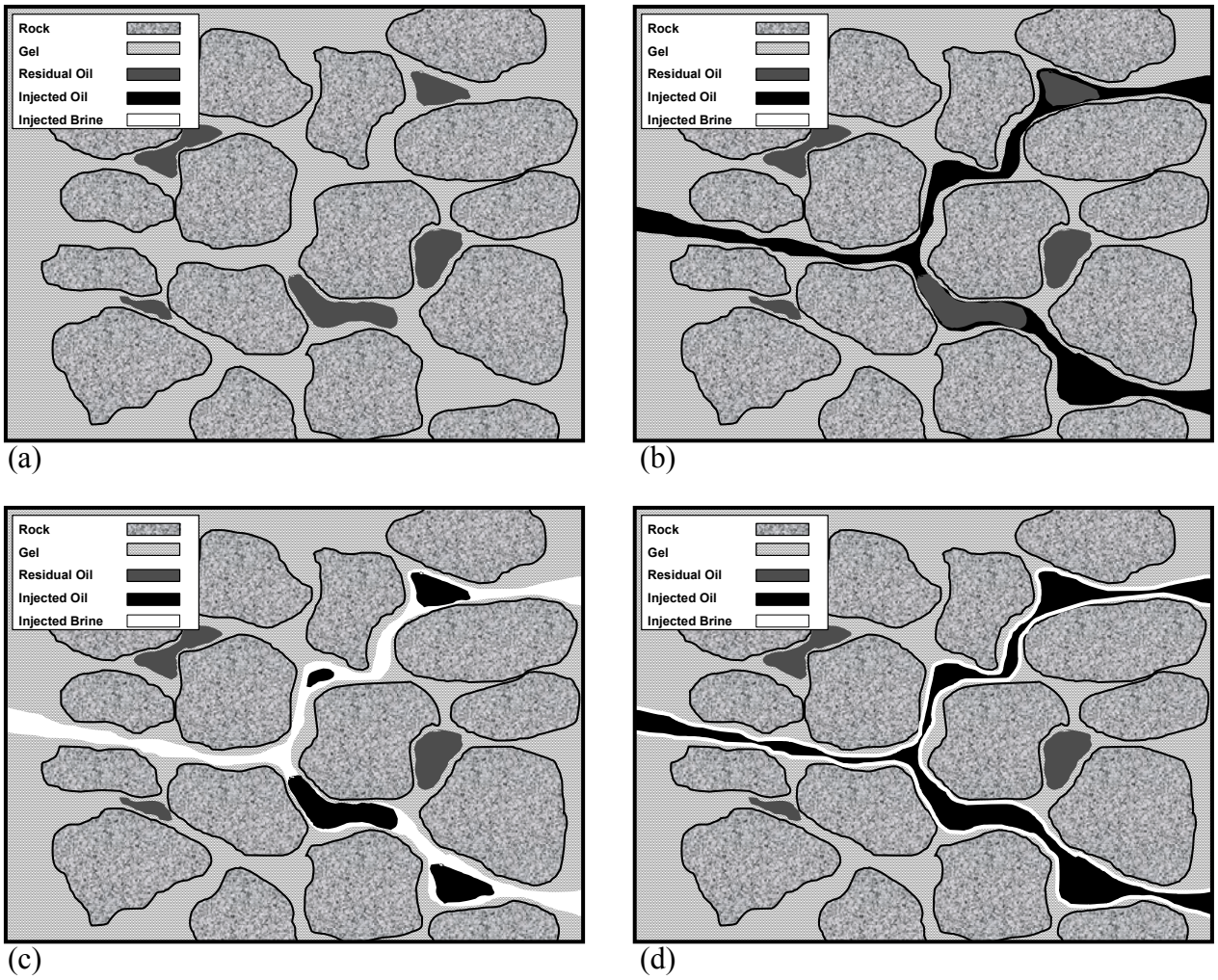

Figure 7.5 – Conceptual model on disproportionate permeability reduction. **(a)** Encapsulation of waterflood residual oil following in situ gelation of chrome-acetate-polyacrylamide gelant. **(b)** Generation of *"new pore space"* when gel is dehydrated by injection of oil. **(c)** Trapping of residual oil in *"new pore space"* during brine flood, leading to disproportionate permeability reduction of brine. **(d)** Flow paths of oil through *"new pore space"*, trapping low saturations of brine.

waterflood. The residual water exists in isolated pockets and in thin films causing little flow resistance to oil. Thus, oil permeability is significantly higher than water permeability because oil flows in most of the *"new pore space"*. The flow of water is impeded by the presence of the residual oil saturation. Residual water distribution in the *"new pore space"* is determined by the pore morphology. Permeability to both oil and water are reduced because a significant part of the original pore space is filled with gel that is impermeable to oil and has a permeability to water in the range of tens to hundreds of microdarcies.

In Berea cores containing an initial oil saturation, brine displacement experiments at the same pressure drop showed that initial brine permeability at waterflood residual oil saturation was

reduced by factors of 100-1000 more than the oil permeability, verifying the existence of disproportionate permeability. When residual oil saturation is initially present as the gelant is placed, the residual oil is encapsulated by the gel, contributing to the disproportionate permeability reduction mechanism by forcing injected fluids to create new flow paths around the trapped oil. Dehydration of the gel reconnects some of the trapped oil as pressure gradients increase with a corresponding increase in effective pore volume and oil permeability.

These experiments show that some oil permeability may be regained in reservoirs that have been treated with a gelled polymer system if the treated interval is subjected to a pressure gradient by injecting oil or by production of oil from that interval under a controlled drawdown. With sufficient pressure gradient, the oil is able to dehydrate the gelled region, creating preferential permeability to oil. Water zones will exhibit larger DPR if residual oil saturation is present in the zone when the gelant is placed.

Conclusions

1. Conclusions are based on the studies of chromium acetate-polyacrylamide gels prepared containing 5000 ppm polymer with a molar mass of 5 million Daltons and 5-10% degree of hydrolysis in unconsolidated sandpacks and Berea sandstone cores.
2. Flow paths for brine and oil after gelation are created primarily by the dehydration of the gel by injection of oil.
3. The effective porosity of the porous matrix was reduced by the gel treatment.
4. The permeability of the porous matrix to oil was reduced significantly by the gel treatment.
5. Disproportionate permeability reduction was observed in sandpacks after dehydration of gel.
6. Disproportionate permeability reduction for brine was observed in Berea sandstone core material.
7. Disproportionate permeability reduction for brine was caused by the trapping of residual oil in the *"new pore space"* created by the dehydration of the gel.
8. Brine and oil flow in the same pore space created by the dehydration of the gel.
9. Smaller brine permeabilities were observed when the porous matrix contained a residual oil saturation prior to gel placement than in a porous matrix that did not have a residual oil saturation.
10. The inferred morphology of the flow paths created by dehydration of the gel is affected by the presence of encapsulated residual oil.
11. Dehydration by oil after in-situ gelation reconnected some of the residual oil saturation encapsulated by the gel treatment.

Nomenclature

k_o = permeability to oil, L^2, md
k_w = permeability to water, L^2, md
S_{gel} =saturation of gel, %
S_o = saturation of oil, %
S_o*= saturation of oil in the effective pore space, %
S_{ot} = saturation of oil encapsulated by gel, %
S_w = saturation of water, %
S_w* = saturation of water in the effective pore space, %
ϕ_{eff} = effective porosity, %

Acknowledgements

Material in this chapter is substantially unchanged from a copyrighted paper published by the Society of Petroleum Engineers. The paper is in the *Soc. of Pet. Engrs Journal*, September, 2002, pp. 309 – 315. The SPE copyright release form grants authority to authors the "nonexclusive right to incorporate all or part of the work in future writings or presentations."

References

1. Al-Sharji, H.H., Grattoni, C.A., Dawe, R.A., and Zimmerman, R.W.: "Pore-Scale Study of the Flow of Oil and Water through Polymer Gels," paper SPE 56738 presented at the 1999 SPE Annual Technical Conference and Exhibition, Houston, TX (3-6 October).
2. Dawe, R.A. and Zhang, Y.: "Mechanistic Study of the Selective Action of Oil and Water Penetrating into a Gel Emplaced in a Porous Medium*," Journal of Petroleum Science and Engineering* (1994) **12**, 113-125.
3. Green, D.W., Willhite, G.P., McCool, C.S., Heppert, J.A., Vossoughi, S. and Michnick, M.J.: "In situ Permeability Modification Using Gelled Polymer Systems," Annual report for the period of April 11, 1997 – April 10, 1998, DOE Contract No. DE-AC22-94PC91008, The University of Kansas.
4. Krishnan, P.K, Asghari, K., Willhite, G.P., McCool, C.S., Green, D.W. and Vossoughi, S: "Dehydration and Permeability of Gels Used in In Situ Permeability Modification Treatments," paper SPE 59347 presented at the SPE/DOE Improved Oil Recovery Symposium, Tulsa, OK (3-5 April 2000).
5. Liang, J. and Seright, R.S.: "Further Investigation of Why Gels Reduce Water Permeability More Than Oil Permeability," *SPEPF* (November 1997) 225-230.
6. Liang, J., Sun, H., and Seright, R.S.: "Reduction of Oil and Water Permeability using Gels," paper SPE 24195 (April 1992) 22-24.
7. Liang, J., Sun, H. and Seright, R.S.: "Why Do Gels Reduce Water Permeability More Than Oil Permeability?," *SPERE* (November 1995), 282-286.
8. Mennella, A., Bryant, S.L. and Lockhart, T.P.: "Propagation of Tracers through Cores with Mass Transfer into an Immobile Fluid Phase," paper SPE 37248 presented at the SPE International Symposium on Oilfield Chemistry, Houston, TX (18-21 February 1997).
9. Miller, J.J. and Fogler, H.S.: "Foamed Gel Barriers in Porous Media: Breakdown and Permeability Evolution", *AIChEJ*, **41,**No. 11(November 1995), 2487-2498.
10. Natarajan, D.;" Study of Gelation and Injection Characteristics of Polyuacrylamide-Chromium(III) systems in the Presence of Excess Acetate Ions", M.S. Thesis, University of Kansas, 1997.
11. Natarajan, D, McCool, C.S., Green, D.W. and Willhite, G.P.: "Control of In-Situ Gelation Time for HPPAM-Chromium Acetate Systems," paper SPE 39696 presented at the 1998 SPE/DOE Improved Oil Recovery Symposium, Tulsa, OK (19-22 April 1998).
12. Nilsson, S. Stavland, A. and Jonsbraten, H.C.: "Mechanistic Study of Disproportionate Permeability Reduction," paper SPE 39365 presented at the SPE/DOE Eleventh Symposium on Improved Oil Recovery, Tulsa, OK (19-22 April 1998).

13. Seright, R., S., and Martin, F., D.: "Inherent Permeability to Water for Several Gels," *Fluid Diversion and Sweep Improvement with Chemical Gels in Oil Recovery Processes*, Second Annual Report, May 1, 1990 through April 30, 1991, DOE Contract No. DE-FG22-89BC14447, Report No. DOE/BC/14447-10, New Mexico Institute of Mining and Technology, Chap. 3, 24-25.
14. Sydansk, R.D. and Southwell, G.P.: "More Than 12 Years of Experience with a Successful Conformance-Control Polymer Gel Technology", paper SPE 49315 presented at the 1998 SPE Annual Technical Conference and Exhibition, New Orleans, LA (27-30 September).
15. Thompson, K.E. and Fogler, H.S.: "Pore-Level Mechanisms for Altering Multiphase Permeability with Gels," *SPEJ* (September 1997) **2**, 350-362.
16. Willhite, G.P., Green, D.W., McCool, C.S., Michnick, M.J., Vossoughi, S., Asghari, K., Krishnan, P., and Natarajan, D., "Permeability and Dehydration of Polymer Gels after Placement," *In situ Permeability Modification Using Gelled Polymer Systems*, Final report for the period of June 10, 1996 – July 31, 1998, DOE Contract No. DE-AC22-94PC91008, The University of Kansas, Chap. 5, 1-18.
17. Willhite, G.P., Zhu, H., Natarajan, D., McCool, C.S., and Green, D.W.: "Mechanisms Causing Disproportionate Permeability in Porous Media Treated with Chromium Acetate/HPAAM Gels" SPE/DOE Paper 59345 presented at the 2000 SPE/DOE Improved Oil Recovery Symposium, Tulsa, Oklahoma, 3-5 April 2000.
18. Yan, Z., McCool, C.S., Green, D.W., and Willhite, G.P.: "Modification of Oil and Water Permeabilities in Berea Sandstone by a Gel Treatment," paper SPE 50753 presented at the International Symposium on Oilfield Chemistry, Houston, TX (16-19 February 1999).

Chapter 8

Effect of Pressure Gradient on Disproportionate Permeability Reduction in Gel-Treated Rock

Researcher Associate: Somenath Ganguly

Introduction

Produced water is a growing concern in mature fields as oil production declines and water cuts increase. Each additional barrel of produced water adds to the cost of (a) lifting the hydrocarbon in a production well, (b) separation of oil and water, (c) protection against corrosion in tubing, and (d) disposal of water. Economic and environmental interests drive development of techniques that can reduce production of water without affecting production of oil significantly. The treatment of a production well with a gelled polymer system is a remedial measure in which the operator would like to preferentially reduce the permeability to water with minimum effect on oil production. Although no treatment has been found that reduces water permeability without affecting oil permeability to some extent, several polymers and gels reduce permeability to water significantly more than to oil when injected into porous rock. This phenomenon, termed disproportionate permeability reduction (DPR), is potentially beneficial for water shut-off treatments in production wells when hydrocarbon-productive zones cannot be protected during gel placement or when the source of water production cannot be determined.

Many production wells have been successfully treated with gelled polymer systems [Sydansk, 1998]. Treatment methodology tends to be empirical in part because there is still uncertainty on how permeability is reduced selectively. The effect of polymer treatments on the permeability to water and oil after gel treatment has been investigated for almost two decades. Research has focused on two general areas: (a) investigation of mechanism(s) leading to disproportionate permeability reduction and (b) estimation of permeability under various fractional flows.

Willhite et al. [2002]. demonstrated that disproportionate permeability is observed when oil and brine flow through the new pore structure created by dehydration of a portion of the gel structure in the treated porous rock by injection of oil. Disproportionate permeability was thought to occur because residual oil was trapped in the new pore structure when oil was displaced by water. Disproportionate permeability reduction was found to be a function of the pressure gradient applied initially to dehydrate the gel, and the flow rate (or pressure gradient) in the new pore structure created by dehydration.

Most of the referenced studies indicate that polymer systems that gel during or after placement exhibit disproportionate permeability reduction in porous media varying from Berea sandstone and carbonate cores to unconsolidated sand packs. In nearly all cases, DPR was found to vary with flow rate. Liang et al. [1995] found that the permeability to brine increased significantly with flow rate but reported insignifcant change in permeability to oil with flow rate. Yan et al. [1999] observed post-treatment permeability to both oil and brine changed with flow rate. The change followed a power-law relationship. A similar observation was made by Willhite et al. [2002] and Seright [1999]. These studies covered a limited range of flow rates.

Experimental Approach

Flow experiments were conducted in Berea sandstone slabs and cores. Results from one slab and four cores are reported. Additional data for the slab runs are reported in Reference 5. The slab was 6 inches by 6 inches by 1 inch thick and the cores were 1 inch by 1 inch by six inches long. Properties of the porous rocks are summarized in Table 8.1. The slab and cores were equipped with inlet and outlet fittings and were coated with epoxy. Two pressure ports were installed at two and four inches along the length of the slab, dividing it into three sections. Pressure was measured across the entire length of the cores. Pressures were measured continuously using Validyne transducers connected to a Camille data acquisition system. The porous rocks were saturated with one percent NaCl, flooded with oil (dodecane) to residual brine saturation, and then waterflooded with brine to residual oil saturation. Permeabilities to brine and oil were each determined at the residual saturation of the other phase. The Berea sandstone rocks were at residual oil saturation prior to the injection of gelant.

Table 8.1 - Properties of Berea sandstone cores used in flow experiments.

	Slab 1	Core 2	Core 3	Core 4	Core 5
Dimension (inches)	6×1×6	1×1×6	1×16	1×1×6	1×1×6
Pore volume (mL)	110	23.2	24.0	24.8	24.5
Porosity, fraction	0.188	0.236	0.244	0.252	0.249
Brine perm (mD)	556	519	500	500	484
Oil perm at interstitial water saturation, mD	265	465	528	506	477
Res. oil perm, mD	51	86	85	88	62
PV gelant injected	6.5	1.5	1.5	2	2
Injection period (hrs)	36	1	1	2	2
Shut-in period (days)	9	6	60	8	8
Oil injection pressure – initial dehydration (psi)	80	20		20	
Brine injection pressure - initial dehydration (psi)	80		20		20

Berea sandstone core contains calcium carbonate which dissolves during brine injection, increasing the effluent pH to the vicinity of 8 or higher. An acetic acid-sodium acetate buffer solution was injected to stabilize the effluent pH to 5 prior to injection of the gelant. This was done to minimize precipitation of chromium from aqueous solutions when the pH rises above 6. The composition of the buffer solution was 0.864% of sodium acetate, 0.23 % of acetic acid, and 1 % NaCl. All compositions are reported in wt%. The pH of the buffer solution was 4.9. The

effluent from displacement of buffer solution turned yellowish after some time indicating dissolution of iron from the rock. The buffer solution was displaced from the porous rock by injection of gelant.

Berea sandstone cores or slabs at residual oil saturation were treated with a chromium acetate-polyacrylamide gelant. The resident brine buffered by sodium acetate was displaced by the gelant leaving a residual oil saturation encapsulated by the gel structure that formed after the core/slab was shut in to permit gelation. Permeability of the gel treated core/slab to brine was on the order of a few microdarcies. The gel-treated slab was impermeable to oil as long as the initial gel structure was intact.

Permeability to oil and brine was created by injection of oil or brine at a constant pressure drop [Willhite, 2002]. When the gel treated core/slab is exposed to oil at low-pressure gradients (40 psi/ft), the gel structure slowly dehydrates as brine is "squeezed" from the gel structure and flows through the core/slab where it is produced. The produced effluent contains some polymer but is primarily brine. Flow channels develop through the gel structure creating a new pore structure within the gel treated pore space. The gel structure remaining in the porous matrix contains a higher polymer concentration than the initial injected gelant.

Experimental Data

Slab Experiments. The initial experiments conducted in the gel-treated slab consisted of a series of runs made at different pressure gradients: (1) oil floods, (2) brine floods, and (3) oil floods. Results from these experiments are presented in this section with the experimental procedures, and were used to develop experiments conducted in the cores.

Figure 8.1 presents an overview of Runs 1.5-1.11 in the slab. The sequence of experiments and data are summarized in Table 8.2. A microwave apparatus was used to obtain saturation maps for experiments conducted in the slab. Further details of the apparatus are given in Reference 5. Saturations measured during brine and oil floods were confirmed by material balance. Saturations and effective porosities in Table 8.2 were estimated from measurement of effluent volumes by material balances using the following assumptions: (1) the gelant displaced all of the resident brine, (2) the residual brine saturation in the new created pore structure was negligible at the end of each oil flood, (3) the amount of oil encapsulated by the gel did not change after the initial dehydration unless a larger pressure gradient was imposed on the slab or core and (4) the newly created pore structure did not change unless a larger pressure gradient was imposed on the slab or core.

The composition of the gelant used in the slab experiment was 0.52% sodium acetate, 0.5% polyacrylamide (Alcoflood 935), and 450 ppm chromium triacetate (112.5 ppm Cr(III)). Sodium acetate was added to delay gelation. The gelant had a pH of 6.2, bottle gel time of 2 ½ days and initial viscosity of 41 cp (at 11.25 sec^{-1}). Bulk-mixed gelant was injected into the rock using either an oil pump or an air source. In this experiment 6.5 PV of gelant was injected over a period of 32 hours. Effluent samples were collected in fractions and were analyzed for pH and gel time.

Table 8.2 - Summary of data-for Slab 1.

Run	Description	S_w (%)	S_{gel} (%)	S_{ot} (encap. by gel) (%)	S_o (not encap. by gel) (%)	Effective Porosity** (%)	S_w* (%)	S_o* (%)
1.1	Pre-treatment brine flood	100	0		0	18.6		
1.2	Oil flood	42	0		58	18.6		
1.3	Brine flood	72	0		28	18.6		
1.4	Gelant Injection	0	74	26	0	0.0		
1.5	Oil flood-dehydration @160 psi/ft	0	60	12	28	5.3	0	100
1.6	Oil flow rate tests	0	60	12	28	5.3	0	100
1.7	Brine flood @160 psi/ft	17	60	12	11	5.3	61	39
1.8	Brine flow rate tests	17	60	12	11	5.3	61	39
1.9	Oil flood @160 psi/ft	0	59	12	29	5.4	0	100
1.10	Oil flood[1]-displace tracer @160 psi/ft	0	59	12	29	5.4	0	100
1.11	Oil rate tests -high pressure drop	0	59	12	29	5.4	0	100
1.12	Oil rate tests -wide pressure drop range	0	59	12	29	5.4	0	100
1.13	Brine flood @160 psi/ft	19	59	12	10	5.4	66	34
1.14	Brine rate tests	19	59	12	10	5.4	66	34

Sw* and So* are based on effective porosity.

**Effective porosity does not include gel or oil encapsulated in the gel.

**Effective porosity based on volume of connected oil in Run 1.10 (32 mL)-volume of residual water is neglected.

Note: Run 1.10-connected oil volume from tracer test was 32 mL.

After a shut-in period, post-treatment flow was established by injecting oil (Run 1.5) at a constant pressure drop of 50 psi (100 psi/ft). Constant injection pressure was obtained by connecting an air source with a pressure regulator to a transfer cylinder containing the injected fluid. The oil was injected at the opposite end of the slab at which the gelant was injected, i.e. the opposite direction to gelant flow.

The injected oil dehydrated the gel, creating flow channels within the gel. The first aqueous effluent sample (~5 mL) was a viscous polymeric solution (31 cp at a shear rate of 11.25 sec^{-1}). Viscosities of subsequent samples were not measured. Dehydration of the gel structure is a slow process as can be seen by the slow change in average water saturation in Figure 8.1. At the end of the initial dehydration at ~100 psi/ft, about 14 mL of brine was displaced by injecting about 425 mL of oil.

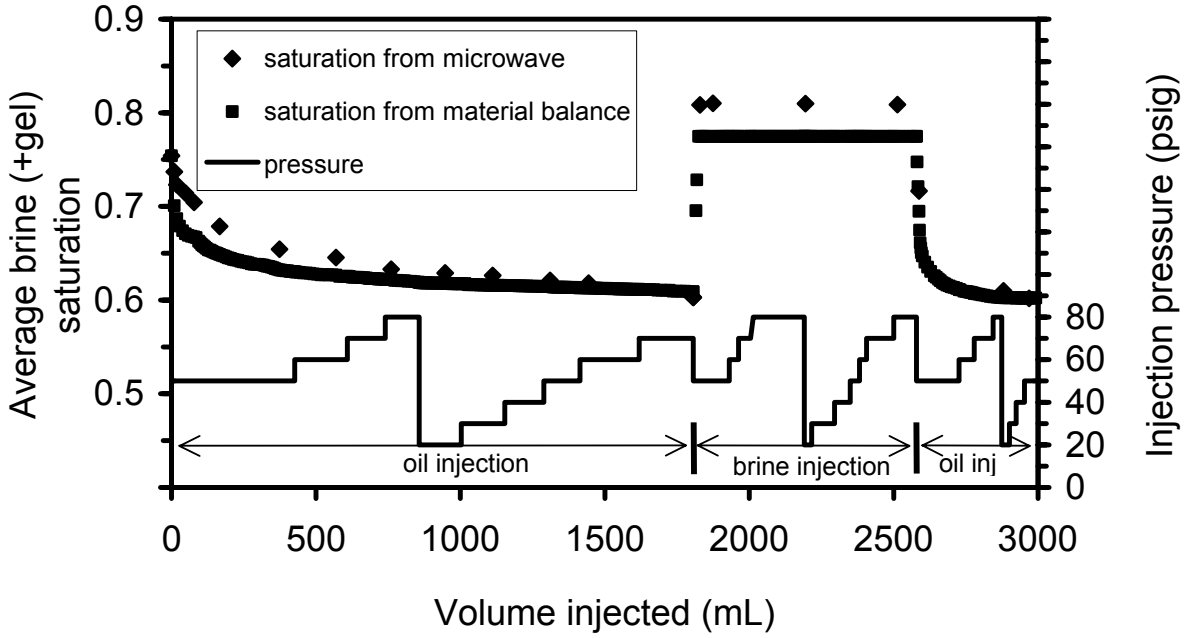

Figure 8.1 - Summary of displacement and pressure drop data for Slab 1; Initial tests (Runs 1.5-1.11).

After the initial dehydration run, oil was injected at different pressure gradients (Run 1.6) beginning at 100 psi/ft and with a maximum of 160 psi/ft. Steady-state flow rates were determined at each pressure gradient. Small amounts of brine were displaced from the gel structure as the pressure gradients were changed. At the end of Run 1.6, the total volume of aqueous phase displaced during oil injection was 16 mL which is equivalent to 20% of the gel volume placed in the pore space. Figure 8.2 presents oil permeability across the slab as a function of pressure gradient. The sequence of pressure gradient changes is indicated on the figure. Permeability to oil was reduced by a factor of about 10 by the gel treatment. Oil permeability decreased when the pressure gradient was reduced from 160 psi/ft to 40 psi/ft suggesting that the gel structure relaxed when the pressure gradient was reduced. Note that permeability to oil increased 50-100% following the pressure cycle in Figure 8.1. This is an indication of the elasticity of the gel structure.

In Run 1.7, the dehydrated, oil saturated slab was flooded with brine at a constant pressure gradient of ~100 psi/ft until oil displacement was completed. Displacement of oil was essentially piston-like with little oil produced after breakthrough of brine. Displacement was analogous to a waterflood of a strongly water-wet rock. Permeability to brine was reduced by a factor of 10-20 after the gel treatment/dehydration process compared to the brine permeability at residual oil saturation.

The effect of flow rate on brine permeability was determined by injecting brine at constant rates in Run 1.8 and measuring the pressure drop. The flow tests (Run 1.8) are indicated by the overall

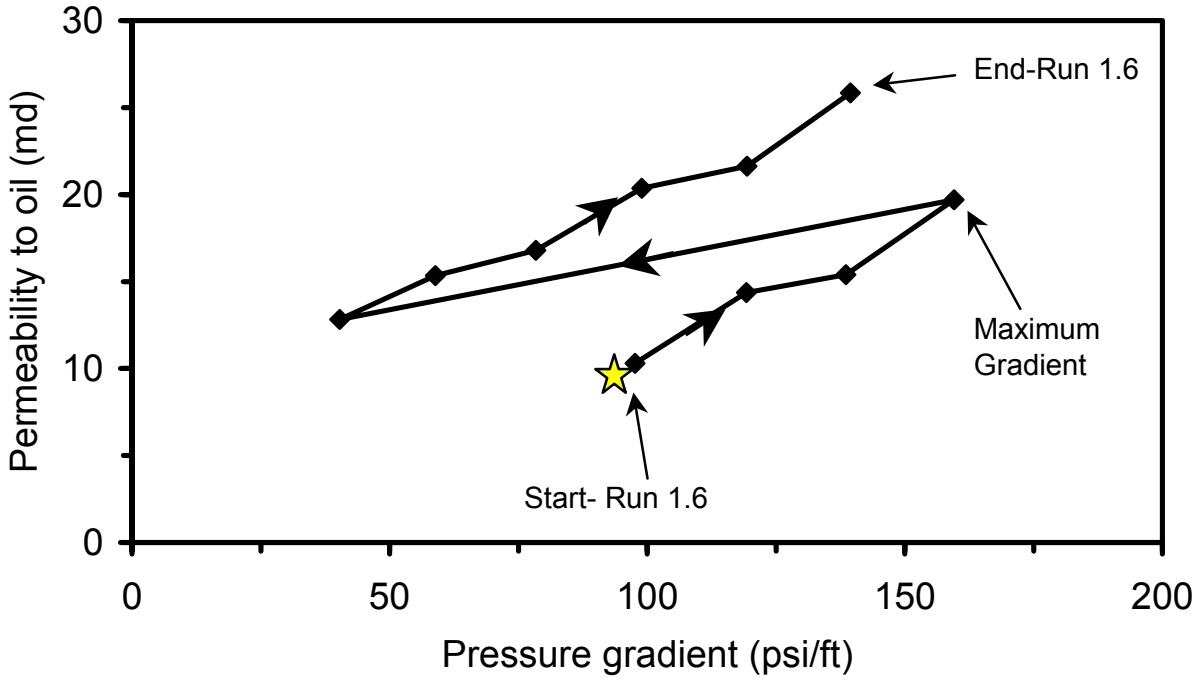

Figure 8.2 - Effect of pressure gradient on the permeability to oil in Slab 1 after dehydration of gel treated slab with oil at 160 psi/ft.

brine permeability data in Figure 8.3. No oil was displaced from the slab during these brine permeability tests.

The variation of brine permeability with pressure gradient is thought to be caused by the elasticity of the gel structure as no additional oil was displaced and the pressure gradient on the gel structure was limited to the maximum gradient applied during the dehydration by oil, Run 1.5. It was not possible to determine if additional dehydration occurred during brine injection tests.

A second oil flood (Run 1.9) was conducted in the slab starting at a pressure gradient of ~100 psi/ft. Oil broke through shortly after the beginning of injection. Brine was produced continuously at slowly decreasing brine cuts. The same sequence of pressure gradient changes applied in Run 1.6 was applied in Run 1.11 as shown in Figure 8.4. There is good agreement between the oil permeability data from Runs 1.6 and 1.11, further reinforcing the observation that oil permeability in the gel-treated rock is a function of the applied pressure gradient, the saturation history and the sequence at which the pressure gradients are applied.

Some of the encapsulated residual oil was reconnected to the flow channels during the dehydration process. An oil tracer test was conducted in Run 1.10 to estimate the oil-contacted volume in the newly created pore space after gel dehydration. An oil soluble tracer (200 ppm of stilbene) was injected and effluent concentrations were analyzed to determine the oil contacted

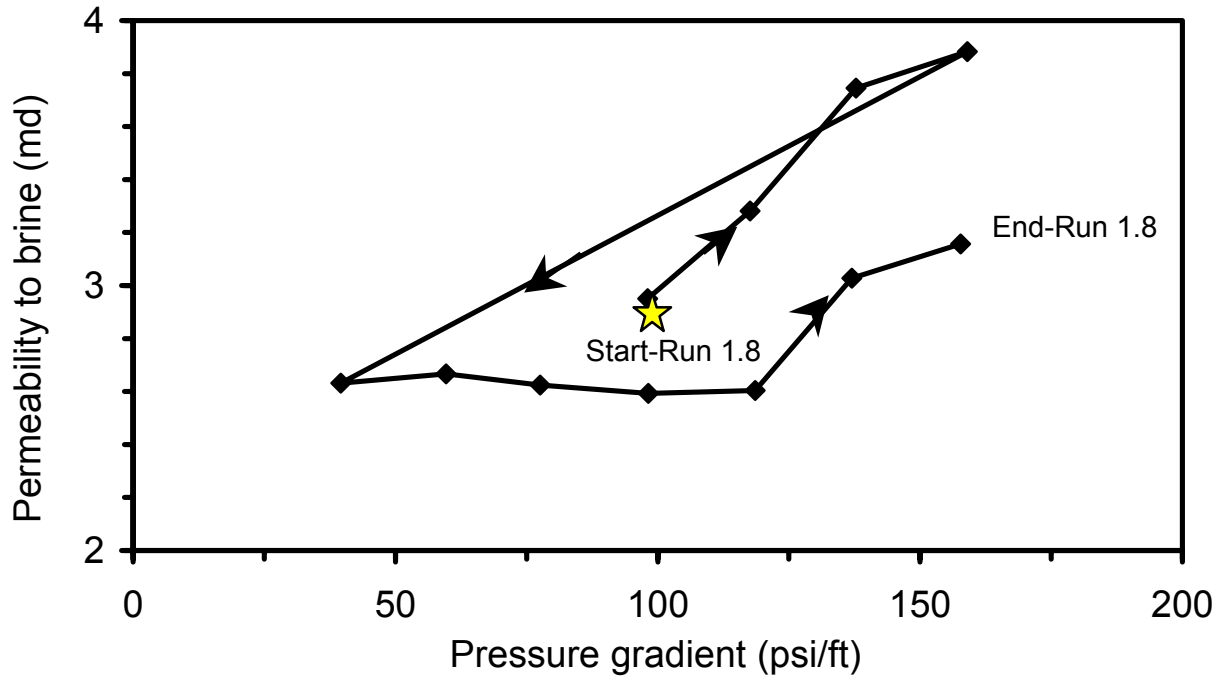

Figure 8.3 - Effect of pressure gradient on the permeability to brine in Slab 1-Run 1.8.

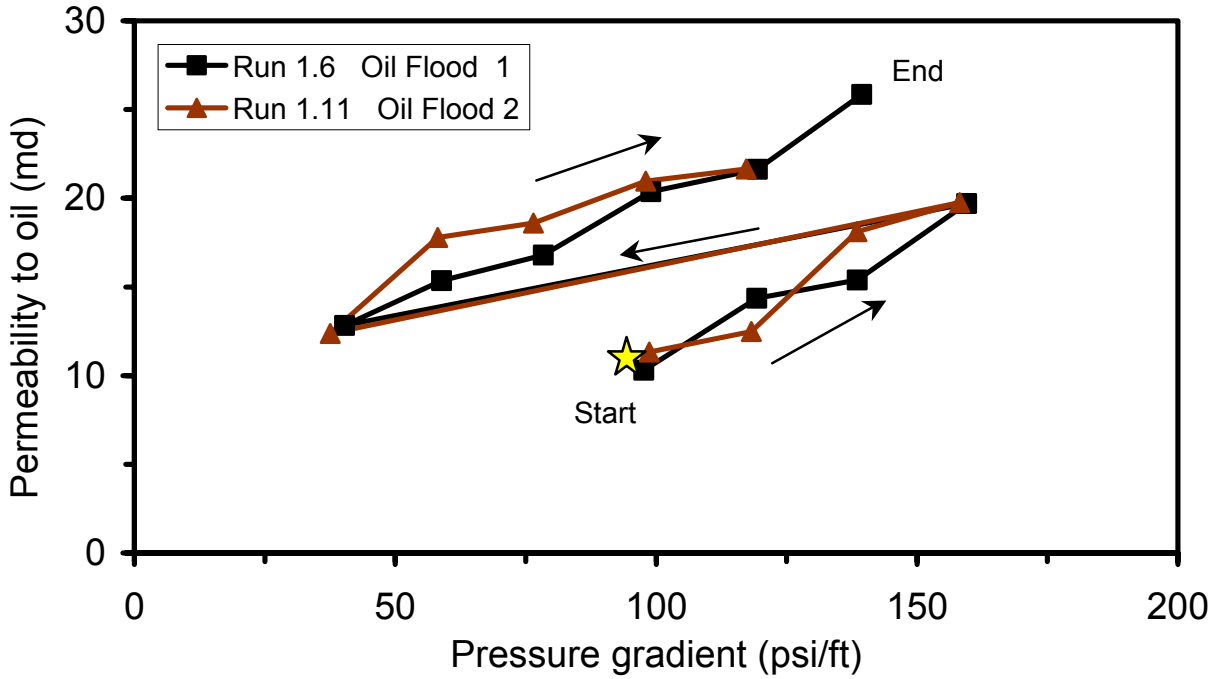

Figure 8.4 - Comparison of Runs 1.6 and Run 1.11 in Slab 1.

pore volume. Experimental data are presented in Reference 5. From these data, the estimated oil contacted pore volume was 32 mL. This volume exceeds the volume of aqueous phase displaced during the initial dehydration (16 mL) and demonstrates that some of the encapsulated residual oil was reconnected to the newly created pore space during the dehydration process. Material balance calculations indicate about 53% or the waterflood residual oil was reconnected to the new flow channels. Oil displaced during the subsequent brine flood was 21 mL (Run 1.13), so that 11 mL of previously mobile oil was trapped as a residual saturation in the newly created pore space.

Data for different sections of the slab are reported in Willhite et al. [2001]. Though the permeability decreased in the direction of post-treatment flow the essential trends for the overall slab apply to the individual sections also. That is, for each section, the permeabilities to oil during both first and second floods were the same, and higher than the permeability to brine for that section.

Disproportionate permeability reduction occurs when the permeability to brine after polymer treatment is reduced by a larger amount than the permeability to oil. This is often expressed in terms of residual resistance factors (RRF) for oil and brine. The residual resistance factor for oil (F_{rro}) is defined as

$$F_{rro} = \frac{k_o}{k_{og}} \qquad \text{Eq.8.1}$$

Similarly, the residual resistance factor for brine (F_{rrw}) is defined as

$$F_{rrw} = \frac{k_w}{k_{wg}} \qquad \text{Eq.8.2}$$

where k_{og} and k_{wg} are the permeabilities to oil and water at endpoint saturations after gel treatment, and k_o and k_w are permeabilities to oil and water before treatment, at interstitial water saturation and residual oil saturation, respectively. Thus, disproportionate permeability reduction occurs when $F_{rro}<F_{rrw}$ at the same pressure gradient.

Figure 8.5 presents the RRF to both oil and brine as a function of pressure gradient. Values of the residual resistance factors are close, particularly at high-pressure gradients. DPR was not evident to any appreciable extent at the pressure gradients between 100 and 160 psi/ft.

The absence of disproportionate permeability reduction at high pressure gradients stimulated a series of flow-rate studies at low pressure gradients. Run 1.12 was a series of oil floods in which oil was injected at constant rates and pressure drops were measured. The slab was first oil flooded at 40 psi/ft. This was followed by an oil flood rate test that began at a pressure gradient of ~0.2 psi/ft, increasing in steps to 40 psi/ft. The series of oil floods was followed by a series of brine floods. The slab was water flooded at a pressure gradient of 133 psi/ft followed by rate tests that began at a pressure gradient of 11.2 psi/ft and increased in steps to 133 psi/ft. Permeability to brine decreased markedly as pressure gradient decreased, probably because the gel structure relaxed as the pressure gradient decreased. The effect of pressure gradient on oil permeability was less pronounced as pressure gradient decreased. Residual resistance factors for rate tests of Runs 1.1 and 1.14 are shown in Figure 8.6. Residual resistance factors for brine are significantly greater than those for oil at the same pressure gradient. Disproportionate

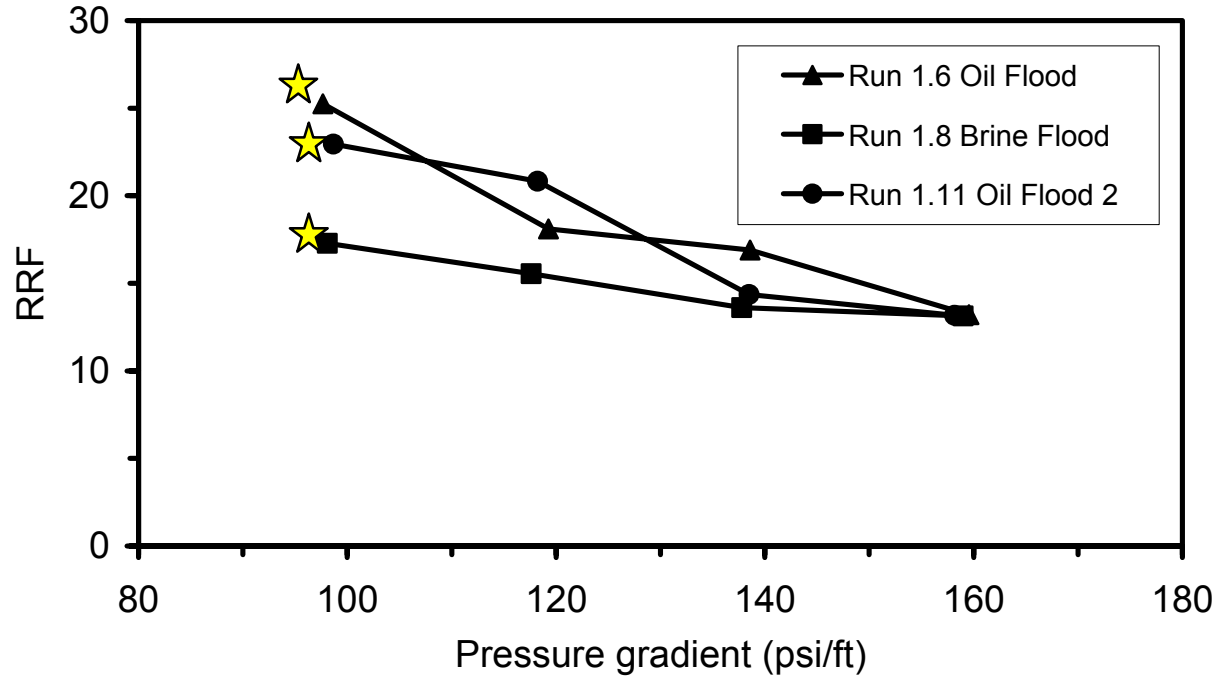

Figure 8.5 - Residual resistance factors for oil and brine in Slab 1 as a function of pressure gradient for Runs 1.5,1.8 and 1.11.

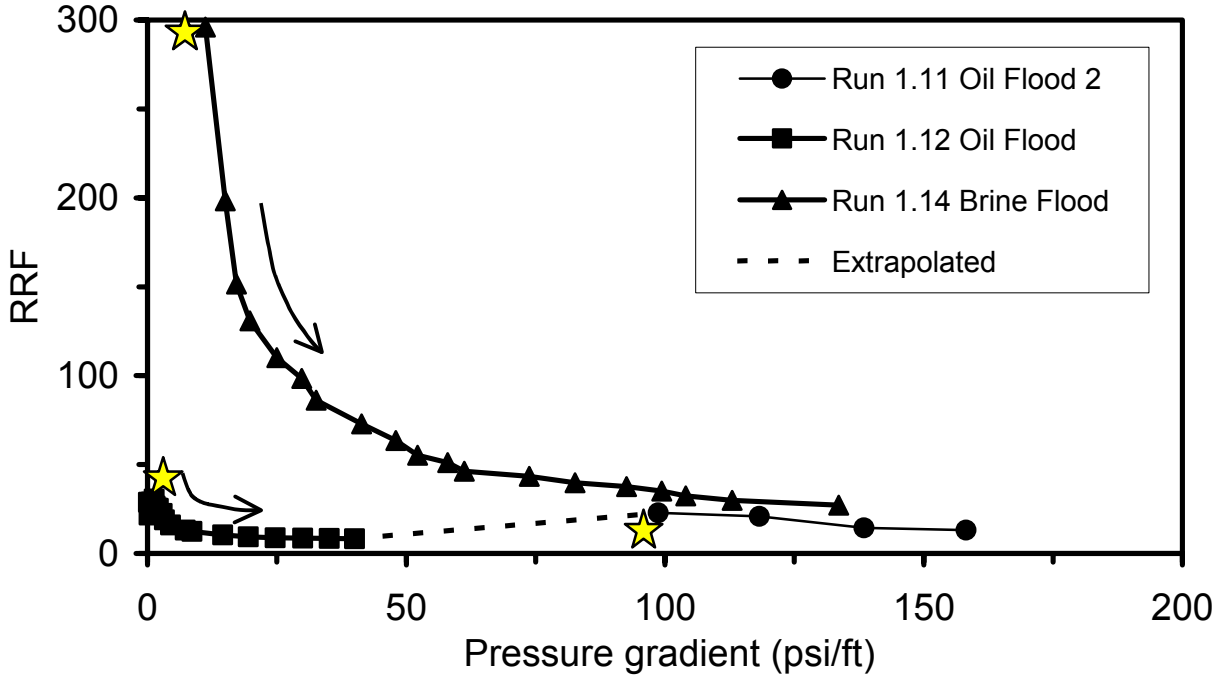

Figure 8.6 - Effect of pressure gradient on residual resistance factors for brine and oil in Slab 1 for Runs 1.12 and 1.14.

permeability reduction is clearly evident as pressure gradient is reduced. These data demonstrate that disproportionate permeability reduction is a function of pressure gradient and that the largest values are observed at small pressure gradients.

Planar Water Saturation Maps. Planar water-saturation maps were determined using a microwave apparatus which is described in Reference 5. The saturations shown in the maps to be presented indicate total aqueous phase saturations, i. e., brine plus gel. It is not possible to differentiate brine from gel with the microwave apparatus. Oil phase saturations are inferred by difference.

Aqueous phase saturations at the end of gel placement are shown in Figure 8.7. Here it is assumed that the phase saturations consist entirely of gel as the gel solutions would have displaced resident brine during the displacement process. As indicated in Table 8.2, a small amount of waterflood residual oil (remaining after Run 1.3) was displaced by the injection of the gel solution which was more viscous than the preceding waterflood (Run 1.3).

Saturations at the end of the first set of oil runs (Runs 1.6) and at the end of the following brine floods (Run 1.8) are shown in Figures 8.8 and 8.9. The flow directions for the different displacements are shown in the upper part of Figures 8.8 and 8.9. There are small saturation gradients across the slab. These are thought to be related to heterogeneities in the rock and the volume of fluids injected.

It is useful to examine saturation changes that occur during a displacement. This is calculated by subtracting the saturations at the start of a flood from those at the end of the flood. Saturation changes for the first few post-gelation floods are shown in Figures 8.10 to 8.13.

The changes in saturations that occurred during the dehydration by oil and subsequent oil floods (Runs 1.5 and 1.6) are shown in Figure 8.10. This change represents the creation of "new" pore space within the gel-treated rock through which injected fluids can flow. As indicated in Table 8.2, the new porosity value is about 5.3%, slightly less than one third of the original porosity. There is a gradient of saturation change across the core, thought to be due to the volume of oil injected. That is, injection of additional oil would have decreased water saturations somewhat more.

Saturation changes that occurred between the end of the oil floods and end of the next series of brine floods (Runs 1.7 and 1.8) are shown in Figure 8.11. These values are slightly larger in magnitude than the negative values shown on Figure 8.10 indicating that the oil floods must have reconnected with some of the oil originally trapped by gel. Some of this reconnected oil was displaced by the brine flow. The net changes in saturation over the oil and brine floods are presented in Figure 8.12.

A second set of oil floods was conducted (Runs 1.9 – 1.12) following the brine floods. The change in saturations between the end of the first set of oil floods and the end of the second set are shown in Figure 8.13. These changes are relatively small indicating that once the dehydration is accomplished, subsequent floods do not change the "new" pore space significantly as long as the pressure gradient used for dehydration is not exceeded.

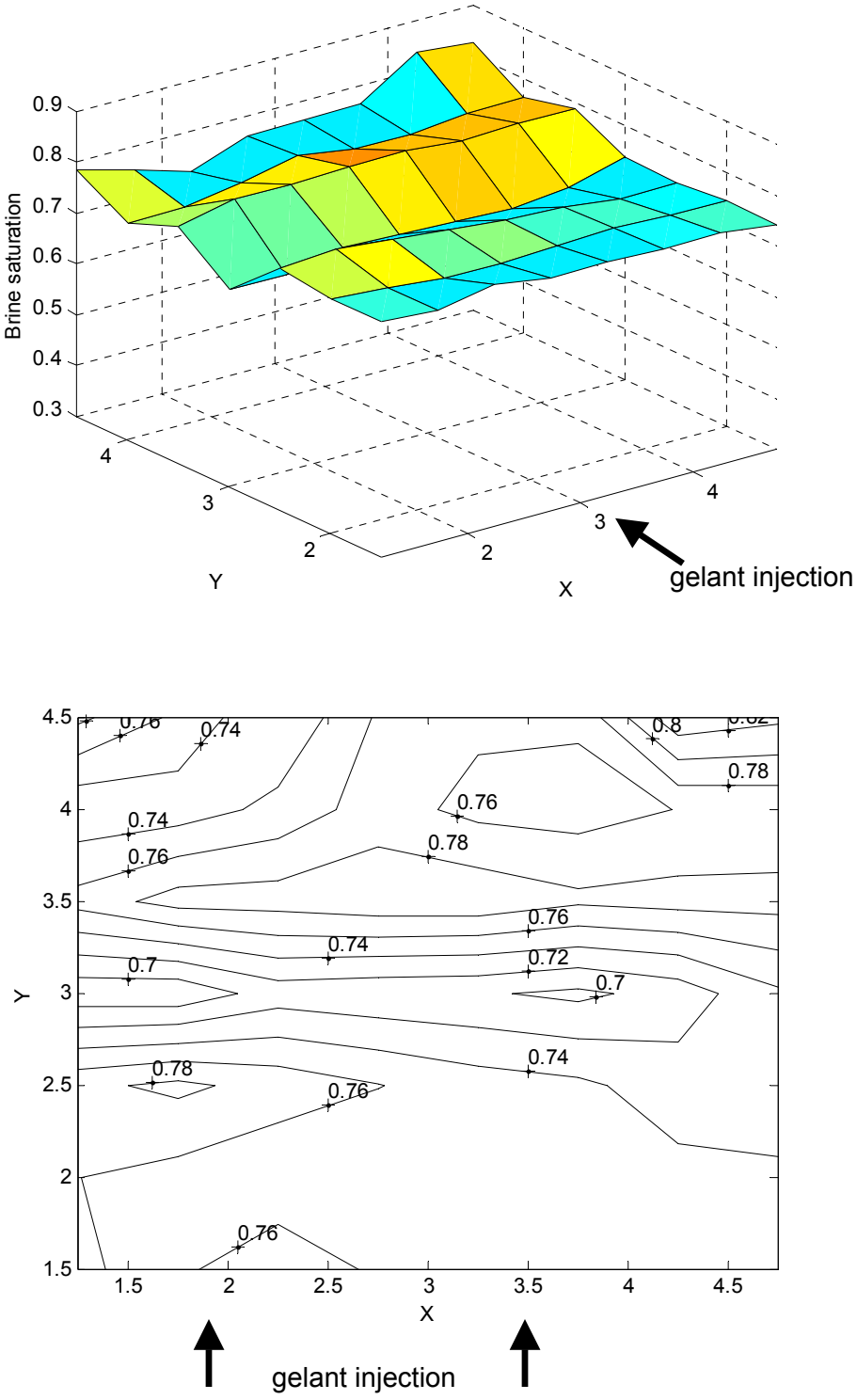

Figure 8.7 – Aqueous phase saturation after injection of gelant Slab1.

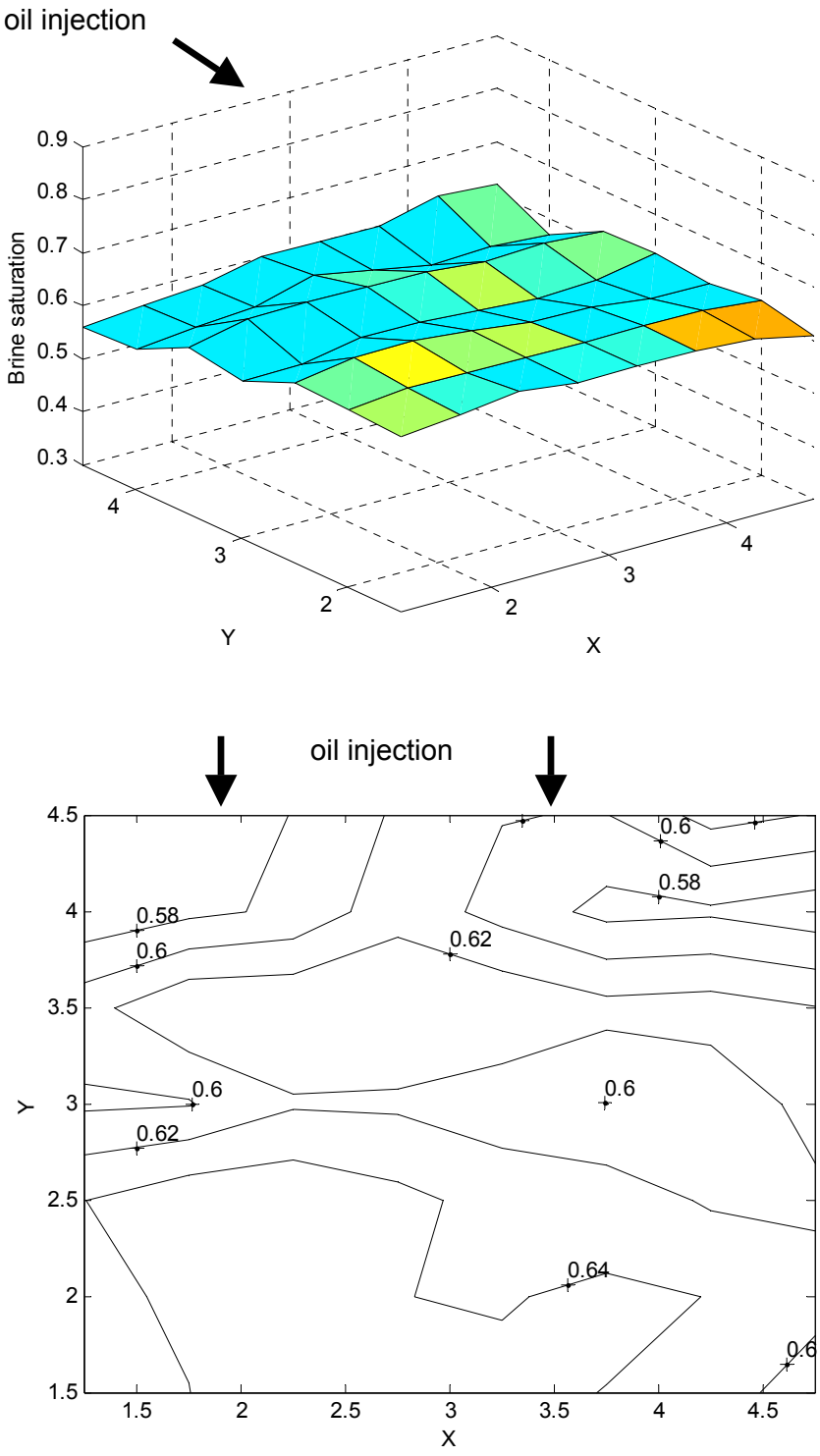

Figure 8.8 – Aqueous saturation after first post-treatment oil flood in Slab1 (Run 1.5).

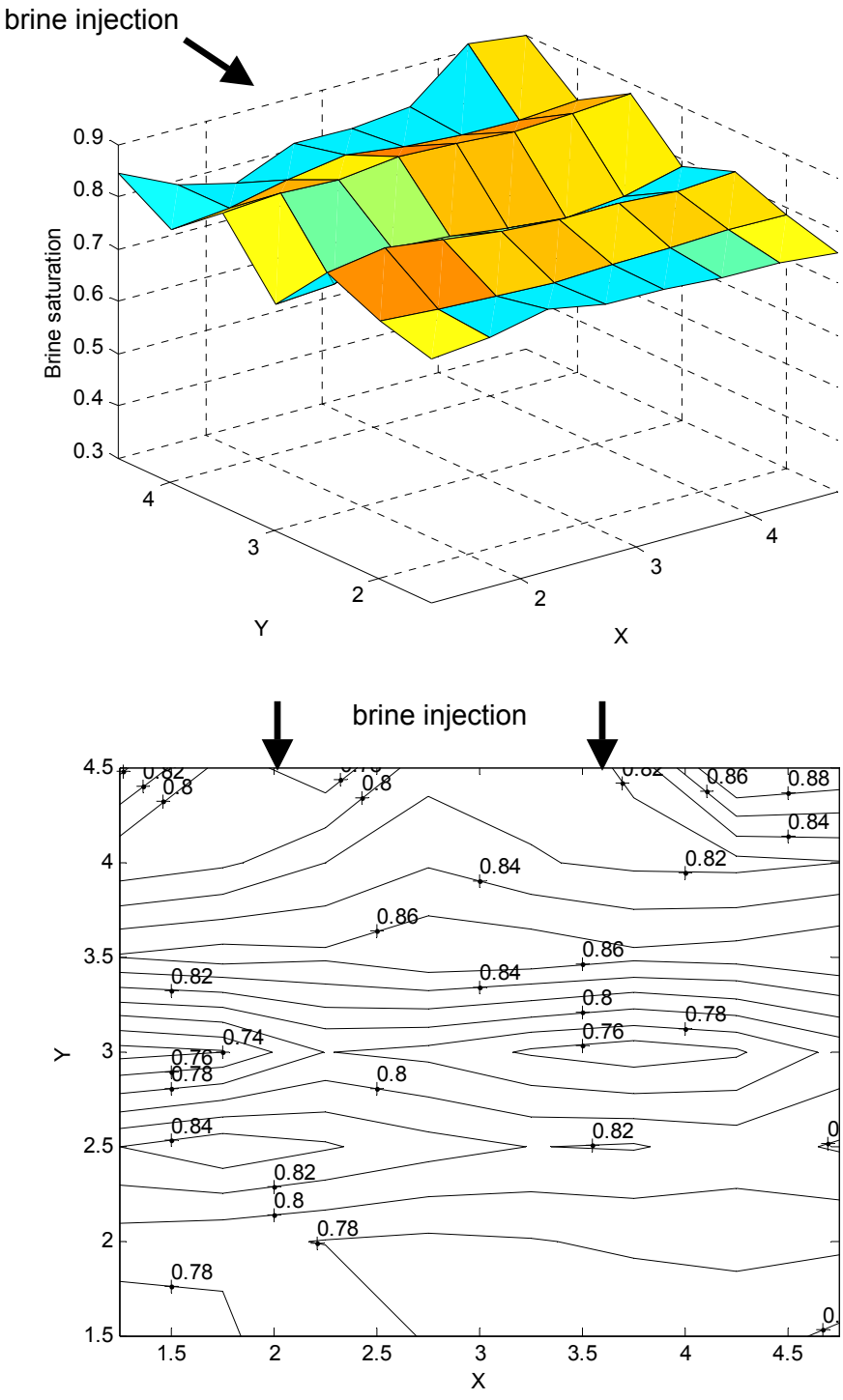

Figure 8.9 – Aqueous saturation after first post-treatment brine flood in Slab1 (Run 1.7).

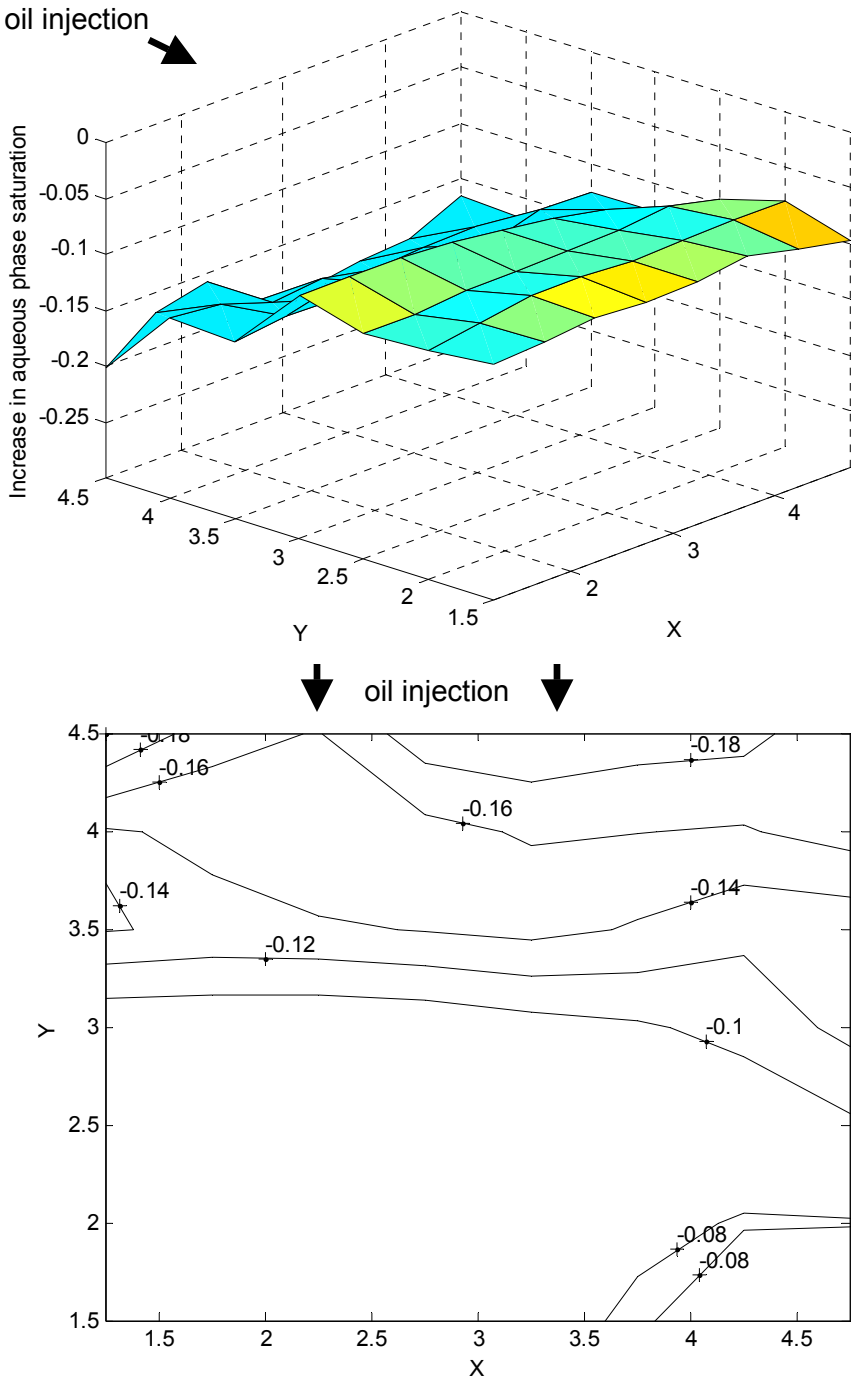

Figure 8.10 – Increase in aqueous saturation during the first post-treatment oil flood in Slab 1 (Run 1.5).

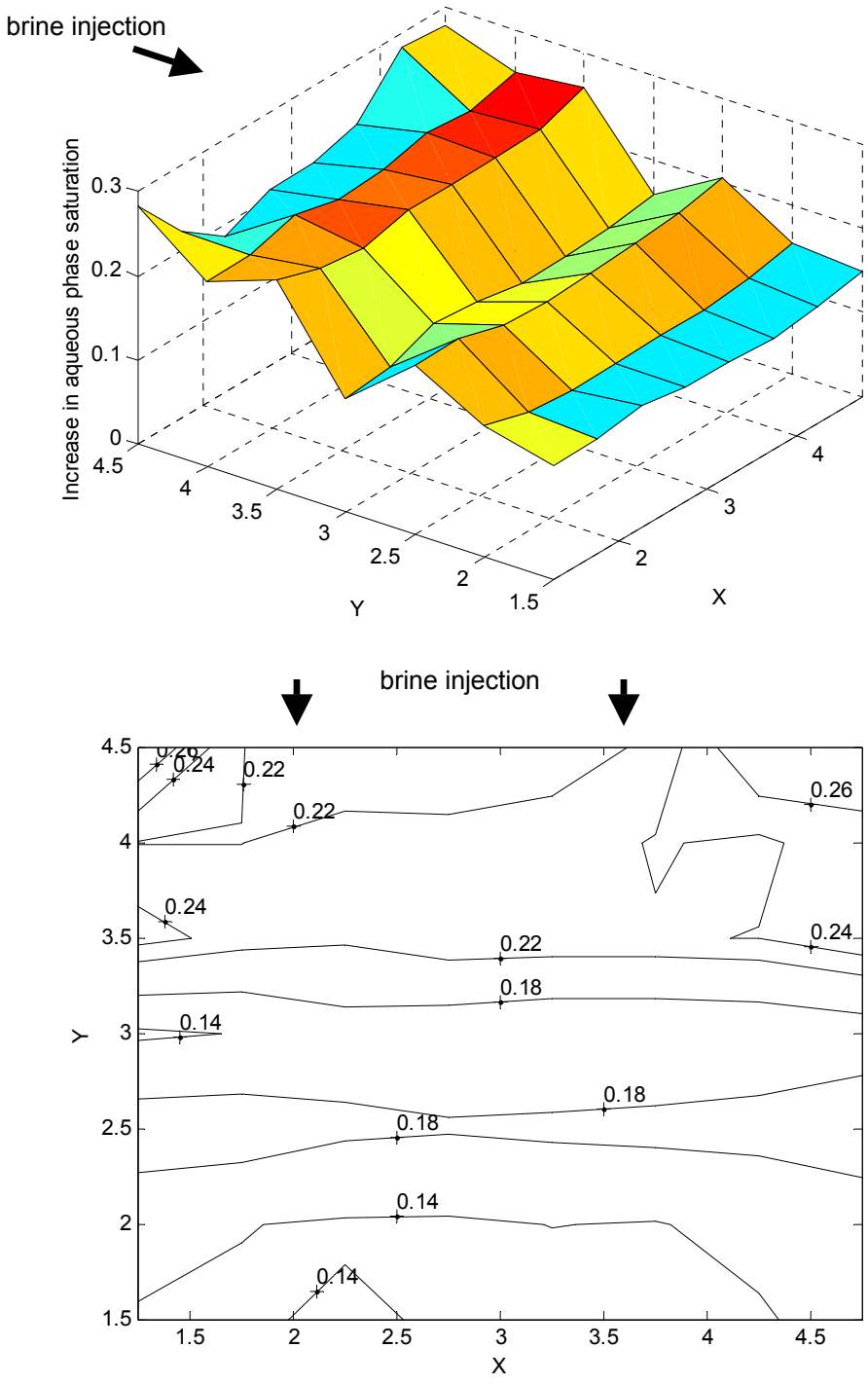

Figure 8.11 – Increase in aqueous saturation during first post-treatment brine flood in Slab 1 (Run 1.7).

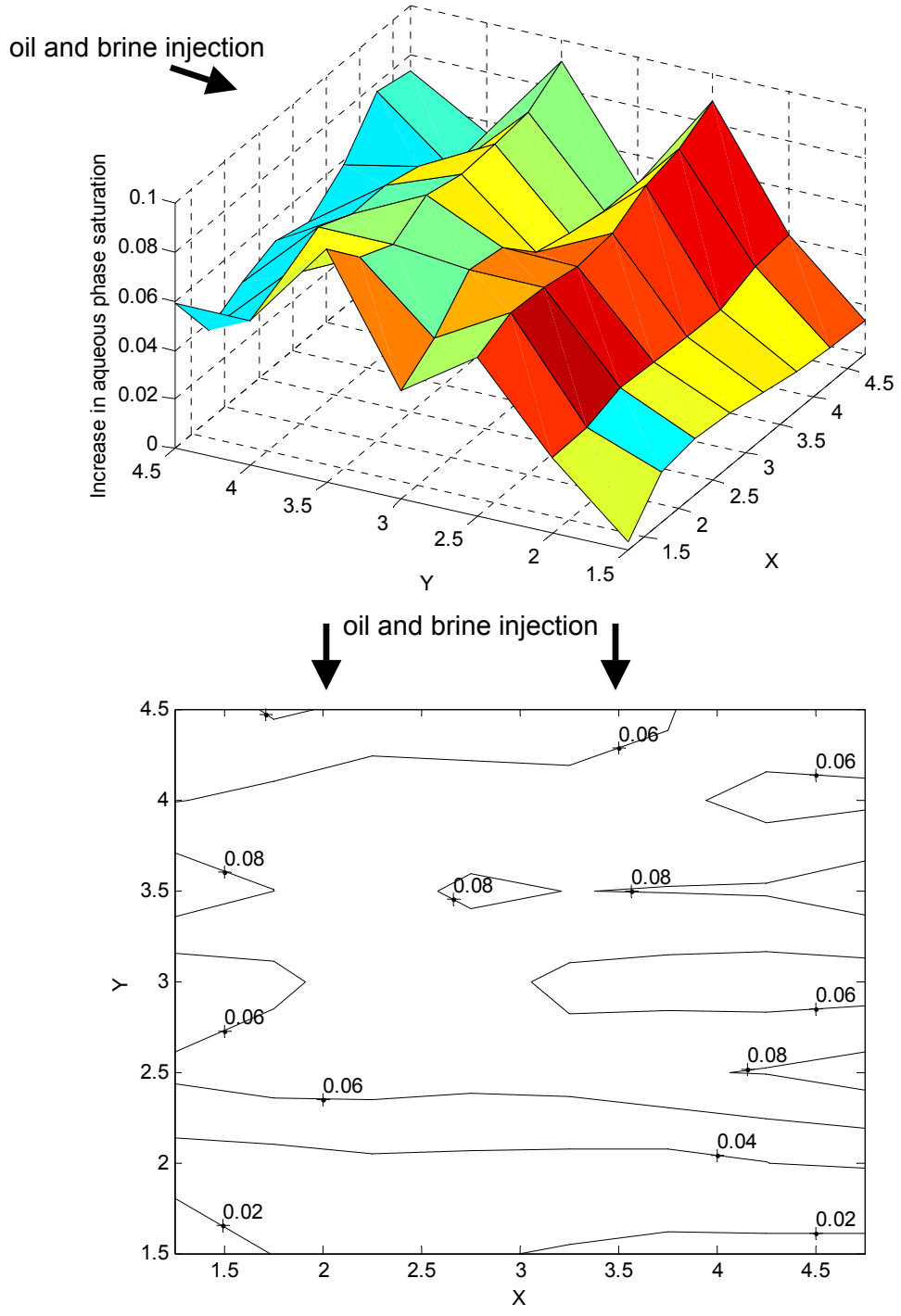

Figure 8.12 – Increase in aqueous saturation during the first post-treatment oil flood *and* the first post-treatment brine flood in Slab 1 (Runs 1.5 and 1.7).

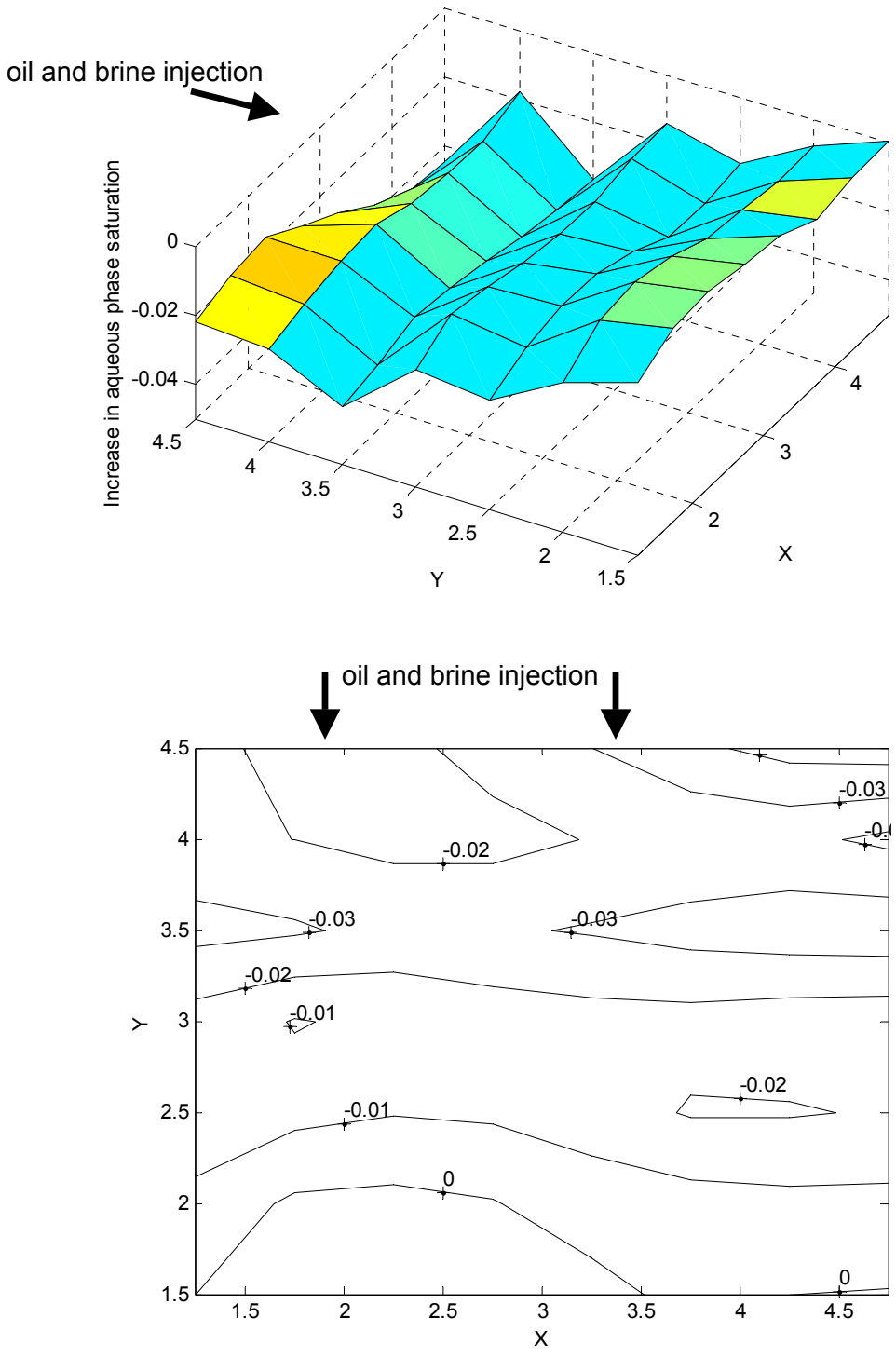

Figure 8.13 - Increase in aqueous saturation during the first post-treatment brine flood *and* the second post-treatment oil flood in Slab 1 (Runs 1.7 and 1.9).

Core Tests. Displacement tests in four linear cores were made to determine if the effect of flow rate observed in the slab was reproducible and to compare permeability reduction when brine or oil was used to dehydrate a treated core. The gelant was injected into Cores 2 and 3 at the same time. Core 2 was treated in a similar manner as the slab including extensive flow-rate tests. Core 3 was shut in for sixty days before dehydration with brine. Gelant was injected into Cores 4 and 5 at the same time. Core 4 was dehydrated with oil and Core 5 was dehydrated with brine to create the initial flow channels after an eight day shut-in period following gel placement.

Composition of the gelant was changed to 0.67% Alcoflood 935, 0.015% Cr(III) acetate, 0.52% sodium acetate. Viscosity of the gelant was 73 cp at a shear rate of 11.25 sec^{-1} and the nominal gel time was 36 hours. A smaller amount of gelant was injected (1.5 or 2 PV) than in the slab experiment and injection was completed within 1 hour after mixing. Experimental data are summarized in Tables 8.3 - 8.6. Saturations and effective porosity were calculated using the assumptions described for Slab 1.

Core 2. The sequence of runs and experimental data are summarized in Table 8.3. The new pore structure was created by dehydration with oil (Run 2.5) containing 200 ppm stilbene as a tracer at a constant pressure gradient of 40 psi/ft until the flow rate was steady and brine production was negligible. Analysis of the stilbene concentration in the effluent indicated that 67% of the residual oil encapsulated by the gelant was reconnected to the flow channels during dehydration. Displacement of the stilbene tracer from the core (Run 2.6) indicated that the effective porosity created by dehydration of the gel was 0.09 and that 92% of the waterflood residual oil was connected to the flow channels.

Flow-rate tests were limited to the maximum pressure gradient used to dehydrate the gel to form the new pore space. Most runs were completed by returning to the pressure gradient at the first rate in a run to verify that the gel structure had not changed during the flow-rate tests. For example, in Run 2.7, pressure drop was measured while injecting oil at various flow rates, starting from the lowest to the highest value, and then back to the lowest one again to determine the oil permeability at each flow rate (pressure gradient).

In Run 2.8, brine was injected at a constant pressure of 20 psi (40 psi/ft), until the permeability became constant. The permeability was measured while changing flow rates (Run 2.9) in the same way as in the previous oil flood. Oil containing stilbene as a tracer was injected in Run 2.10 until brine displacement was negligible. Stilbene was displaced from the core in Run 2.11 and the oil-contacted volume was estimated from the analysis of the effluent concentrations. The effective porosity was 0.09, in good agreement with the previous tracer test (Run 2.6). A series of flow-rate tests was completed in Run 2.12 in which the pressure gradient varied from 0.6 psi/ft to 40 psi/ft to 0.6 psi/ft.

The effect of pressure gradient on the gel structure was investigated by injecting oil at a pressure gradient of 174 psi/ft (Run 2.13) to dehydrate the gel. Further dehydration of the gel occurred as indicated by the displacement of brine, increasing the effective porosity from 0.09 to 0.11. This run was followed by a brine flood at a pressure gradient of 174 psi/ft (Run 2.14) to displace mobile oil from the new pore space. In Runs 2.15 and 2.16, brine flow rates were varied to obtain

Table 8.3 - Summary of data for Core 2.

Run	Description	S_w (%)	S_{gel} (%)	S_{ot} (encapsulated by gel) (%)	S_o (not encap. by gel) (%)	Effective Porosity** (%)	S_w* (%)	S_o* (%)	k_w (mD)	F_{rrw}	k_o (mD)	F_{rro}
2.1	Pre-treatment Brine Flood 1	100	0		0	24			500			
2.2	Oil flood	20	0		80	24					525	
2.3	Brine flood 2	74	0		26	24			85			
2.4	Gelant Injection	0	74	26	0	0			0			
2.5	Oil flood[1] containing stilbene tracer-dehydration @40 psi/ft	0	58	9	33	8	0	100				
2.6	Oil flood[2]-displace tracer @40 psi/ft	0	58	3	39	9	0	100			38	14
2.7	Oil rate tests	0	58	3	39	9	0	100				
2.8	Brine flood 1 @40 psi/ft	16	58	3	23	9	42	58	0.7	121		
2.9	Brine rate tests	16	58	3	23	9	42	58				
2.10	Oil flood containing stilbene tracer @40 psi/ft	0.4	58	3	39	9	1	99			64	8.2
2.11	Displace stilbene tracer[3] at 40 psi/ft	0.4	58	2	39	9	1	99				
2.12	Oil rate tests	0.4	58	2	39	9	1	99				
2.13	Oil flood dehydration @174 psi/ft	0.4	51	2	46	11	1	99			255	2.1
2.14	Brine flood @174 psi/ft	30	51	2	17	11	64	36	7	12		
2.15	Brine rate tests	30	51	2	17	11	64	36				
2.16	Brine rate tests-reproducibility	30	51	2	17	11	64	36				
2.17	Oil flood @174 psi/ft	3	51	2	44	11	6	94			258	2.0
2.18	Oil rate tests	3	51	2	44	11	6	94			258	2.0

Sw* and So* are based on effective porosity.

**Effective porosity does not include gel or oil encapsulated in the gel.

Notes 1. Tracer test-volume of waterflood oil connected during dehydration was 4.05 mL.

2. Tracer test-volume of mobile oil was 9.06 mL.

3. Tracer test-volume of mobile oil was 9.12 mL.

Table 8.4 - Summary of data for Core 3.

Run	Description	S_w (%)	S_{gel} (%)	S_{ot} (encapsulated by gel) (%)	S_o (not encap. by gel) (%)	Effective Porosity* (%)	S_w* (%)	S_o* (%)	k_w (mD)	F_{rrw}	k_o (mD)	F_{rro}
3.1	Pre-treatment Brine Flood 1	100			0	24			500			
3.2	Oil flood	24			76	24					500	
3.3	Brine flood 2	72			28	24			85			
3.4	Gelant Injection	0	72	28	0	0						
3.5	Brine flood-dehydration @40 psi/ft	23	50	7	21	11	52	48	3.8	23		
3.6	Brine rate tests	23	50	7	21	11	52	48				
3.7	Oil flood @ 40 psi/ft	0	50	7	44	11	0	100				
3.8	Oil flood[1] containing stilbene tracer @ 40 psi/ft	0	50	7	44	11	0	100			65	8
3.9	Oil rate tests	0	50	7	44	11	0	100				
3.10	Brine flood at 40 psi/ft	20	50	7	24	11	45	55	1.4	59		
3.11	Brine rate tests	20	50	7	24	11	45	55				
3.12	Brine flood-dehydration @174 psi/ft	32	40	4	24	14	57	43	1.7	49		
3.13	Oil flood @174 psi/ft	0	40	4	56	14	0	100				
3.14	Oil flood[2] containing stilbene tracer @ 174 psi/ft	0	40	4	56	14	0	100			264	2.0
3.15	Brine flood @174 psi/ft	31	40	4	25	14	56	44	19	4.5		

Sw* and So* are based on effective porosity.

**Effective porosity does not include gel or oil encapsulated in the gel.

Notes 1. Tracer test-Run 3.8-continuous oil volume was 10.46 mL.

2. Tracer test-Run 3.14-continuous oil volume was 13.46 mL

Table 8.5 - Summary of data for Core 4.

Run	Description	S_w (%)	S_{gel} (%)	S_o (%)	Permeability (md)	RRF
4.1	Pre-treatment Brine Flood 1	100	0	0	500	
4.2	Oil flood	27	0	73	506	
4.3	Brine flood 2	72	0	28	88	
4.4	Gelant Injection	0	72	28	~0	
4.5	Oil flood-dehydration @40 psi/ft	0	52	48	123	4.1
4.6	Brine flood at 40 psi/ft	21	52	27	8.7	10.1

Table 8.6 - Summary of data for Core 5.

Run	Description	S_w (%)	S_{gel} (%)	S_o (%)	Permeability (md)	RRF
5.1	Pre-treatment Brine Flood 1	100		0	484	
5.2	Oil flood	27		73	477	
5.3	Brine flood 2	73		27	62	
5.4	Gelant Injection	0	73	27	~0	
5.5	Brine flood-dehydration @40 psi/ft	73		27	6.3	9.8
5.6	Oil flood @ 40 psi/ft		47	53	166	2.9
5.7	Brine flood @ 40 psi/ft	23	47	31	11	5.6

a range of pressure gradients that ranged from 0.6 psi/ft to 174 psi/ft to 0.6 psi/ft. Core 2 was flooded with oil at 174 psi/ft in Run 2.17. Oil flow-rate tests conducted in Run 2.18 consisted of twenty-three rate changes in which the pressure drop changed from 0.4 psi/ft to 32 psi/ft to 0.06 psi/ft.

Core 3. Table 8.4 summarizes the sequence of runs and selected experimental data for Core 3. Core 3 was dehydrated by injecting brine at a pressure gradient of 40 psi/ft after being shut-in for 60 days. No oil was produced during dehydration (Run 3.5). A series of brine flow-rate tests was conducted in Run 3.6. The amount of brine displaced during the subsequent oil flood (Run 3.7) was assumed to be equivalent to the amount of gel that was dehydrated during brine injection. About 31% of the gel was dehydrated. Following the oil flood in Run 3.7, stilbene tracer was injected with the oil (Run 3.8) to estimate the continuous oil volume in the new pore space. Permeability to oil was 65 md which gives $F_{rro} = 7.7$. The tracer data indicate that 76% of the waterflood residual oil was connected to the new flow channels following the oil flood, leaving 24% of the waterflood residual oil encapsulated in the gel structure. Oil rate tests were conducted in Run 3.9 following the tracer test. Brine was injected to displace mobile oil in Run 3.10 followed by brine rate tests in Run 3.11. In Run 3.12, brine was injected at a pressure gradient of 174 psi/ft to dehydrate the gel further. A small amount of oil was displaced from the core during this test. Following the subsequent oil flood (Run 3.13) at 174 psi/ft, stilbene tracer was added to

the injected oil (Run 3.14). From these data, the amount of encapsulated waterflood residual oil was estimated to be 13%. Permeability to oil increased to 264 md. Permeability to brine increased to 19 md in Run 3.15 after oil was displaced from the new pore space. Dehydration at 174 psi/ft increased both brine and oil permeability and caused significant reduction in disproportionate permeability reduction. The effective porosity was 14.6% at the end of Run 3.15, which is 60% of the original porosity. The remaining 40% of the original porosity contained gel and encapsulated oil.

Cores 4 and 5. The sequence of tests and experimental data for Cores 4 and 5 are summarized in Tables 8.5 and 8.6. Core 4 was dehydrated by injection of oil and Core 5 was dehydrated by injection of brine, both at a pressure gradient of 40 psi/ft. Tracer and flow-rate tests were not run. Steady flow rates of brine and oil were measured at the end of displacement runs to enable calculation of brine and oil permeability. Gel saturations after dehydration were estimated by assuming that the amount of brine displaced was equal to the amount of dehydration.

Discussion of Results

Injection of a gelant into Berea sandstone reduces the permeability significantly if a gel forms in situ. The gel structure is permeable to brine at low pressure gradients and permeabilities are on the order of a few microdarcies. However, the gel structure is not permeable to oil until the pressure gradient is increased to levels where dehydration of the gel structure begins.

In the experiments described in Slab 1 and Cores 2-5, permeability to oil and brine was created by dehydration of the gel structure by injecting oil or brine at a constant pressure gradient. The dehydration process is slow at low-pressure gradients and the amount of dehydration depends upon the magnitude of the pressure gradient. Table 8.7 summarizes changes of porosity and gel saturation that were estimated from the data in Tables 8.2-8.6. Results from the slab and core tests cannot be compared directly because different amounts of gelant were injected with different compositions. Effective porosity could be estimated only for three runs where oil soluble tracer data were obtained.

Table 8.7 - Comparison of changes in gel saturation and porosity after dehydration.

Experiment	Initial Porosity (%)	Effective Porosity at End of Experiment (%)	Initial Gel Saturation (%)	Estimated Gel Saturation at End of Experiment (%)	Dehydration of Initial Gel Structure (%)
Slab 1	18.6	5.4	74	59	20.3
Core 2	23.6	11.	74	51	31.1
Core 3	24.4	14.6	72	40	44.4
Core 4	25.2		73	53	37.7
Core 5	24.5		73	47	35.6

The data show that the effective porosity following dehydration of the gel treated Berea sandstone was reduced from 30-60% of the original porosity. The gel saturation remaining in the sandstone after the various flow experiments varied from 40 to 59 saturation percent. Thus, substantial amounts of gel remained in the pore space after gel treatment, dehydration and flow tests.

The effects of flow rate on the permeability to brine and oil following dehydration of the gel-treated slab and cores are shown in Figures 8.2, 8.3, 8.4, 8.14, and 8.15, where permeability data are plotted as a function of pressure gradient. Both brine and oil permeability increase with increasing pressure gradient for cores dehydrated at pressure gradients on the order of 40 psi/ft. Permeabilities appear to be reproducible as long as the maximum pressure gradient used to dehydrate the gel structure is not exceeded. The increase in permeability with pressure gradient is attributed to deformation of the newly created flow channels by the pressure gradient. Hysteresis was observed in some runs because permeabilities did not return to the same values at the same pressure gradient at the end of a run.

Brine and oil permeabilities are less than the corresponding endpoint permeabilities prior to gel treatment. When the waterflood residual oil saturation is encapsulated by the gel, 50--85% of this volume can be reconnected to the flow channel when the gel is dehydrated with oil or oil is displaced through the flow channel after dehydration with brine. Oil permeability is increased by connection with the previously encapsulated residual oil. Gel treatment always reduces the permeability to oil and brine even after new flow channels are developed by dehydration of the gel structure to develop flow paths. Residual resistance factors for oil and brine are always greater than 1 and vary with pressure gradient as shown in Figures 8.5, 8.6, 8.16, 8.17 and 8.18. Disproportionate permeability reduction was observed for all core tests because $F_{rro} < F_{rrw}$ at the same pressure gradient.

When the pressure gradient is increased beyond the initial dehydration pressure, further dehydration and possibly rearrangement of the gel structure occurs with a corresponding increase of oil and brine permeabilities. When the pressure gradient was 174 psi/ft, in Core 2 (Run 2.18), oil permeability increased to about 250 md and varied little with pressure gradient in flow-rate tests shown in Figure 8.7. In contrast, brine permeabilities in Core 2 were quite sensitive to pressure gradient as shown in Figure 8.15, varying from 2 to 8 md. Similar data from Core 3 are consistent with Core 2 and are presented as RRF data in Figure 8.11. Core 3 was dehydrated with brine. Brine permeabilities were always less than k_w @ S_{or} and residual resistance factors were greater than 1. Disproportionate permeability reduction was observed in all gel-treated cores and the slab, whether dehydrated by oil or brine. If high pressure gradients are used for dehydration, disproportionate permeability is reduced and can disappear as observed in data from slab flow tests. Disproportionate permeability reduction can still occur at low pressure gradients depending on the amount of permeability reduction that occurred at the maximum pressure used for dehydration.

Residual resistance factors have been determined and reported in other laboratories. Similar data reported by other investigators are presented in Figure 8.19 as a function of pressure gradient. The data from this study are consistent with trends observed by other investigators even though different gel systems were used.

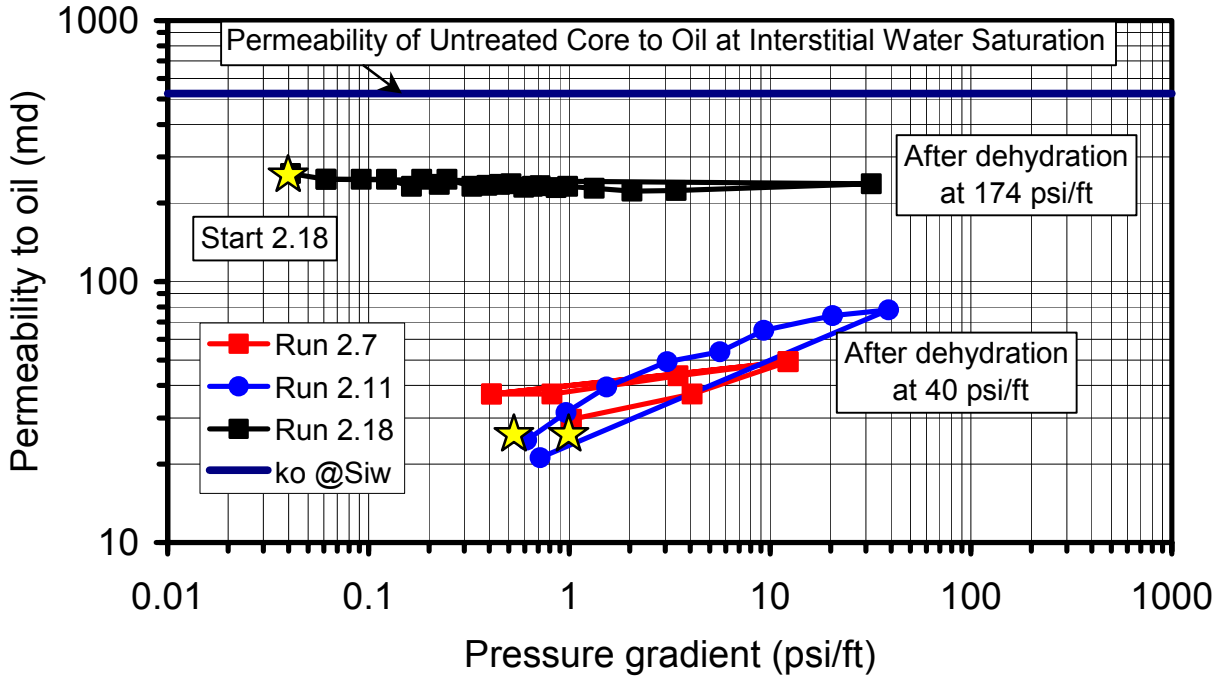

Figure 8.14 - Effect of pressure gradient on the permeability to oil in Core 2 after dehydration at 40 psi/ft and 160 psi/ft.

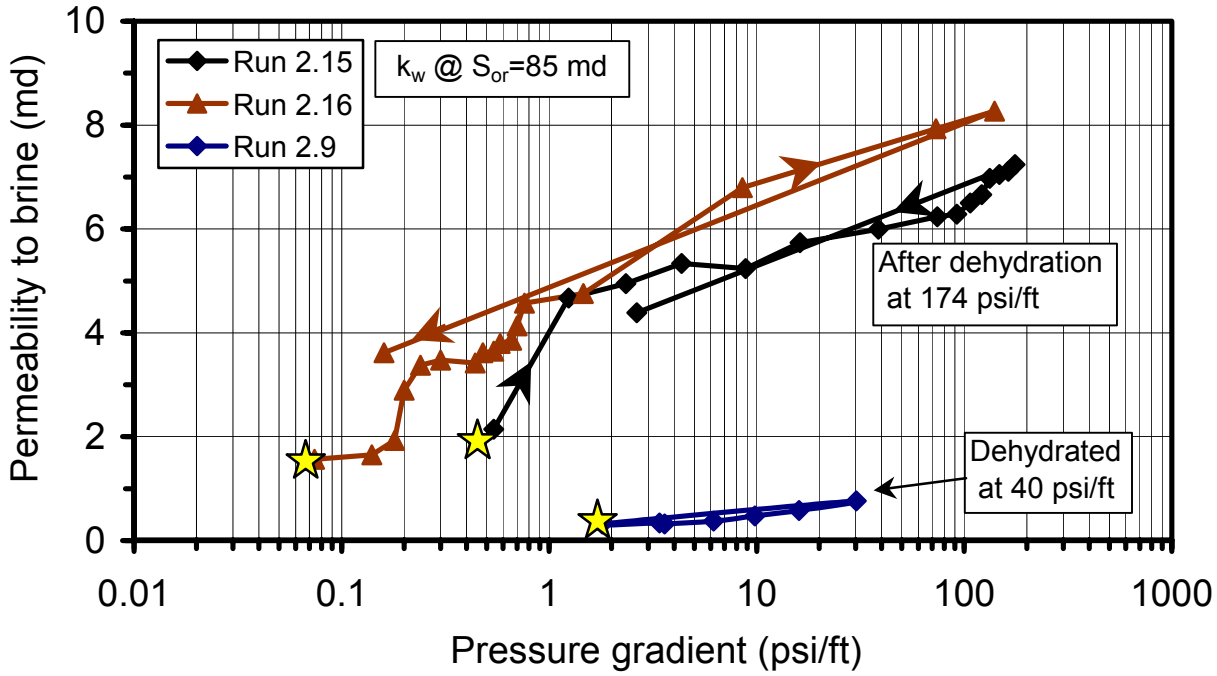

Figure 8.15 - Effect of pressure gradient on the permeability to bring in Core 2 after dehydration at 40 psi/ft and 160 psi/ft.

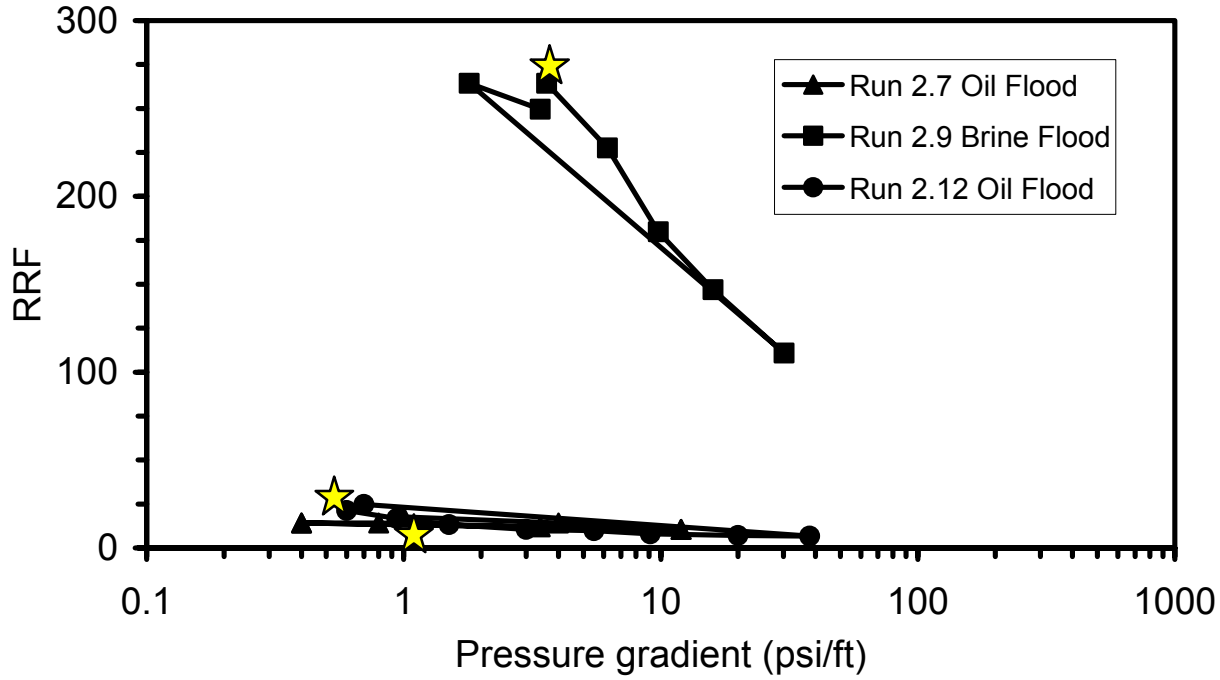

Figure 8.16 - Effect of pressure gradient on residual resistance factors in Core 2 after dehydration at 40 psi/ft.

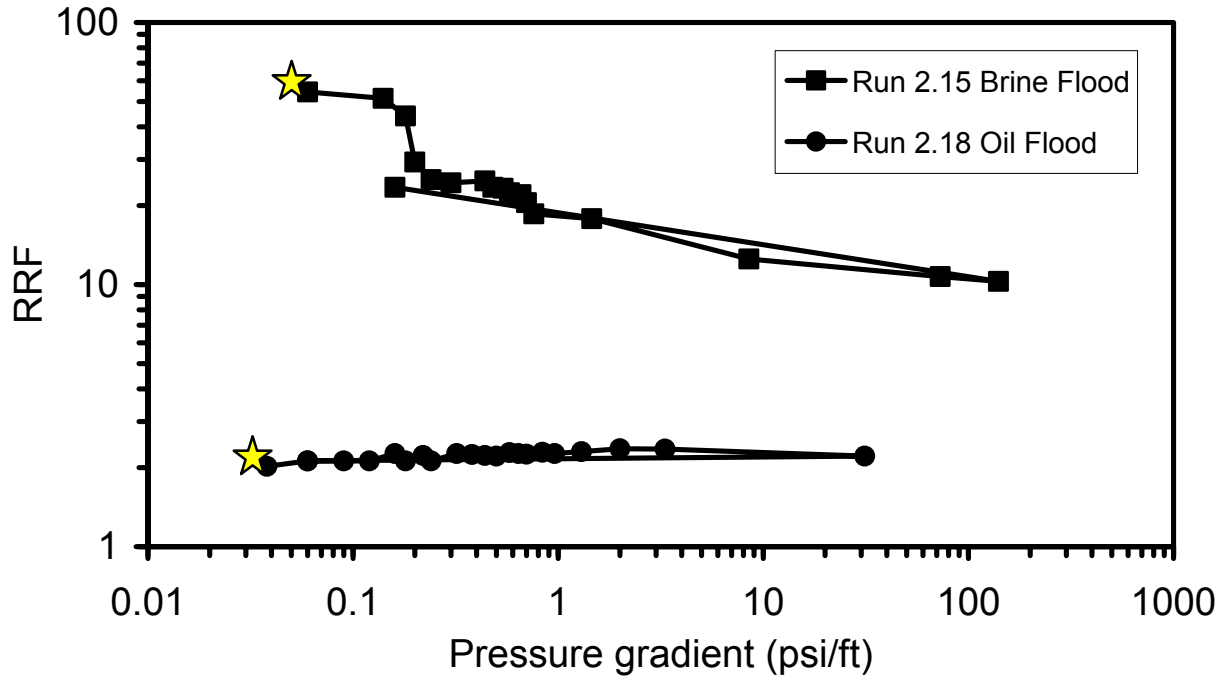

Figure 8.17 - Effect of pressure gradient on residual resistance factors in Core 2 after dehydration at 160 psi/ft.

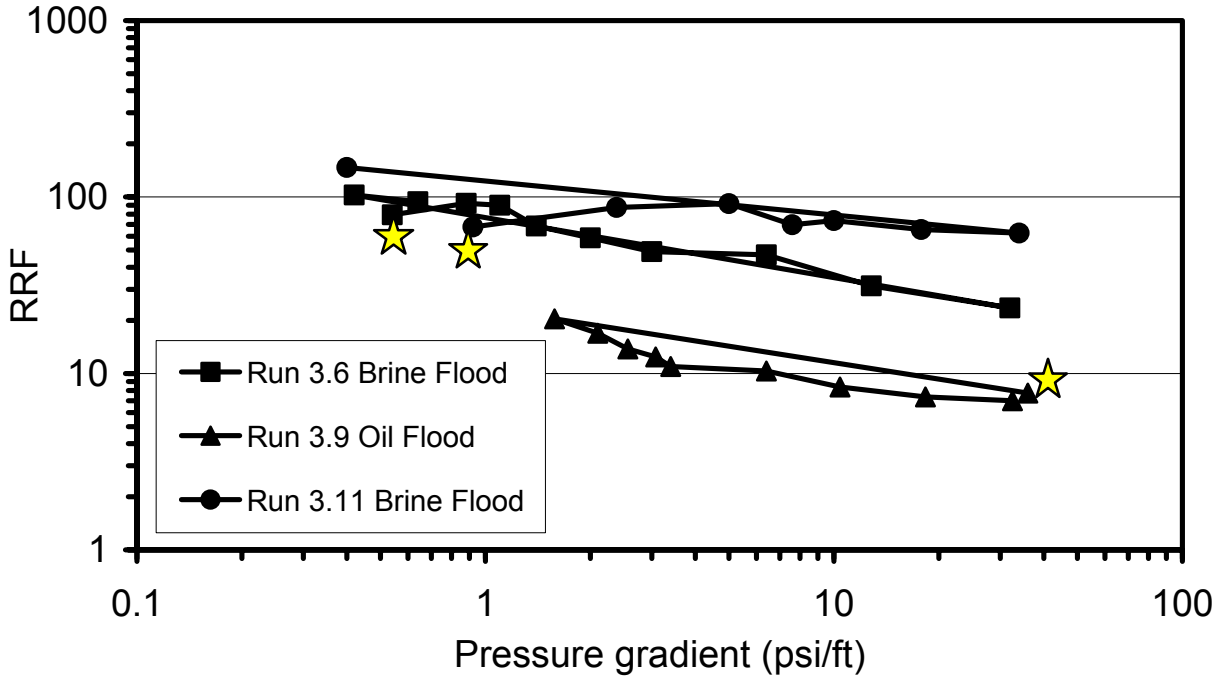

Figure 8.18 - Effect of pressure gradient on residual resistance factors in Core 3 after dehydration with brine at 40 psi/ft.

The results of this study demonstrate that the permeability of brine or oil in a gel-treated sandstone is a function of the pressure gradient used to create the new pore space and the pressure gradient applied during fluid flow. Flowing gels commonly used in profile modification treatments will be dehydrated when subjected to a pressure gradient by either oil or water. New flow channels created in the porous matrix have less permeability than the original matrix. Disproportionate permeability to brine compared to oil is believed to occur when oil is trapped as a residual phase in the new flow channels. The newly created flow channels are strongly water wet and oil is displaced abruptly from flow channels by brine. In contrast, displacement of brine is slow, similar to very strongly water-wet media where brine films slowly thin with continued oil flow.

The experimental observations in this study suggest possible changes in the way that profile modification treatments are applied in production wells where matrix flow dominates. All flowing gels will dehydrate to some extent after placement due to the pressure gradient in the immediate vicinity of a production wellbore. The amount of dehydration can be controlled by controlling the drawdown when the well is placed on production. Alternately, the amount of dehydration can be controlled by injection of oil or brine into a well at a specified pressure gradient after gelation has occurred in the pore structure. This approach differs from the conventional gel placement practice in which small volumes of oil or brine are injected as an overflush to clear tubing and wellbore of the gelant before gelation occurs. The overflush does not dehydrate the gel.

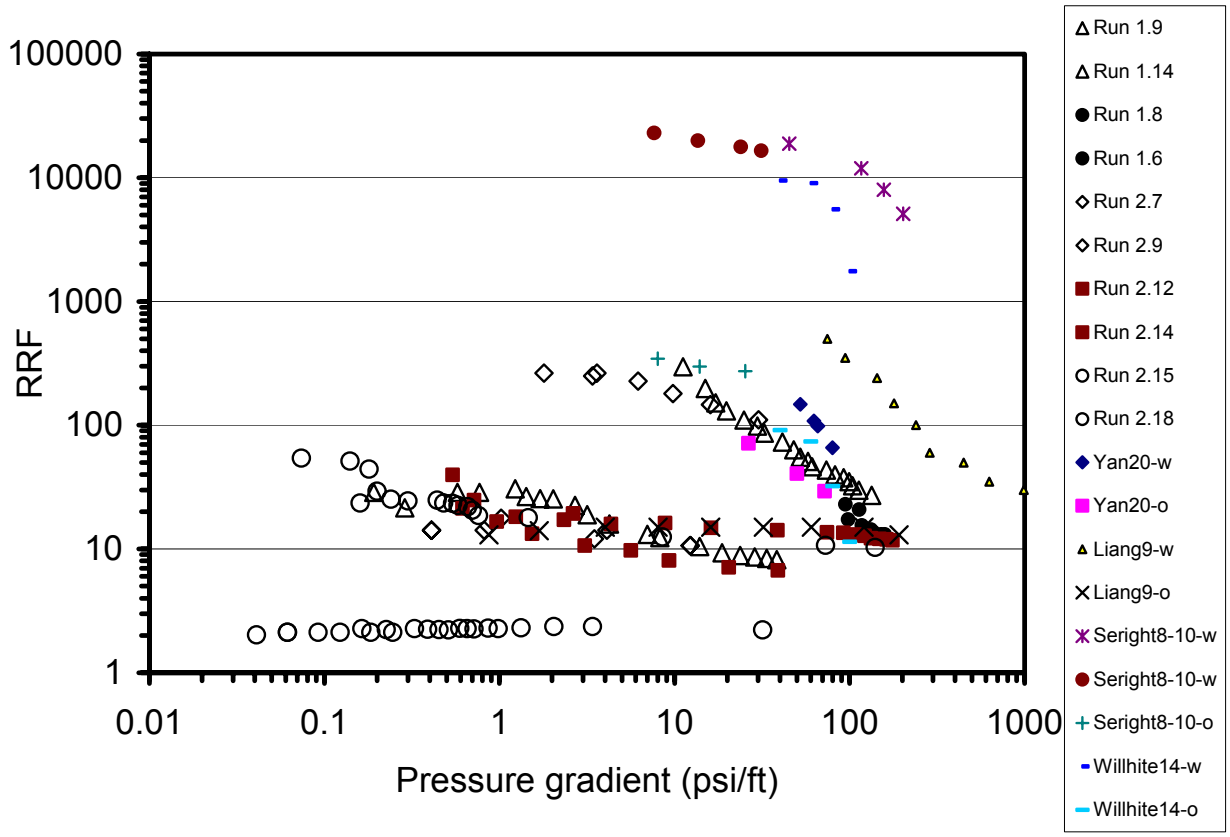

Figure 8.19 - Comparison of the effect of pressure gradient on residual resistance factors for previous studies with results of this study.

Finally we note that a gel-treated matrix may be dehydrated by water produced from a water saturated, gel treated interval. Injection of a small amount of oil after the gel treated matrix has been dehydrated by production of water may allow trapping of residual oil in the dehydrated gel structure with a corresponding reduction in brine permeability when the well is returned to production.

These post-treatment steps are suggested by the research results reported in this paper and may offer a method of controlling the permeability reduction from a gel treatment and the disproportionate permeability reduction. Further testing is needed to determine if laboratory results can be extended directly to the field.

Conclusions

1. Gels formed within the Berea sandstone rocks were dehydrated by injection of oil or water, creating a "new" pore space within the rock-gel system.
2. The volume of dehydration, i.e., the volume of the new pore space, increased with increasing pressure gradient imposed during the dehydration process.
3. Part of the residual oil saturation encapsulated by the gelant was reconnected to the new pore channels during dehydration.

4. Permeabilities to both oil and water, at residual saturations of the other phase, were significantly smaller in the new pore space as compared to the original rock.
5. At the lower range of pressure gradients used for dehydration, permeability to water in the gel treated rock was reduced to a much greater extent than permeability to oil, i.e. there was a significant disproportionate permeability reduction (DPR).
6. Permeabilities to oil and water in the new pore space were a function of imposed pressure gradient, increasing as pressure gradient increased. Pressure gradient had a much larger effect on water permeability than on oil permeability, thus the magnitude of the DPR decreased as pressure gradient was increased.
7. The large DPR values observed at the lower range of pressure gradients are attributed to i) a relatively large residual oil saturation in the new pore space and ii) the extremely water-wet nature of the new pore space.
8. The effect of pressure gradient on brine or oil permeability is attributed to the deformation of the pore structure with pressure gradient.

Nomenclature

DPR = *Occurs when the ratio of F_{rrw}/F_{rro} at the same pressure gradient exceeds 1.0*
F_{rro} = *Residual resistance factor for oil defined by Equation 1*
F_{rrw} = *Residual resistance factor for brine defined by Equation 2*
k_o = *Permeability to oil at residual brine saturation, md*
k_{og} = *Permeability to oil at residual brine saturation of a gel treated porous rock, md*
k_w = *Permeability to brine at residual oil saturation, md*
k_{wg} = *Permeability to brine at residual oil saturation of a gel treated porous rock, md*
S_g = *Saturation of gel in the total pore space*
S_o = *Saturation of non-encapsulated oil in the total pore space*
S_{ot} = *Saturation of gel-encapsulated oil in total pore space*
S_o^* = *Saturation of oil in the newly created, effective pore space*
S_w = *Saturation of brine in the total pore space*
S_w^* = *Saturation of brine in the newly created, effective pore space*
S_{gel} = *Saturation of gel in total pore space*

Acknowledgement

Material in this chapter is substantially unchanged from a copyrighted paper published by the Society of Petroleum Engineers. The paper is in SPE 80205, "Effect of Pressure Gradient on Disproportionate Permeability Reduction," Ganguly et al., presented at the SPE International Symposium on Oilfield Chemistry, Houston, TX, February 5-8, 2003. The SPE copyright release form grants authority to authors the “nonexclusive right to incorporate all or part of the work in future writings or presentations.”

References

1. Ganguly, S., Willhite, G.P., Green, D.W. and McCool, C.S.,“Effect of Pressure Gradient on Disproportionate Permeability Reduction,” paper 80205 presented at the SPE International Symposium on Oilfield Chemistry, Houston, TX (5-8 February 2003).
2. Liang, J., Sun, H., and Seright, R.S., “Why do gels reduce water permeability more than oil permeability,” *SPERE* (November 1995) 282.

3. Seright, R.S. et al., “Using chemicals to optimize conformance control in fractured reservoirs,” Annual Report (U.S.DOE/BC/15110-2, OSTI ID: 11975), U.S.DOE Contract DE-AC26-98BC15110 (September 1999).
4. Sydansk, R.D. and Southwell, G.P., “More Than 12 Years of Experience With a Successful Conformance-Control Polymer Gel Technology,” paper SPE 49315 presented at the 1998 SPE Annual Technical Conference and Exhibition, New Orleans (27–30 September 1998).
5. Willhite, G.P., Green D.W., and McCool, C.S., “Increased oil recovery from mature oil fields using gelled polymer treatments,” Annual Report for the period June 2000 to June 2001, Contract No. DE-AC26-99BC15209, US-DOE, Washington, DC (2001).
6. Willhite, G.P., Zhu, H., Natarajan, D., McCool, C.S., Green, D.W., “Mechanisms causing disproportionate permeability in porous media treated with chromium acetate / HPAAM gels” *SPEJ* (March 2002) 100.
7. Yan, Z., McCool, C.S., Green, D.W., and Willhite, G.P., “ Modification of oil and water permeabilities in Berea sandstone by a gel treatment,” SPE 50753 presented at the 1999 SPE International Symposium on Oilfield Chemistry, Houston, Texas (16-19 February 1999).

Chapter 9

Technology Transfer

Chapters 2 through 8 of this report document and summarize the work performed under this contract in a comprehensive manner. Some minor results of method development of experimental procedures were presented in the annual reports for this contract (No. DE-AC26-99BC15209,"Increased oil recovery from mature oil fields using gelled polymer treatments"):

Annual Report for the period June 1999 to June 2000, Report No. DOE/BC/15209-2, US-DOE, National Petroleum Technology Office, Tulsa, OK (January 2001).

Annual Report for the period June 2000 to June 2001, Report No. DOE/BC/15209-4, US-DOE, National Petroleum Technology Office, Tulsa, OK (March 2002).

The following presentations and technical papers were given/published during the time period between June, 1999 and February, 2003. The presentations and papers were based on work conducted under this contract and the previous contract (DE-AC22-94PC91008).

Presentations

"Dehydration and Permeability of Gels Used in In-situ Permeability Modification", C.S. McCool, paper SPE 59347, presented at the 2000 SPE/DOE Improved Oil Recovery Symposium held in Tulsa, OK, (3-5 April 2000).

"Mechanisms Causing Disproportionate permeability in Porous Media Treated with Chromium Acetate/HPAAm Gels," G.P. Willhite, paper SPE 59345, presented at the 2000 SPE/DOE Improved Oil Recovery Symposium held in Tulsa, OK, (3-5 April 2000).

"A Different Perspective of Disproportionate Permeability Reduction," C.S. McCool, Petroleum Recovery Research Center, New Mexico Tech, Socorro, New Mexico, (2 November 2000).

"Development and Application of Polymer Gels for Water Control," G.P. Willhite, presented at a workshop titled *Gelled Polymers and Their Applications*, Petroleum Technology Transfer Council, Wichita, KS, (6 December 2000).

"Basics of Polymers and Gelled Polymers," C.S. McCool, presented at a workshop titled *Gelled Polymers and Their Applications*, Petroleum Technology Transfer Council, Wichita, KS, (6 December 2000).

"The Effect of Fluid Leakoff on Gel Placement and Gel Stability in Fractures," S. Ganguly (post-doctoral person) paper SPE 64987 presented at the 2001 SPE International Symposium on Oilfield Chemistry held in Houston, TX (13-16 February 2001).

"Propagation of Chromium(III) Acetate Solutions Through Dolomite Rock," H. Jin (graduate student) paper No. 75159 presented at the SPE/DOE Thirteenth Symposium on Improved Oil Recovery, Tulsa, OK (13-17 April 2002).

"The Effect of Effect of Pressure Gradient on Disproportionate Permeability Reduction," Ganguly, S. (post-doctorial person) paper No. 80205 presented at the SPE International Symposium on Oilfield Chemistry, Houston, TX (5–8 February 2003).

Technical Papers

Krishnan,P., Asghari, K., Willhite, G.P., McCool, C.S., Green, D.W. and Vossoughi, S.: "Dehydration and Permeability of Gels Used in In-situ Permeability Modification", paper SPE 59347, presented at the 2000 SPE/DOE Improved Oil Recovery Symposium held in Tulsa, OK (3-5 April 2000).

Zou, B., McCool, C.S., Green, D.W., and Willhite, G.P., "A Study of the Chemical Interactions Between Brine Solutions and Dolomite," *SPE Reservoir Evaluation &Engineering*, **3**, No.3 (June 2000) 209.

McCool, C.S., Green, D.W., and Willhite, G.P., "Fluid/Rock Interaction Between Xanthan-Chromium(III) Gel Systems and Dolomite Core Material," *SPE Production & Facilities,* **15**, No. 3 (August 2000) 159.

Zou, B., McCool, C.S., Green, D.W., and Willhite, G.P., "Precipitation of Chromium Acetate Solutions", *SPE Journal,* **5**, No. 3 (September 2000) 324.

Zhuang, Y., Pandey, S.N., McCool, C.S. and Willhite, G.P., "Permeability Modification with Sulfomethylated Resorcinol-Formaldehyde Gel System," *SPE Reservoir Evaluation & Engineering,* **3** (October 2000) 386.

McCool, C.S., Shaw, A.K., Singh, A., Bhattacharya, S., Green, D.W., and Willhite, G.P "Permeability Reduction by Treatment with KUSP1 Biopolymer," *SPE Journal,* **5**, No. 4 (December 2000) 371.

Willhite, G.P., Zhu, H., Natarajan, D., McCool, C.S. and Greeen, D.W., "Mechanisms Causing Disproportionate Permeability in Porous Media Treated with Chromium Acetate/HPAAm Gels," *SPE Journal,* **7**, No.1 (March 2002) 100.

Ganguly S., Willhite, G.P., Green, D.W. and McCool, C.S., "The Effect of Fluid Leakoff on Gel Placement and Gel Stability in Fractures," *SPE Journal*, **7**, No. 3 (September 2002) 309.

Jin, H., McCool, C.S., Willhite, G.P., Green, D.W. and Michnick, M.J. "Propagation of Chromium(III) Acetate Solutions Through Dolomite Rock," paper No. 75159 presented at the SPE/DOE Thirteenth Symposium on Improved Oil Recovery, Tulsa, OK (13-17 April 2002); accepted for publication in June 2003 issue of the *SPE Journal*.

Ganguly, S.,Willhite, G.P., Green, D.W. and McCool C.S., "The Effect of Pressure Gradient on Disproportionate Permeability Reduction,"paper No. 80205 presented at the SPE International Symposium on Oilfield Chemistry, Houston, TX (5–8 February 2003).